BI-FUNCTIONAL NANOSTRUCTURED NOVEL CATALYSTS FOR DIMETHYL ETHER SYNTHESIS

A THESIS SUBMITTED TO
THE GRADUATE SCHOOL OF NATURAL AND APPLIED SCIENCES
OF
MIDDLE EAST TECHNICAL UNIVERSITY

BY

GÖKHAN ÇELİK

IN PARTIAL FULFILLMENT OF THE REQUIREMENTS
FOR
THE DEGREE OF MASTER OF SCIENCE
IN
CHEMICAL ENGINEERING

JULY 2012

Approval of the thesis:

BI-FUNCTIONAL NANOSTRUCTURED NOVEL CATALYSTS FOR DIMETHYL ETHER SYNTHESIS

submitted by **GÖKHAN ÇELİK** in partial fulfillment of the requirements for the degree of **Master of Science in Chemical Engineering Department, Middle East Technical University** by,

Prof. Dr. Canan Özgen
Dean, Graduate School of **Natural and Applied Sciences**

Prof. Dr. Deniz Üner
Head of Department, **Chemical Engineering**

Prof. Dr. Timur Doğu
Supervisor, **Chemical Engineering Dept., METU**

Prof. Dr. H. Önder Özbelge
Co-Supervisor, **Chemical Engineering Dept., METU**

Examining Committee Members:

Prof. Dr. Göknur Bayram
Chemical Engineering Dept., METU

Prof. Dr. Timur Doğu
Chemical Engineering Dept., METU

Prof. Dr. H. Önder Özbege
Chemical Engineering Dept., METU

Prof. Dr. Pınar Çalık
Chemical Engineering Dept., METU

Assist. Prof. Dr. Dilek Varışlı
Advanced Technologies, Gazi University

Date: 20.07.2012

I hereby declare that all information in this document has been obtained and presented in accordance with academic rules and ethical conduct. I also declare that, as required by these rules and conduct, I have fully cited and referenced all material and results that are not original to this work.

Name, Last name: GÖKHAN ÇELİK

Signature:

ABSTRACT

BI-FUNCTIONAL NANOSTRUCTURED NOVEL CATALYSTS FOR DIMETHYL ETHER SYNTHESIS

Çelik, Gökhan
M.Sc., Department of Chemical Engineering
Supervisor : Prof. Dr. Timur Doğu
Co-Supervisor: Prof. Dr. H. Önder Özbelge

July 2012, 196 pages

Excessive use of fossil fuels shall result in the significant energy problems in the coming century and causes global warming by CO_2 emission. Use of petroleum in transportation constitutes the dominant part of total petroleum use. Researches on non-petroleum based, environmentally friendly alternative fuels have been ascended in last decades. Among the alternative fuels, DME has been considered as an attractive fuel alternate due to high cetane number, low PM (particulate matter) and low NO_x emission. Synthesis of DME is possible with gasification of biowastes or coal and steam reforming of natural gas. DME is produced in two different methods. In the first method, methanol is formed from the synthesis gas, followed by methanol dehydration to DME. In the second method, called as direct synthesis of DME from synthesis gas, methanol formation and dehydration occurs simultaneously at the same location within the reactor. For the direct synthesis of DME, bi-functional catalysts must be used; one site is responsible for methanol synthesis and other site is responsible for methanol dehydration.

Throughout this thesis work, several catalysts were prepared to be used as methanol synthesis component or methanol dehydration component of bi-functional direct

DME synthesis catalyst and bi-functional catalysts were also prepared for the direct synthesis of DME from synthesis gas. Materials were characterized by XRD, EDS, SEM, N_2 physisorption, and DRIFTS characterization techniques. Activity tests were conducted in a high pressure, fixed bed flow reactor at 50 bar and for the feed gas compositions of H_2:CO=50:50 and H_2:CO: CO_2=50:40:10.

Addition of zirconia and alumina promoters, long aging time, calcination temperature of 550 °C and reduction at 250 °C were found to be beneficial in methanol synthesis from the equimolar composition of CO and H_2. Precipitated catalysts were usually active and selective to methanol. However, bi-functional co-precipitated catalyst was not successful in situ conversion of methanol into dimethyl ether. Furthermore, tungstosilisic acid impregnated SBA-15 was physically mixed with commercial methanol reforming catalyst and activity results revealed that high DME yield and selectivity were obtained.

By physically mixing commercial methanol synthesis and reforming catalysts with γ-Al_2O_3 and TRC-75(L) in appropriate proportions or by preparing the reactor bed in a sequential arrangement, very high DME yields were obtained and superiority of direct synthesis to conventional two step synthesis was proven. Presence of CO_2 in the feed stream not only enhanced the catalytic activity but also utilization of the most important greenhouse gas was accomplished. It was seen that synthesized catalysts are very promising in the direct synthesis of dimethyl ether from synthesis gas.

Keywords: Dimethyl ether, Methanol synthesis and dehydration, Bi-functional catalysts, Direct synthesis, Co-precipitated catalysts

ÖZ

DİMETİL ETER SENTEZİ İÇİN ÇİFT FONKSİYONLU NANOYAPILI YENİ KATALİZÖRLER

Çelik, Gökhan
Yüksek Lisans, Kimya Mühendisliği Bölümü
Tez Yöneticisi : Prof. Dr. Timur Doğu
Ortak Tez Yöneticisi : Prof. Dr. H. Önder Özbelge

Temmuz 2012, 196 sayfa

Fosil yakıtlarının aşırı kullanımı önümüzdeki yüzyılda önemli enerji yokluğu problemlerine yol açabilir ve CO_2 salınımıyla küresel ısınmaya neden olmaktadır. Ulaşımdaki petrol kullanımı, toplam petrol kullanımının en büyük yüzdesini oluşturmaktadır. Petrol dışı kaynaklardan çevre dostu alternatif motorlu taşıt yakıtlarının geliştirilmesine yönelik çalışmalar son on yıllarda artmıştır. Araştırılan alternatif yakıtlar içerisinde dimetil eter (DME); yüksek setan sayısı, partikül ve hava kirletici gazların emisyonu açısından üstün özelliklere sahip olması sayesinde öne çıkmıştır. Biyo-atıklar veya kömürün gazlaştırılması ya da doğal gazın reformlanmasıyla elde edilen sentez gazından başlayarak DME üretimi mümkün olabilmektedir. DME sentezi iki farklı yöntemle gerçekleştirilmektedir. Bunlardan birincisinde önce sentez gazından metanol sentezi ve ardından üretilen metanolün dehidrasyonu ile DME oluşumu söz konusudur. İkinci yöntemde ise methanol sentez ve dehidrasyonlarının tek bir reaktörde aynı anda gerçekleştiği, DME'in doğrudan sentez gazından tek aşamada sentezi ile eldesidir. Doğrudan sentez prosesi için hem metanol sentez hem de dehidrasyon özellikleri olan iki fonksiyonlu katalizörlere ihtiyaç duyulmaktadır.

Bu tez çalışmasında, iki basamaklı dimetil eter sentezinin metanol sentez ve dehidrasyon fonksiyonlarında kullanılması amacıyla ve sentez gazından doğrudan dimetil eter eldesi için iki fonksiyonlu katalizörler sentezlenmiştir. Sentezlenen malzemelerin dışında ticari katalizörler ile de çalışmalar yürütülmüştür. Katallitik malzemeler XRD, EDS, SEM, azot adsorplanmasıyla yüzey karakterizasyonu ve DRIFTS teknikleri ile karakterize edilmiştir. Aktivite testleri, yüksek basınçlı sabit yataklı akış reaktör sisteminde 50 bar basıncında ve H_2:CO=50:50 ve H_2:CO: CO_2=50:40:10 besleme gazı kompozisyonlarında test edilmiştir.

Zirkonyum ve alüminyum promotörleri eklenmesi, uzun bekletme süresi, 550 °C'de kalsinasyon sıcaklığı ve 250 °C'de indirgenme sıcaklığı eşit kompozisyonlu CO ve H_2 içeren sentez gazından metanol eldesinde aktiviteyi artırmıştır. Çöktürme katalizörleri genel olarak yüksek aktivite göstermişlerdir. Çöktürme yöntemiyle hazırlanan çift fonksiyonlu katalizör, oluşan metanolü dimetil etere az oranda dönüştürmüştür. Silikotungstik asit emdirilmiş SBA-15'in ticari metanol reformlama katalizörü ile karıştırılmış olarak aktivitesine bakıldığında yüksek seçicilikte dimetil eter elde edildiği görülmüştür.

Ticari metanol sentez ve dehidrasyon katalizörlerin ve silikotungstik asit esaslı mezogözenekli TRC-75(L) katalizörünün uygun oranda karıştırarak veya sıralı olarak hazırlanan reaktörler ile yapılan aktivite testlerinde çok yüksek DME verimi elde edilmiştir ve yapılan deneylerle doğrudan sentezin iki basamaklı senteze olan üstünlüğü ispatlanmıştır. Sentez gazı içinde CO_2 bulunması sadece DME verimini artırmakla kalmamış, aynı zamanda da en önemli sera gazı olan CO_2'in kullanımında başarılı olunmuştur. Çalışma kapsamında sentezlenen katalizörlerin sentez gazından DME sentezinde çok umut verici oldukları görülmüştür.

Anahtar Kelimeler: Dimetil Eter, Metanol sentezi ve dehidrasyonu, İki fonksiyonlu katalizör, Doğrudan sentez, Birlikte çöktürme katalizörleri

To My Family

ACKNOWLEDGEMENTS

I would like to present my sincere thanks to my supervisor Prof. Dr. Timur Doğu for his inspiring guidance, endless support, and continuous encouragement. I also want to thank him for his understanding and kindly attitude in every aspect. He is an example to follow for all graduate students.

I am very grateful to my co-supervisor Prof. Dr. H. Önder Özbelge for his great help, motivation and suggestions not only for my research but also about my future life. I have learned very important things and got a life philosophy from him. If I was far away from his advices for the last five years, I would have very different life style.

I would like to offer my sincere thanks to Prof. Dr. Gülşen Doğu and Prof. Dr. Tülay Özbelge for their positive manner and support for this study. I would like to also thank Dr. Dilek Varışlı for her early studies about DME.

I cannot pass without presenting my sincere thanks to Canan Şener. I felt her motivation and support at any time. I want to thank my lab friend Seval Gündüz for her helps and friendship during my studies and research colleagues Arzu Aslan, Orkide Akgün, Ayşegül Bayat and Birce Pekmezci. Working in such an environment was a great experience for me.

I would like to thank my friends Okan Özkök, İlker Tezsevin, Duygu Gerçeker and Caner Hocaoğlu for their valuable friendship during my studies.

I would like to thank METU Chemical Engineering department staff; Nevzat Bekçi, Turgut Aksakal, İsa Çağlar, Yavuz Güngör, Süleyman Nazif Kuşhan, Kemal Yıldırım, Murtaza Oral, Mahmut Akdağ and Arap İşleyen for their endless support

and positive attitude. I would also like to thank METU Central Laboratory and technical staff for the characterization analyses.

I owe special thanks to my family. It is very difficult to express in words for all the support and encouragement they have given to me. They deserve my special and sincerely gratitude. My very special thanks are due to my mother Serbes Çelik, my father Ramazan Çelik and my lovely brother Volkan Çelik.

METU Scientific Research Coordination is also acknowledged for the financial support with the research fund BAP-03-04-2011-008.

The Scientific and Technological Research Council of Turkey (TÜBİTAK) is also acknowledged for the partial financial support under graduate scholarship of TÜBİTAK BİDEB (2228).

TABLE OF CONTENTS

CHAPTERS

LIST OF FIGURES

FIGURES

LIST OF TABLES

TABLES

NOMENCLATURE

Cp: Heat Capacity (J/mol.K)
DME: Dimethyl Ether
DRIFTS: Diffuse Reflectance Infrared Fourier Transform Spectroscopy
EDS: Energy Dispersive Spectroscopy
ETOH: Ethanol
f: Fugacity (bar)
F: Molar flow rate (mol/hr)
FA: Formic Acid
G: Gibbs Free Energy (kJ/mol)
H: Enthalpy (kJ/mol)
IUPAC: International Union of Pure and Applied Chemistry
K: Equilibrium Constant
MW: Molecular weight (g/mol)
MCM: Mobil Composition of Matter
MeOH: Methanol
n: Mole
P: Pressure (bar)
Q: Volumetric flow rate (ml/min)
R: Gas constant (8.314 J/mol.K)
S: Selectivity
SBA: Santa Barbara Amorphous
SEM: Scanning Electron Microscopy
T: Temperature (°C)
X: Conversion
XRD: X-Ray Diffraction
y: Molar composition
Y:Yield

CHAPTER 1

INTRODUCTION

Fossil fuels have been used extensively as our major energy source for the last century. Their extensive use and fast depletion of reserves may lead to the energy shortage in near future since they are not renewable in the human time scale [1]. Furthermore, carbon dioxide emission upon the fossil fuel use is of great importance due to the global warming. Fast depletion of fossil fuels and global warming issues have initiated new researches on non-petroleum based, environmentally friendly alternative fuel. Dimethyl ether (DME) has attracted the attention of researchers due to its benign characteristics.

DME is a benign chemical in terms of good burning characteristics and environmentally friendly properties. It can be used for various important applications. Physical and fuel properties of DME are given in Chapter 2. In this Chapter, it has been compared with other alternate fuels such as alcohols (methanol, ethanol), natural gas (methane), LPG (propane, butane), diesel, and gasoline. Application areas of DME are also given in this chapter. On the other hand, disadvantages of DME are mentioned and possible solutions are also proposed.

DME can be produced by two processes from the synthesis gas. In the first one, methanol formation from the synthesis gas followed by methanol dehydration step. In the second process, methanol synthesis and dehydration occur simultaneously within the reactor at the same time. For this reason, bi-functional catalyst must have two active sites. One site is responsible from methanol synthesis and copper and zinc containing catalysts function very well in methanol synthesis. Other site is responsible from methanol dehydration and acidic catalysts such as γ-Al_2O_3, aluminum silicates, and zeolites function very well in methanol dehydration. Information about the production routes and catalytic literature review are given in Chapter 3.

In the DME synthesis, amount of produced methanol is very important since it will be converted to DME. However, methanol synthesis is a highly exothermic reaction with thermodynamical limitations. Therefore choice of operating parameters is very significant. In Chapter 4, thermodynamic analyses are conducted to determine to operating parameters. Equilibrium conversion of methanol synthesis reaction and direct DME synthesis reactions are plotted with respect to temperature and pressure.

In Chapter 5, catalysts preparation methods, catalyst treatments and characterization techniques are explained in principal. Precipitated catalysts, impregnated catalysts and ordered molecular materials are basically reviewed. Importance of the catalyst treatments emphasized with characterization methods.

Chapter 6 presents experimental procedures concerning the synthesis of novel materials. Characterization instruments and operating procedures of characterization techniques are presented. In addition, high pressure experimental set-up is explained in detail with reactor properties.

In Chapter 7, activity results of synthesized and commercial catalysts are given and in Chapter 8, activity results are illustrated. In the activity test results, conversions and selectivities are investigated with respect to temperature. Finally, conclusions are given in Chapter 9.

CHAPTER 2

DIMETHYL ETHER AS A CHEMICAL

The vast amount of energy needs of the Earth has been covered by the fossil fuels, starting with coal, petroleum oil, and natural gas. These fossil fuels have been used in the last century extensively resulting in the today's advanced world, technology and prosperity. However, fossil fuels are not infinite and being depleted rapidly. Their use is limited with what we have as resources since fossil fuels are not renewable on the human time scale [1].

One of the most important problems with the fossil fuels is the carbon dioxide emission. Since the fossil fuels are carbon containing materials, carbon dioxide which is the major greenhouse gas contributing to the global warming is released to atmosphere upon combustion. Among the fossil fuels, excessive use comes from transportation. Transportation constitutes 57% of oil use in the world. At this rate of use, rapid depletion for transportation can cease the synthesis of many of the oil based petrochemical products. Oil is too valuable to be burned for transportation [2].

If humanity keeps excessive use of fossil fuels as their major energy source, fast depletion can result in the significant shortage of energy problems in the coming century. If current consumption rates continue, fossil fuels will be depleted to a large extent. In addition to this, greenhouse effect due to the excessive carbon dioxide emissions could result in devastating impacts on the world. For these reasons, researches on seeking for non-petroleum based alternative fuels have started. Among the alternative fuels that can replace petroleum based fuels, dimethyl ether (DME) can be considered as the best candidate.

Dimethyl ether, also known as methoxy methane, is the simplest ether having a chemical formula of CH_3OCH_3. DME is in the gas form at standard temperature and pressure and can be liquefied at 6 atm or -25 °C. It is volatile but non-toxic, non-carcinogenic, non-teratogenic, and non-mutagenic. It burns with a visible blue flame and it has sweet ether like odor [3].

DME can be synthesized in at least two minimum steps. First step is converting fossil fuels including natural gas or coal and renewable materials (biomass, waste and agricultural products) into the synthesis gas. As it can be seen, there are several feedstocks for the DME synthesis. Therefore, DME synthesis is not limited to the one feedstock. Second step is transforming syngas to DME either by conventional methanol synthesis and dehydration or by direct synthesis from syngas [3,4]. Synthesis gas is composed of carbon monoxide, carbon dioxide and hydrogen. Use of carbon dioxide containing syngas in the DME synthesis is very promising since it is an excellent solution candidate for global warming and depletion of oil reserves. By this way, carbon dioxide can be converted to the valuable non-petroleum based fuel DME [2].

For the fuel characteristics, which are given in Table 1, DME has a cetane number of 60 which is higher than the conventional diesel fuel whose cetane number is around 50. Cetane number is the combustion characteristic of diesel fuel indicating the auto ignition property of the fuel under high temperature and high pressure. Ignition point of DME is also very close to the ignition point of diesel fuel. High cetane number, low boiling point of DME (-25 °C) and high oxygen content (35 wt%) are important fuel characteristics allowing fast vaporization and smokeless operation. DME combustion does not produce soot. In addition, DME fueled diesel engines are quieter than the conventional diesel fuel fueled cars. There is no SO_x emission coming from DME use since DME is sulfur free chemical and NO_x emission is also

Table 1. Comparison of Dimethyl Ether and Other Alternative Fuels' Physical Properties* (Adapted from [4, 8])

Properties	**DME**	**Methanol**	**Methane**	**Ethanol**	**Propane**	**Butane**	**Gasoline**	**Diesel**
Chemical Structure	CH_3OCH_3	CH_3OH	CH_4	C_2H_5OH	C_3H_8	C_4H_{10}	C_7H_{16}	$C_{14}H_{30}$
Molecular Weight , g/mol	46	32	16	46	44	58	100	-
Liquid density , g/cm^3	0.67	0.79	0.42	0.79	0.49	0.57	0.73-0.76	0
Vapor pressure , bar	5.3	0.13	0.05	0.06	9.30	2.40	-	-
Explosion limit , vol %	3.4 -18.6	6.7-36	5-15	3.3-19	2.1-9.4	1.9-8.4	1.4-7.6	0.6-6.5
Cetane number	55-60	5	0	40,50	5	10	5-20	40-55
Normal Boiling point, °C	-24.9	64	-162	78	-42	-0.5	38-204	125-400
Net Calorific Value , kcal/kg	6900	4800	12000	-	11100	10900	-	10200
Sulfur content , ppm	0	0	7-25	0	-	-	~200	~250
Carbon Content , wt.%	30.8	37.5	74	29.4	81.8	82.8	85.5	87
Specific gravity of gas	1.6	1.1	0.6	1.6	1.5	2.0	-	-
Ignition Temperature , K	350	385	540	365	470	430	228	-
Heat of evaporation , kJ/mol	21.5	35.2	8.2	38.9	18.7	22.3	-	-

*Values are at standard temperature and pressure low [1, 4, 5] The comparison of benign properties of DME can be made as in the Figure 1.

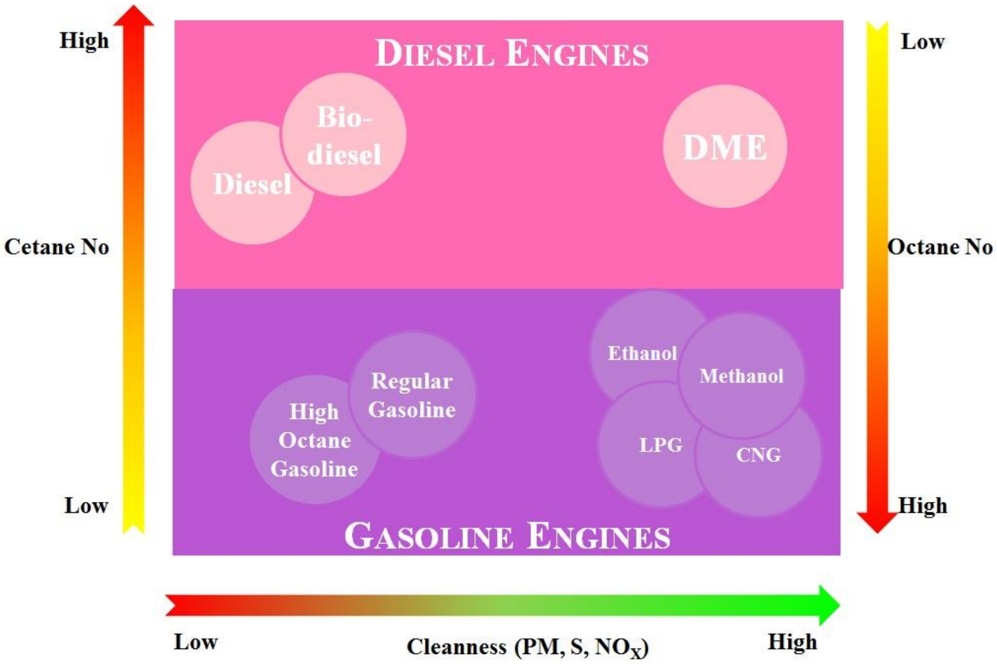

Figure 1. Fuels comparisons with respect to fuel quality and cleanness [6]

Use of DME in the diesel engines is possible with some minor modifications on the fuel injection system. Since the energy densities of diesel fuel and DME are different, storage tanks should also be modified. For the same amount of energy, DME storage tank requires a 1.7 times the volume of the storage tank of diesel fuel. In the ordinary diesel engine with a new fuel injection system, cars fueled with DME have been tested and it has been shown that same performance has been obtained with great amount of emission reducing when compared to the conventional diesel [7].

DME can be used for residential purposes such as heating and cooking. DME has quite similar properties with natural gas and Wobe indexes of natural gas and DME are almost same, indicating the interchangeability of fuels. For cooking and heating purpose, there is no need to change the equipment which has been originally designed for natural gas [7].

There are several similar properties of DME with LPG. DME can be handled in a safe manner as LPG and minor changes are necessary in the storage and distribution. With these minor changes, there will be no need of investment on the infrastructure since existing LPG refilling stations can also be used for DME refilling. This makes the use of DME as economically feasible since building a new infrastructure requires time and large amount of capital [4]. DME can also be blended with LPG (up to 20%) to use in the residential home heating and cooking without modifications to the existing equipment and distribution [9].

Use of DME as a starting raw material for the synthesis of olefins is also possible in which methanol has been already used since enthalpy of DME is lower than the enthalpy of methanol. By this way, heat of reaction in which DME is raw material could be lowered. In addition to this, transformation of DME into the olefins is important since olefins are the basic raw materials of the petrochemical industry [1].

DME has been used as propellant in consumer applications such as personal care, paints and finishes, insect control, etc. By these uses, DME has replaced the harmful chloroluorocarbon gases which contribute to the ozone depletion in the upper atmosphere [10].

DME can also be used in fuel cells and is considered to be one of the best alternate fuels in portable fuel cells. Unlike the other liquid fuels, DME is free from the disadvantages of low performance of ethanol, high corrosion of formic acid and toxicity of methanol. In addition to these, DME has smaller dipole moment which decreases the crossover of it from anode side to cathode side and complete oxidation is possible with a minimum kinetic energy loss since there is no C-C bond in DME. When DME is used as fuel in fuel cells, theoretical fuel requirements decreased since DME has high electron transfer number [11].

DME possesses some drawback regarding to the physical characteristics. Viscosity of the DME is lower than the commercial diesel by a factor of 20. This could result in the leakage in fuel injectors and pumps. Lubrication issues are another handicap of

DME. In the solution of these problems, additives could be used to increase the lubricity. Moreover, additives used in the commercial diesel fuels have been also used in the DME as a lubricity enhancer [4].

CHAPTER 3

SYNTHESIS OF DIMETHYL ETHER

In this chapter, a literature survey on the production routes of dimethyl ether and methanol is given with the highlights from the catalytic material development on direct DME synthesis, methanol synthesis, and methanol dehydration.

3.1. DIRECT SYNTHESIS OF DIMETHYL ETHER FROM SYNTHESIS GAS

In dimethyl ether synthesis, two minimum steps are necessary. First step is converting fossil fuels including natural gas, coal and renewable materials (biomass, waste and agricultural products) into the synthesis gas. There are several feedstocks for DME synthesis. Therefore, DME synthesis is not limited to the one feedstock [3]. After syngas is obtained, it is converted to DME. Conversion to DME could be accomplished in two ways. One way is the conventional two-step process of DME synthesis in which methanol is synthesized from synthesis gas, followed by methanol dehydration at different reactor. Other way is the direct synthesis of DME in one step from the synthesis gas. Direct synthesis of DME is gaining importance because of its thermodynamical and economical properties [12].

In the direct synthesis of dimethyl ether from the synthesis gas, there are mainly two overall reactions, reaction-1 and reaction-2. Methanol synthesis from the synthesis gas is given with reaction-3 and methanol dehydration is given with reaction-4. Reaction-1 is a combination of reactions 3, 4, and 5 and reaction-2 is a combination of reactions 3 and 4 [13]. Reaction-5 is the water gas shift reaction which occurs very fast on the copper-zinc based catalyst and overall direct synthesis of DME reaction turns into reaction-1 [14].

$3CO + 3H_2 \rightarrow CH_3OCH_3 + CO_2 \quad \Delta H_{rxn} = -246$ kJ/mol [1]

$2CO + 4H_2 \rightarrow CH_3OCH_3 + H_2O \quad \Delta H_{rxn} = -205$ kJ/mol [2]

$CO + 2H_2 \rightarrow CH_3OH \quad \Delta H_{rxn} = -90$ kJ/mol [3]

$2CH_3OH \rightarrow CH_3OCH_3 + H_2O \quad \Delta H_{rxn} = -25$ kJ/mol [4]

$CO + H_2O \rightarrow CO_2 + H_2 \quad \Delta H_{rxn} = -41$ kJ/mol [5]

Direct dimethyl ether synthesis reactors usually operate at a temperature range of 240 °C - 280 °C and at a pressure range of 30 bar – 70 bar. Due to the exothermic nature of DME synthesis reactions, temperature control and heat removal are very important to achieve high conversions [13].

Zhang et al. [14] studied dimethyl ether synthesis from CO hydrogenation on HY zeolite and zeolites were modified by incorporation of several metals. Methanol dehydration of synthesized catalysts was also tested. Activity tests were performed at 245 °C and 20 bar for a feed gas of $H_2/CO=1.5$. They reported that dual catalyst must be prepared by coupling the methanol synthesis and dehydration sites completely. Modification of HY zeolites by Fe, Co, and Cr did not show stability due to the carbon deposition. However, modification by Zr and Ni exhibited very high activity and stability. Moreover, activity of dual catalyst can be changed with the ratio of methanol synthesis component to methanol dehydration component. To produce more methanol, fraction of methanol synthesis component could be increased.

Sun et al. [15] studied low temperature synthesis of DME from carbon dioxide containing synthesis gas over Pd modified Cu-ZnO-Al_2O_3/HZSM5 catalyst. Activity tests were conducted at 200 °C and 30 bar. Activity results indicated that palladium addition to the catalyst hindered CO formation and selectivity of DME increased. Lowest catalytic activities were attributed to the increase in the particle size of CuO and ZnO. On the other hand, strong interactions at the interface could be the main reason of high activity. This effect was called as synergistic effect.

Yoo et al. [16] studied the effect of solid acid catalyst on the direct synthesis of DME. Different SAPO catalysts were prepared having different pore structures and different acidities. Catalytic activity was tested in a fixed bed reactor operating at 42 bar and 260 °C from a feed mixture of $H_2/CO=1.5$. Activity results revealed that highest acidity materials exhibited very high initial activity whereas they were exposed to high amount of coke formation within the pores and activity decreased considerably. On the other hand, moderate acidic materials with desired pore structures were more stable than the high acidic materials. In the activity tests of direct synthesis of DME, hydrocarbon byproducts were hardly observed with any of the catalysts. In the direct synthesis of DME, highest carbon monoxide conversion was obtained as 55 % with a DME selectivity of nearly 63% for the admixed catalyst, in which SAPO composition was 10% in weight.

Mao et al. [17] investigated the effect of sulfate content and calcination conditions on the activity of the methanol dehydration component of hybrid catalyst. Impregnation method was used in the incorporation of sulfate and sulfate content was altered up to 15%. Calcination temperature was varied in between 350 °C - 750 °C. Activity tests were carried out in a fixed bed flow reactor operating at 40 bar and 260 °C for the feed gas of $H_2:CO:CO_2=66:30:4$. Activity results showed that catalytic activity was enhanced when calcination was carried at 550 °C instead of 350 °C. Formation of CO_2 was prevented when calcination was carried at 550 °C. With the further increase in the calcination temperature, a sharp decline of CO conversion and DME selectivity was observed. Moreover, with increase in the sulfate ratio, slight decrease of DME selectivity was observed due to CO_2 formation. However, CO conversion also increased. Highest activity was obtained with 10% sulfate impregnated $SO_4^{-2}/\gamma\text{-}Al_2O_3$ sample which was calcined at 550 °C. Catalytic activity upon sulfate impregnation was attributed to the number and strength of acid sites.

Sofianos and Sourrell et al. [18] investigated the activity of different methanol dehydration components such as alumina, amorphous silica-alumina, Y zeolite, mordenite, and ZSM-5 zeolites. By mixing the powders of methanol synthesis component and methanol dehydration component, bi-functional catalyst beds were prepared. Activity tests were conducted at 40 bar for H_2:CO=2:1 feed gases and small amount of CO_2 was also added to feed gas. Results indicated that, in the presence of suitable acidic methanol dehydration catalyst, methanol can be converted to DME over γ-alumina, alumina-silica, and zeolite. Comparison between methanol synthesis and direct DME synthesis was made and it was seen that DME synthesis was more favored than the methanol synthesis, indicating thermodynamic advantage of direct synthesis. Moreover, presence of CO_2 in the feed stream was found to be beneficial in CO conversion and DME selectivity.

Sun et al. [19] investigated the effect of surface properties on the catalytic performance. Bi-functional catalysts which were composed of CuO/ZnO/ZrO_2/HZSM-5 were prepared by coprecipitating sedimentation and modified by different ZrO_2 content. Catalytic activity was tested at 30 bar for a feed gas of CO:CO_2:H_2=30:3:67. Very high DME selectivity at around 83% and reasonable CO conversion at around 73% were obtained. Catalytic activity was attributed to the Cu^+ species which were formed upon ZrO_2 incorporation. In addition, ZrO_2 incorporation also increased the dispersion of active sites and enhanced synergistic effect, which are beneficial in catalytic activity.

Regeneration study of the direct DME synthesis catalyst of CuO-ZnO-Al_2O_3/γ-Al_2O_3 was made by Sierra et al. [20]. Regeneration of the catalysts could be achieved by the oxygen and helium and regeneration temperature was 325 °C. Temperature was reported to be important since copper could sinter at this temperature readily. Deactivation of catalyst was due to coke formation and copper sintering, the latter was irreversible. Although DME direct synthesis catalysts undergo fast deactivation, initial activity of the catalyst could be achieved after regeneration. However, sintering of copper which is an irreversible process can be prevented by adding promoters such as alumina.

3.2. METHANOL SYNTHESIS

Methanol synthesis was first made by destructive distillation of wood. For this reason; methanol is also called as wood alcohol. Methanol demand of 19th century was met by this method and methanol was used for lighting, heating and cooking purposes [1]. High pressure operation was first conducted by BASF. Operating parameters were in the range of 250 bar - 350 bar and 320 °C - 450 °C. The catalyst was highly poison resistant, $ZnO-Cr_2O_3$ and this high pressure process was used for 45 years from the synthesis gas, which was obtained by German low quality coal/lignite.

In the 1960s, Imperial Chemical Industries (ICI) was used copper in methanol synthesis with Zn promoter, which was enhancing the dispersion of copper and prevent agglomeration of it. By this catalyst, operating pressure was dropped to 35 bar - 55 bar, which is known as low pressure process [21].

In the methanol synthesis, three main reactions are involved. Reaction 3 and 6 are the hydrogenation of carbon oxides to methanol and reaction-5 is the water gas shift reaction which occurs over the copper-zinc based catalyst.

$CO + 2H_2 \rightarrow CH_3OH$ [3]

$CO + H_2O \rightarrow CO_2 + H_2$ [5]

$CO_2 + 3H_2 \rightarrow CH_3OH + H_2O$ [6]

While reactions 3, 6 and 5 are occurring, number of moles decrease. As a result, volume is reduced to some extent. These reactions are also exothermic in nature. For these reasons, high pressure and low temperature favor activity [22].

Although methanol is one of the top chemicals, there are still controversial points about the catalytic behaviors of the methanol synthesis catalyst. Nature of active site, formation mechanism and role of ZnO and other promoters are still in debate.

However, a consensus of methanol synthesis occurs via CO_2 hydrogenation on metallic copper of copper/zinc oxide catalyst has been reached by many authors [23].

Sintering of the copper is one of the most important reasons of catalyst deactivation. Copper is one of the least stable metals and sintering may happen readily above 300 °C. Sintering also increases the particle size and XRD results of used catalyst revealed that particle size could increase from 7 nm to 20 nm due to sintering [23, 24].

Arena et al. [25] has given basic evidents of methanol synthesis catalyst in his recent study. In this study, methanol synthesis from CO_2 was conducted due to importance of CO_2 as a greenhouse gas. $Cu/ZnO/ZrO_2$ catalyst was chosen due to the water adsorption capacity of ZrO_2 with respect to γ-alumina which is highly hydrophilic. Catalytic activity tests showed that methanol selectivity is highly dependent on the reduction temperature. Results showed that $Cu^{\delta+}/Cu^0$ ratio was the key parameter to obtain high selectivity.

Saito et al. [26] investigated the role of metal oxides such as Al_2O_3, Ga_2O_3, and Cr_2O_3 for methanol synthesis from CO_2 hydrogenation. Reaction conditions were 5 mPa and 523 K and catalysts were reduced in H_2 flow at different temperatures. Activity results indicated that Al_2O_3 and Zr_2O_3 metal oxides increased the copper dispersion and improved copper surface area whereas it had no effect on catalytic activity. On the other hand, Ga_2O_3 and Cr_2O_3 had no effect on copper dispersion but increased catalytic activity. This increment in activity was a result of the Cu^+/Cu^0 ratio which was optimized by Ga_2O_3 and Cr_2O_3 metal oxides. Catalyst activity was decreasing with increase in pretreatment temperature due to sintering of copper. However, it was seen that sintering of copper can be suppressed by the addition of metal oxides.

Meshkini et al. [27] investigated the promoting effect of different metal oxide additives of a co-precipitated methanol synthesis catalyst from syngas. Catalytic activity tests were conducted in a stainless steel fixed bed reactor operating at 50 bar and 513 K, from a reactant gas of gaseous mixture $CO/CO_2/H_2=1/1/4.5$ at gas hourly space velocity of 12400 /hour. Among the studied promoters (Mn, Zr Mg, Cr, W, Ce, Ba) Mn and Zr promoted catalysts were the most active catalysts. It was also reported that addition of promoters also changed the copper dispersion and number of active sites. For example, Mn-Zr promoted catalysts offered the Cu metal surface area as 41.1 m^2/gcat and copper dispersion was the highest in this catalyst.

Dai et al. [28] made XPS studies of methanol synthesis catalyst prepared by the oxalate gel co-precipitation method for the feed mixture of CO_2-H_2 and CO_2-CO-H_2. They have found that reduction by H_2/Ar at 240 °C reduced copper to metallic state and had no effect on the chemical state of zinc. This result indicated that copper and zinc are 0 and +2 at the chemical valence states. Furthermore, they have shown that carbon dioxide containing methanol synthesis catalyst undergoes partial oxidation to $Cu^{\delta+}$ when exposed to pure carbon dioxide where $0<\delta<1$. This result was also supported by another study of Spencer et al. [29]. In this study, Spencer reviewed the benefits of zinc in methanol synthesis catalyst in addition to having copper as main active component.

Ma et al. [30] prepared methanol synthesis catalyst from CO_2 hydrogenation via oxalate co-precipitation methanol by changing the solvent. They investigated the properties of solvent on catalyst characterization and activity and concluded that large viscosity and small surface tension solvent have given the best structure and activity in oxalate co-precipitated catalysts. They conducted catalytic activity tests at 20 bar for a feed gas of $CO_2:H_2 = 1:3$ in a continuous tubular flow fixed bed microreactor. Obtained CO_2 conversions and methanol selectivity were in the range of 18-20% and 35-45%.

Raudaskoski et al. [31] have studied the effect of aging time on copper, zinc and zirconia co-precipitated catalyst via CO_2 hydrogenation. They prepared catalysts by conventional co-precipitation method by changing the aging time for 0.5 gr, 12 hr and 24 hr. Methanol activity results which were conducted at pressure of 30 bar and space velocity of 50 ml/min.gcat. Feed gas ratio was $H_2/CO_2=3$ and 1 gr catalyst was loaded into reactor. Results showed that as aging time increased, methanol yields increased. It was also seen that the catalyst which aged for 24 hours contain the least amount of sodium. In catalytic activities, CO_2 conversion as high as 20% and methanol selectivities as high as 30% were obtained at 250 °C.

Zirconium takes attention from many researchers because of showing a good effect for methanol synthesis from synthesis gas. Zirconia was investigated by Sun et al. [32] using Cu-ZnO-ZrO_2/HZSM-5 catalyst including different Zirconia amounts to observe its catalytic performance for direct DME synthesis. According to results, ZrO_2 addition increased the formation and stabilization of Cu^+ which is partly responsible for methanol formation. ZrO_2 provides a strong promoting effect on CO conversion and DME yield.

Effect of zirconia on copper based catalysts was also investigated by Flores et al. [33] and it was seen that zirconia addition increased the copper surface area. ZrO_2 addition affected the copper dispersion and changed the morphology of copper particles and increased the dispersion of Cu crystallites resulting more active sites and higher conversions. According to Słoczynski et al. [34], incorporation of ZrO_2 not only increased the catalytic activity but also decreased H_2O adsorption capability. As a result of this, methanol yield and catalytic performance increased. They also reported that, when oxide additives, B, Ga, In, Gd, Y, Mg and Mn, introduced to the Cu/ZnO/ZrO_2 catalyst, highest methanol yield was obtained with catalyst Ga_2O_3 and lowest activity was observed with In_2O_3.

Zhang et al. [14] studied the effect of zirconia impregnation on γ-alumina in methanol synthesis from CO_2 hydrogenation. They examined the effect of temperature, space velocity and molar ratio of reactants and find out that high space velocity and low temperature were the parameters to obtain high activity. In addition, zirconia addition to γ-alumina enhanced the CuO dispersion and as a result, zirconia addition increased the catalytic performance.

Ceria has been used as a promoter or doper to the copper zinc containing methanol synthesis catalyst. Shen et al. [35] studied the methanol synthesis from the feed gas of carbon monoxide and carbon dioxide over ceria supported copper catalyst and found that ceria enhanced the dispersion of copper. They compared the activity results with conventional copper zinc based catalyst and synthesized catalyst was more active than the conventional one. In carbon monoxide hydrogenation, Pokrovski et al. [36] investigated the effects of cerium incorporation into the Cu/ZrO_2 methanol synthesis catalyst. They showed that presence of ceria was beneficial to increase the adsorption capacity of oxides and made the concentration of methoxide species higher. For these reasons, ceria incorporation increased the activity.

Another study conducted by Kaluza et al. [37] was about a novel promising alternative to conventional process. Preparation of $Cu/ZnO/Al_2O_3$ catalyst was made by using micromixer cascade as continuous catalyst. Continuous and consecutive precipitation was achieved and by using spray dryer. Quenching was also achieved. By this technique, homogeneity and reproducibility of the catalyst enhanced. Furthermore, catalytic activity which was conducted at 60 bar and 250 °C for a gas mixture of CO, CH_4, CO_2 and H_2 has given 50% higher conversion than the commercial catalyst.

Guo et al. [38] synthesized catalyst by glycine-nitrate combustion method and examined the catalytic properties in the methanol synthesis from CO_2 hydrogenation. They have changed the amount of glycine which is the complexing agent for metal ions in the methanol synthesis catalyst. They have conducted catalyst activity testing at 30 bar and 493 K for the feed gas of $CO_2:H_2 = 1:3$ and 12% CO_2 conversion and 71.1% methanol selectivity was obtained for gas hourly space velocity of 3600 /hr. As glycine amount increased, decreases were observed in BET surface areas and CO_2 conversion. Methanol selectivity exhibited a volcanic trend with respect to glycine amount.

3.3. METHANOL DEHYDRATION

The conventional method to obtain DME is the methanol dehydration. Since DME is produced from the methanol, DME is more expensive than methanol in spite of being relatively simple process [5]. Methanol dehydration for the synthesis of DME is the conventional way of obtaining DME and synthesis can be accomplished by solid acidic catalysts at atmospheric pressure. For this purpose, zeolites, aluminas, aluminosilicates, mixed metal oxides, and impregnated materials of metal oxides as nanocomposites have been used in methanol dehydration. Methanol dehydration occurs via the following reaction-4.

$$2CH_3OH \rightarrow CH_3OCH_3 + H_2O \qquad [4]$$

Kim et al. [39] studied DME synthesis and investigated the role of acidity in methanol dehydration on Na-ZSM-5 and H-ZSM-5 catalysts with different Si/Al ratios. Based on the activity and NH_3-TPD results, highest dehydration rate was seen on the catalyst with highest acidity. Optimal reaction parameters were also found in this study and it was concluded that overall reaction rate of direct synthesis is possible to control by lowering the acid strength of the catalyst and therefore, by slowing down the dehydration rate.

Yaripour et al. [40] prepared γ-alumina and aluminum phosphate modified catalysts with co-precipitation method to be used in the methanol dehydration to dimethyl ether. Phosphorus modification affected the catalytic activity in a positive way. Almost 100% DME selectivity and nearly 80% conversions was obtained at reaction conditions of 573 K and 16 barg. Optimum phosphorus content was found to be as Al/P=1.5 and they concluded that moderate acid sites were the best candidates for activity in methanol dehydration reactions.

Methanol dehydration to dimethyl ether was also studied by the same group Yaripour et al. [41]. They prepared silica-titania and aluminium phosphate catalysts and conducted activity tests in a fixed bed reactor operating at temperature of 300 °C and gas hourly space velocity of 15600 h^{-1}. Results showed that silica-titania catalyst had no significant activity in methanol dehydration. However, phosphorus modified aluminum catalysts were active DME as the major product with the formation of methane as a byproduct. Formation of methane was attributed to the strong acidic sites whereas medium acidity was claimed to be key factor to obtain high selectivity.

Khaleel [42] studied methanol dehydration to dimethyl ether over highly porous xerogel alumina catalysts and investigated the flow rate effect on the catalytic activity. Synthesis of mesoporous γ-alumina was achieved with high surface area and catalytic activity was found to be highly dependent on the product distribution. High flow rates of methanol favored DME formation whereas low flow rates caused carbon dioxide and methane formation. Moreover, synthesized mesoporous alumina was better than commercial γ-alumina.

Fu et al. [43] investigated the effect of surface acidity on the methanol dehydration to dimethyl ether and prepared several catalysts such as H-ZSM-5 and steam de-aluminated H-Y zeolite (SDY), γ-Al_2O_3 and $Ti(SO_4)_2/\gamma$-Al_2O_3. Methanol dehydration reactions were carried out in a fix bed reactor operating in a temperature range of 400 K – 600 K with gas hourly space velocity of 3400 ml/gcat.h. Catalytic activities can be ordered as H-ZSM-5 > SDY > $Ti(SO_4)_2/\gamma$-Al_2O_3 > γ-Al_2O_3 and highest activity was obtained with H-ZSM-5 at 423 K. However, significant formation of coke was observed and this could hinder the use of these catalysts in the direct synthesis of DME from synthesis gas. On the other hand, titania modified alumina ($Ti(SO_4)_2/\gamma$-Al_2O_3) had comparable acid sites with the H-ZMS-5 and carbon deposition was absent for this catalyst. Therefore, this catalyst could be used in the direct synthesis of DME from synthesis gas as methanol dehydration component.

Vishwanathan et al. [44] studied the dehydration of crude methanol to dimethyl ether over sodium modified H-ZSM-5 catalysts. They altered the sodium content by impregnation and conducted the activity test at 230 °C- 340 °C with a feed rate of 25 ml/min. From the activity results, it was seen that dimethyl ether selectivity increased with a decrease in the surface acidity and decrease in the surface acidity was achieved with increase in the sodium content. By changing the sodium content, hydrocarbon formations as side products were prevented. This study was also important in term of the purity of the feed since crude methanol was transformed to DME instead of pure methanol, which is more expensive.

Methanol dehydration on aluminum impregnated SBA-15 was studied by Tokay et al. [45]. They synthesized alumina impregnated one-pot hydrothermal synthesis of SBA-15. Activity tests were conducted in a temperature range of 120 °C - 450 °C at atmospheric pressure. According to the results, aluminum impregnation decreased the pore volume and surface area of synthesized SBA-15. The reaction results show that aluminum impregnated SBA-15 was highly active in methanol dehydration and gave almost equilibrium conversions with DME selectivity values approaching 100% at temperatures over 300 °C.

A comprehensive study was made by Xu et al. [46] in synthesis of DME from methanol. They prepared several solid acid catalysts such as γ-Al_2O_3, H-ZSM5, amorphous silica-alumina and titania modified alumina and zirconia. They conducted the activity studies in a plug flow reactor operating at a range of temperatures around 280 °C and reported that all catalysts were active and selective in DME formation. γ-Al_2O_3 catalyst exhibited 90% methanol conversion at 250 °C. However, effect of presence of water in the product stream was examined by changing the water partial pressure and methanol conversion decreased from 17.5% to 5.8% at 188 °C. Based on this finding, direct synthesis of DME from synthesis gas was proposed to enhance the catalytic activity since typical methanol synthesis catalyst $Cu/ZnO/Al_2O_3$ accelerates the water gas shift reaction. Hence, excess water could be eliminated and catalytic activity could be enhanced. Zirconia addition to titania increased the catalytic activity. Nevertheless, these catalysts suffered from the low acidity and low conversion values were reported.

Çiftçi et al. [47] prepared mesoporous nafion-silica nanocomposites by one pot acidic hydrothermal synthesis procedure and obtained well dispersion of nafion on the support of silica with very high BET surface areas (600 m^2/g - 800 m^2/g).

Activity of the nanocomposites was tested in dimethyl ether synthesis from methanol dehydration in a temperature range of 120 °C – 300 °C. Activity results revelaed that almost 100% DME selectivity was obtained with very high yields and optimal nafion to silica ratio was found to be 0.15. At higher ratios, brönsted acidity decreased together with catalytic activity. Another type of the methanol dehydration catalysts was also made by Çiftçi et al. [48]. They synthesized nanocomposite catalysts by the hydrothermal synthesis and silicotungstic acid was incorporated before hydrothermal syntheses. They altered the W/Si ratio and conducted methanol dehydration studies to obtain DME. Low temperature activities at 200 °C – 250 °C with very high DME selectivities were obtained with the catalyst having the W/Si ratio 0.40 and this catalyst was called as TRC-75(L). This catalyst was used also in this study as methanol dehydration component of direct synthesis.

CHAPTER 4

THERMODYNAMIC ANALYSIS

Thermodynamic analysis of the reactions involved in DME synthesis is very important to determine the operating parameters of the experiments. For DME synthesis, high pressures (30 bar and above) and moderate temperatures (200 °C - 300 °C) are needed to achieve high conversion values. In this section, thermodynamic analyses of the reactions 1, 2, and 3 are made considering equimolar feed composition of carbon monoxide and hydrogen.

$3CO + 3H_2 \rightarrow CH_3OCH_3 + CO_2$ [1]

$2CO + 4H_2 \rightarrow CH_3OCH_3 + H_2O$ [2]

$CO + 2H_2 \rightarrow CH_3OH$ [3]

For the methanol synthesis reaction (reaction-3), thermodynamic analysis can be applied as follows:

For the thermodynamic analysis of this reaction, firstly, constant pressure heat capacity values were taken from literature as a function of temperature [49]. Heat capacity of any species can be represented by Equation 4.1.

$$C_{p,i} = a + b \times T + c \times T^2 + d \times T^3 \quad Cp[=]\,J/(mol \times K)\ \text{and}\ T[=]K \qquad 4.1.$$

Heat capacity coefficients of species involved in DME synthesis are given in Table 2.

Table 2. The molar heat capacity coefficients of species involved in DME synthesis [49]

Species	**a**	**b × 10^2**	**c × 10^5**	**d × 10^9**
H_2	29.088	-0.192	0.400	-0.870
CO	28.142	0.167	0.537	-2.221
CO_2	22.243	5.977	-3.499	7.464
H_2O	32.218	0.192	1.055	-3.593
CH_3OH	19.038	9.146	-1.218	-8.034
CH_3OCH_3	17.02	17.91	-5.234	-1.918

To calculate the heat of reaction at a particular temperature, the constants in the heat capacity equation can be summed after multiplied with the stoichiometric coefficients. Resulting constant pressure heat capacity expression for the Reaction-3 can be given with Equation 4.2.

$$\mathrm{Cp} = \Delta a + \Delta b \times T + \Delta c \times T^2 + \Delta d \times T^3 \qquad 4.2.$$

To determine the reaction enthalpy and equilibrium constants, standard enthalpies and Gibbs free energies of formation at reference temperature 25 °C are found and given with Table 3.

Table 3. Standard enthalpies and gibbs energies of formation at 298.15 K for one mole of each substance from its elements in gas phase [49]

Species	**$\Delta H°_f$, kJ/mol**	**$\Delta G°_f$, kJ/mol**
H_2	0	0
CO	-110.5	-137.2
CO_2	-393.5	-394.4
H_2O	-241.8	-228.6
CH_3OH	-200.7	-162.0
CH_3OCH_3	-184.2	-113.0

Then, heat of reaction as a function of temperature can be calculated as in equation 4.3.

$$\Delta H_{rxn}\ \Delta H° + \int(\Delta a + \Delta bT + \Delta cT^2 + \Delta dT^3)dT \qquad 4.3.$$

Equilibrium constant is calculated by integrating the Van't Hoff relation over the studied range of temperature. Van't Hoff relation is given in the differential form as

$$d(\ln K) = \frac{\Delta H_{rxn}}{RT^2}\, dT \qquad 4.4.$$

To integrate the Van't Hoff relation, equilibrium constant must be given for integration and equilibrium constant at reference temperature can be calculated as

$$K_{298} = \exp(-\Delta G°/RT) \qquad 4.5.$$

After integrating equation 4.4, Equation 4.6 is obtained.

$$K(T) = K(298\ K) \times \exp\left(\int_{298}^{T} \frac{\Delta H_{rxn}}{RT^2}\, dT\right) \qquad 4.6.$$

In equilibrium conversion calculations, the limiting reactant for equimolar mixture is carbon monoxide. For this reason, hydrogen conversion results are given.

Since DME synthesis is a high pressure process, it is necessary to consider the non-idealities. For this reason, Peng-Robinson equation of state was used. Fugacity coefficient of each species at different conditions and K_{ϕ} values were evaluated and given in Appendix-A.

$$K = K_{\phi} \times K_P \qquad 4.7.$$

$$K_{\phi} = \frac{\phi_{CH3OH}}{\phi_{CO} * (\phi_{H2})^2} \qquad 4.8.$$

$$K_P = \frac{P_{CH3OH}}{P_{CO} * (P_{H2})^2} = \frac{y_{CH3OH}}{y_{CO} * (y_{H2})^2} \times \frac{1}{P^2} \qquad 4.9.$$

For the 100 mole/hour basis, the inlet flow rates and equilibrium composition calculations were tabulated as in Table 4.

Table 4. The inlet flow rates and equilibrium composition calculations for Reaction-3 ($CO + 2H_2 \rightarrow CH_3OH$)

Species	Initial Flow Rate	Equilibrium Value	Molar Composition
CO	50	$50(1\text{-}X_{eq})$	$50(1\text{-}X_{eq})$ / $100\text{-}100\ X_{eq}$
H_2	50	$50(1\text{-}2\ X_{eq})$	$50(1\text{-}2\ X_{eq})$ / $100\text{-}100\ X_{eq}$
CH_3OH	-	$50\ X_{eq}$	$50\ X_{eq}$ / $100\text{-}100\ X_{eq}$
Total	100	$100\text{-}100\ X_{eq}$	1

For the equimolar mixture of carbon monoxide and hydrogen, equilibrium conversions with respect to temperature and pressure are given in Figure 2.

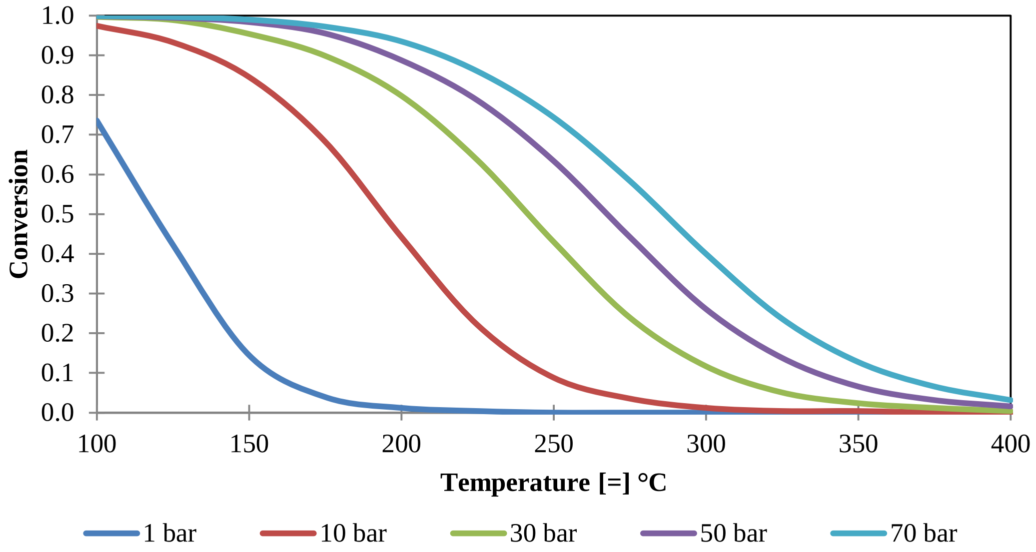

Figure 2. The equilibrium conversion curves for reaction-3 ($CO + 2H_2 \rightarrow CH_3OH$) with respect to temperature and pressure for a feed ratio of H_2:CO=1:1

As temperature increases, equilibrium conversion decreases since methanol synthesis is an exothermic reaction. At atmospheric pressure, there is no conversion at temperatures in which methanol synthesis catalyst is active and increase in the pressure favors conversion. For these reasons, methanol synthesis should be carried out at high pressures. Similar analyses can be applied to other reactions and equilibrium conversions are given in Figures 3 and 4.

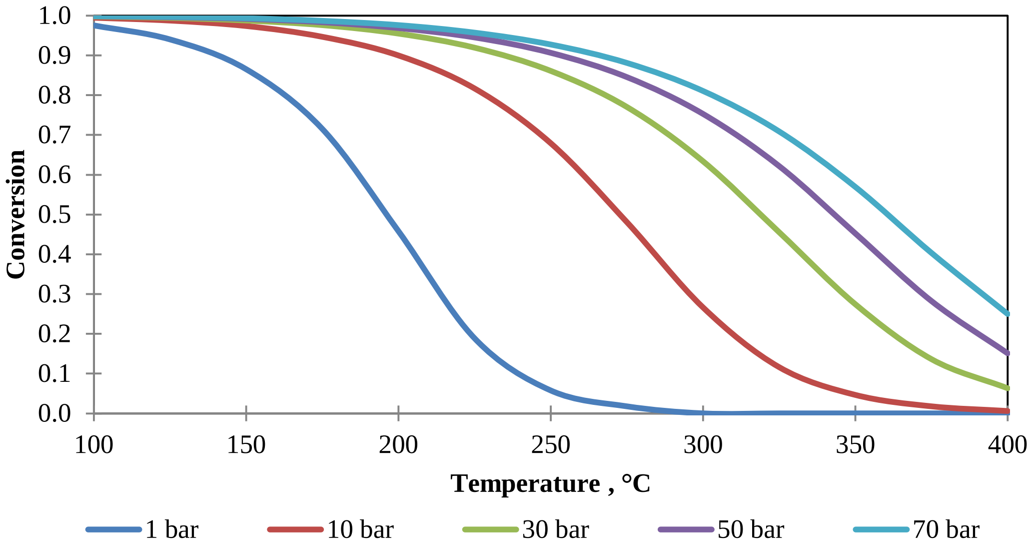

Figure 3. The equilibrium conversion curves for reaction-1 ($3CO + 3H_2 \rightarrow CH_3OCH_3 + CO_2$) with respect to temperature and pressure for a feed ratio of H_2:CO=1:1

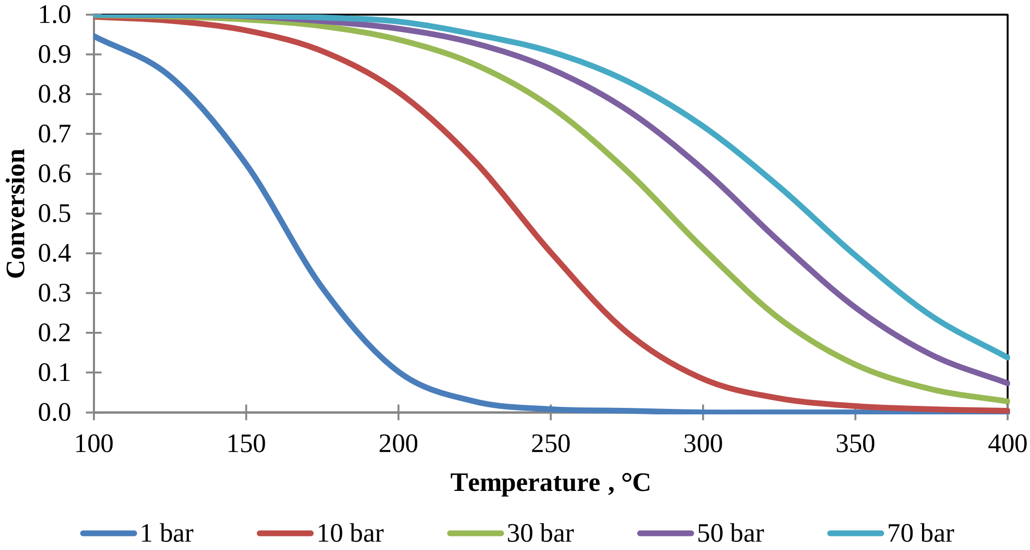

Figure 4. The equilibrium conversion curves for Reaction-2 ($2CO + 4H_2 \rightarrow CH_3OCH_3 + H_2O$) with respect to temperature and pressure for a feed ratio of H_2:CO=1:1

For all the reactions, it could be seen that reactions are highly pressure dependent. Among the methanol synthesis reaction, reaction-3, and direct synthesis of dimethyl ether reactions, reactions 1&2, equilibrium conversion of methanol synthesis is the lowest whereas reaction-1 has the highest conversion at 50 bars. This could be seen in Figure 5.

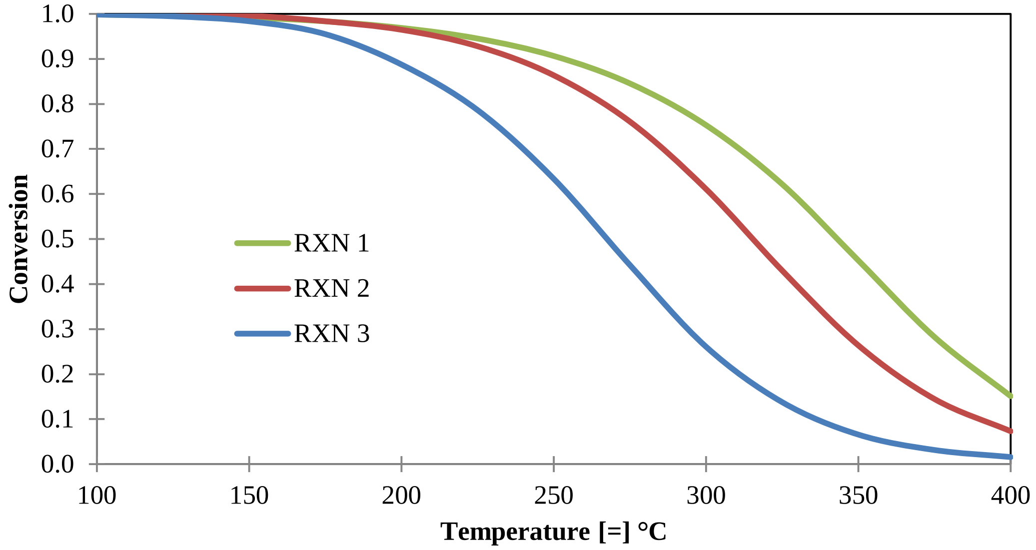

Figure 5. The equilibrium conversion curves for Reaction-1, 2, and 3 at 50 bars with respect to temperature for a feed ratio of H_2:CO=1:1

Thermodynamic analysis of DME synthesis indicated that high pressures are necessary for high conversion per pass. After the pressure of 50 bars, further increase in pressure did not have significant effect on conversion. In addition, working at high pressure increases the compressor cost and high pressures are risky to operate. When all these factors are considered, 50 bars was chosen as the operating pressure of the direct synthesis of dimethyl ether system. Thermodynamic analysis also gives information about the temperature range in which the experiments must be conducted. Since the methanol and dimethyl ether synthesis are exothermic reactions, at high temperatures conversion drops significantly. At 300 °C and 50 bar, methanol synthesis reaction gives an equilibrium conversion 26.1%. For this reason, choice of 300 °C as the highest temperature seems appropriate.

Based on the thermodynamic analysis, it is proven that direct synthesis reactions give more conversion than the methanol synthesis reaction. This could be considered as the thermodynamic advantage since conversion increases at the same operating parameters.

CHAPTER 5

CATALYTIC MATERIALS

For the direct synthesis of dimethyl ether synthesis from the syngas, several catalysts have been prepared including co-precipitated catalysts, ordered mesoporous materials and impregnation catalysts. In this part, firstly catalyst preparation methods including precipitation, impregnation and ordered molecular materials are given in detail. Then, catalyst treatment steps such as hydrothermal synthesis, calcination, drying and washing are mentioned. Finally, characterization methods applied in this study are explained in detail.

5.1. CATALYST PREPARATION METHODS

5.1.1. Precipitation and co-precipitation

Precipitation refers to the obtaining a solid from a liquid solution. Typically, two or more solutions and suspensions of materials which could cause precipitation of an amorphous or crystalline precipitate or gel are mixed as a first step of precipitation. In the preparation, precipitating solid is obtained due to the super saturation. By either reducing the solubility or initiating a chemical reaction, solid formation is induced [50, 51].

The demands for precipitated catalysts are very high since product separation after precipitation is necessary and large volumes of metal salts solutions are used in precipitation process. The main advantages of the precipitated catalysts are obtaining very pure materials and flexibility of the process with respect to the final product quality. Precipitation is preferred method of the catalyst preparation for the high amount of the loading starting from 10% - 20% [52].

In the precipitated catalysts, catalyst with more than one component can be prepared and called as co-precipitation. According to the International Union of Pure and Applied Chemistry (IUPAC) nomenclature, precipitation refers to the simultaneous precipitation of a soluble component with a macro component from the same solution by mechanical entrapment, adsorption or occlusion. On the other hand, co-precipitation in catalysis area is used for simultaneous precipitation of more than one component [53]. Precipitation scheme of a precipitated catalyst can be given in Figure 6.

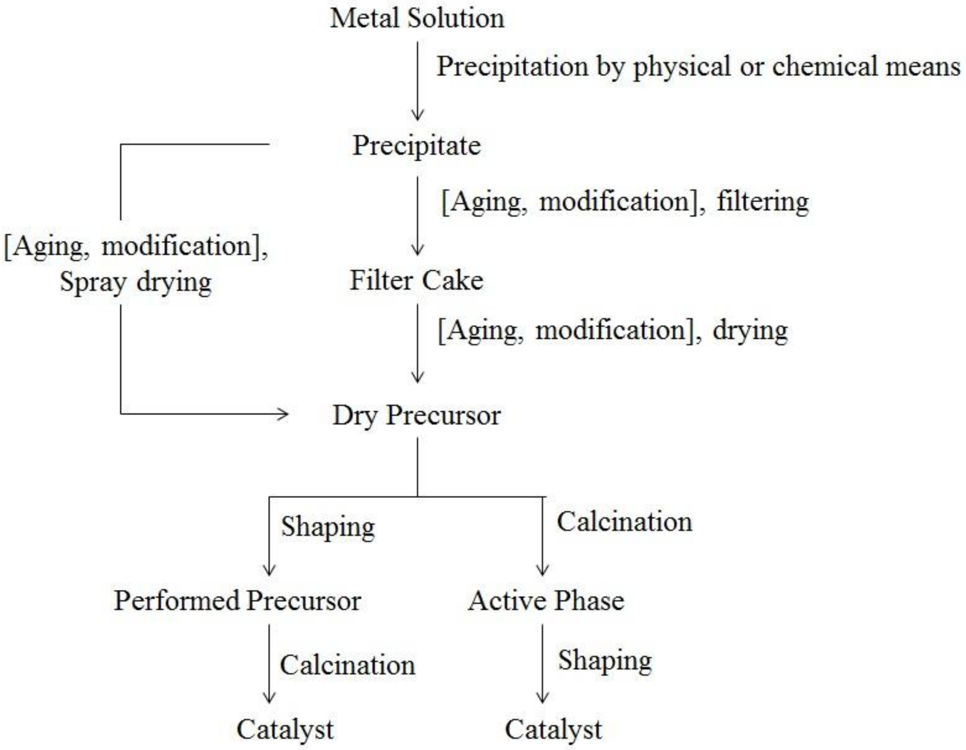

Figure 6. Preparation scheme for precipitated catalysts.
Optional steps are indicated by square buckets [53]

When physical chemistry considerations are taken into account, a nucleus has to form. This is the first step of formation of a solid from solution. From free energy of agglomerates of the constitutes of solutions, formation of the particles are governed. Total free energy change due to agglomeration is determined by equation 5.1.

$$\Delta G = \Delta G_{bulk} + \Delta G_{interface} + \Delta G_{others} \qquad 5.1.$$

where ΔG_{bulk} refers to the difference of the free energy between solution species and solid species

$\Delta G_{interface}$ refers to the free energy change related to the formation of the interface

ΔG_{others} refers to the all other contributions such as strains and impurities [53].

Bulk energy change is always negative. However, energy is needed to create an interface, indicating that energy change is positive for the interface. Bulk energy change is proportional to the volume of the particles whereas interface energy change is proportional to the surface area. Therefore, there is a critical size of the agglomerate from which bulk energy change dominates the total energy change and interface energy change decreases upon the agglomeration of the particle. This critical size is called as the size of nucleus. Nucleus formation occurs when precursor concentration exceeds a critical threshold concentration. The nucleus is defined as “smallest solid-phase aggregate of atoms, molecules or ions which is formed during a precipitation and which is capable of spontaneous growth”. As long as concentration of precursor is above the nucleation threshold, formation of new particle is possible. When the precursor concentration decreases, then particle growth of the formed particles becomes dominant [53].

For the success in the preparation methods, super saturation is necessary. To achieve super saturation, physical and chemical treatments can be made. Some physical treatments are changing the temperature of the reaction mixture and evaporating the solvent. Chemical treatments are changing of the precipitating agent which changes pH [52]. For co-precipitated catalysts, knowledge of relative solubilities of precipitates is important since it could result in sequential precipitation.

Raw material can influence the final product characteristics. Choice of raw material should be made as to having counter ions in decomposition to volatile products. By changing the raw materials, morphologies, phases and sizes could change [53, 54]. By changing concentration and composition of the solutions, final product characteristics could be altered. Usually, high concentrations are advantageous for precipitation. High concentrations are also advantageous for fast production in plants since high concentrations increase the space time by decreasing the vessel volume for the same amount of precipitate. In precipitated catalysts high amount of solvents are used and solvent type influences the product characteristics. Most of the time, water has been used extensively since it is abundant and economically feasible. Organic solvents could enhance the material properties and can give superior product qualities. Nevertheless, use of them is limited due to the environmental regulations and price difference with the conventional solvent water [53].

Temperature in which precipitation is conducted is one of the most important parameter influencing the properties of the final product. Since nucleation rates are highly temperature dependent, temperature plays a key role in tuning the crystallite sizes, surface areas and formed phases. Although suitable precipitation temperature should be determined experimentally, precipitation is usually conducted at high temperatures around 100 °C which is beneficial to obtain super saturation. Aging time has great influences on the catalyst properties. Aging time can be defined as the time in which precipitate is left under the mother liquor solution at either precipitation conditions or different conditions. While aging is taking place, precipitated catalyst undergoes size increment by Ostwald ripening and recrystallization which could directly affect the catalytic performance [53]. Although pH effect on the catalyst performance and catalytic activity is not well studied, pH directly affects the degree of the super saturation. Likewise temperature, optimal pH should be determined experimentally [53]. In the precipitation, pH can be either kept constant at a desired value or variable pH to desired end point [54].

5.1.2. Impregnation

One of the widely used catalytic materials preparation method is the impregnation of an active component with its solution to the catalysts or porous support. In the absence of specific interactions between support and components of impregnation, the impregnation process steps are quite simple. In impregnation, a solution of active component is slowly added to the suspension of catalysts or support with porous structure. Adsorption depends on the concentration of the active component solution and penetration of it into the support. After adsorption is completed, excess water in the structure of the support should be removed so as to keep the active component within the pores of the support. This step is important since water presence could result in the migration of the metal salts to the exterior surface. Calcination should be conducted to convert the metal salts to the metal oxides [50].

Uniformity is an important phenomenon in impregnated catalysts since the degree of it depends on the adsorptive properties of the carrier and the solvent. If alcoholic solutions are used as solvents, then different concentration distributions are obtained than the aqueous solution. When the multicomponent impregnation is desired, uneven distribution of the components could arise because of the chromatographic effect. Depending on the adsorption capability, impregnation could be conducted in different places. If the adsorption capability of the component is high, then the adsorption occurs on the surface. If the adsorption capability of the component is low, then penetration of the active components through the pores of the support occurs. This could be prevented by keeping the impregnated catalysts in a moist state for some time to enable the equilibrium [50].

Unless interactions between active components and support are strong, drying of the impregnated supports leads to uneven distribution of the active components. Moreover, crystallization occurs if saturation limit of the active component solution is exceeded. For these reasons, water evaporation and drying must be done spontaneously. If the evaporation rate is slow, soluble active materials migrate to the smaller pores in which water evaporation rate is slow. Such a catalyst allows hardly to the access of reactants to active components within the catalyst.

Impregnated catalysts are highly advantageous. Main advantage of impregnated catalysts is their pore structure and surface area. Since supports at several desired ranges of surface areas are commercially available, desired properties could be obtained easily. Impregnated catalysts contain fewer amounts of active components when compared to the precipitated catalysts and this can be considered as an economical advantage. On the other hand, disadvantage of the impregnation comes from the limited amount of material that can be incorporated into the support [50].

Impregnation can be achieved by different methods. In this study, two methods have been used together.

Impregnation with an excess of solution: In this method, catalyst is exposed to the excess solution and impregnation is slow and can take several hours to days. Excess liquid is evaporated quickly. By this method, surface is restructured extensively and distribution of the species can be controlled and very high dispersion values could be obtained. This method could be considered as the best method among the others [51]

Co-impregnation: In a single step, incorporation of two or several active components is done. In this method, it is difficult to obtain a high dispersion and segregation can easily occur [51].

5.1.3. Ordered mesoporous materials

Ordered porous materials can be classified with respect to their pore size. According to the IUPAC definition, porous solids are divided into three categories.

Microporous materials: Their pore size is smaller than 2 nm. Zeolites are the well-known examples of microporous solids. Microporous materials have crystalline network structure and as a result they offer extremely narrow pore size distribution which is the key factor in guest-host chemistry and shape selective catalysis. However, they suffer from the small pore openings due to mass transfer limitations.

Mesoporous materials: Their pore size is in between 2 -50 nm. Having a broad pore size distribution allows the use of mesoporous materials in the place of zeolites since mesoporous materials break the pore size constraints of microporous materials. Famous examples of mesoporous materials are M41S family and aluminosilicate molecular sieves

Macroporous materials: Their pore size is greater than the 50 nm. Alumina membranes and porous glasses are the examples of macroporous materials [55].

Porous materials offer the advantage of tunable properties, high chemical, thermal, and mechanical stabilities with high surface area and large pore volumes. Pore size distribution flexibility is very important for size specific applications in which host-guest interactions are quite strong. Ordered mesoporous materials were obtained by the Mobil Corporation Scientists and MCM-41(Mobil Composition of Matter No.41) exhibits a highly ordered hexagonal array of unidimensional cylindrical pores with a narrow pore size distribution. These materials have long range order with a surface area of above 1000 m^2/g. These properties make them attractive catalyst supports. The walls of MCM-41 are amorphous. There are also other types of mesoporous materials such as MCM-48 which is in the cubic form and MCM-50 which is in the lamellar structure [56].

Specific formation of pores with a predetermined size distribution is enabled by liquid crystals forming template, which is the characteristic approach of MCM type materials. Liquid crystal templating mechanism was proposed by Kresge et al. [57] and two possible synthesis routes were proposed for the formation of the MCM-41 as shown in Figure 7.

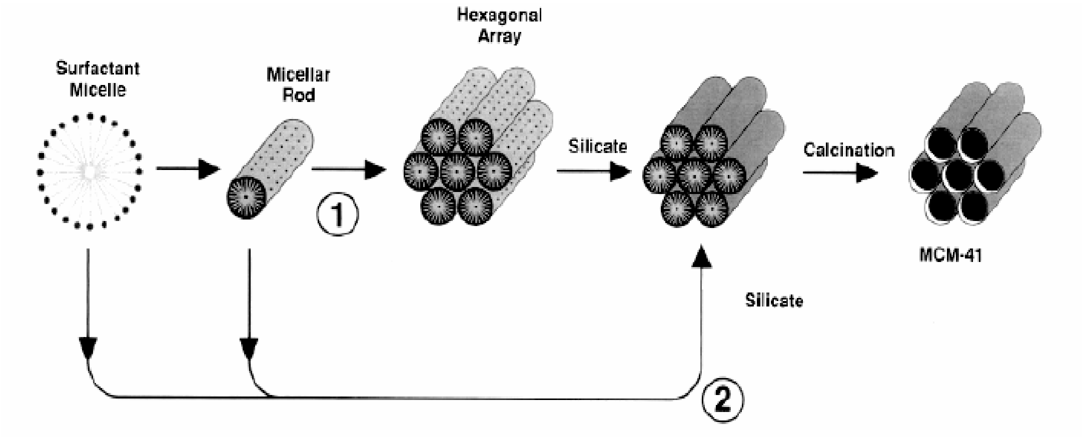

Figure 7. Liquid crystal templating (LCT) mechanism representing two possible formation routes of MCM-41 [57]

In the first route, aggregation of surfactant molecules as surfactant micelles are known to exist in a hexagonal arrangement within the solution and silicate present in the synthesis solution penetrate to the surfactant structure and form an inorganic structure. For MCM-41 synthesis to undergo from pathway-1, concentration of the surfactant molecules should be as low as critical micelle concentration (CMC). In pathway 2, silicate influences the formation of liquid crystal phase. No matter which pathway is followed, hexagonally shaped silicate surrounded MCM material is obtained upon calcination [57].

Although M41S family materials have the excellent catalytic properties such as narrow pore size distributions, high surface area, high mechanical and thermal strength, they are inert for most of the reactions and their acidity is quite low [57]. To improve the catalytic performance of such mesoporous materials, metals, metal oxides or acidic sites were incorporated into their structure and they have showed very good catalytic performances [48, 58-61].

Thermal stability of M41S type materials is reported as low due to their low pore wall thickness (1-2 nm) and limited pore diameter (80 Å). Because of these limitations of M41S family, Zhao et al. [62] developed SBA-15 type catalysts. SBA-15 can be synthesized at low temperatures in between 35 °C - 80 °C with uniform pore sizes and pore wall thicknesses by using triblock copolymers as structure directing agents. PEO-PPO-PEO is used as triblock copolymer due to its mesostructural ordering properties, amphilic character, low cost, commercial availability and biodegradability. It is reported that the synthesized SBA-15 has a wall thickness larger than MCM-41 which makes SBA-15 hydrothermally more stable. Zhao et al. also stated that the pore size and wall thickness of SBA-15 material can be adjusted by changing the heating temperature between 35 °C and 140 °C and by changing the aging time between 11 to 72 hours. Moreover, the effect of boiling water on SBA-15 and MCM-41 is found out that MCM-41 became amorphous after 6 hours whereas SBA-15 retained stable after 24 hours. SBA-15 could only be synthesized at strongly acidic conditions, pH<1. Higher pH values results deformation of the material. Aktas et al. [63] investigated the importance of pH for SBA-15 synthesis. SBA-15 and SBA-15 like materials are synthesized at acidic conditions, pH<1 and pH>1, respectively. It is found that deformation of the material increases and pore diameters decrease as the pH increases.

5.2. CATALYST TREATMENTS

5.2.1. Hydrothermal transformations

In the synthesis of ordered mesoporous materials and most of the zeolites, hydrothermal synthesis has been used. Hydrothermal transformation is usually carried out at low to moderate temperatures in the range of 100 °C – 300 °C in the autoclaves. Mother liquor which is usually water was subjected to several structural and textural transformations in the hydrothermal synthesis step. These transformations can be given as

- Small crystals and amorphous particles grow to large crystals and amorphous particles
- Amorphous particles are crystallized
- Crystalline structures change to other crystalline structures
- Pores of the gels shrink

These transformations tend to reach to the thermodynamic equilibrium, so there is a decrease of the free energy of the system in the hydrothermal synthesis [52].

In the hydrothermal synthesis, several parameters such as the temperature, pressure, pH, and concentration influence the final product properties as well as the hydrothermal synthesis duration. It is possible to tune the catalyst properties by changing these parameters. Resultant mixture from the hydrothermal synthesis must be followed by filtration, washing, drying, and calcination [52].

5.2.2. Washing

Washing is used to remove the undesired and useless ions from the suspension of product containing solution. In ordered mesoporous material, washing can remove the surfactant to an extent. For some applications, hot washing water could increase the efficiency of the washing by increasing the exchange rate of ions [52].

5.2.3. Drying

The main function of drying is the removal of solvent, which is usually water, from the pores of the catalyst. Removal of solvent must be controlled since it can result in the collapse of mesostructure, decrease the porosity, and loss of pore volume. Therefore, drying affects the quality of the final product to a large extent. Collapse of the structure could happen due to the internal pressure of water which remains in the small pores of the catalyst after the water in the larger pores is removed. This situation can be prevented by carrying out drying at low temperatures and in vacuum. By this way, large capillary stresses can be prevented [52].

5.2.4. Calcination

Calcination is a heat treatment of the catalysts under the flow of fluid. Several fluids can be used such as dry air, nitrogen, helium or mixture of these. The processes occurring in the calcination can be described as follows, [50,52]

- Chemically bonded water is removed.
- Small crystals and particles grow to large crystals and particles
- Structural modification, phase change, and generation of active phase occur
- Mechanical properties are stabilized.
- Thermally unstable compounds such as carbonates, nitrates, hydroxides, and organic salts are converted to oxides.

5.3. CHARACTERIZATION METHODS

5.3.1. X-Ray Diffraction (XRD)

X-ray diffraction is one of the oldest, basic techniques for the characterization of materials. Crystalline phases can be identified and particle sizes can be obtained by the XRD. Atoms scatter the X-rays and direction of them is given by the Bragg's law. Bragg's law is given in the equation 5.2 [64].

$$n\lambda = 2d\sin\theta \quad n = 1,2,3,\ldots \tag{5.2.}$$

where λ is the wavelength of the X-rays

d is the distance between two lattice planes

θ is the angle between the incoming X-rays

Calculated lattice spacings are characteristics for the particular compound and used in the identifying the particle. By this characterization technique, mesoporous two-dimensional hexagonal structure is also well demonstrated and it provides information about the pore structure of the mesoporous materials. In a typical XRD pattern of a mesoporous material, a major diffraction peak (100) and two to five reflection peaks, i.e. (110), (200) and (210) are observed before 2θ value of 10^{o} which are caused by well-ordered two-dimensional hexagonal structure [65]. For pure siliceous mesoporous materials, at higher degrees of 2θ values, no peaks are observed, because the walls are composed of amorphous silica, the ordering lies in the pore structure [55]. On the other hand, for the active site incorporated mesoporous materials, at high angles, peaks of incorporated crystalline metal structures are observed. This is also the case for the co-precipitated catalysts in which mesoporous structure is absent. For this reason, only high angle X-ray diffraction was applied for co-precipitated catalysts whereas high and low angle diffraction was applied for the ordered mesoporous materials.

5.3.2. Nitrogen Physisorption

One of the primary methods for characterization of porous materials is physisorption. Mainly, physisorption analysis is performed by cooling the material to a temperature near the normal liquefaction point (77 K for nitrogen) and measuring the amount of nitrogen is measured with changing nitrogen pressure. An isotherm is obtained by this procedure and the pore structure information including pore sizes, surface area, and pore size distribution are obtained. Different models have been developed to calculate the pore size distribution such as BET (Bruanauer, Emmett, Teller) and BJH (Barrett, Joyner, Halenda) [66].

5.3.3. Scanning Electron Microscopy (SEM)

Scanning electron microscopy is a characterization technique used to obtain information on morphology, crystallography, and chemical composition. Information is obtained from electron beams which transmit the sample [64].

For the inspection of the surface morphology of the catalytic materials, scanning electron microscopy is wildly used. It is analogous to scanning transmission electron microscopy. This method involves detection of black-scattered and secondary electrons as well as X-rays that are black-scattered from the sample. This technique can be used on thick samples [55].

5.3.4. Energy Dispersive Spectroscopy (EDS)

An approximate composition of the bulk is obtained by energy dispersive spectroscopy which is mounted to the SEM apparatus. It is based on collecting and energy dispersion of characteristic X-rays. Relative amount of each element in the catalyst is obtained by the resulting X-ray spectrum [55].

5.3.5. Diffuse Reflectance Infrared Fourier Transform Spectroscopy (DRIFTS FTIR)

Acid sites of the catalysts can be determined by DRIFTS of pyridine adsorption. Brönsted and lewis acid sites of the synthesized catalysts can be identified in this technique. When light hits to the surface of a material, it is partially reflected and transmitted. Moreover, light which has passed the material is absorbed and reflected again. The sum of these radiations is the diffuse reflectance of the sample [67].

CHAPTER 6

EXPERIMENTAL

In the present study, several catalysts were prepared for methanol synthesis, methanol dehydration and direct synthesis of dimethyl ether from synthesis gas. Several catalyst preparation methods, including co-precipitation, one-pot direct synthesis and impregnation have been used. Moreover, bi-functional catalyst beds were prepared by dry physical mixing. In this chapter, catalyst preparation methods are explained in detail. Characterization results which have been applied for the synthesized catalysts are also presented. Finally, high pressure reactive flow system, which was constructed to carry out methanol synthesis, methanol dehydration, and direct synthesis of DME is described in detail.

6.1. CATALYST SYNTHESIS

6.1.1. Synthesis of Co-Precipitated Catalysts

Co-precipitated catalysts were prepared by modifying the procedure of co-precipitation method reported by Saito et al. [26]. For the synthesis of the co-precipitated catalysts, following chemical reagents were used.

Source of Metals :Copper nitrate trihydrate, $Cu(NO_3)_2.3H_2O$, Merck
Zinc nitrate tetrahydrate, $Zn(NO_3)_2.4H_2O$, Merck
Cerium(III) nitrate hexahydrate, $Ce(NO_3)_3.6H_2O$, Merck
Zirconyl nitrate monohydrate, $ZrO(NO_3)_2.H_2O$, Aldrich

Aluminium nitrate nonahydrate, $Al(NO_3).9H_2O$, Merck

Source of Medium :Deionized water (Millipore Ultra-Pure Water System, Milli-QPlus)

Source of precipitant: Sodium carbonate, Na_2CO_3, Merck

Synthesis of co-precipitated catalyst consists of five important steps: preparation of synthesis solution, aging, washing, drying, and calcination.

In the synthesis 600 ml of deionized water was heated to the 70 ºC while mixing with a magnetic stirrer. 1 M metal solution was prepared by dissolving the required amounts of metal salts in water and 1.1 M precipitant solution was prepared by dissolving the required amounts of sodium carbonate in water.

Precipitation of 1 M metal solutions was made with the 100 ml solution. Such a solution requires the addition of 0.1 mole metals to the solution and metal ratio was chosen as Cu:Zn:Al =6:3:1 in mole basis.

Metal and precipitant solutions were fed to burettes and simultaneous and dropwise additions of the solutions were started. While simultaneous addition was taking place, pH of the main solution was measured. pH of the solution changes by the addition of solutions. Metal solution decreased the pH whereas carbonate solution was increasing it. Choice of the pH is very important since it directly affects the precipitation quality and it was determined to be kept constant at 7. For this reason, flow rate of the metal salts and carbonate solutions were kept controlled and pH was kept constant at 7.0-7.2 successfully. Time in which solutions were added to the mixture was recorded and it took about 30 minutes for 100 ml of metal solution. After metal and carbonate solutions were added, aging was started at 70ºC while mixing the main solution. When aging was completed at different durations, main solution was allowed to cool to room temperature.

Washing of the co-precipitated catalyst was done via the filtered washer with a membrane filter having the porosity-4. During the washing step, solution was fed to the washer and resultant precipitant was accumulated on the filter. After 2 liters of deionized water was passed through the accumulated solid, it was taken to the beaker and mixed with 500 ml of deionized water, for 30 minutes. After mixing, the solution was again fed to the washer and solid accumulation was observed while all water was filtered. Then, 3 liters of deionized water was passed again over the sample.

After the washing, drying was necessary and it was done in the oven at 120 °C. The material was taken from the filter and placed in oven, which was at 120 °C. Drying period was 24 hr.

For the calcination of the dried samples, catalyst was placed in a quartz tubular reactor with a membrane filter of porosity-2. The main purpose of the membrane filter was to prevent the removal of solid particles via air flow. The reactor was placed into the middle of the tubular furnace and air was passed through the sample at a rate of 1 dm^3/min and at a pressure of 4 bar. Furnace was heated from the ambient temperature to the final calcination temperature of 350 ºC at a rate of 1 ºC/min and kept at 350 ºC for 6 hr. The exit of the reactor was connected to the ventilation system so that exhaust gas is sent to vent. After 6 hours was completed, material was allowed to cool and air flow was continued until the furnace temperature was decreased to nearly 80 ºC.

Several catalysts were prepared by the co-precipitation method. Experimental procedure is depicted in Figure 8**.** Effect of promoter, promoter type, aging time, washing water temperature, calcination temperature, and reduction temperature were investigated by preparing different catalysts.

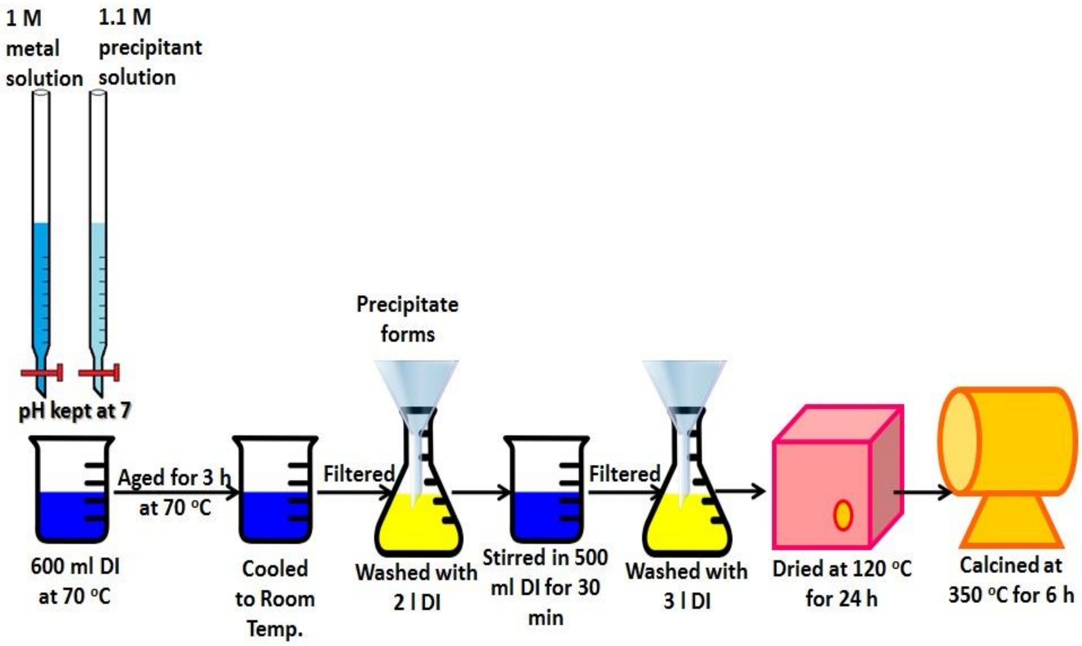

Figure 8. Experimental procedure for the co-precipitated catalysts

Reduction of synthesized materials was performed with pure hydrogen flow at a flow rate of 1 dm^3/min at two different temperatures; 225 °C and 250 °C. Reduction period was five hours. The reactor was placed into the middle of the tubular furnace and inert gas composed of He (30%) /N_2 (70%) was passed through the sample and heating at a temperature ramp of 1 °C/min until the desired temperature and flow gas was switched to the hydrogen. After five hours, flowing hydrogen gas was switched to inert gases and reactor was allowed to cool.

To investigate the effect of promoter, catalyst with only Cu-Zn was prepared. Promoter types were investigated by the addition of aluminum, zirconium and ceria to the Cu-Zn containing metal solutions. For the aging time, Cu-Zn-Al catalysts were aged for 1 hour, 3 hours and 6 hours. In the washing step, Cu-Zn-Al catalysts washed with hot deionized water, which is nearly at 95 °C, instead of cold deionized water, which is at room temperature. Effect of calcination was studied by conducting the calcination at 550 ºC instead of 350 ºC and reduction of the catalyst was done with the pure H_2 flow at two different temperatures; 225 ºC and 250 ºC.

The co-precipitated catalysts described above are for the methanol synthesis from the synthetic gas. Based on the above experimental procedure, a bi-functional co-precipitated catalyst for the direct synthesis of DME was also made. Experimental procedure is summarized in Figure 9. In the synthesis, γ-Al_2O_3 commercial methanol dehydration catalyst obtained from TOYO was used. Characterization results of Toyo catalyst are given in Section 7.3. It was crushed and dried in oven at 120 °C for two hours. 12.6 gr dried material was added into 600 ml of deionized water, which was at room temperature. Suspension containing the pulverized Toyo catalysts was mixed with magnetic stirrer at room temperature for 24 hours and its temperature was increased to 70 ºC at the end of 24 hours. 1 molar and 100 ml metal solution composed of copper, zinc and aluminum salts with a molar ratio of Cu:Zn:Al=6:3:1 and 1.1 molar precipitant solutions were fed to burettes and simultaneous and dropwise additions of the solutions were started. The rest of the preparation method was the same.

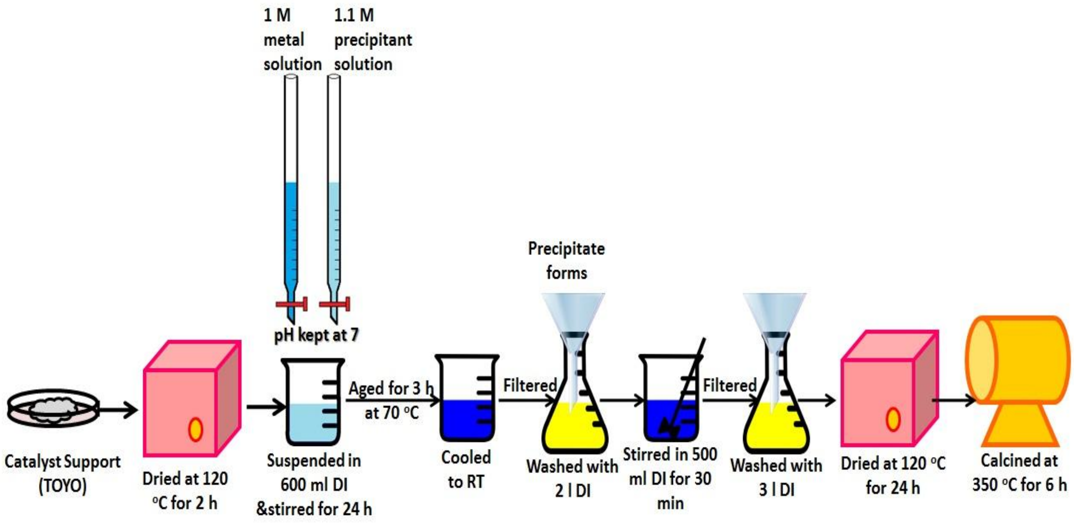

Figure 9. Experimental procedure for the bi-functional co-precipitated catalyst H-CZA-TOYO

Nomenclature for these catalysts is given in the Table 5.

Table 5. Nomenclature for co-precipitated catalysts

Nomenclature	**Content**	**Aging Time**	**Washing Water**	**Calcination Temp. , ºC**	**Reduction Temp. , ºC**
CZ	Cu-Zn	3 hr	Cold	350	-
CZA	Cu-Zn-Al	3 hr	Cold	350	-
CZCe	Cu-Zn-Ce	3 hr	Cold	350	-
CZZr	Cu-Zn-Zr	3 hr	Cold	350	-
CZA-1hr	Cu-Zn-Al	1 hr	Cold	350	-
CZA-6hr	Cu-Zn-Al	6 hr	Cold	350	-
CZA-Hot	Cu-Zn-Al	3 hr	Hot	350	-
CZA-C550	Cu-Zn-Al	3 hr	Cold	550	-
CZA-R225	Cu-Zn-Al	3 hr	Cold	350	225
CZA-R250	Cu-Zn-Al	3 hr	Cold	350	250
H-CZA-TOYO	Cu-Zn-Al, γ Al_2O_3	3 hr	Cold	350	-

6.1.2. Synthesis of SBA-15 and Impregnation of STA

Synthesis of SBA-15 and impregnation was co-worked with Arslan A. and synthesis procedure was also reported in elsewhere [68].

Source of Silica	: TEOS (Tetraethylorthosilicate) $C_8H_{20}O_4Si$ (Merck)
Source of Surfactant	: Pluronic P123
Source of Water	:Deionized water, obtained from Millipore Ultra-Pure Water System (Milli-QPlus)
Source of Acid	: Tungstosilisic acid hydrate (STA), (Sigma-Aldrich) Hydrochloric acid fuming 37% (Merck)

Synthesis of ordered mesoporous material, SBA-15 consists of five important steps: preparation of synthesis solution, hydrothermal synthesis, washing, drying, and calcination.

For the synthesis of SBA-15, a similar procedure described by Mbaraka and Shanks [69] was followed. Triblock copolymer, poly (ethylene glycol)-block-poly (propylene glycol)-block-poly (ethylene glycol) (Pluronic P123) was used as the surfactant and TEOS (tetraethyl-ortosilicate) was used as the silica source. 4 g of triblock copolymer was mixed with 125 ml deionized water and 25 ml concentrated HCl solution. The mixture was stirred at room temperature until triblock copolymer was completely dissolved. After that, the temperature of the mixture was raised to 40℃ and 8.2 ml TEOS was added drop wise. The solution was stirred at this temperature for 40 min. For hydrothermal synthesis part, the solution kept at 100℃ for 24 hour. The obtained solid was filtered and washed with deionized water and dried in oven at 120 °C. The calcination was performed in a quartz tubular reactor placed in a tubular furnace heated from ambient temperature to 600℃ at a rate of 1 ℃/min and kept at 600℃ for 6 hours in a flow of dry air. Experimental procedure is given in the Figure 10.

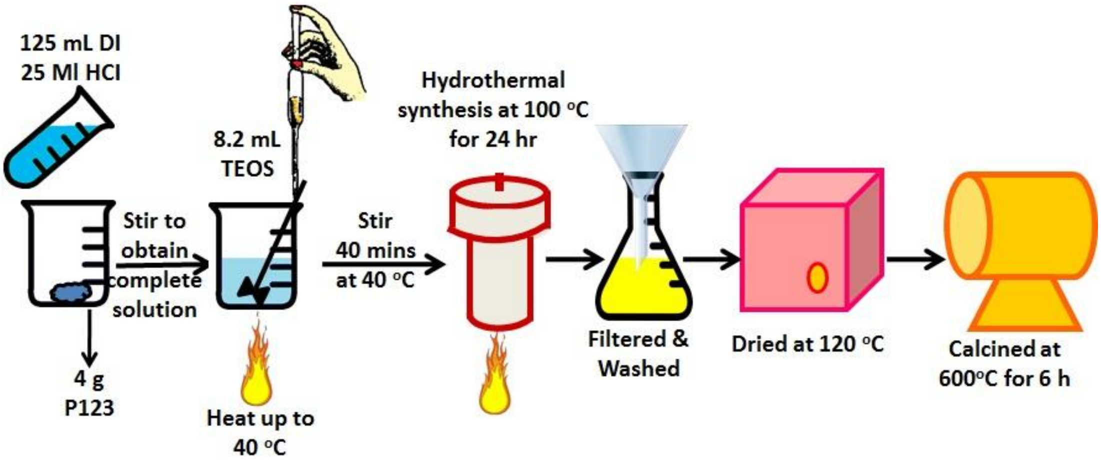

Figure 10. Experimental procedure for ordered mesoporous material SBA-15

Tungstosilisic acid was impregnated onto synthesized SBA-15. Experimental procedure is depicted in Figure 11. The molar ratio of tungsten to silica was adjusted to one (W/Si = 1). For this purpose, the procedure for impregnation of STA onto MCM-41 catalysts described by Varisli [70] was followed. 0.4 g SBA-15 was dissolved with 20 ml of deionized water at room temperature and 1.6195 g of STA was dissolved with 10 ml of deionized water. STA solution was added dropwise to the SBA-15 suspension and stirred at 30℃. The temperature was than raised to 50℃ and solution was left for mixing about 65 hour at this temperature to evaporate bulk water. After evaporation, material was taken to oven at 120 °C for 24 hours for further drying. Calcination was performed in a quartz tubular reactor placed in a tubular furnace heated from ambient temperature to 350 °C at a rate of 1 °C/min and kept at 350 °C for 6 hours in flow of dry air. This catalyst was denoted as STA@SBA-15.

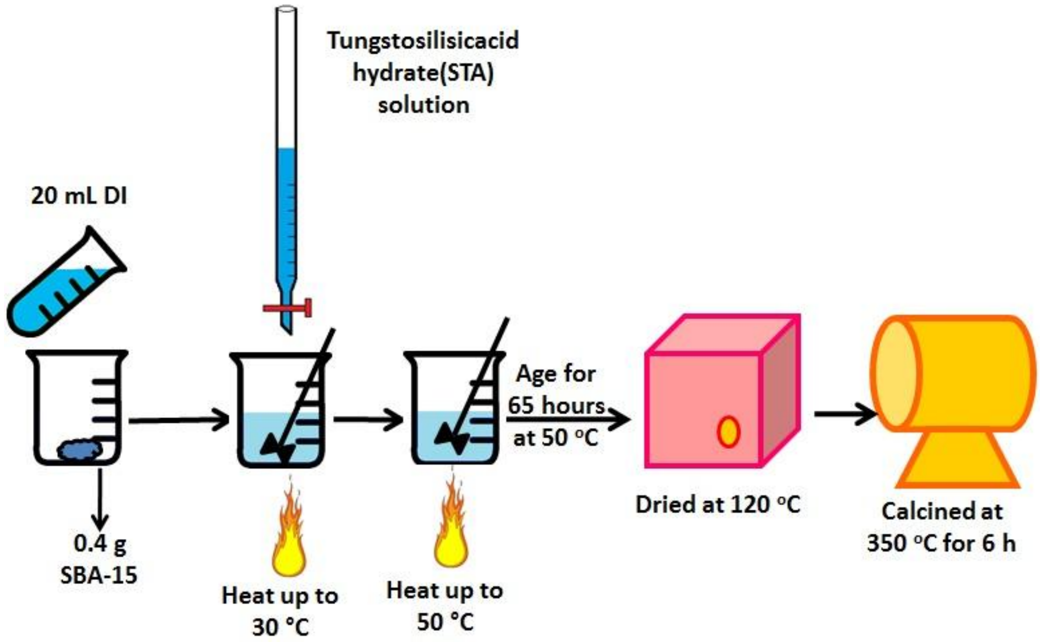

Figure 11. Experimental procedure for STA impregnation to ordered mesoporous material SBA-15

6.1.3. Dry-Physical Mixing and Sequenced Catalysts

In the direct synthesis of dimethyl ether, bi-functional catalysts containing methanol synthesis and dehydration sites are required. One function is to synthesize methanol from the synthetic gases whereas the other function is to convert synthesized methanol into the dimethyl ether. For this purpose, several catalysts were prepared and their preparation procedure and synthesis details were given in previous sections; Section 6.1.1 and 6.1.2.

Among the synthesized catalysts, some of them are able to perform only methanol synthesis and some of them are able to perform only methanol dehydration. An alternative approach is physical dry mixing of two catalysts to obtain a hybrid bi-functional catalyst. For this purpose, methanol reforming catalyst, Hifuel R120, denoted as “MRC”, and commercial methanol synthesis catalyst, obtained from Alfa-Aesar and denoted as “MSC”, were mixed with the methanol dehydration catalysts; TOYO and TRC-75(L) type catalysts. TOYO catalyst was γ-Al_2O_3 based methanol dehydration catalyst and obtained from Toyo Engineering Corporation. TRC-75(L) is a novel solid acid methanol dehydration catalyst prepared by a one-pot hydrothermal procedure. It was tungsten containing, silicate based, and in the structure of M41S family. This catalyst was synthesized in our laboratory and details of the synthesis procedure are given early publications of our group [48, 59]. It was shown that TRC-75(L) catalyst functioned very well in methanol dehydration with very high conversion and selectivity values. Characterization results of commercial catalysts are given in Sections 7.3. and 7.4.

In addition to the physical mixing of catalysts, another type of catalyst bed was prepared by placing catalysts in a sequential way. That is, firstly methanol synthesis catalysts was placed into the reactor and after that methanol dehydration catalyst was placed. By this way, reactant gases encountered with methanol synthesis catalysts first and then methanol dehydration catalyst. This type of reactor bed arrangement is important to see the effect of the one step DME synthesis over two step DME synthesis since such a reactor bed behaves like two reactors in series; one of them is operating for methanol synthesis whereas other was operating for methanol dehydration.

For nomenclature, a letter “C” is added to the end of the catalyst name if the catalyst within the reactor bed is a mixed catalyst and a letter “S” is added to the end of the catalyst name if catalysts in the reactor bed are arranged in a sequenced way.

6.2. CHARACTERIZATION TECHNIQUES

Synthesized catalysts were characterized by using several techniques to understand the physical and chemical structure of the catalysts. In the scope of this study, X-ray diffraction, nitrogen physisorption, energy dispersive spectroscopy, scanning electron microscopy, and diffuse reflectance infrared fourier transform spectroscopy of pyridine adsorption were used.

6.2.1. X-Ray Diffraction (XRD)

For the X-ray diffraction analysis, XRD Rigaku Ultima-IV X-Ray diffractometer in the METU-Central laboratory was used. In the device, CuK is the radiation source with a 2θ scanning ranges of low angle (0.2° to 10°) and high angle (10° to 80°).

6.2.2. Nitrogen Physisorption

Nitrogen adsorption-desorption analyses were made by a Quantachrome Autosorb-1-C/MS instrument in the METU Central Laboratory. Degassing was done at 120 °C for 6 hours before the analyses and the analyses were performed at a relative pressure range of 5x10-2 to 0.99 at liquid nitrogen temperature. Multipoint BET surface area values, BJH adsorption and desorption pore diameters and pore volumes of samples were determined by this characterization technique. Nitrogen adsorption and desorption isotherms were plotted and the pore size distributions were determined.

6.2.3. Scanning Electron Microscopy (SEM)

Scanning electron microscopy (SEM) analyses were done in the Middle East Technical University (METU) Central Laboratory by a Quanta 400F field emission SEM high resolution instrument. Before the analyses, samples were coated with a gold-palladium alloy.

6.2.4. Energy Dispersive Spectroscopy (EDS)

For the energy dispersive spectroscopy (EDS), SEM instrument Quanta 400F in the Middle East Technical University-Central Laboratory was used. Before the analyses, samples were coated with a gold-palladium alloy.

6.2.5. Diffuse Reflectance Infrared Fourier Transform Spectroscopy (Drifts) Of Pyridine Adsorption

Diffuse reflectance infrared fourier transform spectroscopy of pyridine adsorption analyses were done at Kinetic Laboratory at Middle East Technical University. Perkin Elmer Spectrum One instrument was used. 0.035 gr samples were covered with 1 ml of pyridine. After pyridine covered samples were dried, a prescribed amounts of pyridine covered and non-covered samples were mixed with KBr in an amount of 40 times of the sample which is to be analyzed. A reference spectrum was recorded with KBr. Acidic sites were determined by the subtraction of absorbance of pyridine covered samples from the absorbance of non-covered samples.

6.3. REACTION SET-UP

The reaction set-up in our laboratory is a high pressure, continuous flow system used for methanol synthesis and direct synthesis of DME. This experimental set-up was first built by Arınan A. [8] and it was improved to a large extent in the duration of this study. A schematic representation of experimental set-up is given in Figure 12.

The reactant gases of CO, CO_2, and H_2 are fed from the pressurized tanks and gas flow rates are controlled by the Omega FMA-800A series mass flow controllers.

Before mass flow controllers, a vent system is placed for proper operation of flow controllers. Pressures before the flow controllers are measured by gas regulators and pressure gauges. Pressure of the controller inlet is adjusted to 10 bars higher of the operating system pressure. There is a by-pass line near controllers to allow for operations without the use of flow controllers. After the flow controllers, another pressure gauge is placed to see the operating pressure of the reaction set-up. A tubular furnace is placed to keep supply necessary heat to the reactor. After furnace, a metering valve with an on- off valve and GO BP60 type back pressure regulator are placed to keep the pressure of the reactive side constant and to arrange the flow rate of the exhaust line. Before the reactor, pre-heating is achieved at 150 ºC and after the reactor, heating is done at the same temperature to prevent condensation of products. An online gas chromatography is present in the reaction set-up to analyze products and unconverted gases. At the end of the reaction set-up, a soap bubble flow meter is connected to measure the exit flow rate.

Products and unconverted gases were analyzed online by a SRI 3680 multigas #1 gas chromatography (GC) equipped with Carbosphere column and a thermal conductivity detector (TCD). The carrier gas of the GC is helium with a flow rate of 20 cc/min and at a pressure of 4 bar. In the GC, a temperature ramped program is used and operation parameters are given in the Table 6. Calibration factors and retention times of the GC are given in the Table 7.

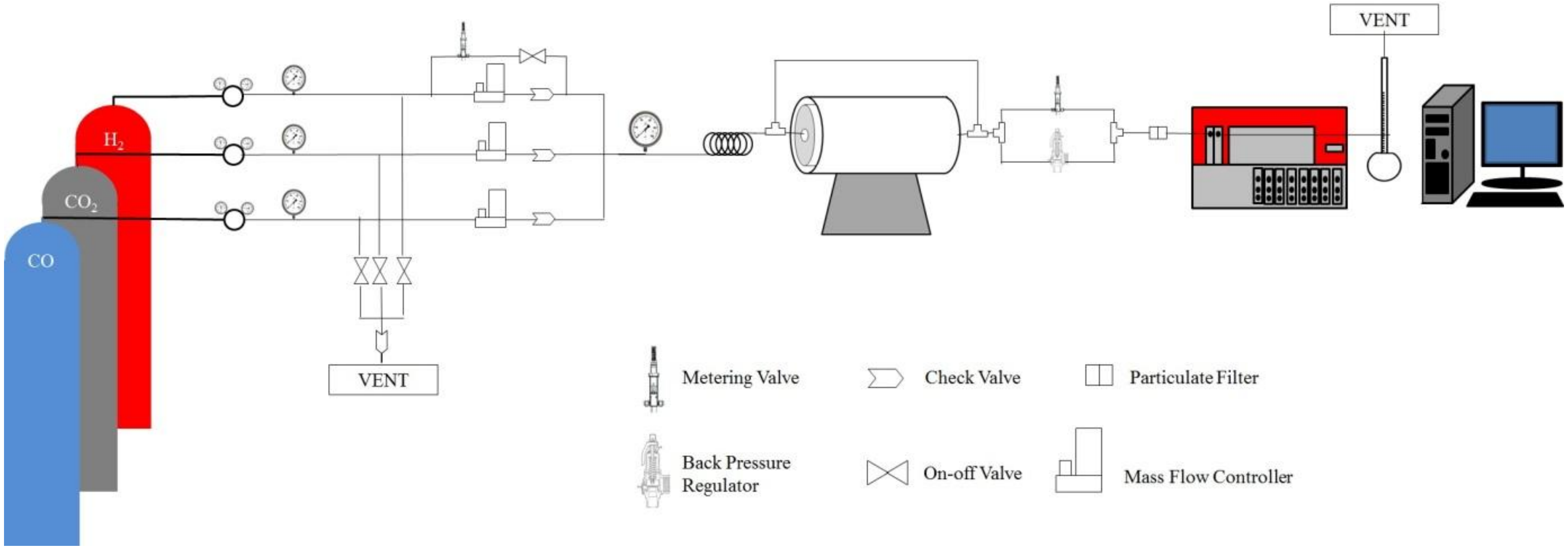

Figure 12. High pressure experimental set-up

Table 6. Temperature Program of Gas Chromatograph

Initial Temp. , ºC	Time , min	Ramp , ºC/min	Final Temp. , ºC
130	7	-	130
130	3	40	250
250	18	-	250

Table 7. Calibration Factors and Retention Times of Gas Chromatograph

Component	Retention Time , min.	Calibration Factor
Carbon Monoxide	1.3 – 1.4	1.00
Carbon Dioxide	4.2 - 4.3	0.83
Methane	2.4 - 2.6	1.36
Methanol	13.9 - 14.2	1.40
Dimethyl Ether	23.3 - 23.5	0.49
Ethanol	25.8 - 26.0	1.44
Formic Acid	11.8 - 11.9	1.80

Since high pressures are required in the methanol and DME synthesis, all the connections and construction materials have been chosen as stainless-steel which can withstand high pressures. Direct synthesis of DME from synthetic syngas mixtures was investigated in a fixed bed tubular flow reactor, which was made of ¼ inch stainless steel tubing. Catalyst was packed to the center of the reactor and supported from both ends by quartz wool. In most of the experiments, reactor was charged with 0.2 g catalyst.

Catalytic activity tests were conducted in temperature ranges from a minimum of 200 ºC to a maximum of 400 ºC. Catalyst amount charged to the reactor was 0.2 gr and reactant gas flow rate was adjusted to either 50 cc/min or 25 cc/min. Space time based on these flow rates at atmospheric pressure and temperature was 0.24 g.s/ml and 0.48 g.s/ml. However, actual space time at reaction conditions is expected to be quite different.

Steady state was reached in usually 30 minutes for most of the experiments, which nearly corresponds to duration of one complete GC analysis. Four successive data points at steady state were taken from each temperature and averages of these values were used in the conversion and selectivity calculations. Carbon monoxide and carbon dioxide conversions (when applicable) and selectivity of the products were calculated.

CO conversion was defined as the ratio of amount of CO reacted to amount of CO fed to reactor and product selectivities were defined as the ratio of moles of CO converted to a specific component to total moles of CO converted to the products. According to these definitions, conversion and DME, methanol, and CO_2 selectivities were expressed as;

X = (Moles of CO fed to system – Moles of CO emerged from system)/ Moles of CO fed to system 6.1.

S_{DME} = 2(Moles of DME formed)/ (Moles of CO converted to products) 6.2.

S_{MEOH}= (Moles of MEOH formed)/ (Moles of CO converted to products) 6.3.

S_{CO_2} = (Moles of CO_2 formed)/ (Moles of CO converted to products) 6.4.

In the experiments performed with the feed stream containing only 50% CO and 50% H_2, (Mixture-1), formation of CO_2 was observed together with DME. However, in the case of experiments performed with a feed stream containing some CO_2 (Mixture-2), carbon dioxide also acted as a reactant at low temperatures. For such experiments, CO and CO_2 conversions were calculated and product selectivities were defined as the ratio of moles CO and CO_2 converted to specific component to total moles of CO and CO_2 converted to products. According to these definitions, CO and CO_2 conversions and DME and methanol selectivities were expressed as;

X_{CO} = (Moles of CO fed to system – Moles of CO emerged from system)/ Moles of CO fed to system 6.5.

X_{CO_2} = (Moles of CO_2 fed to system – Moles of CO_2 emerged from system)/ Moles of CO_2 fed to system 6.6

S_{DME} = 2(Moles of DME formed)/ (Moles of CO&CO_2 converted to products) 6.7.

S_{MEOH}= (Moles of MEOH formed)/ (Moles of CO&CO_2 converted to products) 6.8.

For comparative purposes, product yields were also calculated. Yield was expressed as the ratio of moles of desired product formed to moles of reactant fed to the system.

Y_{MEOH}= (Moles of MEOH formed)/ (Moles of CO fed to system) 6.9.

Sample conversion, selectivity, and yield calculations are illustrated in the Appendix B.

CHAPTER 7

CHARACTERIZATION RESULTS

In this chapter, characterization results of catalytic materials are presented. X-Ray diffraction (XRD), nitrogen physisorption, energy dispersive spectroscopy (EDS), scanning electron microscopy (SEM), and diffuse reflectance infrared fourier transform spectroscopy of pyridine adsorption techniques were used in characterization of these materials.

7.1. CHARACTERIZATION RESULTS OF CO-PRECIPITATED CATALYSTS

7.1.1. X-Ray Diffraction (XRD)

X-Ray diffraction patterns of the co-precipitated copper and zinc containing catalyst, CZ, are given in Figure 13. Diffraction peaks of CuO and ZnO in the 2θ angles of 10° - 80° were wide and not well-defined, indicating well dispersion of metals and metal oxides. Since the catalyst was composed of only copper and zinc metals, no other elements were searched for. Two major peaks of CuO at 35.2° and 38.5° were observed and a major peak of ZnO was observed at 31.7°. In addition to observed peaks, ZnO and CuO diffraction peaks overlap at $30° < 2\theta < 50°$. For this reason, it was not possible to identify all peaks of ZnO since their intensities were lower than CuO peaks. At high 2θ angles, several peaks of CuO and ZnO were also observed. These points will be further discussed at XRD analysis of reduced samples, CZA-

R225, CZA-R250. Particle sizes of the metals and metal oxides were calculated by Scherrer's equation [71]. Calculations were illustrated in Appendix C.

$$d_i = \frac{K \times \lambda}{\beta \times \cos(\theta)} \qquad 7.1.$$

where, d_i = particle size of i,

K = shape factor

λ = X-Ray wavelength

β = Full width at half max

θ = Bragg's angle

For CZ catalyst, diffraction lines of CuO and ZnO were identified and particle size of CuO and ZnO were calculated from the Scherrer's equation. To determine CuO particle size, peak at 2θ=35.6 °C was used and peak at 2θ=31.7 °C was used in determination of ZnO. Particle sizes of CuO and ZnO were calculated as 4.3 nm and 4.9 nm, respectively.

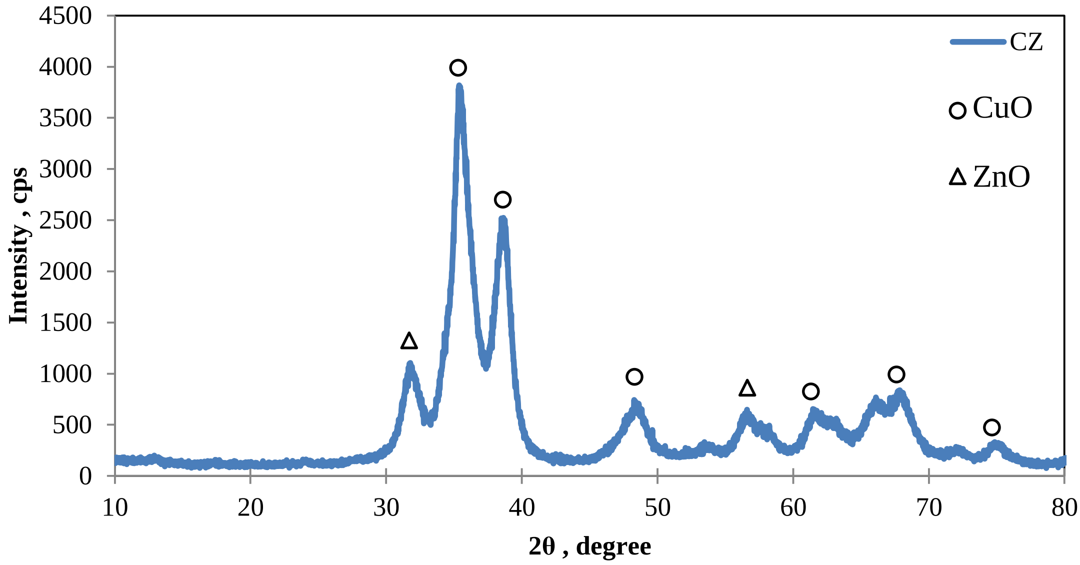

Figure 13. X-Ray diffraction pattern of copper and zinc containing co-precipitated catalyst, CZ

Several promoters including alumina, zirconia and ceria were incorporated to copper-zinc containing co-precipitated catalyst and x-ray diffractions are given in Figure 14. Synthesized catalysts showed very similar diffraction patterns to the catalyst with no promoter. Highly intense CuO and ZnO peaks were recorded at 35.2°, 38.5°, 48.5° and 31.7°. Peaks were wide and not well defined in the range of 10° - 80° and peaks of promoters were not observed. Thus, metals and metal oxides in the crystalline structure were well dispersed. Addition of promoters to the copper-zinc containing catalyst decreased the intensity of the peaks, resulting in more amorphous structure. For the ceria co-precipitated catalyst, intensity of the peaks was lowest when compared to other catalysts. As a result, it was more amorphous than other promoted catalysts.

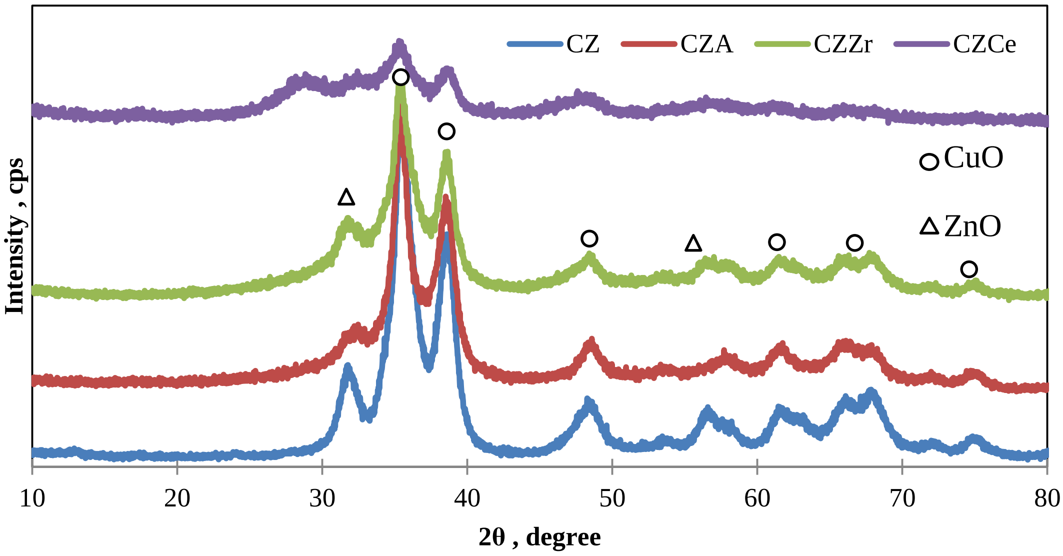

Figure 14. X-Ray diffraction patterns of copper, zinc and promoter containing co-precipitated catalysts; CZ, without promoter; CZA, Alumina promoter; CZCe, Ceria promoter; CZZr, Zirconia promoter.

Particles sizes were calculated and given in Table 8. CuO particle size increased with loadings of promoters alumina and zirconia. For the ZnO particles, co-precipitation with alumina and zirconia promoters decreased the ZnO particle size. For the ceria co-precipitated catalyst, CZCe, best dispersion was obtained among other promoted catalysts as it can be seen from Figure 14. No peak was observed for ZnO at 2θ of 31° and particle size of CuO was very small, indicating the well dispersion.

Table 8. Particle sizes of copper, zinc and promoter containing co-precipitated catalysts; CZ, without promoter; CZA, Alumina promoter; CZCe, Ceria promoter; CZZr, Zirconia promoter.

	d_{CuO} , nm	d_{ZnO} , nm
CZ	4.3	4.9
CZA	8.1	4.1
CZZr	5.0	2.5
CZCe	2.8	-

Copper, zinc and alumina containing co-precipitated catalysts were aged for different times; one hour, three hours, and six hours. Figure 15 shows the diffraction patterns of these catalysts. As it can be seen from Figure 15, aging time did not influence the diffraction patterns. Peaks for the CZA catalyst were obtained at same 2θ angles and their intensities were almost same.

Particles sizes of different aging time catalysts were calculated and given in Table 9. CuO particle shrink with aging time and the smallest crystallites were observed for the 6 hour aged catalyst. For the ZnO particles, particle sizes of ZnO almost remained constant.

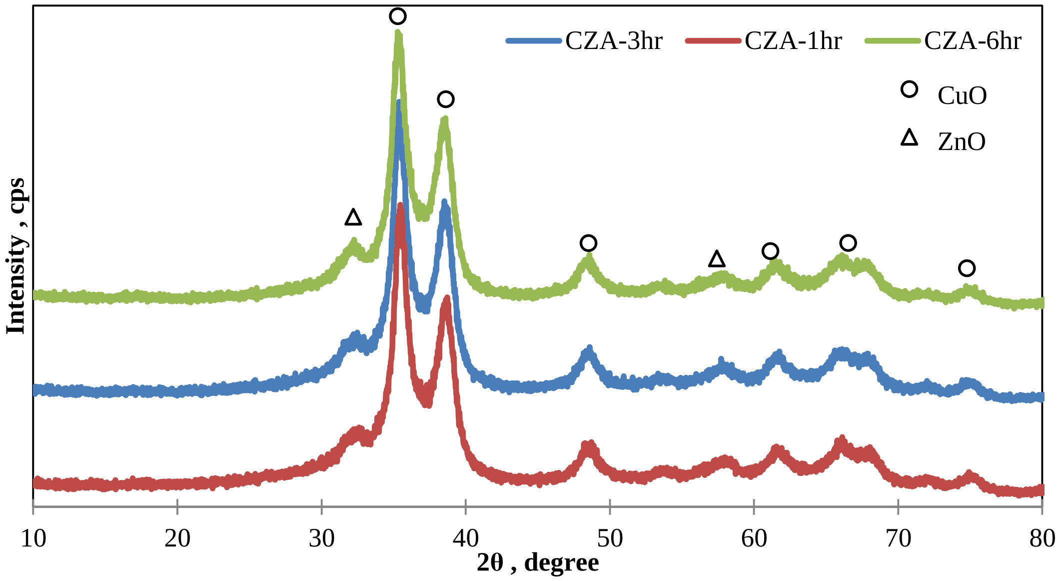

Figure 15. X-Ray diffraction patterns of copper, zinc and alumina containing co-precipitated catalysts for different aging time; CZA-1 hr, aged for one hour; CZA-3 hr, aged for three hours; CZA-6hr, aged for six hours.

Table 9. Particle sizes of copper, zinc and alumina containing co-precipitated catalysts for different aging time; CZA-1 hr, aged for one hour; CZA-3 hr, aged for three hours; CZA-6hr, aged for six hours.

	d_{CuO} , nm	**d_{ZnO} , nm**
CZA-1hr	9.4	4.0
CZA-3hr	8.1	4.1
CZA-6hr	7.6	4.7

Different washing procedures were applied to copper, zinc and alumina containing co-precipitated catalysts. Catalysts were washed with hot deionized water and denoted as “CZA-Hot”. Figure 16 shows the diffraction patterns of these catalysts. Although there is no change in the diffraction patterns of differently washed catalysts, intensities were slightly different. CZA-Cold catalyst had slightly higher intense peaks than CZA-Hot. Peaks for the CZA catalyst were obtained at almost same 2θ angles with same strength. Particles sizes of the CZA-Hot were calculated from Scherrer's equation and CuO particle size of CZA-Hot was calculated as 8.4 nm whereas CuO particle size of CZA-Cold was 8.1 nm.

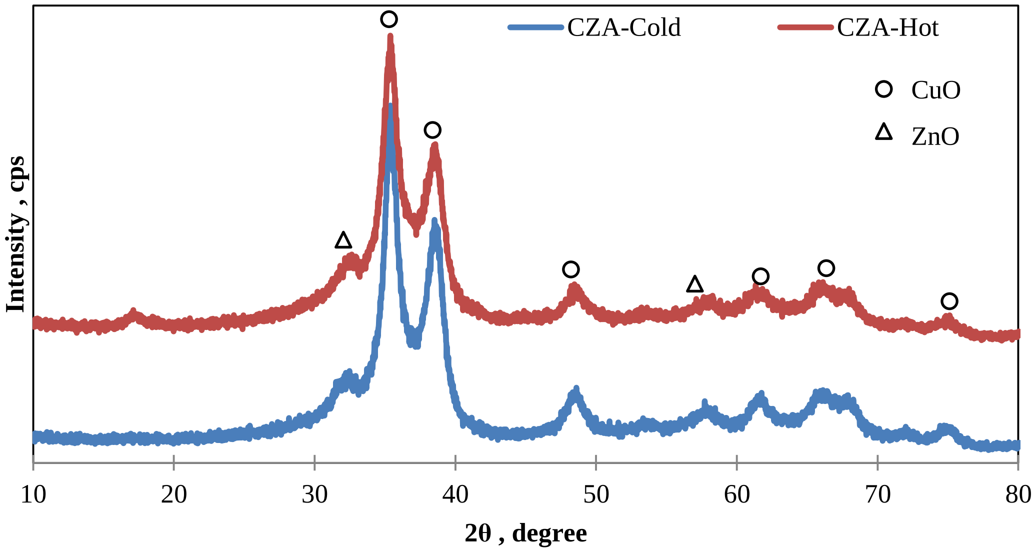

Figure 16. X-Ray diffraction patterns of copper, zinc and alumina containing co-precipitated catalysts for different washing conditions; CZA-Hot, washed with hot water; CZA-Cold, washed with cold water.

Calcination temperature is one of the most important catalyst treatment and catalyst properties change with temperature to a large extent. To investigate the effect of calcination temperature; copper, zinc, and alumina containing co-precipitated catalyst were calcined at high temperature at 550 °C, CZA-C550, and low temperature at 350 °C, CZA-C350. The result of XRD characterization (Figure 17) showed that more intense peaks were obtained in high temperature calcined catalyst, indicating more crystalline structure. Peaks of alumina promoter would be seen at high temperature calcined catalyst since the intensity of peaks increased. However, to determine the alumina peaks, different composition catalysts should be prepared. Dispersion of metals and metal oxides suffered from high temperature calcination since peaks at low temperature calcined catalyst were less intense than high temperature calcined catalyst.

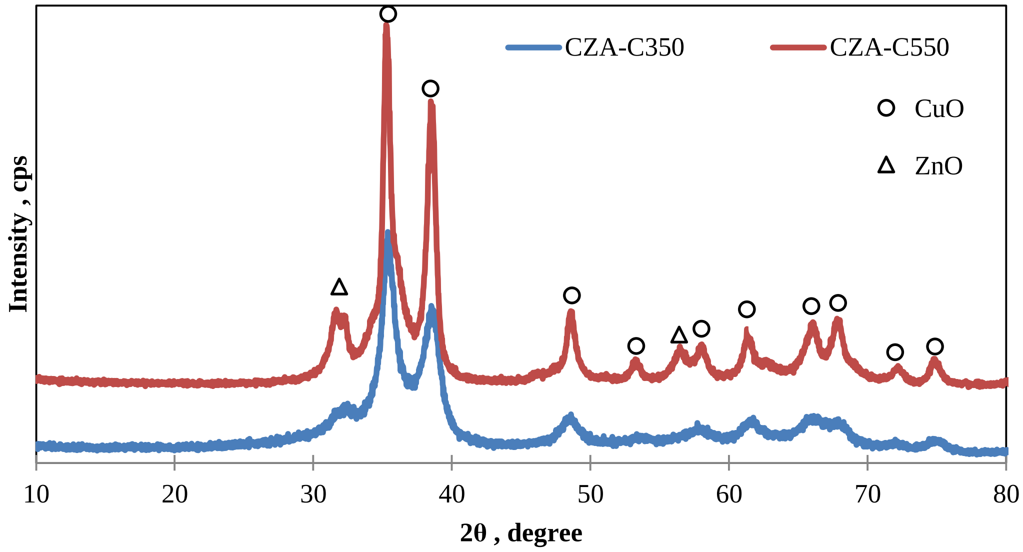

Figure 17. X-Ray diffraction patterns of copper, zinc and alumina containing co-precipitated catalysts for different calcination temperature; CZA-C550, calcined at 550 °C; CZA-C350, calcined at 350°

The mean crystalline size of CuO and ZnO were determined from the Scherrer's equation and results are given in Table 10. From the increase in the particle size, it can be understood that CuO particles agglomerated and sintering occurred. Particle size of CuO increased from 8.1 nm to 13.0 nm as calculated from the Scherrer's equation. Size of ZnO particles also increased and their particle sizes increased from 4.1 nm to 8.1 nm.

Table 10. Particle sizes of copper, zinc and alumina containing co-precipitated catalysts for different calcination temperature; CZA-C550, calcined at 550 °C; CZA-C350, calcined at 350 °C

	d_{CuO} , nm	**d_{ZnO} , nm**
CZA-C350	8.1	4.1
CZA-C550	13.0	8.1

Among the synthesized co-precipitated catalysts, X-Ray diffraction patterns were affected mostly by reduction treatment. Among the reduction, copper particles were reduced to the metallic state. X-Ray diffraction patterns of reduced catalysts are given in Figure 18. For the copper zinc alumina containing co-precipitated catalyst, mostly Cu^{+2} peaks were present. Among the reduction, oxidation level of copper particles was reduced to either +1 or 0 state. Reduction was not complete at 225 °C since Cu^{+1} peaks were still present. However, as reduction temperature increased to 250 °C, only metallic copper was present. Intensity of metallic copper peak of 250 °C-reduced catalyst (CZA-R250) was lower than the intensity of metallic copper peak of 225 °C reduced catalyst (CZA-R225). By comparing the intensities, it was concluded that catalyst reduced at 250 °C was of more crystalline structure than the catalyst reduced at 225 °C. Furthermore, for the CZA catalyst, ZnO and CuO peaks overlapped and only CuO peaks were observed because of their high intensities. When the oxidation level of copper was changed upon reduction, ZnO peaks appeared in the overlapping range of $30° < 2\theta < 50°$.

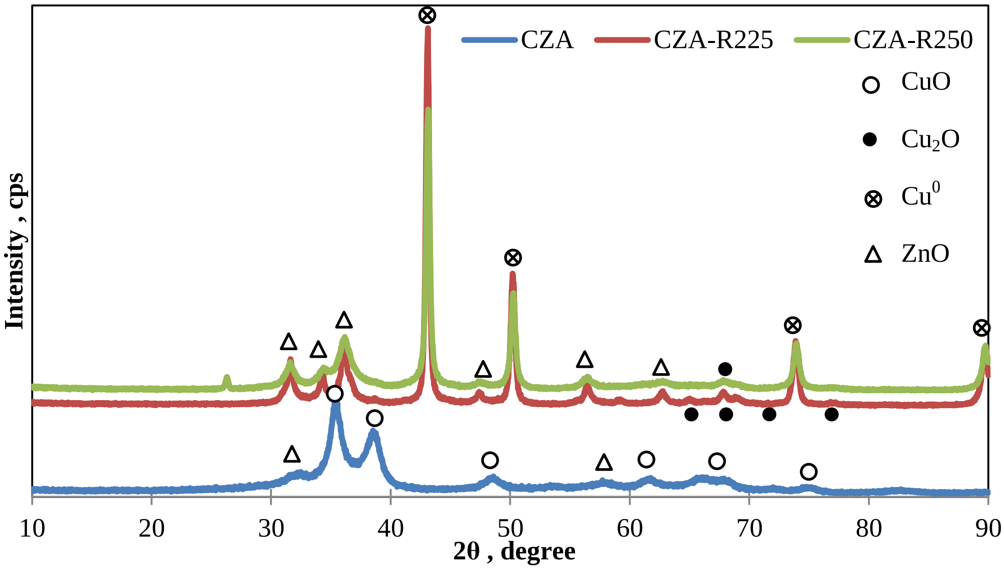

Figure 18. X-Ray diffraction patterns of copper, zinc and alumina containing co-precipitated catalysts for different reduction temperature; CZA, no reduction; CZA-R225, reduced at 225 °C; CZA-R250, reduced at 250°C;

In the reduced samples, Cu^{+2} in the unreduced sample was disappeared and turned into the Cu^{+1} and Cu^0. With further increase in reduction temperature, almost all Cu^{+1} peaks were also turned into the metallic copper. Particle sizes of present metals and metal oxides are given in Table 11.

Particle size of copper was calculated from the metallic copper peak at $2\theta=43.1°$ and particle size of Cu^{+1} was calculated from the oxide peak at $2\theta=64.9°$. As reduction occured CuO particles turned to Cu_2O and subsequently to the metallic copper. Metallic copper particle size reached to the 26.8 nm at 250 °C. Reduction also agglomerated ZnO particles, resulting in the size increase. However, no change of oxidation state was observed indicating that ZnO was not reduced under H_2 flow at 225 °C and 250 °C.

Table 11. Particle sizes of copper, zinc and alumina containing co-precipitated catalysts for different reduction temperature; CZA, no reduction; CZA-R225, reduced at 225 °C; CZA-R250, reduced at 250°C.

	d_{CuO} , nm	**d_{Cu2O} , nm**	**d_{Cu} , nm**	**d_{ZnO} , nm**
CZA	8.1	-	-	4.1
CZA-R225	-	18.5	-	10.3
CZA-R250	-	-	26.8	10.6

XRD diffraction pattern of bi-functional co-precipitated catalyst H-CZA-TOYO is given in Figure 19. As it can be seen from figure, most of the CuO and ZnO peaks of CZA catalyst were disappeared for the bi-functional catalyst. Since bi-functional catalyst was co-precipitated on the suspension of TOYO catalyst, it exhibited γ-Al_2O_3 peaks at 45.9° and 66.7°. However, peaks were wide and not well defined indicating the well dispersion of metals and metal oxides in the structure.

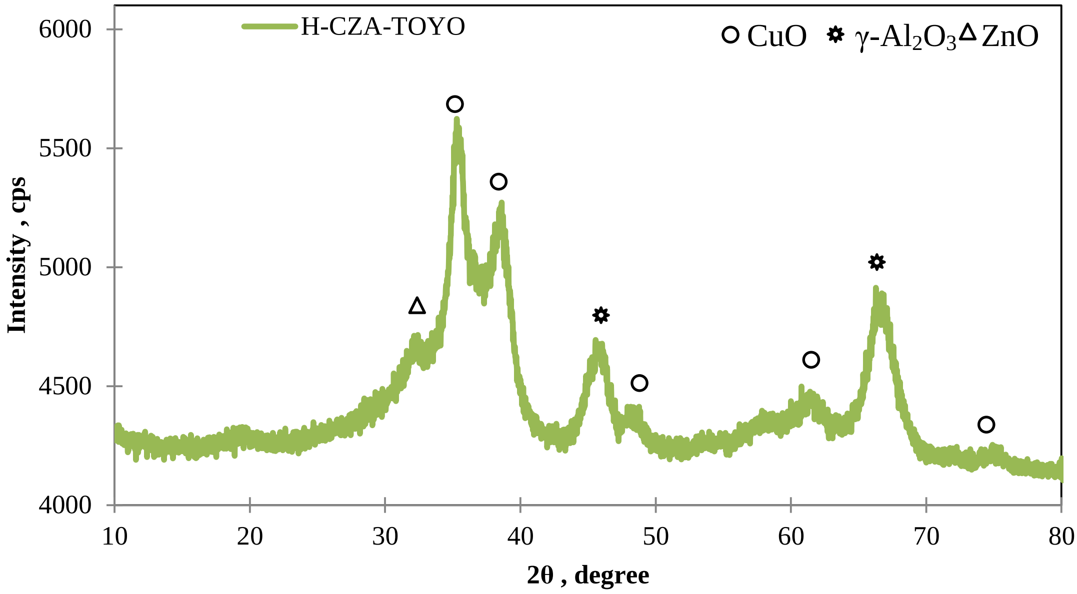

Figure 19. X-Ray diffraction patterns of bi-functional co-precipitated catalyst H-CZA-TOYO with comparison of CZA and TOYO catalysts

The mean crystalline size of CuO, ZnO, and γ-Al_2O_3 were determined from the Scherrer's equation and results are given in Table 12. Particle size of γ-Al_2O_3 was calculated from 2θ=66.7°. H-CZA-TOYO, bi-functional catalyst prepared by co-precipitation of metal salts into the suspension of TOYO, exhibited smallest particle sizes than the CZA and TOYO catalysts. Dispersion of the bi-functional catalyst is better than the TOYO and CZA.

Table 12. Particle sizes of bi-functional co-precipitated catalyst H-CZA-TOYO

	d_{CuO} , nm	d_{ZnO} , nm	$d_{\gamma\text{-}Al_2O_3}$, nm
H-CZA-TOYO	6.9	< 2	3.9

7.1.2. Nitrogen Physisorption

Nitrogen physisorption was applied to co-precipitated catalysts and information about the multipoint BET surface areas, pore volumes, and pore sizes was obtained. The nitrogen physisorption results are given in Table 13. Nitrogen physisorption results of co-precipitated catalysts had surface areas in between 22 m^2/g and 107 m^2/g and pore diameters were in between 2.13 nm to 17.7 nm, within the mesoporous range. Copper-zinc containing co-precipitated catalyst had a surface area of 61.5 m^2/g with a pore volume of 0.62 cc/g and 9.5 nm.

Table 13. Nitrogen physisorption results of co-precipitated catalysts

	Multipoint BET Surface area , m^2/g	**BJH Method Desorption Pore Volume , cc/g**	**BJH Method Desorption Pore Diameter , nm**
CZ	61.52	0.62	9.55
CZA	57.23	0.45	7.85
CZZr	106.7	0.51	9.68
CZCe	97.18	0.77	3.84
CZA-1hr	68.97	0.49	17.5
CZA-6hr	49.98	0.37	7.85
CZA-C550	41.09	0.62	2.14
CZA-Hot	76.99	0.51	17.7
CZA-R225	22.10	0.11	2.13
CZA-R250	53.03	0.27	17.7
H-CZA-TOYO	115	0.67	9.67

Upon the promoter loading, catalytic surface area enhanced for zirconia and ceria containing co-precipitated catalysts whereas slight decrease was observed for alumina promoted catalyst. Nitrogen physisorption results of co-precipitated catalysts are given in Table 14. As it can be seen from Table 14, zirconia promoted co-precipitated catalyst had a surface area of 106.7 m^2/g and pore diameter was 9.86 nm. Moreover, their pore volumes were close to each other. All the pore diameters were in the mesoporous region.

Table 14. Nitrogen physisorption results of copper, zinc and promoter containing co-precipitated catalysts; CZ, without promoter; CZA, Alumina promoter; CZCe, Ceria promoter; CZZr, Zirconia promoter.

	Multipoint BET Surface area , m^2/g	**BJH Method Desorption Pore Volume , cc/g**	**BJH Method Desorption Pore Diameter , nm**
CZ	61.52	0.62	9.55
CZA	57.23	0.45	7.85
CZZr	106.7	0.51	9.68
CZCe	97.18	0.77	3.84

Adsorption desorption isotherm of the copper and zinc containing co-precipitated catalyst is given in Figure 20 and adsorption desorption isotherms of co-precipitated catalysts were similar to each other and given in Appendix D.

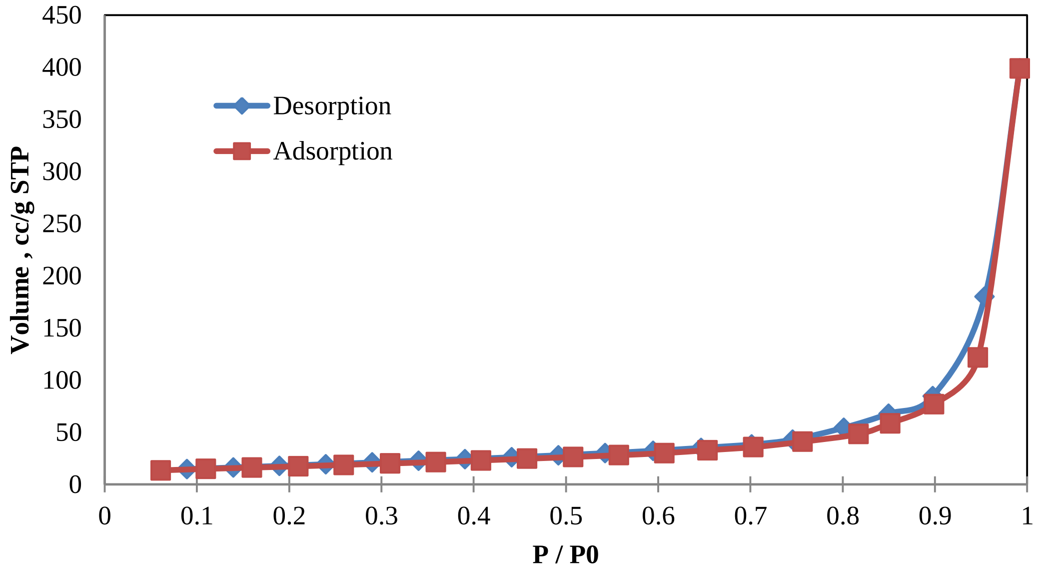

Figure 20. Adsorption-desorption isotherm of copper and zinc containing catalyst, CZ.

Nitrogen physisorption results of different timely aged catalysts are given in Table 15. Upon the increase in the aging time, multipoint BET surface areas decreased. Highest surface area obtained with the one hour aged catalyst as 69.0 m^2/g and its pore diameter was calculated as 17.5 nm. Increase in the aging time from one hour to three hours reduced the pore diameter from 17.5 nm to 7.85 nm. However, further increase in the aging time had no effect on the size of the pores

Table 15. Nitrogen physisorption results of copper, zinc and alumina containing co-precipitated catalysts for different aging time; CZA-1 hr, aged for one hour; CZA-3 hr, aged for three hours; CZA-6hr, aged for six hours.

	Multipoint BET Surface area , m^2/g	**BJH Method Desorption Pore Volume , cc/g**	**BJH Method Desorption Pore Diameter , nm**
CZA-1 hr	68.97	0.49	17.5
CZA-3 hr	57.23	0.45	7.85
CZA-6 hr	49.98	0.37	7.85

Copper-zinc and alumina precipitated catalyst was washed with hot deionized water and nitrogen physisorption results are given in Table 16 in comparison with cold deionized water. Surface area increase from 57.2 m^2/g to 77.0 m^2/g was observed upon the washing with hot deionized water and pore diameter was almost two times of the cold water washed catalyst.

Table 16. Nitrogen physisorption results of copper, zinc and alumina containing co-precipitated catalysts for different washing conditions; CZA-Hot, washed with hot water; CZA-Cold, washed with cold water.

	Multipoint BET Surface area , m^2/g	**BJH Method Desorption Pore Volume , cc/g**	**BJH Method Desorption Pore Diameter , nm**
CZA-Cold	57.23	0.45	7.85
CZA-Hot	76.99	0.51	17.7

To investigate the effect of calcination temperature on the copper, zinc, and alumina containing co-precipitated catalyst, high temperature calcination was conducted and nitrogen physisorption results of co-precipitated catalysts are given in Table 17. Surface area decreased upon calcination at high temperature and pore diameter was decreased to 2.14 nm. Decrease in the surface area can be attributed to the thermal sintering.

Table 17. Nitrogen physisorption results of copper, zinc and alumina containing co-precipitated catalysts for different calcination temperature; CZA-C550, calcined at 550 °C; CZA-C350, calcined at 350 °C

	Multipoint BET Surface area , m^2/g	**BJH Method Desorption Pore Volume , cc/g**	**BJH Method Desorption Pore Diameter , nm**
CZA-C350	57.23	0.45	7.85
CZA-C550	41.09	0.62	2.14

Reduction was carried out at 225 °C and 250 °C under hydrogen flow and reduced catalysts were characterized by N_2 physisorption. Nitrogen physisorption results are given in Table 18 with comparison of non-reduced sample. Slight decrease of surface area was observed and this could be attributed to the thermal sintering. Pore volume was decreased from 0.45 cc/g for un-reduced sample to around 0.11 cc/g for reduced samples.

Table 18. Nitrogen physisorption results of copper, zinc and alumina containing co-precipitated catalysts for different reduction temperature; CZA, no reduction; CZA-R225, reduced at 225 °C; CZA-R250, reduced at 250°C.

	Multipoint BET Surface area , m^2/g	**BJH Method Desorption Pore Volume , cc/g**	**BJH Method Desorption Pore Diameter , nm**
CZA	57.23	0.45	7.85
CZA-R225	22.1	0.11	2.13
CZA-R250	53.03	0.27	17.7

Bi-functional catalyst, H-CZA-TOYO prepared by the co-precipitation of copper, zinc, and alumina into TOYO suspension was of a surface area 111 m^2/g with a pore size of 9.7 nm within the mesoporous range. Surface area of bi-functional catalyst was greater than the other co-precipitated catalysts because of the high surface area of TOYO catalyst. Moreover, adsorption-desorption isotherm of the bi-functional catalyst is given in Figure 21 and pore size distribution is shown in Figure 22.

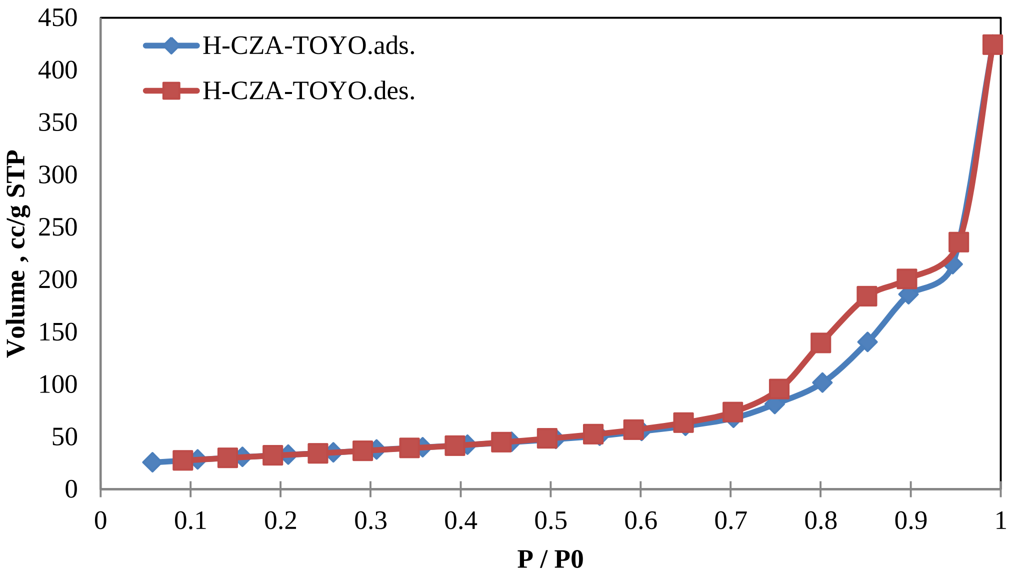

Figure 21. Adsorption-Desorption Isotherm of bi-functional copper, zinc, and alumina containing catalyst, H-CZA-TOYO.

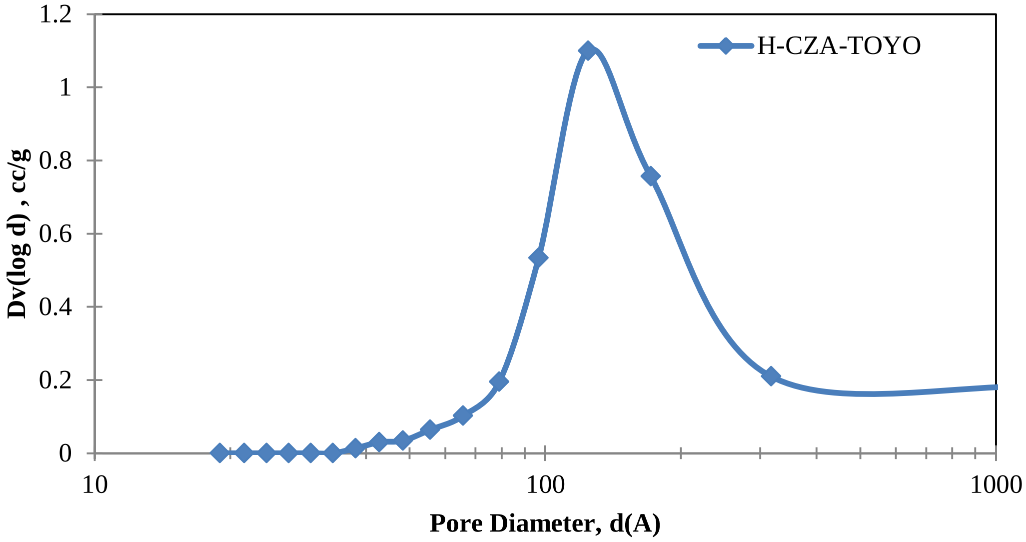

Figure 22. Pore size distribution of bi-functional copper, zinc, and alumina containing catalyst, H-CZA-TOYO.

As it can be seen from Figure 22, pore size distribution is wide and obtained at around average pore size of 9.7 nm.

7.1.3. Energy Dispersive Spectroscopy (EDS)

The results of EDS analyses are given in Table 19. Results showed that in the preparation of catalysts, compositions of many catalysts were well preserved. However, some composition changes can be seen from the Table 19. Among the synthesized co-precipitated catalysts, molar metal ratio of copper to zinc was preserved as prepared in the promoter changed catalysts. Slight changes occurred on co-precipitated catalysts that were exposed to high calcination temperature and reduction treatment. These operations affected the catalyst compositions.

Table 19. Energy dispersive spectroscopy results of co-precipitated catalysts

	Copper		**Zinc**		**Alumina**		**Promoter (Zr, Ce)**	
	Prepared (moles%)	**Obtained (moles%)**	**Prepared (moles%)**	**Obtained (moles%)**	**Prepared (moles%)**	**Obtained (moles%)**	**Prepared (moles%)**	**Obtained (moles%)**
CZ	66.7	66.7	33.3	33.3		-	-	-
CZA	60	71.8	30	19.6	10	8.4	-	-
CZZr	60	57.39	30	30.48	-	-	10	12.13
CZCe	60	59.9	30	29.8	-	-	10	10.3
CZA-1hr	60	67.2	30	21.5	10	6.6	-	-
CZA-6hr	60	80.1	30	16.5	10	3.4	-	-
CZA-C550	60	65.2	30	22.7	10	12.1	-	-
CZA-Hot	60	67.2	30	21.5	10	11.3	-	-
CZA-R225	60	42.7	30	30.72	10	26.6	-	-
CZA-R250	60	53.2	30	28.08	10	18.72	-	-
H-CZA-TOYO	17.8	9.67	8.9	4.2	76.3	86.13	-	-

7.1.4. Scanning Electron Microscopy (SEM)

Morphologies of the samples were observed by SEM analyses and SEM images of the co-precipitated catalysts are given in Figures 23-33. Due to the oxides present on the catalyst, vibration occurred during the analyses. For this reason, images having vibrations should be viewed accordingly. In the copper and zinc containing catalyst, CZ, small rod-like structures were observed and uniformity of these structures was very high as it can be seen from Figure 23.

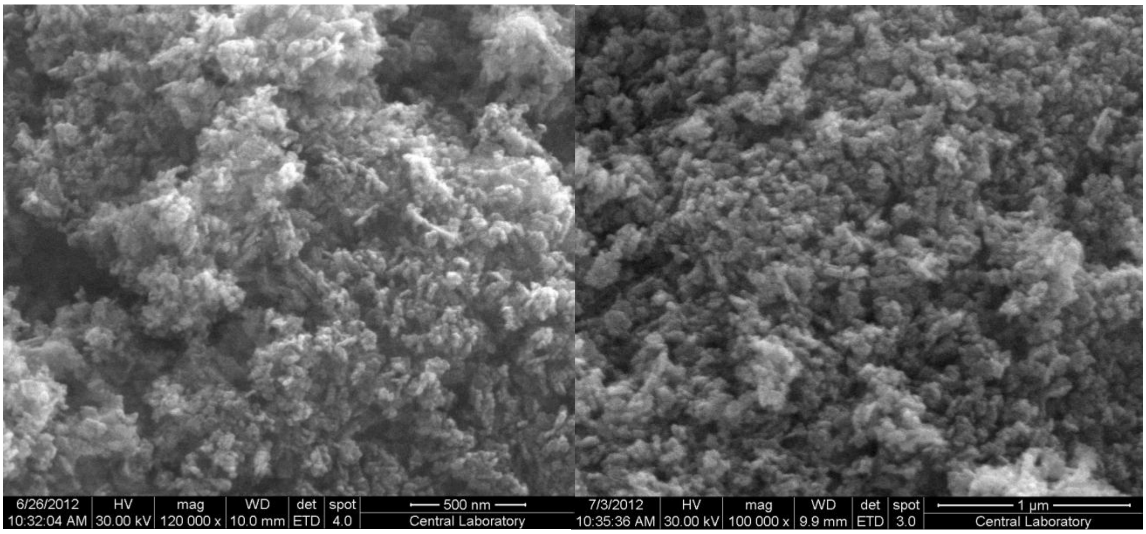

Figure 23. SEM images of copper and zinc containing co-precipitated catalyst, CZ

Promoter incorporated copper and zinc containing co-precipitated catalysts exhibited similar morphologies with the no-promoter catalyst. Formation of rod-like structures on the copper, zinc, and alumina co-precipitated catalyst can be more clearly seen in Figure 24. Two different sized fragments were dispersed uniformly on the bulk of the catalyst. However, dispersion of two different sized fragments on zirconia promoted catalyst was not as good as alumina promoted catalyst. SEM images of zirconia promoted catalyst is given in Figure 25 and ceria incorporated catalyst is given in Figure 26.

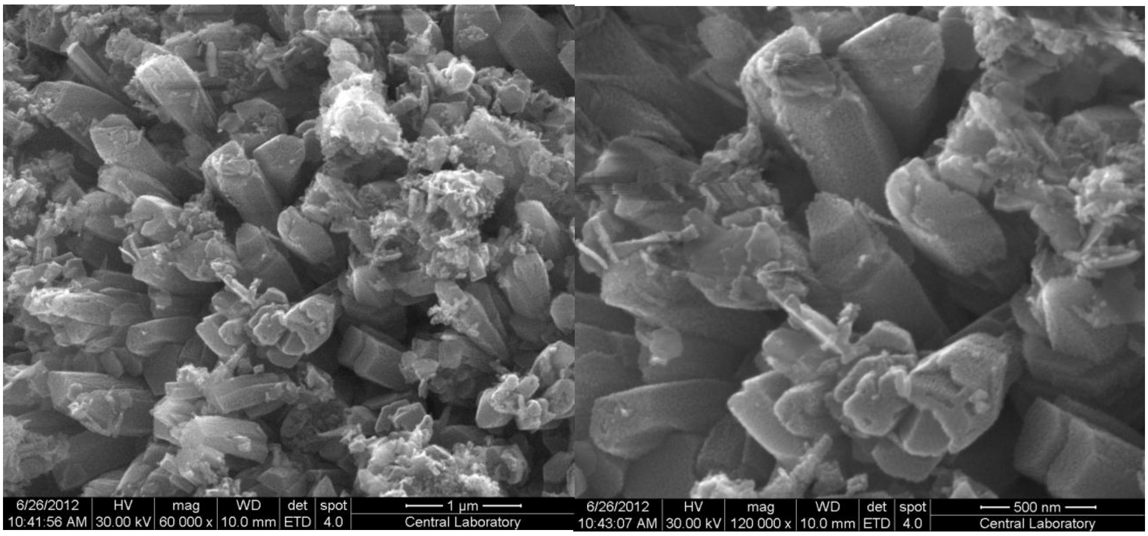

Figure 24. SEM images of copper, zinc, and alumina containing co-precipitated catalyst, CZA

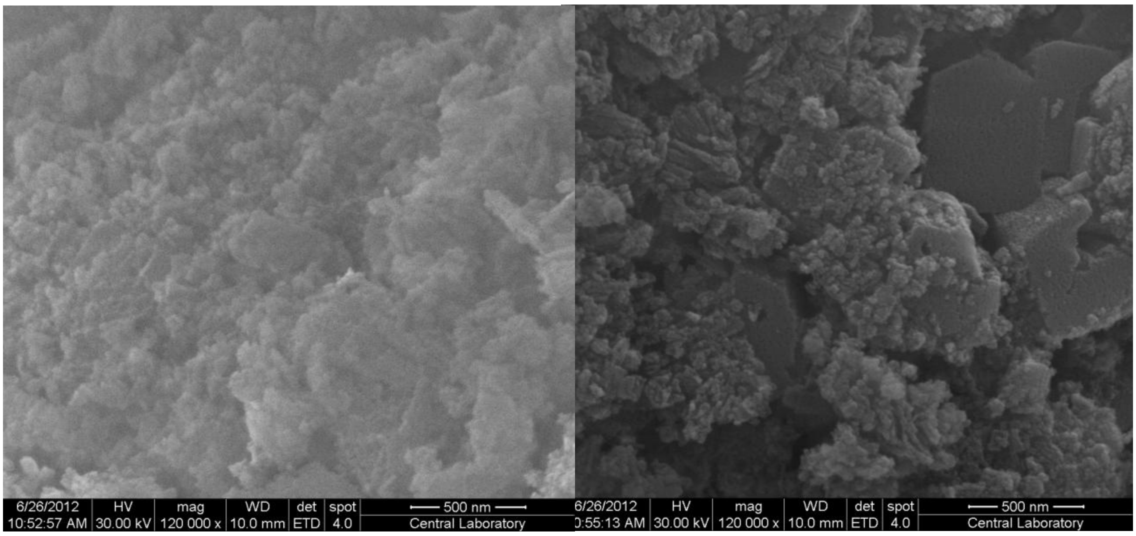

Figure 25. SEM images of copper, zinc, and zirconia containing co-precipitated catalyst, CZZr

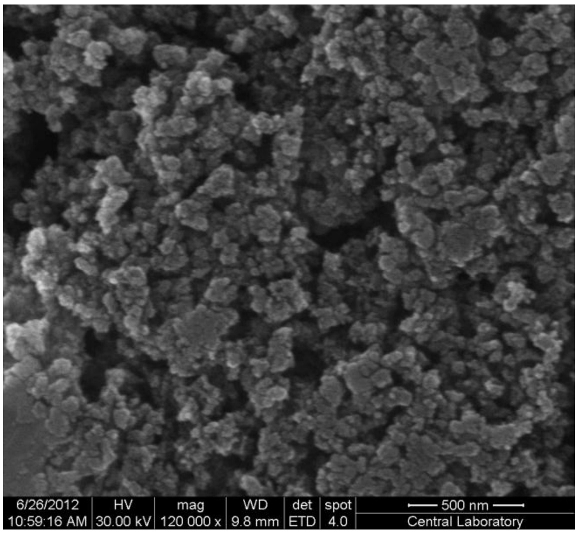

Figure 26. SEM images of copper, zinc, and ceria containing co-precipitated catalyst, CZCe

SEM images of copper, zinc, and alumina containing co-precipitated catalyst calcined at 550 °C is given in Figure 27. Upon calcination at high temperatures, small sized particles were agglomerated and two different sized fragments were observed. This could be attributed to the sintering.

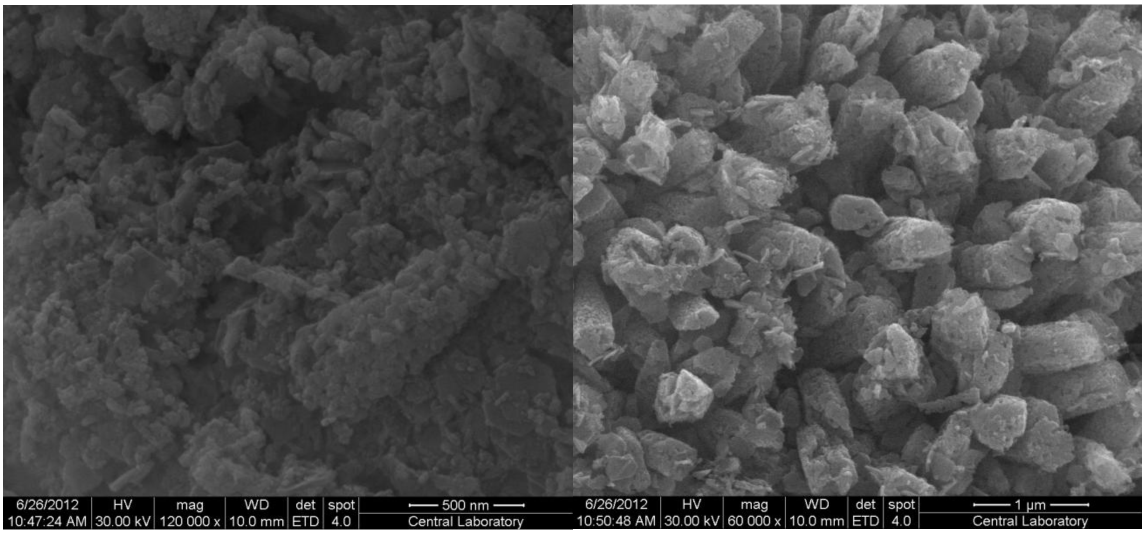

Figure 27. SEM images of copper, zinc, and alumina containing co-precipitated catalyst calcined at 550 °C, CZA-C550

SEM images of reduced catalyst at 225 °C are given in Figure 28 and reduced catalyst 250 °C is given in Figure 29. When compared to non-reduced catalyst, morphology changes to quasi-spherical particles were observed.

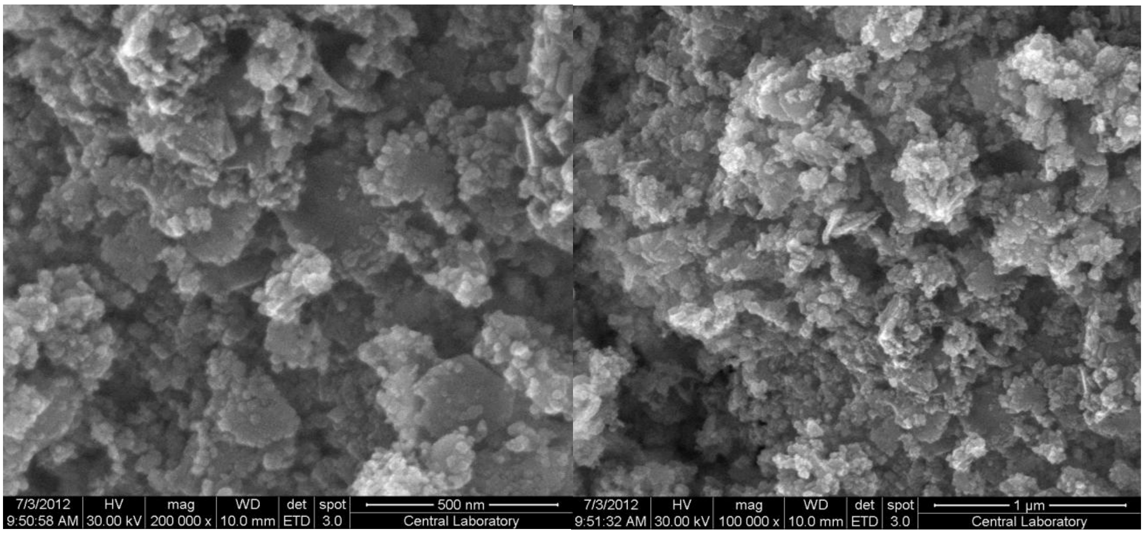

Figure 28. SEM images of copper, zinc, and alumina containing co-precipitated catalyst reduced at 225 °C, CZA-R225

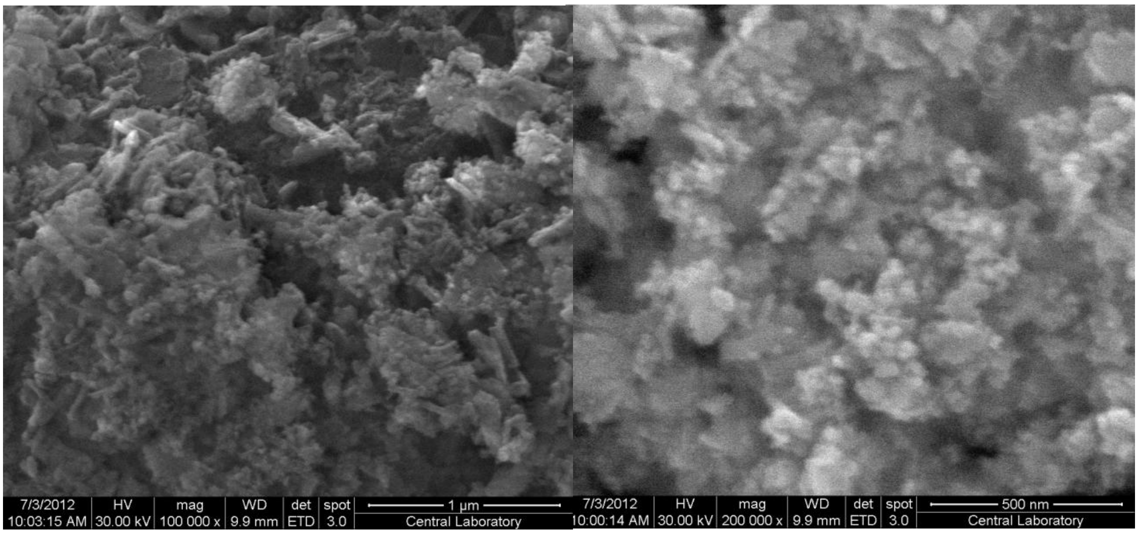

Figure 29. SEM images of copper, zinc, and alumina containing co-precipitated catalyst reduced at 250 °C, CZA-R250

SEM images of copper, zinc, and alumina containing co-precipitated catalysts aged for 6 hours are given in Figure 30 and aged for one hour is given in Figure 31. In 6 hours aged catalyst, rod-like structures with sharp corners were observed and uniformity was high. For 1 hour aged catalyst, similar morphology was obtained. However, uniformity in the 1 hour aged catalyst was lower and two different sized fragments could be easily seen. Based on these findings, it could be concluded that as aging time increased, uniformity enhanced.

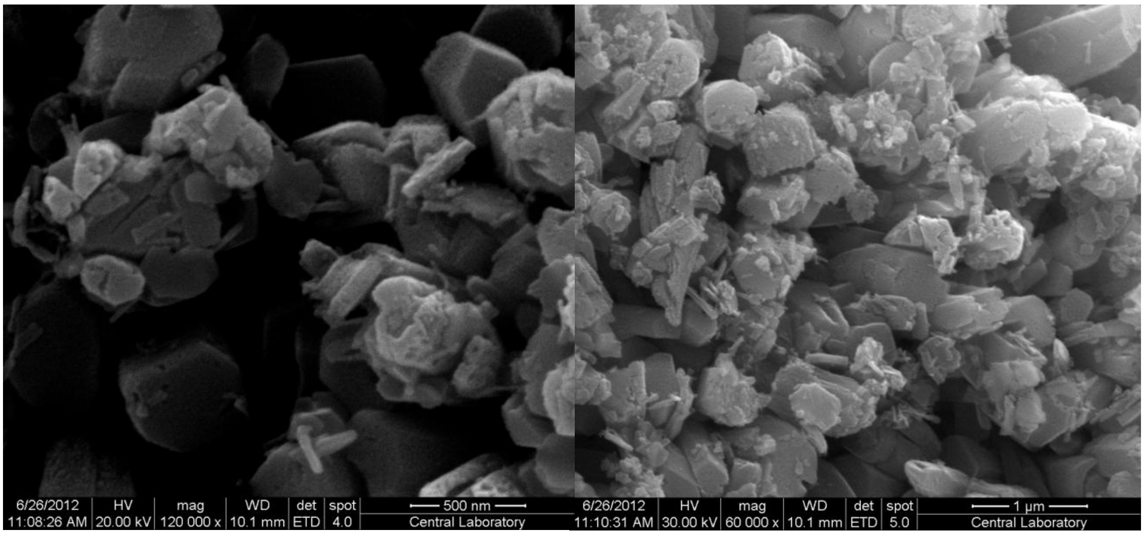

Figure 30. SEM images of copper, zinc, and alumina containing co-precipitated catalyst aged for 6 hours, CZA-6 hr

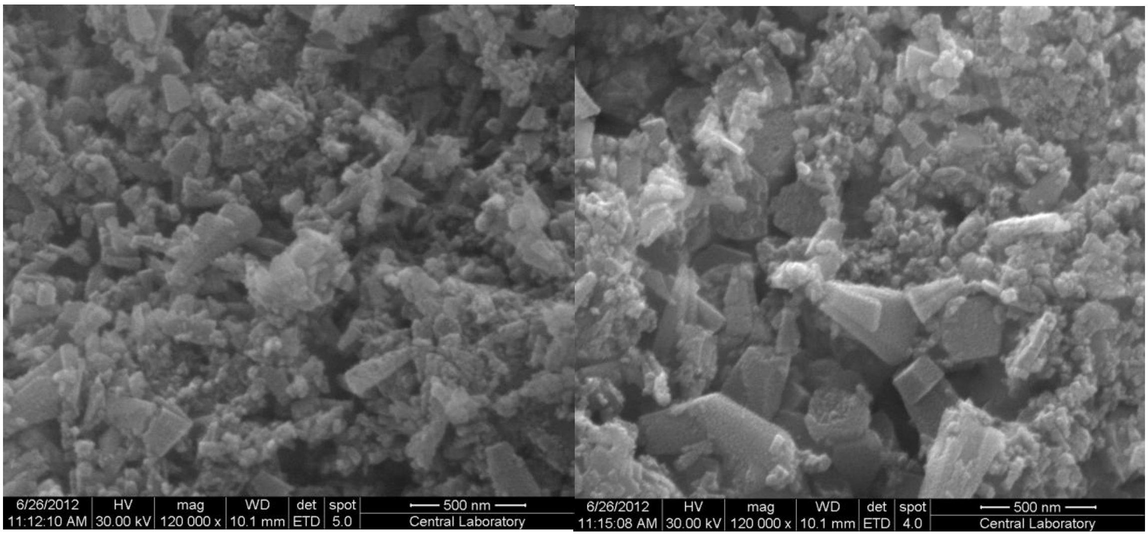

Figure 31. SEM images of copper, zinc, and alumina containing co-precipitated catalyst aged for 1 hour, CZA-1 hr

SEM images of copper, zinc, and alumina containing catalyst washed with hot deionized water are given in Figure 32. Formation of rod-like structures with sharp corners was observed. Upon washing with hot water, rod-like structures were favored.

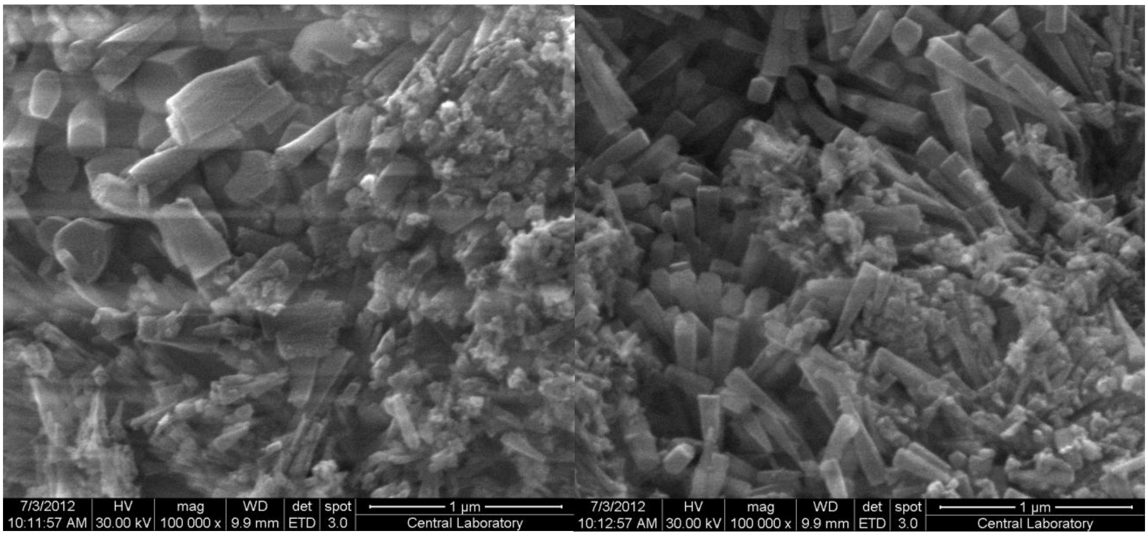

Figure 32. SEM images of copper, zinc, and alumina containing co-precipitated catalyst washed with hot water, CZA-Hot

Morphology of the bi-functional copper, zinc and alumina containing catalyst is illustrated with Figure 33. In the SEM images, similar morphology with other precipitated catalysts was obtained. Formation of rod-like structures with two different sized fragments were observed.

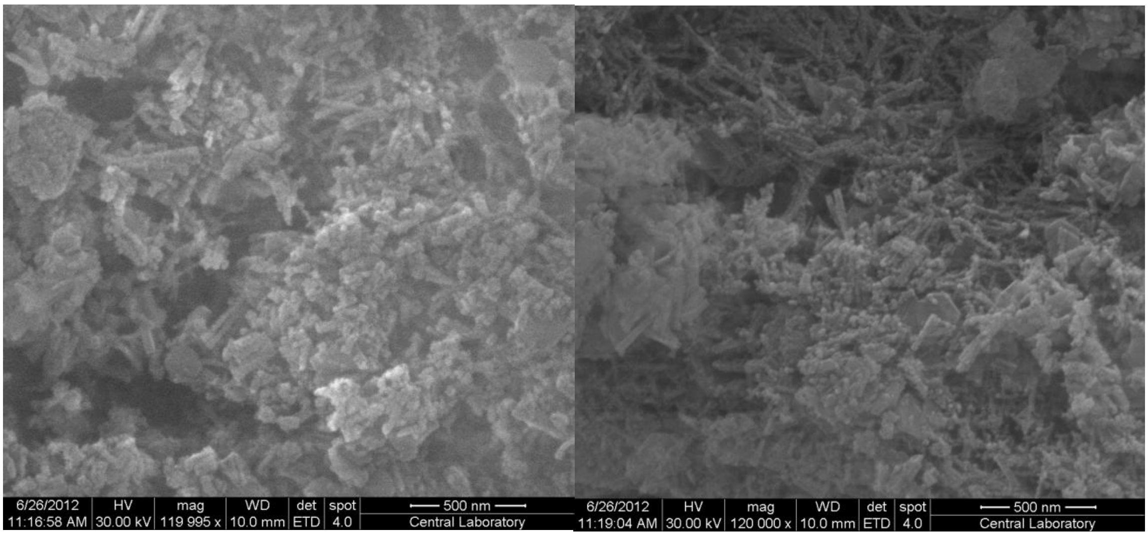

Figure 33. SEM images of bi-functional, copper, zinc, and alumina containing co-precipitated catalyst, H-CZA-TOYO

7.1.5. Diffuse reflectance infrared fourier transform spectroscopy of pyridine adsorption

DRIFTS analyses were made for copper, zinc containing co-precipitated catalyst CZ, copper, zinc, and alumina containing co-precipitated catalyst CZA, and bi-functional co-precipitated catalyst H-CZA-TOYO and absorbance results are given in Figure 34. As it can be seen from the figure, catalysts did not exhibit peaks in the wave number range of 1400 cm^{-1} – 1600 cm^{-1} due to non-presence of acidic sites. Pyridine adsorbed samples exhibits Levis acid site peak which appears at around 1450 cm^{-1}. Peak at 1490 cm^{-1} corresponds to the adsorption of pyridinium ions on the both Lewis and Brönsted acid sites. Peak at 1540 cm^{-1} is associated with the Brönsted acid sites of the catalysts [72]. No observance of peaks can be attributed to the low acidity of the catalysts.

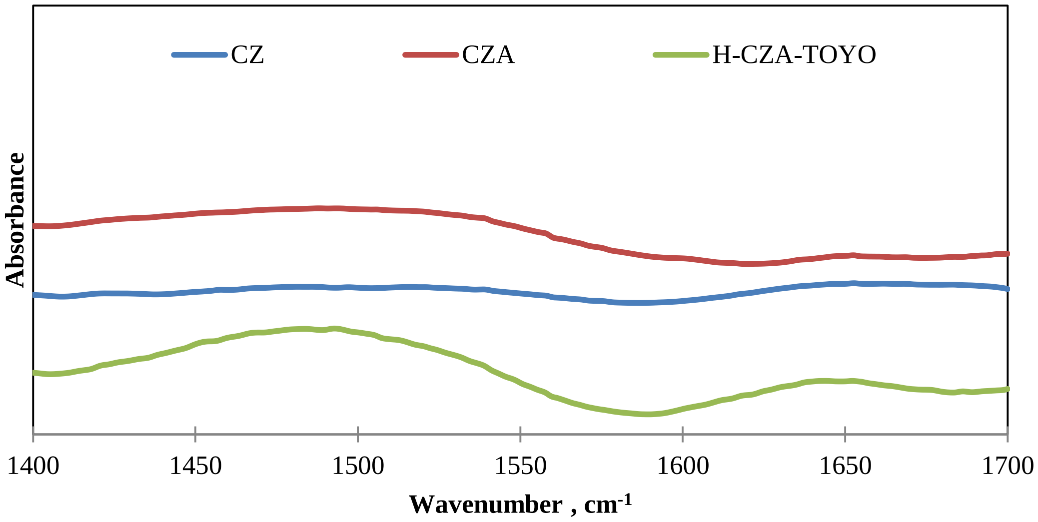

Figure 34. DRIFTS spectra of CZ, CZA, and H-CZA-TOYO catalysts

7.2. CHARACTERIZATION RESULTS OF STA IMPREGNATED SBA-15

In this part, characterizations of SBA-15 and STA impregnated sample have been done and results were also reported in elsewhere [69].

7.2.1. X-Ray Diffraction (XRD)

SBA type materials were characterized in order to analyze their structural and physical properties. The X-Ray diffraction patterns of the synthesized SBA-15 support and STA impregnated SBA-15 catalyst having W/Si molar ratio of 1 (STA@SBA-15) were analyzed and given in Figure 35 and Figure 36.

Low angle XRD pattern of SBA support (Figure 35) showed that synthesis of SBA-15 was successfully accomplished. When the small angle X-Ray diffraction pattern of pure SBA-15 is compared with the STA@SBA-15, low angle reflection peaks could no longer be observed. Loss of reflection peaks indicated that high STA loading resulted in poorer mesoscale ordering and destruction of mesostructure. For the high angle XRD diffraction (Figure 36), no diffraction line for STA was seen, indicating the well dispersion of STA within the silicate based support of SBA-15.

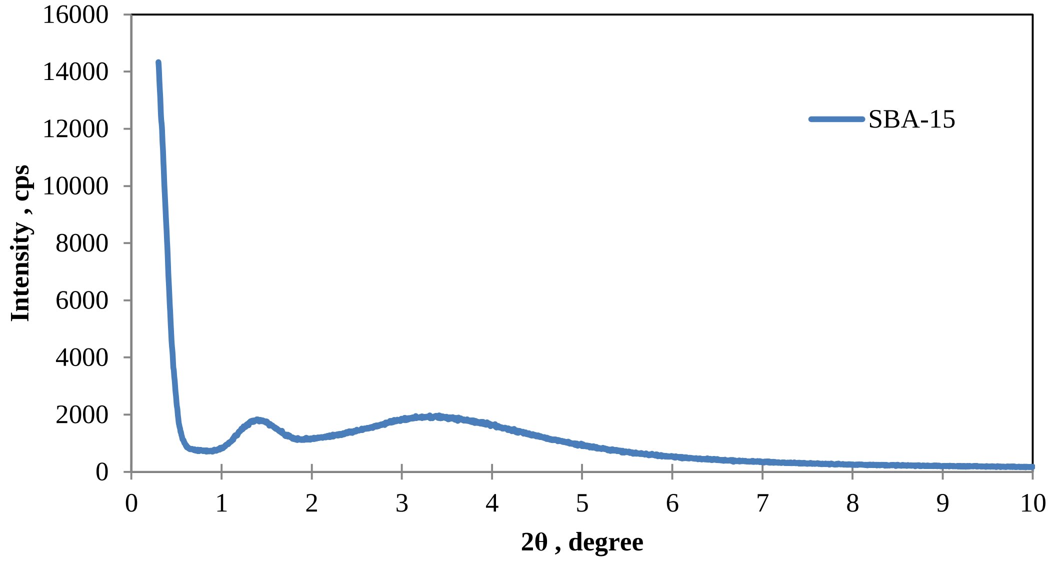

Figure 35. Low angle XRD pattern of SBA-15

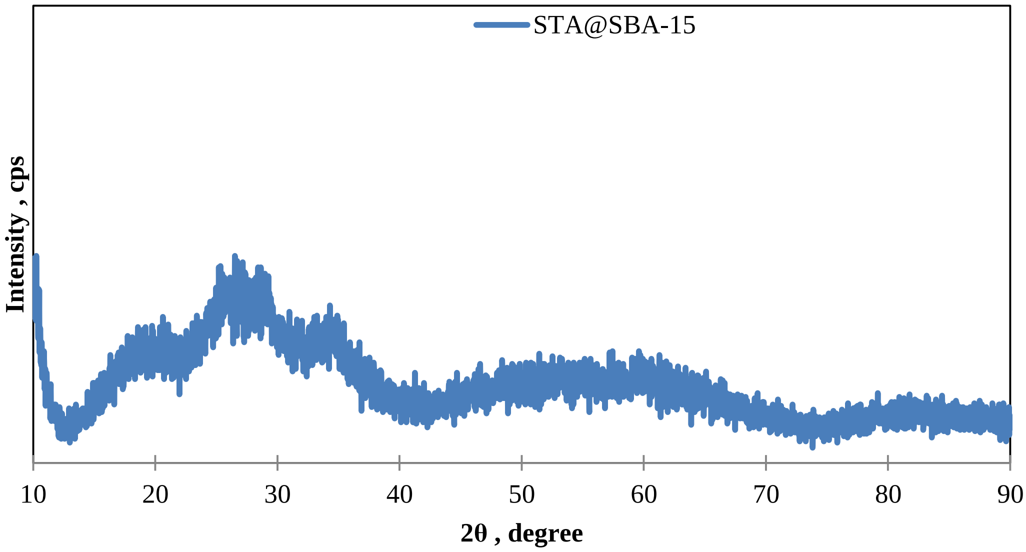

Figure 36. High angle XRD pattern of STA impregnated SBA-15.

7.2.2. Nitrogen Physisorption

The textural properties such as multipoint BET surface area, pore volume and pore diameter of synthesized materials were obtained with the nitrogen physisorption analyses and presented in Table 20. Support material SBA-15 had a promising BET surface area of 808.2 m^2/g with a pore diameter of 7.82 nm which is in the mesoporous region. Upon the impregnation of STA onto the SBA-15 support, huge amount of surface area was lost due to the blockage of pores with STA.

Table 20. Nitrogen physisorption results of SBA-15 and STA@SBA-15

	Multipoint BET Surface area , m^2/g	**BJH Method Desorption Pore Volume , cc/g**	**BJH Method Desorption Pore Diameter , nm**
SBA-15	808.20	1.33	7.82
STA@SBA-15	72.69	0.13	7.65

The nitrogen isotherms and the pore size distributions of pure SBA-15 and STA impregnated SBA-15 is plotted in Figure 37 and 38, respectively. Type IV hystherisis loop is observed with both SBA-15 and STA@SBA-15 indicating the mesoporous structure of the materials. The adsorption amount of nitrogen considerably differed between SBA-15 and STA@SBA-15. This was also consistent with the decrease of the pore volume from 1.33 cc/g to 0.13 cc/g. Also, the desorption band was shifted to a higher relative pressure after STA impregnation suggesting a partial loss of structural organization and the formation of some narrower pores. Nevertheless, the main part of this hysteresis is still between P/P_0 values of 0.6-0.8.

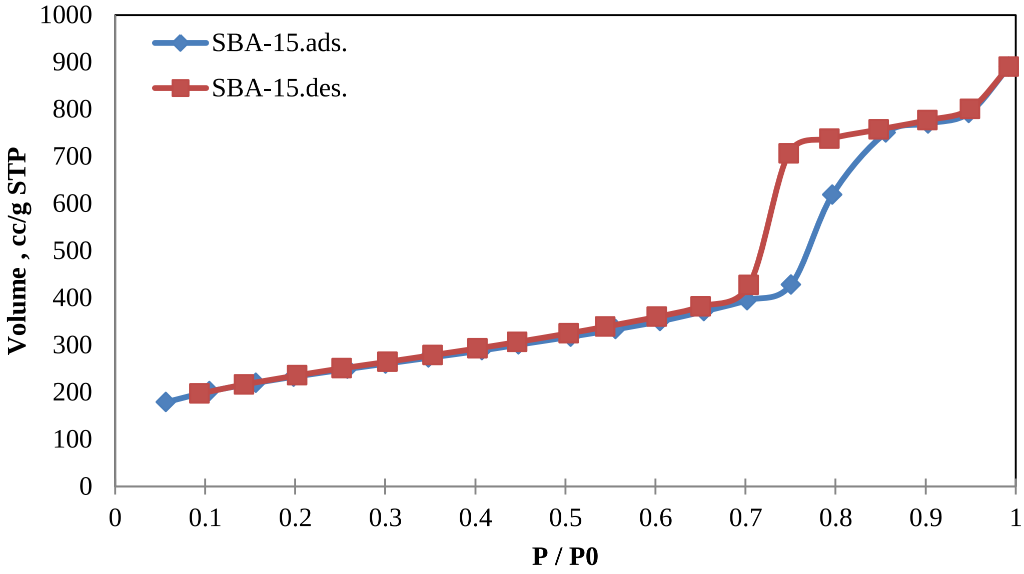

Figure 37. Adsorption- desorption isotherm of SBA-15

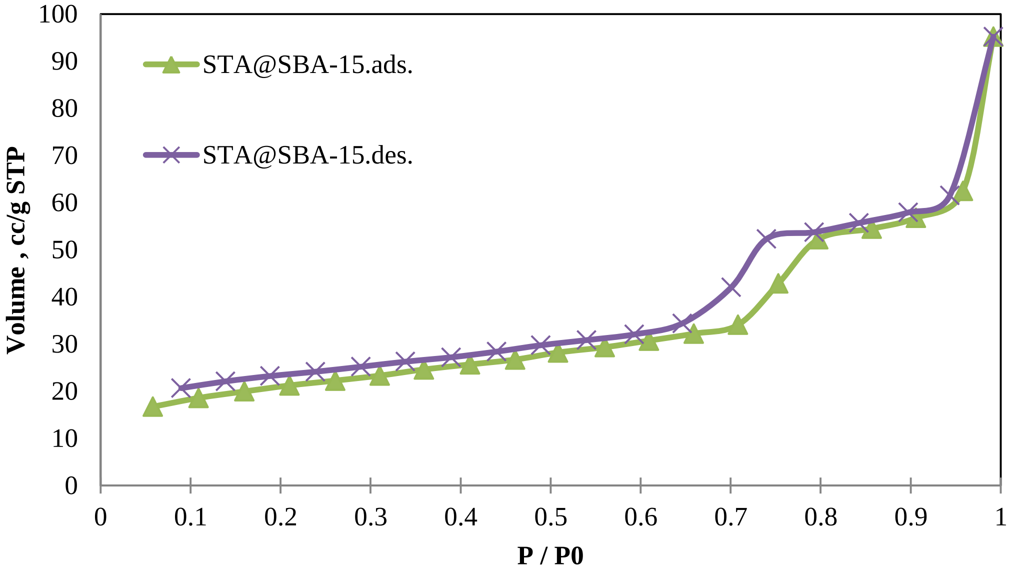

Figure 38. Adsorption- desorption isotherm of STA@SBA-15

7.2.3. Diffuse reflectance infrared fourier transform spectroscopy of pyridine adsorption

DRIFTS analysis was made for STA impregnated SBA-15 catalyst, STA@SBA-15, and acidity results are given in Figure 39. As it can be seen from the figure, catalyst exhibited Levis acid site peak which appeared at around 1438 cm^{-1}. At 1485 cm^{-1}, peak corresponding to the adsorption of pyridinium ions on the both Lewis and Brönsted acid sites was obtained. Last peak was obtained at 1538 cm^{-1} due to the Brönsted acid sites of the catalysts [72]. STA impregnated SBA-15 catalyst had strong acidity and Brönsted acid sites were stronger than Lewis acid sites.

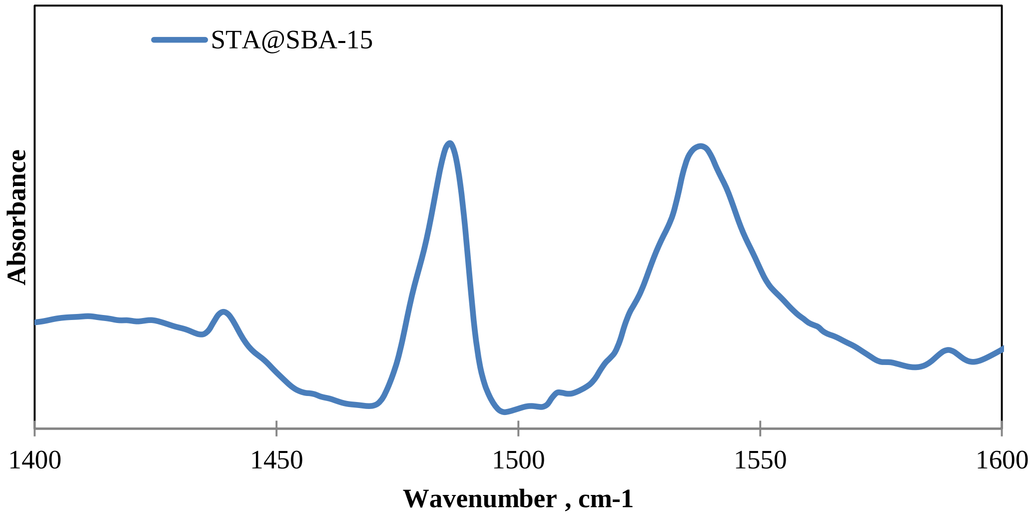

Figure 39. DRIFTS spectra of STA impregnated SBA-15 catalyst (STA@SBA-15)

7.3. CHARACTERIZATION RESULTS OF COMMERCIAL γ-Al_2O_3 CATALYST

7.3.1. X-Ray Diffraction

XRD characterization technique was applied to TOYO catalyst and high angle X-ray diffraction results are given in Figure 40. Toyo was composed of γ-Al_2O_3 alumina and all reflection peaks of it were observed. Particle size of γ-Al_2O_3 calculated from Scherrer's equation was 4.8 nm.

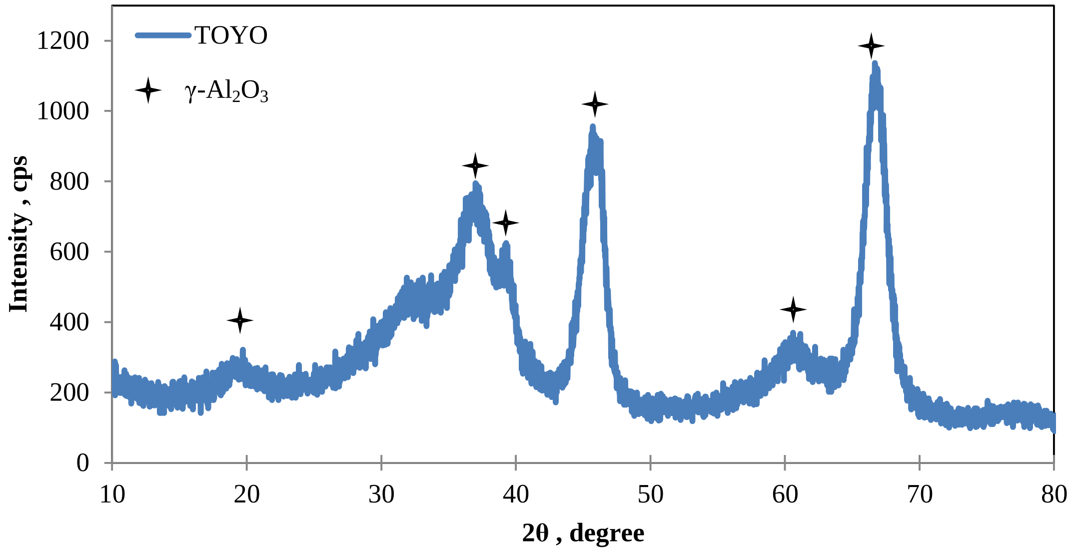

Figure 40. X-Ray diffraction pattern of commercial methanol dehydration catalyst TOYO

7.3.2. Nitrogen Physisorption

Nitrogen physisorption characterization exhibited that TOYO catalysts had a BET surface area of 147.7 m^2/g. It has a pore volume of 0.57 cc/g with a pore diameter of 9.5 nm, which was within the mesopores region. Pore size distribution of the catalysts is given in Figure 41. Narrow pore size distributions at around average pore diameter of 9 nm were obtained. Moreover, adsorption desorption isotherms TOYO is shown in Figure 42.

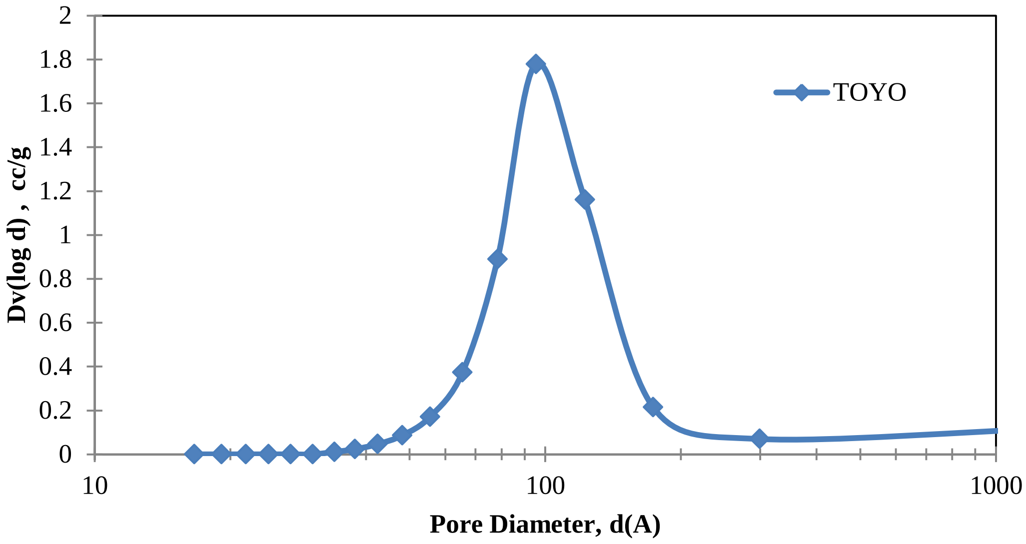

Figure 41. Pore size distributions of methanol dehydration catalyst TOYO

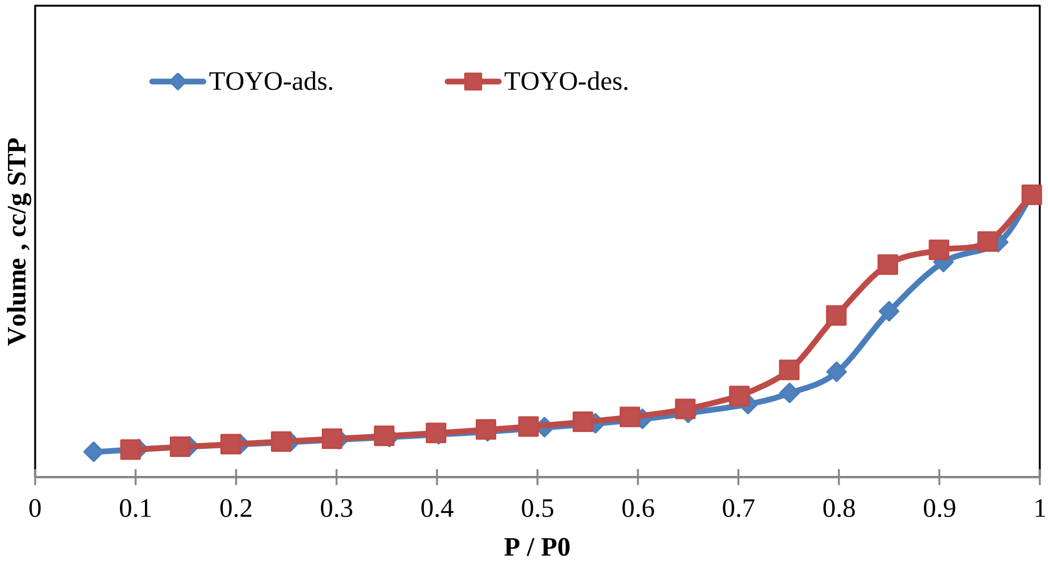

Figure 42. Adsorption–desorption isotherm of methanol dehydration catalyst TOYO

7.3.3. Energy Dispersive Spectroscopy (EDS)

EDS results of TOYO confirmed that only alumina was present within the material.

7.3.4. Scanning Electron Microscopy (SEM)

SEM images of commercial methanol dehydration catalyst TOYO is given in Figure 43.

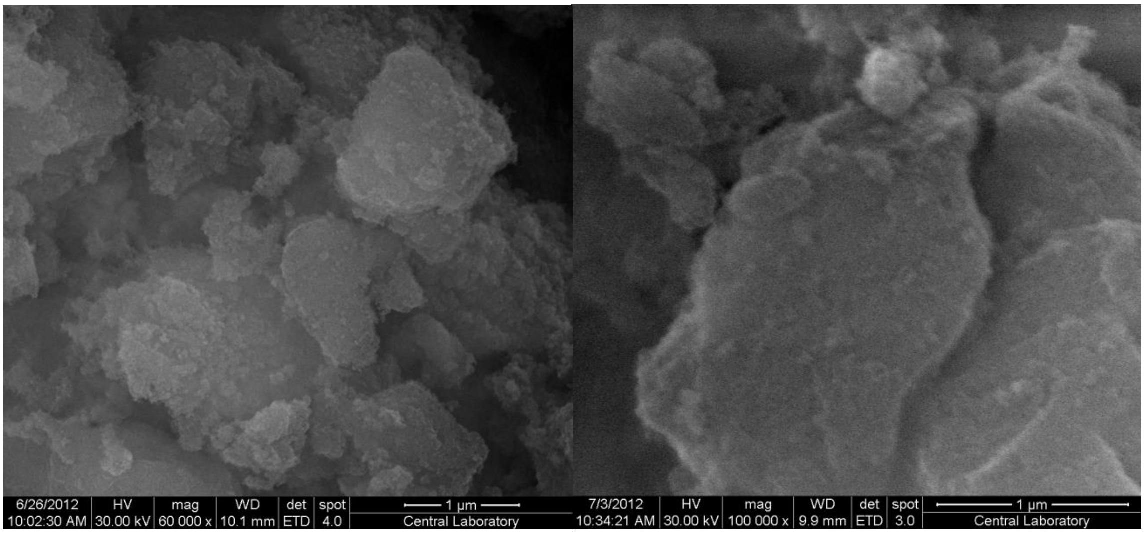

Figure 43. SEM images of methanol dehydration catalyst TOYO

7.3.5. Diffuse reflectance infrared fourier transform spectroscopy of pyridine adsorption

DRIFTS analysis was made for commercial γ-Al_2O_3 TOYO catalyst and DRIFT spectra is given in Figure 44. TOYO catalyst did not exhibit peaks in the wave number range of 1400 cm^{-1} – 1600 cm^{-1} due to non-presence of Brönsted and Lewis acidic sites. No observance of peaks can also be attributed to the low acidity of the catalysts.

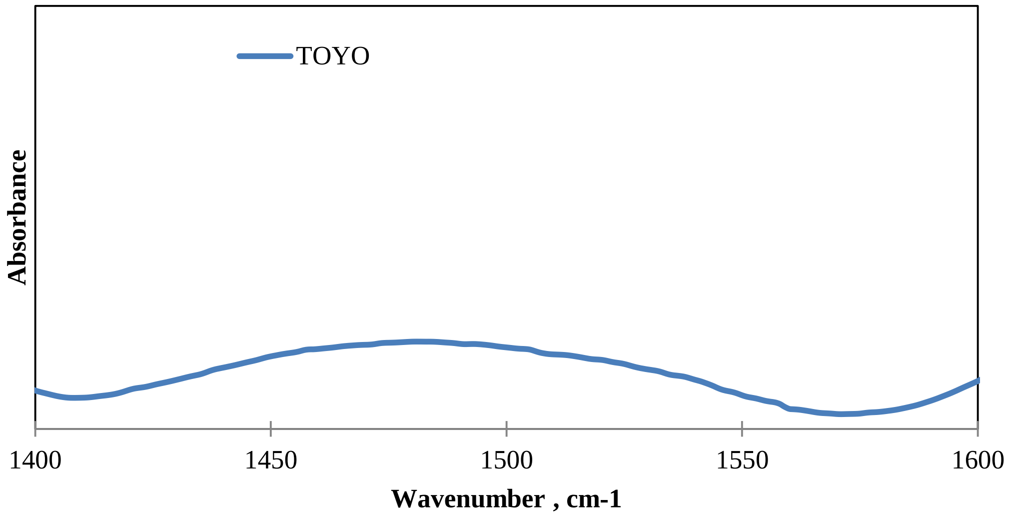

Figure 44. DRIFTS spectra of methanol dehydration catalyst TOYO

7.4. CHARACTERIZATION RESULTS OF COMMERCIAL METHANOL REFORMING CATALYST, MRC, AND METHANOL SYNTHESIS CATALYST, MSC

7.4.1. X-Ray Diffraction (XRD)

High angles X-Ray diffraction patterns of methanol reforming catalyst, MRC, and methanol synthesis catalyst, MSC (Figure 45) were recorded and the peaks were identified as the diffraction lines of SiO_2, CuO, and ZnO. Silicon oxide peak was observed at around 26° and ZnO and CuO peaks were obtained at similar positions to the synthesized methanol synthesis co-precipitated catalysts. Diffraction peaks for MRC and MSC were wide and not well defined, indicating well dispersion of metal and metal oxides.

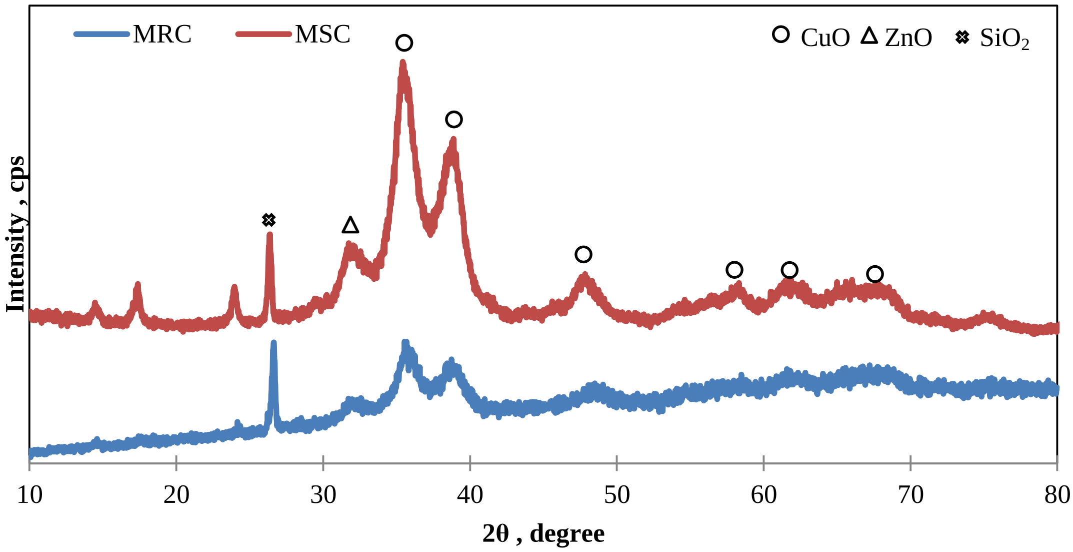

Figure 45. X-Ray diffraction patterns of methanol reforming catalyst, MRC, and methanol synthesis catalysts, MSC.

The mean particle sizes of the CuO, ZnO, and SiO_2 were calculated by Scherrer's equation and results are given in Table 21. As it can be seen from the table, there was no change of particle size of silica. However, smaller particle sizes were obtained in the methanol synthesis catalyst, MSC.

Table 21. Particle sizes of methanol reforming catalyst, MRC, and methanol synthesis catalysts, MSC.

	d_{CuO} , nm	**d_{ZnO} , nm**	**d_{SiO_2} , nm**
MRC	6.5	6.4	29.3
MSC	4.6	3.4	29.8

7.4.2. Nitrogen Physisorption

Nitrogen physisorption technique was applied to methanol synthesis catalyst and methanol dehydration catalyst and information about BET surface area, pore volume and pore diameter were obtained and given in Table 22. Methanol synthesis catalyst

MSC is better than the methanol reforming catalyst MRC in terms of textural properties. MSC catalyst had a BET surface area of 100 m^2/g with a pore size of 6.51 nm which is in the mesoporous materials region.

Table 22. Nitrogen physisorption results of MRC and MSC

	Multipoint BET Surface area , m^2/g	**BJH Method Desorption Pore Volume , cc/g**	**BJH Method Desorption Pore Diameter , nm**
MRC	67.55	0.20	3.81
MSC	99.47	0.24	6.51

Adsorption-desorption isotherms of the commercial catalysts are given in Figure 46.

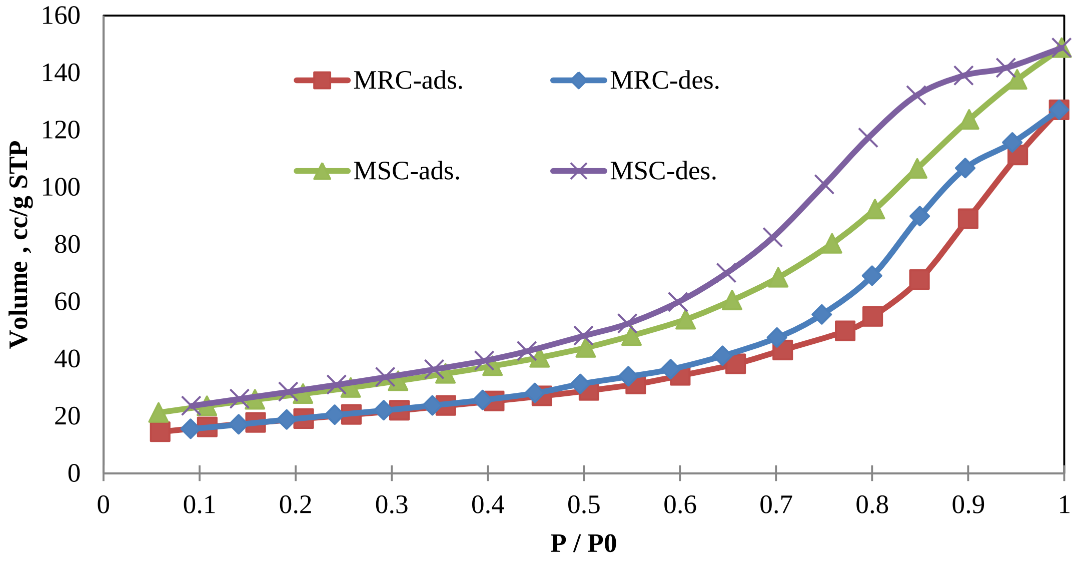

Figure 46. Adsorption-Desorption isotherm of commercial catalysts MRC and MSC

7.4.3. Energy Dispersive Spectroscopy (EDS)

The results of EDS analyses for commercial catalysts are given in Table 23. It has been found that methanol synthesis catalyst contains more alumina than the methanol reforming catalysts. Moreover, no silica was found by EDS analyses.

Table 23. EDS results of MRC and MSC

	Copper , moles %	**Zinc , moles %**	**Alumina , moles %**
MRC	53.4	28.5	18.1
MSC	54.6	21.1	24.3

7.4.4. Scanning Electron Microscopy (SEM)

SEM images of commercial methanol reforming catalyst, MRC, is given in Figure 47 and methanol synthesis catalyst, MSC, is given in Figure 48. SEM images of MSC and MRC revealed that very small particles were formed and much larger particles were also observed.

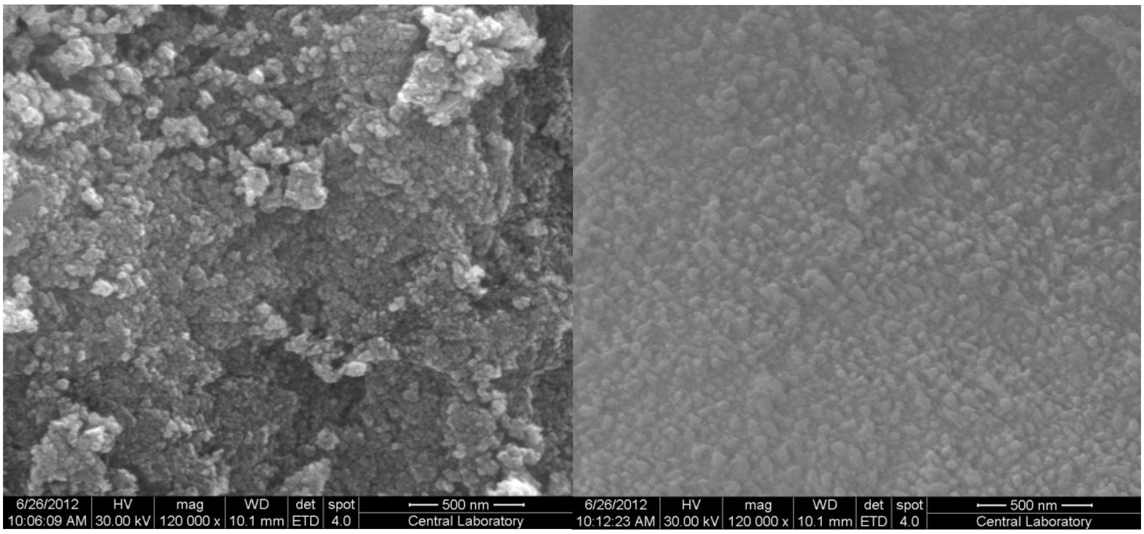

Figure 47. SEM images of commercial methanol reforming catalyst, MRC

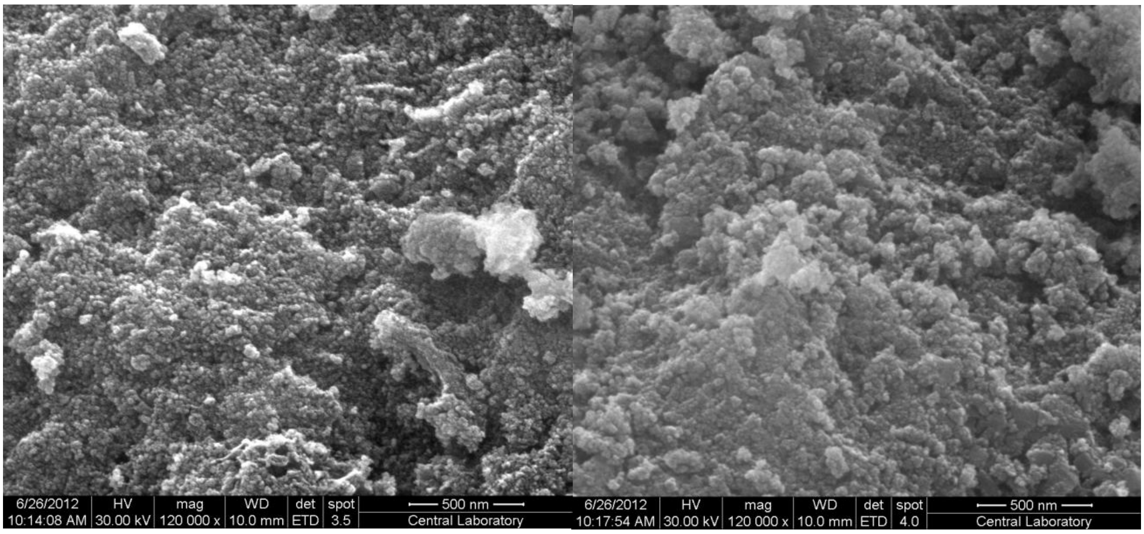

Figure 48. SEM images of commercial methanol synthesis catalyst, MSC

7.4.5. Diffuse reflectance infrared fourier transform spectroscopy of pyridine adsorption

DRIFTS analyses were made for commercial methanol synthesis catalyst, MSC, and methanol reforming catalyst, MRC. DRIFT spectra of these catalysts are given in Figure 49. TOYO catalyst did not exhibit peaks in the wave number range of 1400 cm^{-1} – 1600 cm^{-1} due to non-presence of Brönsted and Lewis acidic sites. No observance of peaks can also be attributed to the low acidity of the catalysts.

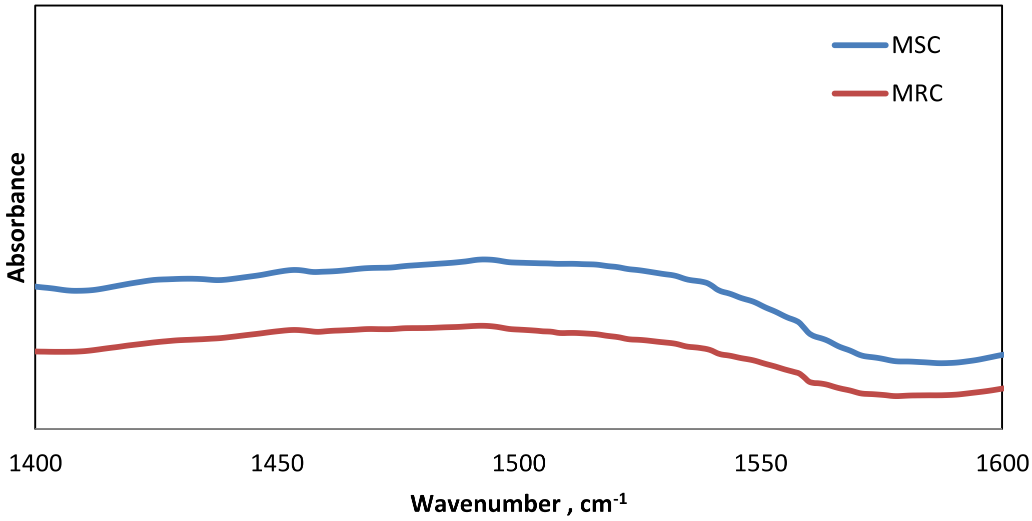

Figure 49. DRIFTS spectra of commercial methanol synthesis catalyst, MSC, and methanol reforming catalyst, MRC.

CHAPTER 8

ACTIVITY RESULTS

In this part, activity results of characterized catalysts are given in the direct synthesis of DME. Since some catalysts are methanol synthesis catalysts, some are methanol dehydrations catalysts, or direct DME synthesis catalysts, their activities are given on the basis of what they are responsible for. The carbon monoxide and carbon dioxide conversions (when applicable) and selectivity of the products are given in graphical forms as a function of temperature.

8.1. ACTIVITY RESULTS OF COMMERCIAL CATALYSTS

Activity results of commercial methanol reforming catalyst and methanol synthesis catalyst were made for different flow rates and different reactant gas mixtures. Methanol reforming catalyst was obtained from the Alfa- Aesar and denoted as “MRC” whereas methanol synthesis catalyst was also obtained from the Alfa – Aesar and denoted as “MSC”. Characterization results of these commercial catalysts were discussed in Section 7.4. Activity test of MSC was done in another study at the same experimental set-up and experimental data was taken for the comparative purposes [8].

8.1.1. Activity results of MRC from Mixture-1 ($CO:H_2=50:50$)

Activity tests of MRC were conducted for methanol synthesis from the syngas. Since there was no methanol dehydration component, methanol formation was expected, mainly.

For the equimolar feed mixture ($CO:H_2=1:1$), namely Mixture-1, the activity test was carried at 50 bar and in a temperature range of 200 ºC – 400 ºC. Reactant flow rate was adjusted to 50 cc/min (at standard temperature and pressure) for the 0.2 gr catalyst. Carbon monoxide conversion values are given in the Figure 50.

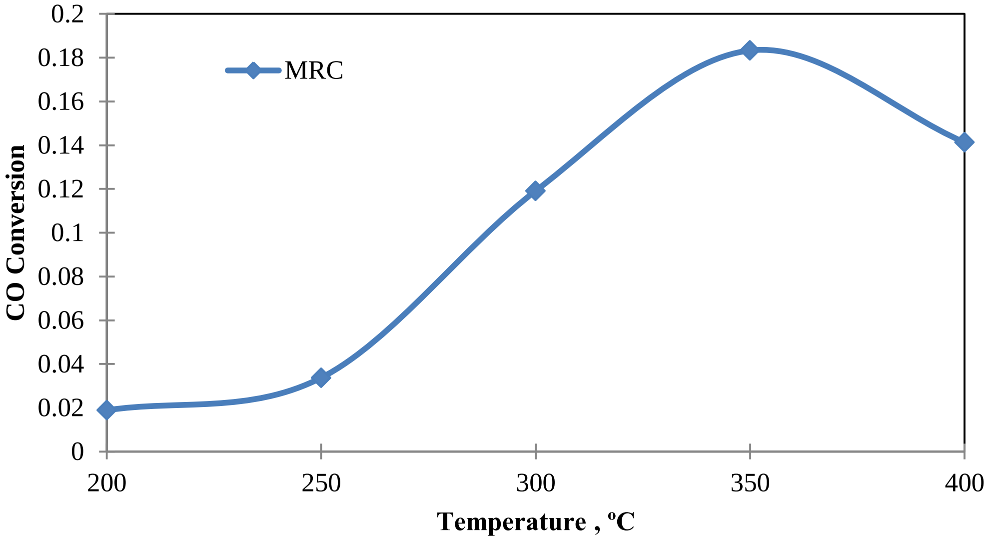

Figure 50. Carbon monoxide conversion values obtained with methanol reforming catalyst, MRC, (Space time of 0.24 s.gr/cc, catalyst amount: 0.2 gr, Mixture-1 feed stream: 50% CO + 50% H_2)

As it can be seen from Figure 50, carbon monoxide conversions increased with increasing temperature until 350 °C. At 350 °C, 18.3% conversion was obtained and after this temperature and a decrease was observed at 400 °C. In the methanol synthesis, catalysts are usually active in the temperature range of 250 °C – 275 °C. For this temperature range, catalytic activity varied from 3.4% to 8.0%.

Product distribution of methanol reforming catalyst, MRC, is given in Figure 51. As it can be seen from the figure, most abundant product was methanol for the temperature range of 200 °C to 300 °C. The selectivity of methanol was very high as 93.7% at 200 °C and it was reduced to 67.3% at 300 °C. As temperature increased, methanol selectivity decreased since methanol synthesis is an exothermic reaction. Formations of side products were observed at high temperatures. Starting from 250

°C, some methanol was converted to the dimethyl ether at a selectivity value of nearly 15%. After 300 °C, carbon dioxide and methane formation increased in a similar fashion. This could be attributed to the reverse dry reforming of methane, reaction 7.

$$2CO + 2H_2 \rightarrow CH_4 + CO_2 \qquad [7]$$

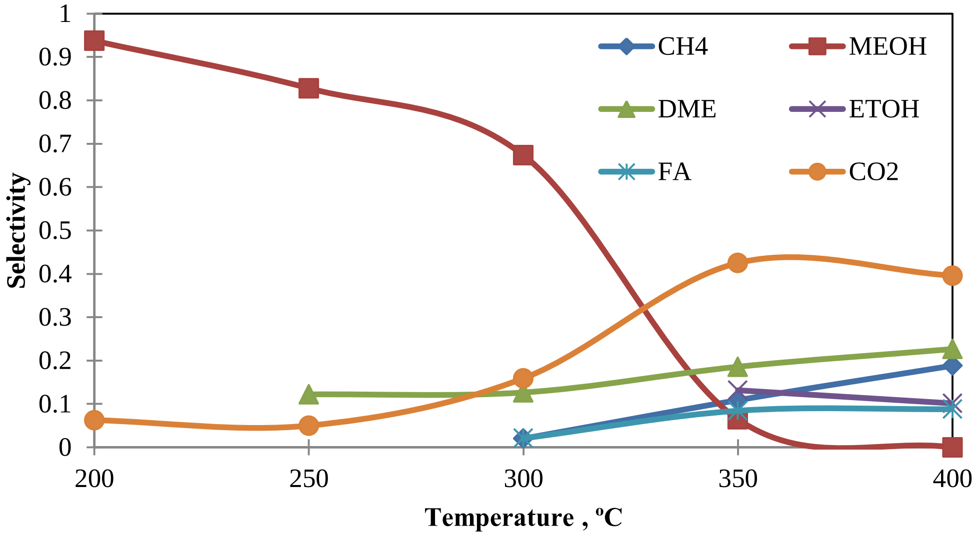

Figure 51. Product distribution obtained with methanol reforming catalyst, MRC, (Space time of 0.24 s.gr/cc, catalyst amount: 0.2 gr, Mixture-1 feed stream: 50% CO + 50% H_2)

Deactivation of the copper, zinc, and alumina based catalyst affects the conversion and product distribution. Deactivation is mainly because of the sintering of the copper particles at temperatures higher than 300 °C [24]. Conversion decrease of MRC catalyst after 350 °C could be due to the sintering. Decrease of methanol selectivity was mainly because of the exothermic nature of thermodynamically limited methanol synthesis reactions.

For the same catalyst, MRC, another study was done by changing the reactant gas flow rate. Activity test was conducted for a temperature range of 200 °C - 400 °C at

50 bar and for the mixture-1 ($CO:H_2$=1:1). When the flow rate of reactant gas was changed from 50 cc/min to 25 cc/min, conversion values came out to be nearly same as it can be seen from Figure 52.

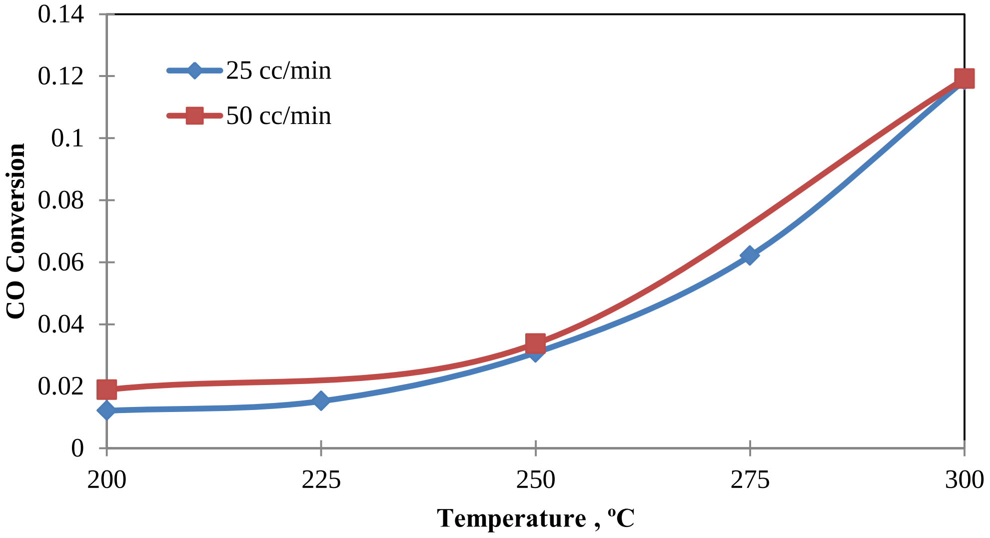

Figure 52. Comparison of carbon monoxide conversion values obtained with methanol reforming catalyst, MRC, for reactant gas flow rate of 25 cc/min and 50 cc/min. (catalyst amount: 0.2 gr, Mixture-1 feed stream: 50% CO + 50% H_2)

When it comes to product distribution which is shown in Figure 53, lowering the reactant flow rate did not change methanol selectivity significantly. For the lower flow rate, more robust selectivity values were obtained at the temperature range of 200 °C to 275 °C. Even at 300 °C, methanol selectivity was 63.2%. DME synthesis was started at 225 °C whereas DME synthesis was first observed at 250 °C for the reactant flow rate of 50 cc/min.

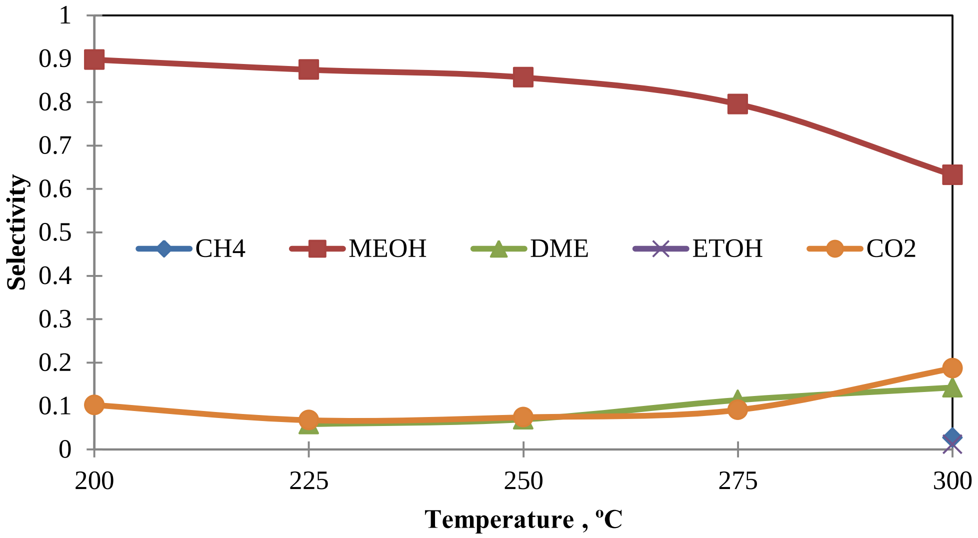

Figure 53. Product distribution obtained with methanol reforming catalyst, MRC, for reactant gas flow rate of 25 cc/min (Space time of 0.48 s.gr/cc, catalyst amount: 0.2 gr, Mixture-1 feed stream: 50% CO + 50% H_2)

8.1.2. Activity results of MRC from Mixture-2 ($CO:CO_2:H_2$=40:10:50)

Last activity test of MRC is with carbon dioxide containing feed gas mixture (40% CO, 10% CO_2, and 50% H_2). When the product distribution of MRC catalyst with mixture-1 was examined, it was seen that there was carbon dioxide as a major side product at all temperatures. Based on the product distribution of MRC, it was proposed that having a small amount of carbon dioxide in the feed mixture could prevent the formation of carbon dioxide according to Le chatelier principle. Presence of carbon dioxide in the feed mixture could also prevent the formation of methane by inhibiting reverse methane dry reforming.

When the activity test was made with a feed mixture of $CO:CO_2:H_2$=4:1:5, namely mixture-2, at 50 bar, very high conversion values were obtained as compared to the equimolar feed of CO and H_2. This could be seen from Figure 54. For the mixture-2, 49.2% carbon monoxide conversion was obtained at 350 °C whereas conversion was 18.3% for the activity with the feed gas of mix-1 at the same temperature.

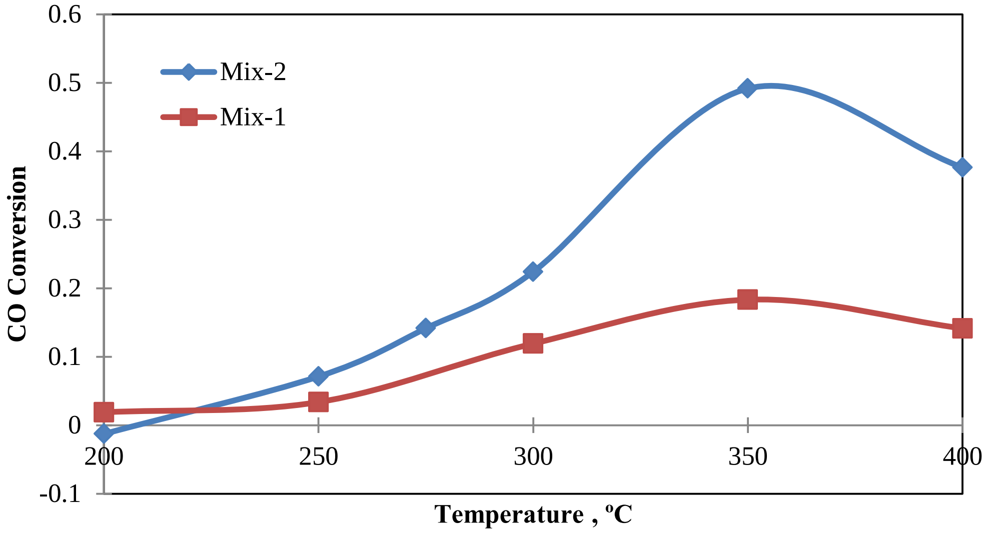

Figure 54. Comparison of carbon monoxide conversion values obtained with methanol reforming catalyst, MRC, for the mixture-1 (50% CO + 50% H_2) and mixture-2 (40% CO, 10% CO_2, 50% H_2) (Space time of 0.24 s.gr/cc, catalyst amount: 0.2 gr)

At 200 °C, activity with carbon dioxide containing feed gas, Mix-2, gave negative carbon monoxide conversion. The reason why carbon monoxide conversion was negative is because of the presence of carbon dioxide in the feed. Carbon dioxide acted as a feed and carbon monoxide was a product rather than a reactant at 200 °C. Carbon dioxide conversion with respect to temperature is given in Figure 55 for methanol reforming catalyst and carbon dioxide conversion was positive from 200 °C to 250 °C. Effluent gas of MRC was composed of only carbon monoxide and carbon dioxide as carbon containing products at 200 °C. When these results were considered, it was concluded that reverse water gas shift reaction was occurring since carbon dioxide was converted to carbon monoxide in the presence of H_2.

$$CO_2 + H_2 \rightarrow CO + H_2O \qquad [8]$$

After 250 °C, more carbon dioxide was emerged from the reactor than it was fed to it and for this reason; negative conversion of carbon dioxide was obtained.

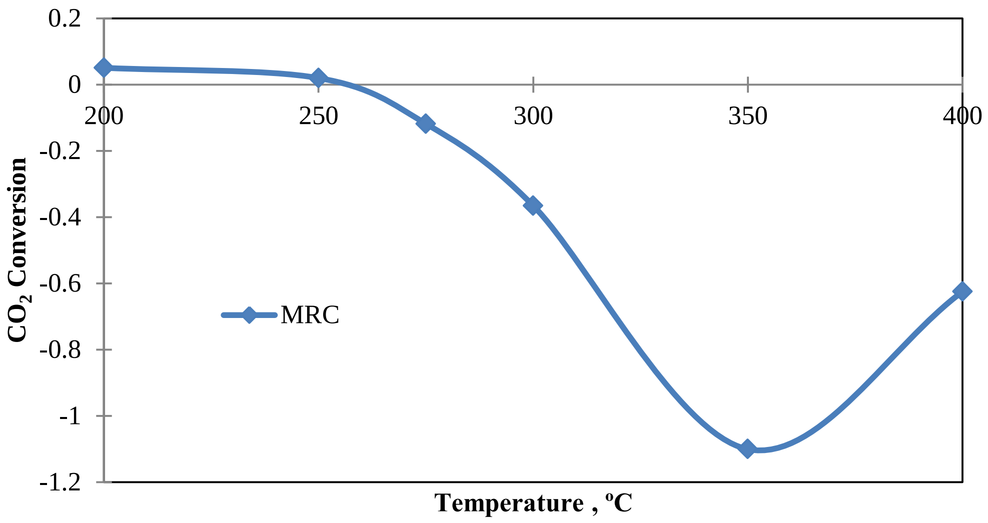

Figure 55. Carbon dioxide conversion values obtained with methanol reforming catalyst, MRC, (Space time of 0.24 s.gr/cc, catalyst amount: 0.2 gr, Mixture-2 feed stream: 40% CO, 10% CO_2, 50% H_2)

Selectivities which were calculated with respect to carbon monoxide for mixture-2 are given in Figure 56. Since there is no carbon containing product rather than CO and CO_2 at 200 °C in the effluent gas, selectivities were zero. As temperature increased, formations of other products were observed. At 250 °C, there is still positive carbon dioxide conversion and carbon monoxide conversion was changed from negative to positive, which means both carbon monoxide and carbon dioxide were reactants at 250 °C. Because of this reason, selectivity definitions must be made with respect to overall carbon content at 250 °C. That is, selectivities were defined with respect to total moles of converted CO+CO_2. Overall selectivities calculated with respect to total carbon are given in Table 24. Sample conversion and selectivity calculations are given in Appendix B.

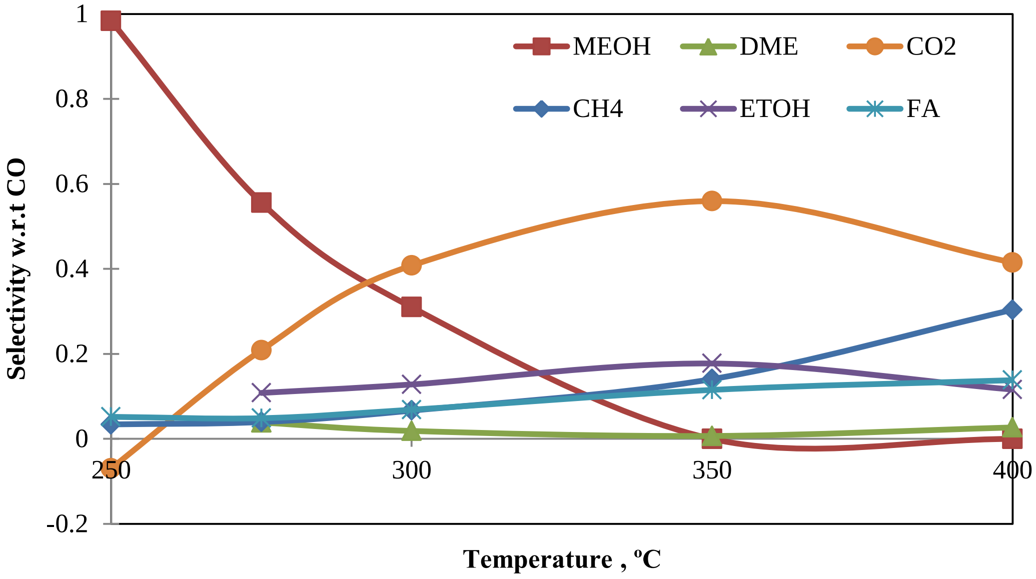

Figure 56. Product distribution obtained with methanol reforming catalyst, MRC, which were calculated with respect to carbon monoxide at a space time of 0.24 s.gr/cc for Mixture-2: 40% CO, 10% CO_2, 50% H_2)

Due to the exothermic nature of the methanol synthesis reaction, selectivity of methanol decreases as temperature increases. Starting from 300 °C, carbon dioxide was the most abundant gas in the product line and formation of formic acid was observed.

Table 24. Overall selectivities obtained with methanol reforming catalyst, MRC, which were calculated with respect to converted CO&CO_2 at temperature of 250 °C and a space time of 0.24 s.gr/cc for Mixture-2: 40% CO, 10% CO_2, 50% H_2)

	Methanol	Methane	Formic Acid
Overall Selectivity	91.9%	3.2%	4.9%

8.1.3. Activity results of MSC from Mixture-1 ($CO:H_2$=50:50)

Activity tests were conducted with commercial methanol synthesis catalyst, denoted as "MSC", at 50 bar. The studied temperature range was 200 °C - 300 °C and feed gas was the equimolar mixture of carbon monoxide and hydrogen. The reactant gas flow rate was 25 cc/min.

The comparison of carbon monoxide conversion with respect to temperature for the MSC and MRC is given in Figure 57. Based on the carbon monoxide conversion results, nearly same carbon monoxide conversions were obtained. However, at 200 °C, methanol synthesis catalyst was giving higher activity than the methanol reforming catalyst.

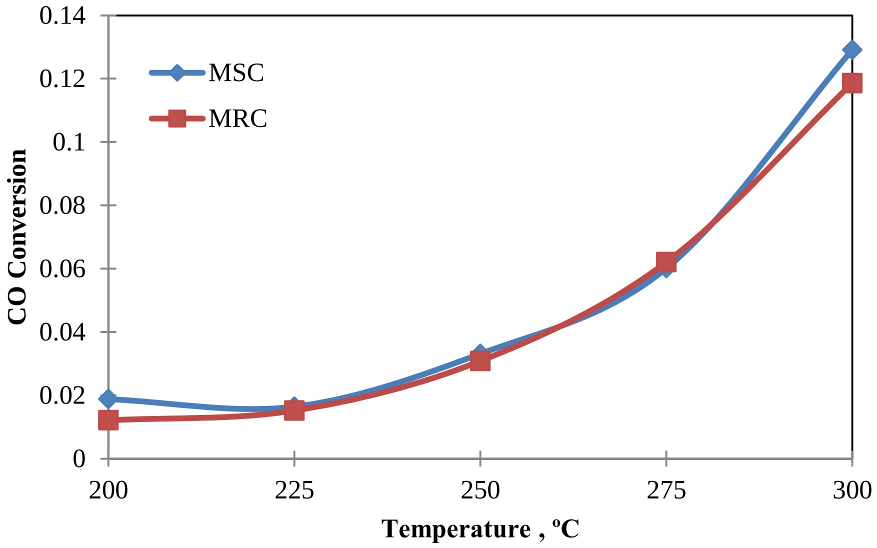

Figure 57. Comparison of carbon monoxide conversion values obtained with methanol reforming catalyst (MRC) and methanol synthesis catalyst (MSC) (space time of 0.48 s.gr/cc, catalyst amount: 0.2 gr, mixture-1 feed stream: 50% CO + 50% H_2)

When the product distribution of methanol synthesis catalyst was examined, it was seen that methanol was the main product as expected. This can be seen in Figure 58. Methanol selectivity values were very high for the studied range of temperature.

Major side product was carbon dioxide at all temperatures and dimethyl ether formation was observed at 275 °C. Selectivity of dimethyl ether at 275 °C was 1.8%.

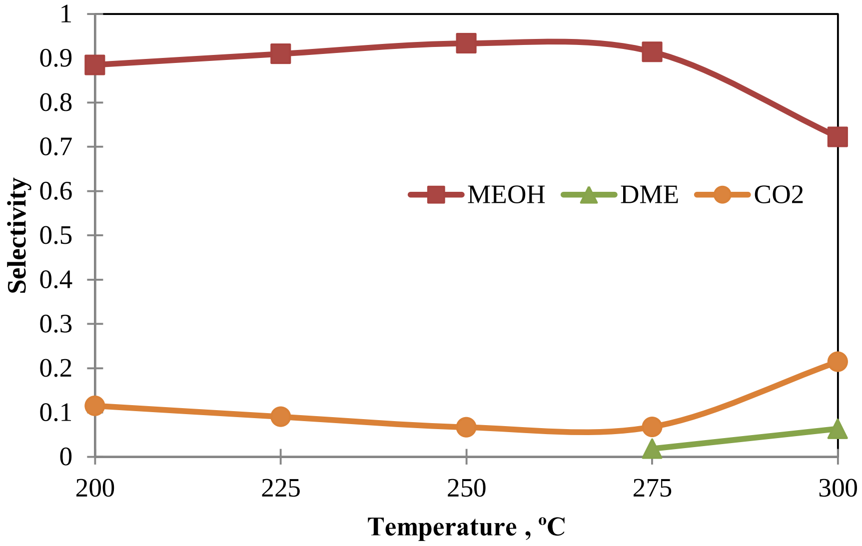

Figure 58. Product distribution obtained with methanol synthesis catalyst (MSC) (space time of 0.48 s.gr/cc, catalyst amount: 0.2 gr, Mixture-1 feed stream: 50% CO + 50% H_2)

Comparison of methanol selectivities obtained with MRC and MSC is given in Figure 59. Methanol selectivity of MSC was higher than MRC. At 275 °C, methanol selectivity of methanol synthesis catalyst was 91.4% whereas methanol selectivity was 79.5% for methanol reforming catalyst.

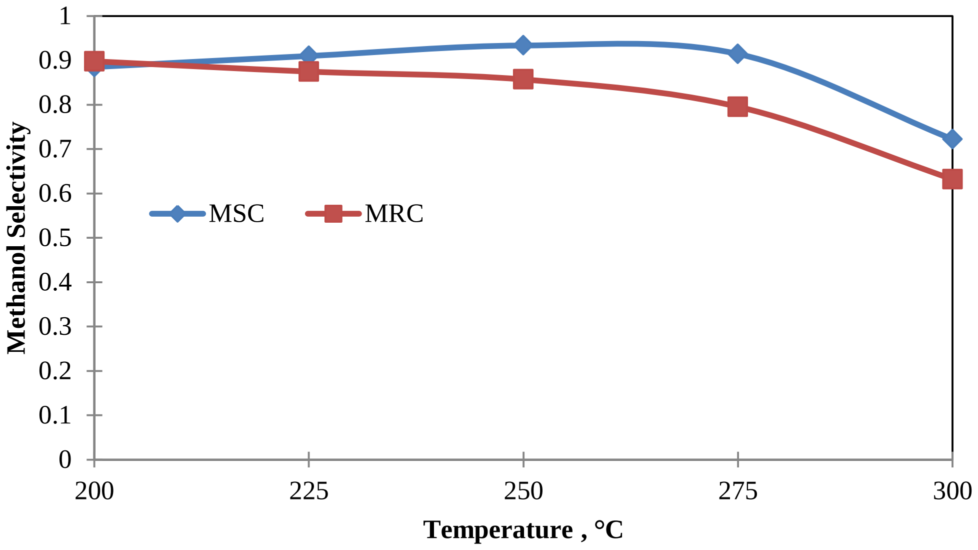

Figure 59. Comparison of methanol selectivities obtained with methanol reforming catalyst (MRC) and methanol synthesis catalyst (MSC) (space time of 0.48 s.gr/cc, catalyst amount: 0.2 gr, mixture-1 feed stream: 50% CO + 50% H_2)

8.2. ACTIVITY RESULTS OF PHYSICALLY MIXED CATALYSTS

In this part, methanol reforming catalyst and methanol dehydration catalysts, either TOYO or TRC-75(L) were physically mixed in equal weights. That is, a mixed catalyst mixture was prepared by mixing the 0.1 gr of catalysts which is responsible for methanol synthesis and 0.1 gr catalysts which is responsible for methanol dehydration. For the comparative purposes, experimental data of TRC-75(L)-C at a reactant flow rate of 50 cc/min is taken from another study [8].

0.1 gr of methanol reforming catalyst, MRC, and 0.1 gr of methanol dehydration catalyst were physically mixed and it was denoted as TRC-75(L)-C. Its activity was tested with feed Mixture-1 (50% CO, 50% H_2) and feed Mixture-2 (40% CO, 10% CO_2, 50% H_2). Sample conversion and selectivity calculations are given in Appendix B for Mixture-1 and Mixture-2.

8.2.1. Activity results of TRC-75(L)-C from Mixture-1 ($CO:H_2$=50:50)

TRC-75(L)-C was tested in our experimental set-up operating at 50 bar and at a flow rate of 50 cc/min in the temperature range of 200 °C – 400 °C from mixture-1. Carbon monoxide conversion values are given in Figure 60.

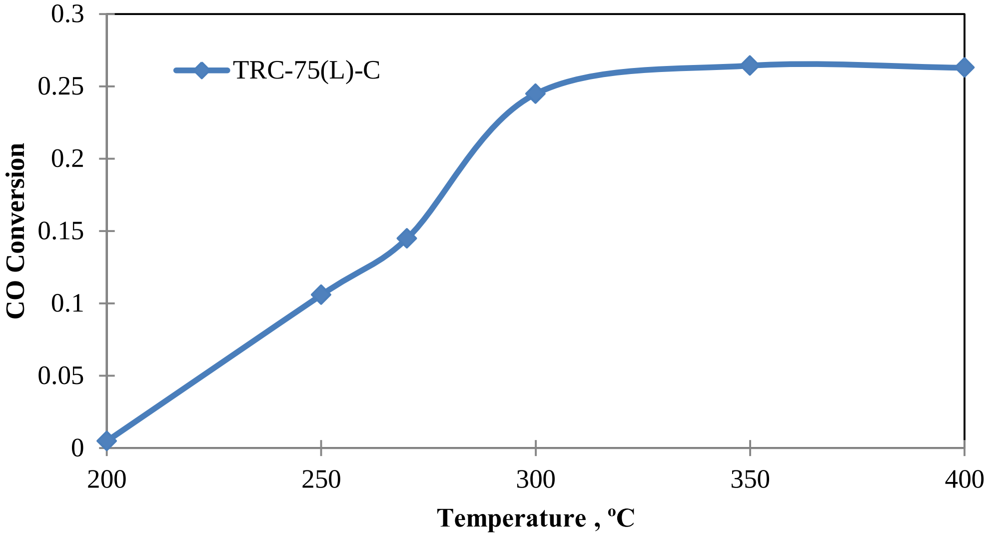

Figure 60. Carbon monoxide conversion values obtained with TRC-75(L)-C (space time of 0.24 s.gr/cc, catalyst amount: 0.2 gr, Mixture-1 feed stream: 50% CO + 50% H_2)

As it can be seen from Figure 60, conversion of the hybrid catalyst mixture reached to a maximum at 300 °C. Conversion at 300 °C was 24.5% and hybrid catalyst exhibited catalytic activity starting from 200 °C. The comparison of carbon monoxide conversions of TRC-75(L)-C and MRC is given in Figure 61.

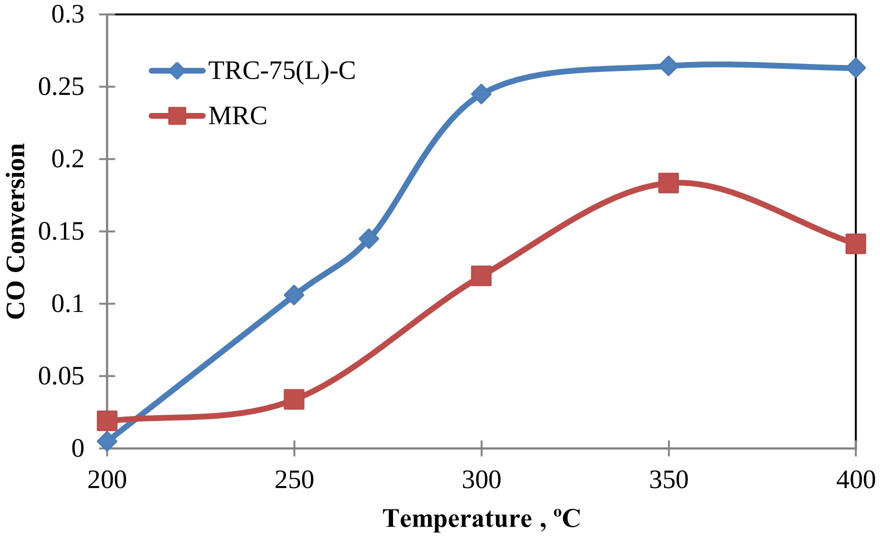

Figure 61. Comparison of carbon monoxide conversion values obtained with TRC-75(L)-C and methanol reforming catalyst (MRC) (space time of 0.24 s.gr/cc, catalyst amount: 0.2 gr, Mixture-1 feed stream: 50% CO + 50% H_2)

The carbon monoxide conversions for TRC-75(L)-C was quite higher than the methanol reforming catalyst at the same experimental conditions. This situation can clearly be seen in Figure 61. Carbon monoxide conversion of MRC was 11.9% at 300 °C whereas it was 24.5% for the bi-functional catalyst at the same temperature, which is more than two times of the MRC conversion. The reason why there occurs such a big conversion difference is because of the nature of the bi-functional catalyst mixture. In the bi-functional catalyst mixture, produced methanol was continuously converted to products and this shifts the methanol synthesis reactions, which is equilibrium limited, towards the products. This is the thermodynamic advantage of one step synthesis. Moreover, methanol synthesis is a highly exothermic reversible reaction with thermodynamical limitations [23]. Thermodynamic analysis of methanol synthesis reaction from carbon monoxide and hydrogen, reaction-3, revealed that equilibrium conversion was 26.1% at 300 °C as calculated in Chapter 4.

$$CO + 2H_2 \rightarrow CH_3OH \qquad [3]$$

When the product distribution of TRC-75(L)-C was examined, main product was dimethyl ether in the temperature range of interest as it can be seen from Figure 62. Main product was methanol in the catalytic activity of methanol reforming catalyst from carbon monoxide hydrogenation and results showed that methanol was successfully converted to DME. However, there was also unconverted methanol at low temperatures. At 250 °C, DME selectivity of 56.1% was obtained. Methane formation together with carbon dioxide underwent a parallel trend indicating the occurrence of reverse dry reforming of methane.

$$2CO + 2H_2 \rightarrow CH_4 + CO_2 \qquad [7]$$

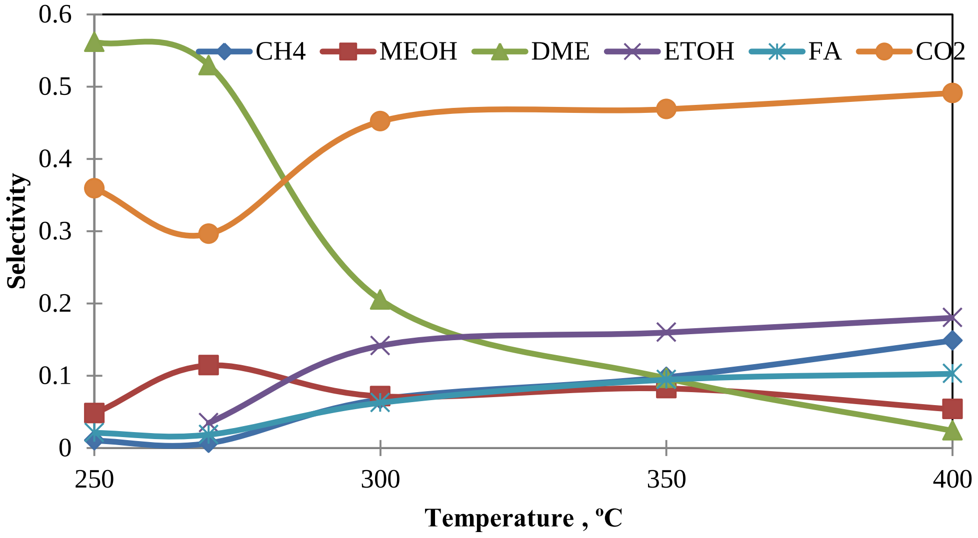

Figure 62. Product Distribution obtained with TRC-75(L)-C (space time of 0.48 s.gr/cc, catalyst amount: 0.2 gr, Mixture-1 feed stream: 50% CO + 50% H_2)

Formation of ethanol was started at 275 °C and ethanol was the main side product at high temperatures. In addition, formic acid was also observed. After 275 °C, increase in the carbon monoxide conversion was due to the formation of formic acid and ethanol through the reactions 9, 10, and 11. In addition, in-situ conversion of methanol to dimethyl ether also increased the conversion.

$2CO + 4H_2 \rightarrow C_2H_5OH + H_2O$ [9]

$3CO + 3H_2 \rightarrow C_2H_5OH + CO_2$ [10]

$CO + H_2O \rightarrow CH_2O_2$ [11]

Carbon dioxide was the major side product at 250°C. Beside reverse methane dry reforming reaction, direct dimethyl ether synthesis reaction, reaction-1, was majorly responsible for the production of carbon dioxide. For each one mole of DME produced, one mole of carbon dioxide should also form. In reaction 1, selectivity ratio of DME to CO_2 is equal to two since the former contains two carbon atoms whereas the latter contains one. DME selectivity of TRC-75(L)-C catalyst at 250 °C 0.56 and CO_2 selectivity at the same temperature is 0.36, respectively. Selectivity ratio of DME to CO_2 is 1.6 and quite consistent with the expected results from reaction-1. Formation of CO_2 with methane reverse dry reforming decreased the selectivity ratio. All these results indicated that DME formation was essentially due to methanol synthesis from CO (reaction-3) and dehydration of methanol to DME (reaction-4).

$3\ CO + 3\ H_2 \rightarrow DME + CO_2$ [1]

$CO + 2H_2 \rightarrow CH_3OH$ [3]

$2CH_3OH \rightarrow DME + H_2O$ [4]

Formation of water was occurred by reaction-4 and water reacted with carbon monoxide through water gas shift reaction. CO_2 was also produced by water gas shift reaction.

$CO + H_2O \rightarrow CO_2 + H_2$ [5]

Comparison of DME selectivities of MRC and TRC-75(L)-C for the Mixture-1 is given in Figure 63. For the MRC, DME was produced with low selectivity which was being equal to 12.2% at 250°C. When the bi-functional catalyst TRC-75(L)-C was used, DME selectivity increased to 56.2%. Increase in DME selectivity for bi-functional catalyst can be attributed to the Brønsted acid sites of bi-functional catalyst, which functioned in methanol dehydration to DME. Methanol dehydration component of bi-functional catalyst, TRC-75(L), had both Brønsted and Lewis acid sites and Brønsted acid sites were stronger than Lewis acid sites. Presence of Brønsted acid sites in the catalyst is the major indication of activity in methanol dehydration reactions [48, 59].

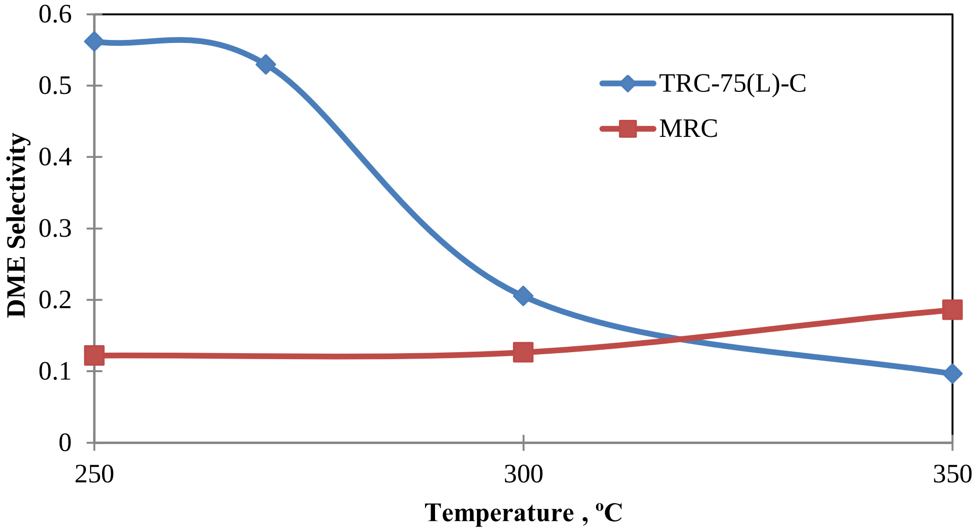

Figure 63. Comparison of carbon monoxide conversion values obtained with TRC-75(L)-C and methanol reforming catalyst(MRC) (space time of 0.24 s.gr/cc, catalyst amount: 0.2 gr, Mixture-1 feed stream: 50% CO + 50% H_2)

8.2.2. Activity results of TRC-75(L)-C from Mixture-2 ($CO:CO_2:H_2$=40:10:50)

It was proposed that having carbon dioxide in the feed could possibly decrease the formation of methane by inhibiting the methane reverse dry reforming, DME selectivity could increase and CO_2 utilization could be possible. Based on these proposals, the activity test of TRC-75(L)-C was conducted with mixture-2 (40% CO, 10% CO_2, and 50% H_2) at a reactant gas flow rate of 50 cc/min. The conversions of carbon monoxide and carbon dioxide were calculated separately to understand whether they were converted to products or not.

CO_2 conversion and CO conversions of TRC-75(L)-C catalysts are given in Figure 64 and Figure 65. When Figure 64 was examined, it was seen that CO_2 conversion was positive at 200 °C and conversion is at around 5.8%. This is an important result since carbon dioxide utilization was accomplished. However, as temperature increased, CO_2 conversion decreased and it is negative for all other temperatures, indicating that it was a product rather than a reactant at these temperatures.

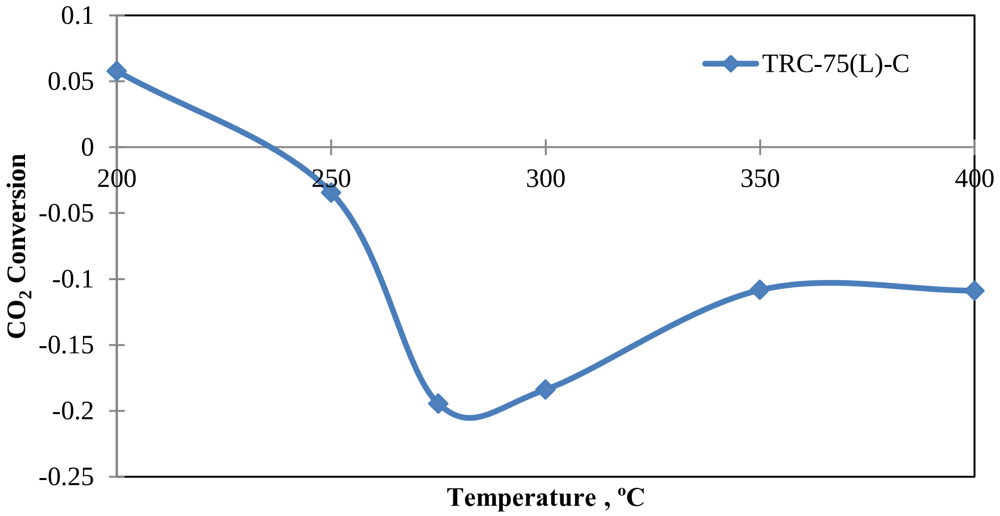

Figure 64. Carbon dioxide conversion values obtained with TRC-75(L)-C (space time of 0.24 s.gr/cc, catalyst amount: 0.2 gr, Mixture-2 feed stream: 40% CO + 10% CO_2 + 50% H_2)

Figure 65 shows the carbon monoxide conversions with respect to temperature. Carbon monoxide conversion reached to the maximum at 275 °C as 18.3% and it was negative at 200 °C, indicating that it was a product rather than a reactant.

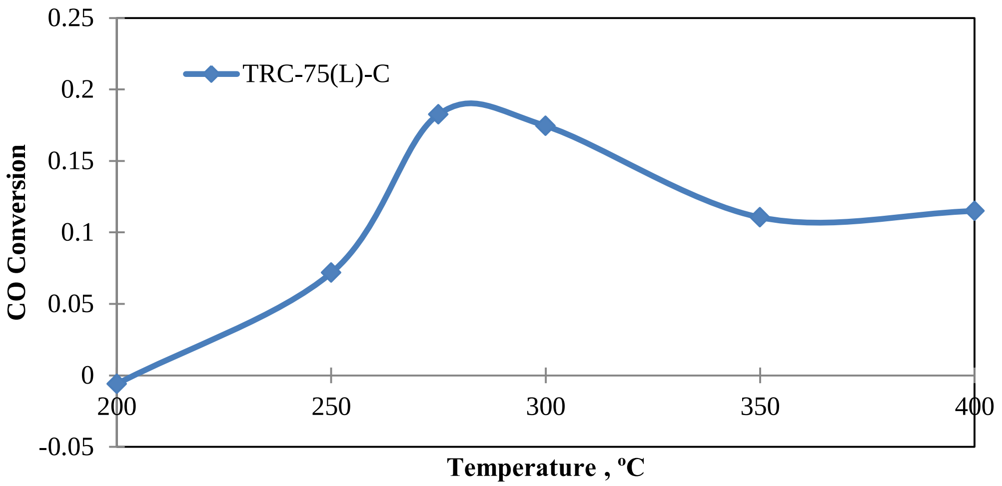

Figure 65. Carbon monoxide conversion values obtained with TRC-75(L)-C (space time of 0.24 s.gr/cc, catalyst amount: 0.2 gr, Mixture-2 feed stream: 40% CO+ 10% CO_2 + 50% H_2)

Product distribution of TRC-75(L)-C catalyst with respect to carbon monoxide for mixture-2 is given in Figure 66. As it can be seen from the figure, main product was DME until 350 °C. When the activity result of MRC at the same experimental conditions was examined, it was seen that major product was methanol. Formation of DME is an indication of the successful conversion of all methanol to DME. DME selectivity is 84.5% at 250 °C and as temperature increased, DME selectivity decreased as expected since fewer methanol was produced at high temperatures. Further increase in the temperature resulted in the increase of carbon dioxide selectivity and formation of ethanol, formic acid and methane occured at high temperatures. At low temperatures, reverse methane dry reforming was hindered and methane formation at low temperatures was insignificant.

Product distribution with respect to moles of converted carbon monoxide was meaningless at 200 °C since carbon monoxide conversion at this temperature was negative. Instead of defining the selectivity with respect to moles of carbon monoxide converted, it could be defined as the total moles of carbon atoms entering to the reactor system, that is, selectivity was defined with respect to total moles of converted CO and CO_2 as in Equations 6.7 and 6.8. Based on the new selectivity definition, DME had a selectivity of 1 at 200°C. At this temperature, only carbon containing product was DME beside carbon monoxide and it was formed by CO_2 hydrogenation. DME selectivity at 250 °C was 0.96. These results are very promising since utilization of carbon dioxide in the production of DME was successful at temperatures less than 250 °C. DME synthesis from carbon dioxide can be expressed as,

$$2\ CO_2 + 6\ H_2 \rightarrow DME + 3H_2O \qquad [12]$$

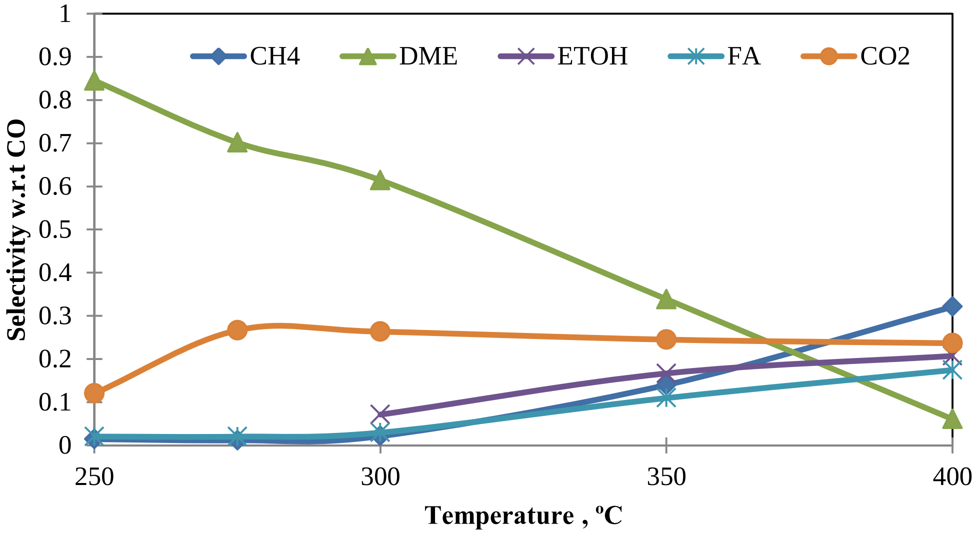

Figure 66. Product distribution obtained with TRC-75(L)-C (space time of 0.24 s.gr/cc, catalyst amount: 0.2 gr, Mixture-2 feed stream: 40% CO + 10% CO_2 + 50% H_2)

Having carbon dioxide in the feed mixture was beneficial on DME selectivity. On the other hand, addition to CO_2 the feed mixture resulted in the decrease of carbon dioxide selectivity. Positive effects of addition of CO_2 to the feed gas on DME and CO_2 selectivities can be more clearly seen with Figure 67.

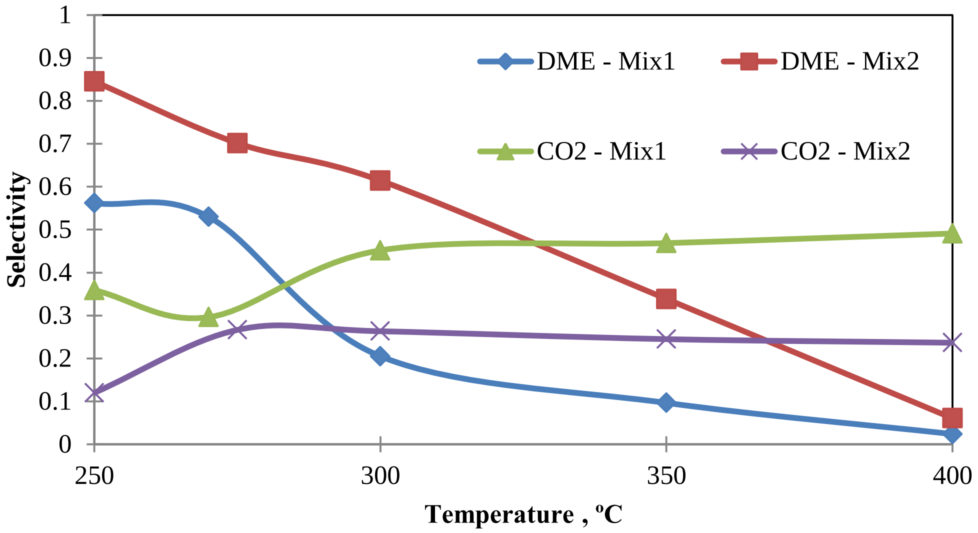

Figure 67. Comparison of product distributions obtained with TRC-75(L)-C for Mixture-1(50% CO + 50% H_2) and Mixture-2 (40% CO + 10% CO_2 + 50% H_2) (space time of 0.24 s.gr/cc, catalyst amount: 0.2 gr)

DME selectivity obtained with Mixture-1 was equal to 56.2% at 250 °C and DME selectivity obtained with Mixture-2 was equal to 84.5% at 250 °C. By introducing CO_2 into the system, reaction-1 has affected negatively as expected. Addition of CO_2 into the feed gas did not alter CO conversions considerably. However, Mixture-2 has given 18.3% CO conversion whereas Mixture-1 has given 14.5% at 275 °C. Based on all these results, addition of CO_2 into the feed mixture enhanced the CO conversion and DME selectivity.

$3\ CO + 3\ H_2 \rightarrow DME + CO_2$ [1]

$2\ CO + 4\ H_2 \rightarrow DME + H2O$ [2]

8.2.3. Activity results of HF-AL-C from Mixture-2 ($CO:CO_2:H_2$=40:10:50)

In the direct synthesis of DME from synthesis gas, another physical mixing catalyst was tested. For the methanol synthesis, methanol reforming catalyst was used and for methanol dehydration, an alumina based commercial catalyst obtained from TOYO was used. Since the catalysts was in the pellet form, they were crushed and brought to the same size of approximately 0.2 mm. Catalyst was prepared by mixing 0.1 gr methanol reforming catalyst and 0.1 gr methanol dehydration catalyst and prepared catalyst was denoted as HF-AL-C. Activity tests were made with the carbon dioxide containing feed Mixture-2 (40% CO, 10% CO_2, 50% H_2) and at a flow rate of 50 cc/min.

Carbon monoxide conversions of HF-AL-C with respect to the temperature are given in Figure 68. As it can be seen from the figure, carbon monoxide conversion has reached to maximum at 300 °C and it had no CO conversion at 200 °C.

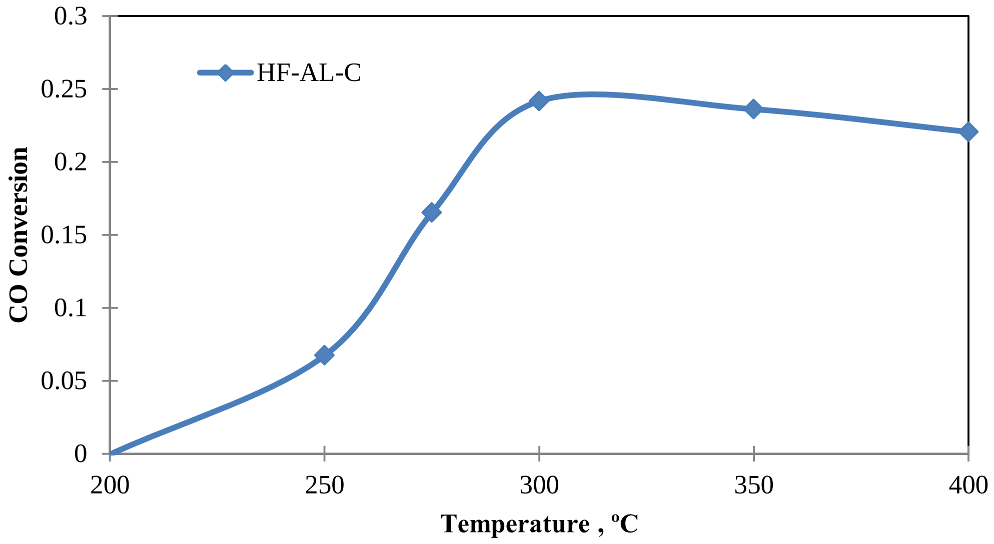

Figure 68. Carbon monoxide conversion values obtained with HF-AL-C (space time of 0.24 s.gr/cc, catalyst amount: 0.2 gr, Mixture-2 feed stream: 40% CO + 10% CO_2 + 50% H_2)

Product distribution of HF-AL-C catalyst is given in Figure 69. Selectivities were defined with respect to CO since only reactant throughout the experiment was carbon monoxide. DME selectivity is 69.9% at 250 °C and selectivity of DME decreased with increasing temperature. As temperature increased, equilibrium limitations of DME appear and formation of side products began. Formation of methane together with CO_2 and increase of its selectivity could be attributed to the reverse methane dry reforming.

$2CO + 2H_2 \rightarrow CH_4 + CO_2$ [7]

DME selectivity was around 70% whereas CO_2 selectivity was around 10% at 250 °C. Based on these selectivities, DME synthesis is likely to occur via reaction 2.

$2\ CO + 4\ H_2 \rightarrow DME + H_2O$ [2]

As temperature increased further, DME selectivity decreased and CO_2 selectivity increased. With the increase in temperature, reaction-1 was also gaining importance.

$3\ CO + 3\ H_2 \rightarrow DME + CO_2$ [1]

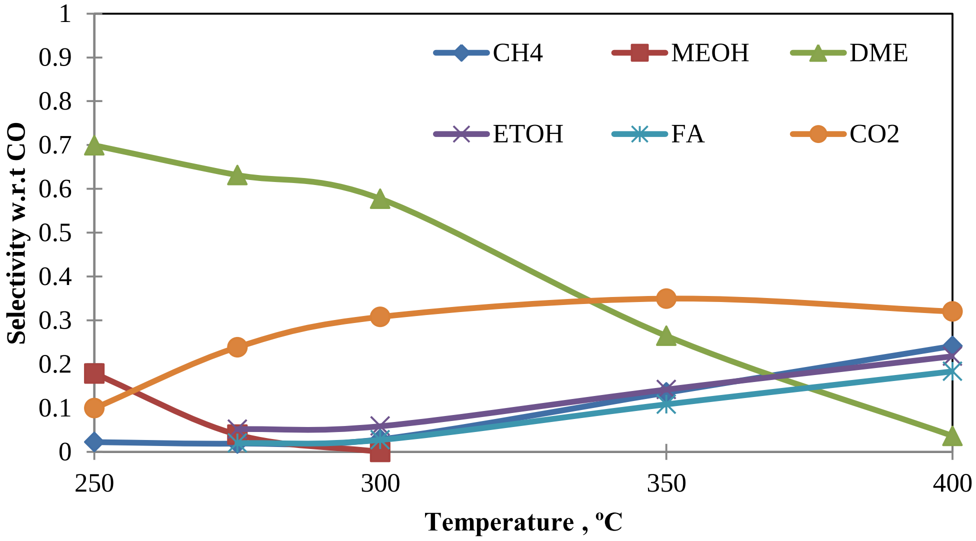

Figure 69. Product distributions obtained with HF-AL-C (space time of 0.24 s.gr/cc, catalyst amount: 0.2 gr, Mixture-2 feed stream: 40% CO + 10% CO_2 + 50% H_2)

When product distribution of HF-AL-C for Mixture-2 was examined, methanol presence was noticed at 250 °C and 275 °C. This is an indication of not all methanol was converted to DME due to the lack of the acidity. The acidity of the bi-functional catalysts could be enhanced by increasing the weight ratio of methanol dehydration catalysts, which was alumina based TOYO catalyst. For this purpose, a catalyst bed of 0.2 gr hybrid catalyst was prepared by mixing 0.08 gr methanol reforming catalyst and 0.12 gr methanol dehydration catalyst. This hybrid bi-functional catalyst was denoted as HF(40)-AL(60)-C. Activity test conducted at 50 bar and 200 °C - 400 °C for the reactant flow rate of 50 cc/min. Feed gas was Mixture-2. In Figure 70, CO conversion values of two mixed catalysts, one of them is equally weighted whereas other was favored for the dehydration, were plotted in comparison with respect to temperature.

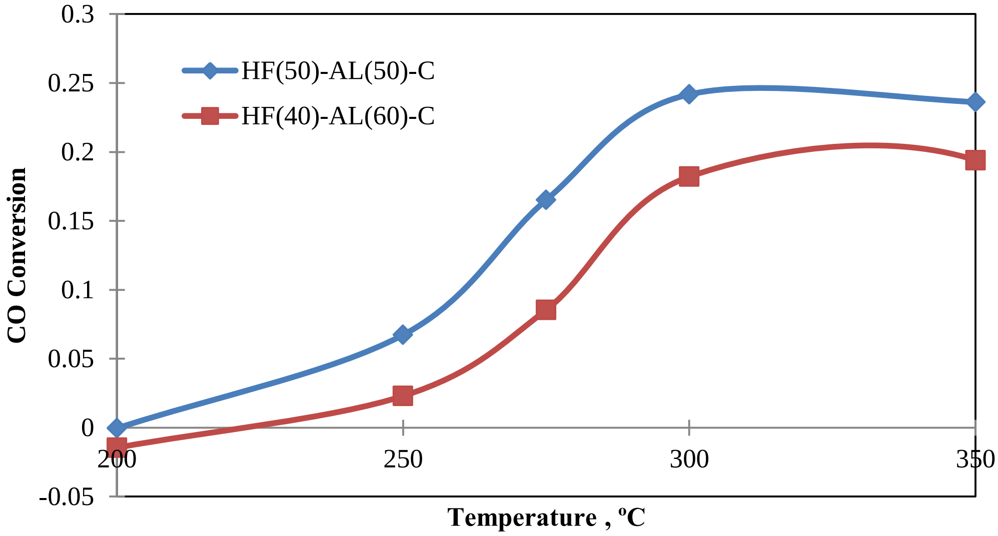

Figure 70. Comparison of carbon monoxide conversion values obtained with acidity increased catalyst (HF(40)-AL(60)-C) and equally weighted catalyst (HF(50)-AL(50)-C) (space time of 0.24 s.gr/cc, catalyst amount: 0.2 gr, Mixture-2 feed stream: 40% CO + 10% CO_2 + 50% H_2)

It was seen that for all temperatures, carbon monoxide conversion were lower for HF(40)-AL(60)-C catalyst. This was an expected result because by decreasing the mass ratio of methanol reforming catalyst to the methanol dehydrating catalyst, fewer methanol was produced and as a consequence, less methanol was converted to DME. For the acidity increased bi-functional catalysts (HF(40)-AL(60)-C), carbon dioxide conversion exhibited interesting results. CO_2 conversion with respect to temperature is given in Figure 71.

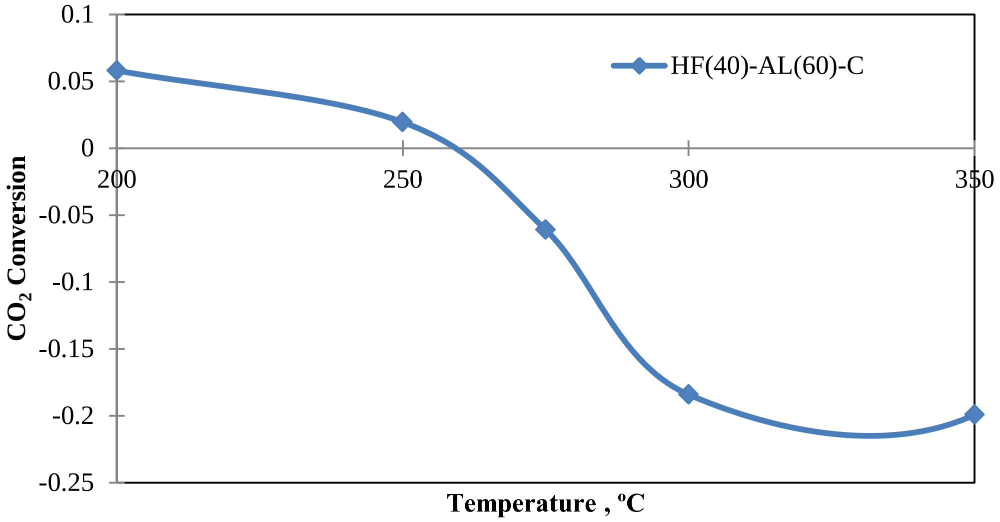

Figure 71. Carbon dioxide conversion values obtained with HF(40)-AL(60)-C (space time of 0.24 s.gr/cc, catalyst amount: 0.2 gr, Mixture-2 feed stream: 40% CO + 10% CO_2 + 50% H_2)

As it can be seen from Figure 71, 5.8% carbon dioxide conversion at 200 °C and 1.9% CO_2 conversion at 250 °C were obtained. At 200 °C, CO_2 was converted to the carbon monoxide via the reverse water gas shift reaction and as a result, CO was produced. This explains why negative CO conversion was obtained. On the other hand, carbon dioxide conversion was always negative for the HF(50)-AL(50)-C catalyst indicating that CO_2 was always a product.

$$CO_2 + H_2 \rightarrow CO + H_2O \qquad [8]$$

Product distribution of HF(40)-AL(60)-C was calculated with respect to carbon monoxide and given in Figure 68. Very high selectivity values of DME were obtained at all temperatures and methanol selectivity was quite low, indicating that all methanol was successfully converted to the DME. As it can be seen from Figure 72, DME selectivity defined with respect to total amount CO converted to products was greater than 100% (around 120%) at 250 °C indicating that CO_2 was also reacted to form DME. Negative CO_2 selectivity confirmed this conclusion. This was a very important result since the catalyst was able to utilize the most important greenhouse gas to the diesel fuel alternate DME.

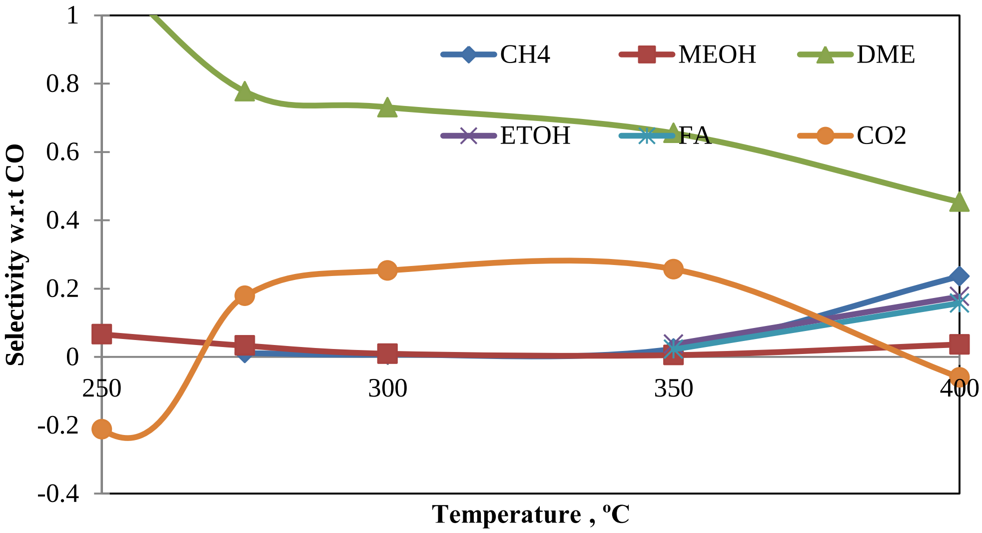

Figure 72. Product distributions obtained with acidity increased HF(40)-AL(60)-C catalyst (space time of 0.24 s.gr/cc, catalyst amount: 0.2 gr, Mixture 2 Feed Stream: 40% CO + 10% CO_2 + 50% H_2)

Selectivity definition with respect to CO was meaningless at 200 °C and 250 °C since CO conversion was negative at 200 °C and CO_2 was reactant at 200 °C and 250°C. Instead of defining the selectivity with respect to moles of carbon monoxide converted, it could be defined as the total moles of carbon atoms entering to the reactor system, that is, selectivity was defined with respect to total moles of converted CO+CO_2 as in Equations 6.7 and 6.8. The overall selectivity is given in Figure 73. Based on overall selectivity definition, DME had an overall selectivity at around 95% from 200 °C to 250 °C. This was a quite important result since CO_2 utilization to the diesel fuel alternate was accomplished via the following reaction.

$$2\ CO_2 + 6\ H_2 \rightarrow DME + 3H_2O \qquad [12]$$

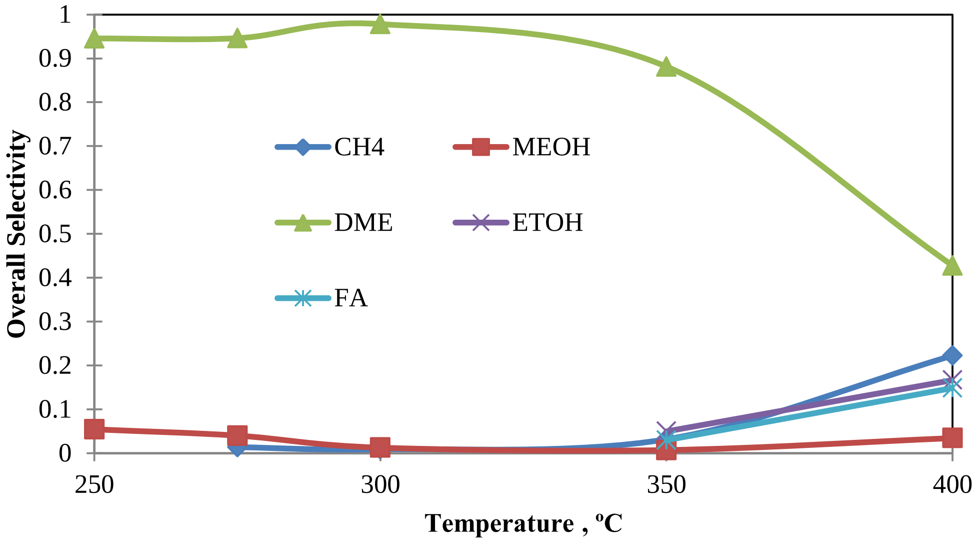

Figure 73. Overall product distributions defined with respect to converted CO&CO_2 to products and obtained with acidity increased HF(40)-AL(60)-C catalyst (space time of 0.24 s.gr/cc, catalyst amount: 0.2 gr, Mixture-2 Feed stream: 40% CO + 10% CO_2 + 50% H_2)

A comparison of DME selectivities of equally weighted hybrid catalyst HF(50)-AL(50)-C and acidity improved HF(40)-AL(60)-C catalyst is given in Figure 74. As it can be seen, changing the ratio of methanol synthesis catalyst to the methanol dehydration catalyst enhanced the dimethyl ether selectivity by increasing the acidity of bi-functional catalyst. Almost all methanol was converted to DME. On the other hand, CO selectivity decreased upon the increase on the ratio of methanol dehydration component to methanol synthesis component. Decrease in CO conversion for acidity improved catalyst HF(40)-AL(60)-C can be seen in Figure 75.

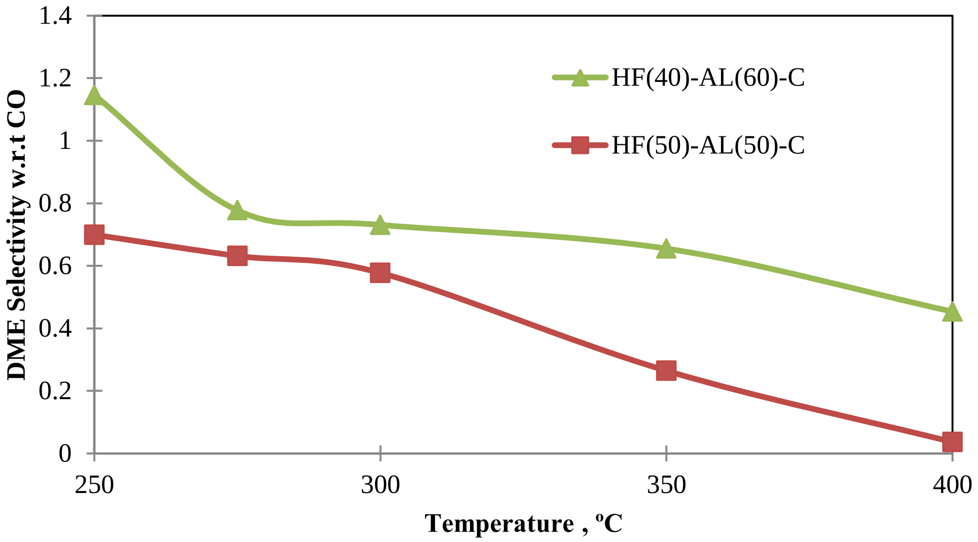

Figure 74. Comparison of DME selectivities obtained with acidity increased HF(40)-AL(60)-C catalyst and equally weighted catalyst HF(50)-AL(50)-C (space time of 0.24 s.gr/cc, catalyst amount: 0.2 gr, Mixture-2 Feed stream: 40% CO + 10% CO_2 + 50% H_2)

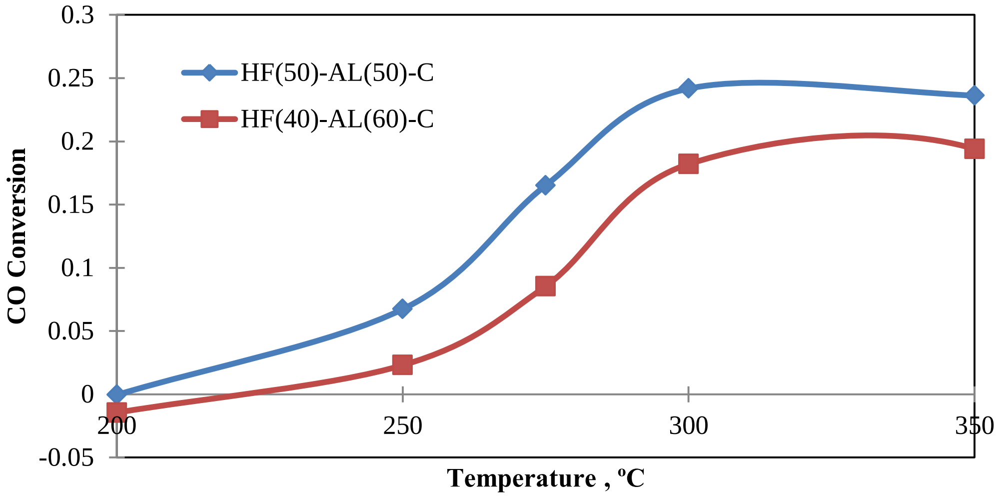

Figure 75. Comparison of CO conversions obtained with acidity increased HF(40)-AL(60)-C catalyst and equally weighted catalyst HF(50)-AL(50)-C (space time of 0.24 s.gr/cc, catalyst amount: 0.2 gr, Mixture-2 Feed stream: 40% CO + 10% CO_2 + 50% H_2)

8.3. ACTIVITY RESULTS OF REACTOR ARRANGEMENTS

Another set of experiments was performed with a sequential catalyst bed. In this reactor bed arrangement, catalyst bed was first loaded with methanol synthesis catalyst and then methanol dehydration catalyst. This arrangement is quite different than previous arrangements in which reactor bed was loaded with bi-functional physically mixed catalyst, allowing simultaneous synthesis of methanol and conversion of methanol to products at the same location within the reactor. In sequentially prepared reactors, syngas is first exposed to the methanol synthesis catalyst and as a result, methanol is produced. After that, methanol, other products if any, and unconverted gases pass over the methanol dehydration catalyst and methanol dehydration takes place. Results obtained in this series arrangement were denoted as TRC-75(L)-S.

Comparison of carbon monoxide conversions obtained with TRC-75(L)-C and TRC-75(L)-S is given with Figure 76. Activity test with the carbon dioxide containing feed stream, Mixture-2, showed the superiority of the mixed reactor bed to the sequential reactor bed. In the mixed catalyst bed, carbon monoxide conversions reached 18.3% at 275 °C whereas sequential catalyst bed showed carbon monoxide conversion as 6.0% at the same temperature. Results indicated the positive effect of in-situ conversion of produced methanol to DME on the carbon monoxide conversion.

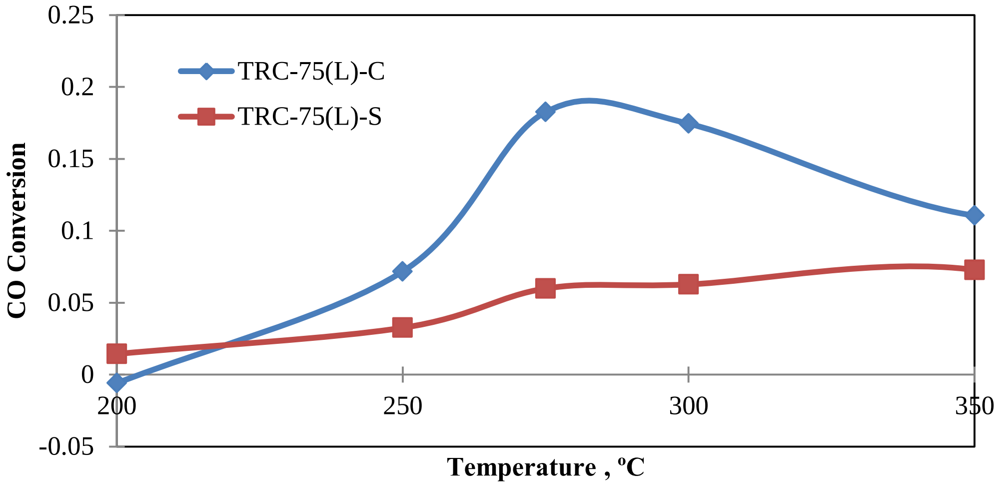

Figure 76. Comparison of carbon monoxide conversion values obtained with mixed reactor bed (TRC-75(L)-C) and sequential reactor bed (TRC-75(L)-S) (space time of 0.24 s.gr/cc, catalyst amount: 0.2 gr, Mixture-2 feed stream: 40% CO + 10% CO_2 + 50% H_2)

Comparison of DME selectivity obtained from the carbon dioxide containing feed gas, namely Mixture-2, of TRC-75(L)-C and TRC-75(L)-S is given in Figure 77. Mixed catalyst bed also gave the higher DME selectivity than the sequential catalyst bed. DME selectivity was 84.5% at 250 °C for mixed catalyst system (TRC-75(L)-C) and 13.3% for the sequential catalyst system at the same temperature. Results showed that DME synthesis directly from the synthesis gas is much more advantageous than the DME synthesis from a two-step procedure in which methanol synthesis and methanol dehydration reactors operate in series.

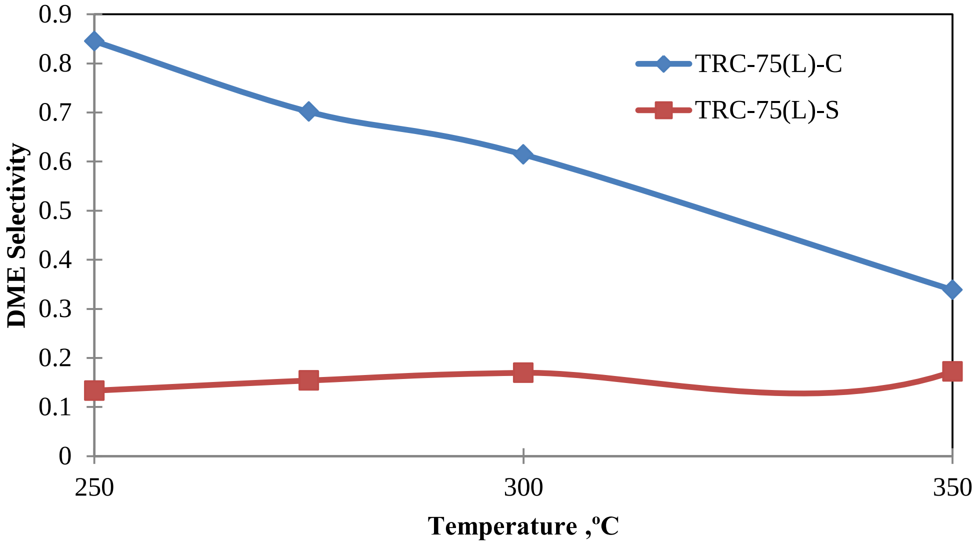

Figure 77. Comparison of DME selectivities obtained with mixed reactor bed (TRC-75(L)-C) and sequential reactor bed (TRC-75(L)-S) (space time of 0.24 s.gr/cc, catalyst amount: 0.2 gr, Mixture-2 feed stream: 40% CO + 10% CO_2 + 50% H_2)

8.4. ACTIVITY RESULTS OF CO-PRECIPITATED CATALYSTS

Activity results of co-precipitated catalysts were conducted at a temperature range of 200°C - 300 °C and at 50 bar for a reactant flow rate of 25 cc/min at standard temperature and pressure. Feed gas was an equimolar mixture of carbon monoxide and hydrogen, namely Mixture-1. 0.2 gr catalyst was loaded into the reactor and space time was calculated as 0.48 s.gr/cc.

8.4.1. Activity results of co-precipitated catalysts from Mixture 1($CO:H_2$=50:50)

In the catalysts preparation, several parameters such as effect of promoter, promoter type, aging time, washing water temperature, calcination temperature, and reduction temperature were investigated and their characterization results were discussed in Section 7.1 and activity results are given in this part.

The carbon monoxide conversion values obtained with the copper-zinc containing co-precipitated catalyst, CZ, is given in Figure 78. As it can be seen from the figure, catalyst conversion was around 1% up to the 250 °C. On the other hand, further increase in temperature increased carbon monoxide conversion and conversion reached to 18.6% at 300 °C.

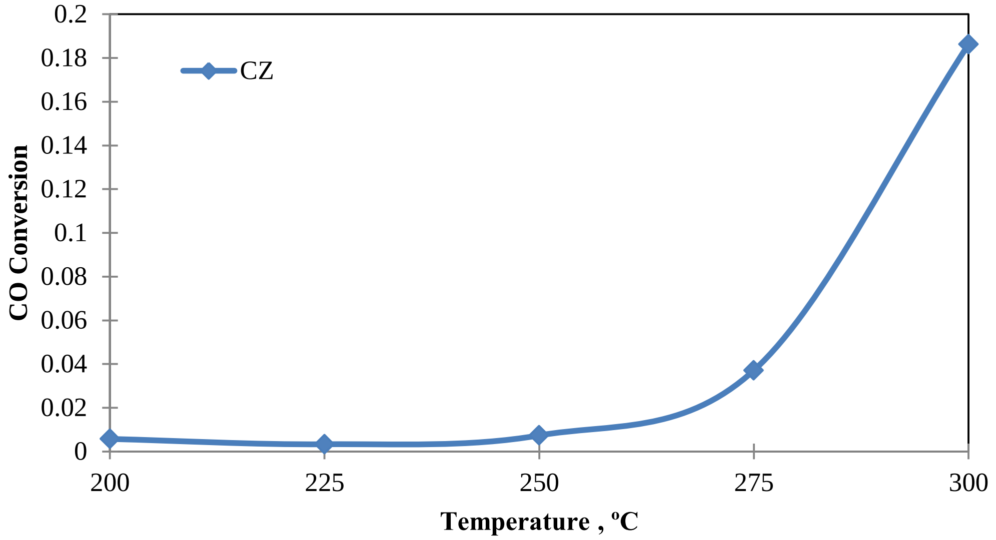

Figure 78. Carbon monoxide conversion values obtained with copper and zinc containing co-precipitated catalyst, CZ, (Space time of 0.48 s.gr/cc, catalyst amount: 0.2 gr, Mixture-1 feed stream: 50% CO + 50% H_2)

When the product distribution of CZ catalyst, which is given in Figure 79, was examined, it was seen that highest methanol selectivity was obtained at 200 °C as 66.0%. Methanol selectivity decreased by increasing temperature since methanol synthesis is an exothermic reaction. At all the temperatures in which activity test was conducted, significant amount of carbon dioxide was present. Selectivity of carbon dioxide also increased upon the increase in temperature. At 275 °C and 300 °C, methane, ethanol and formic acid were formed as side products. Methanol was produced by reaction-3 No dimethyl ether formation was observed since the CZ catalyst was not a strong acid catalyst as shown by drift spectra of pyridine adsorption in Figure 34.

$CO + 2H_2 \rightarrow CH_3OH$ [3]

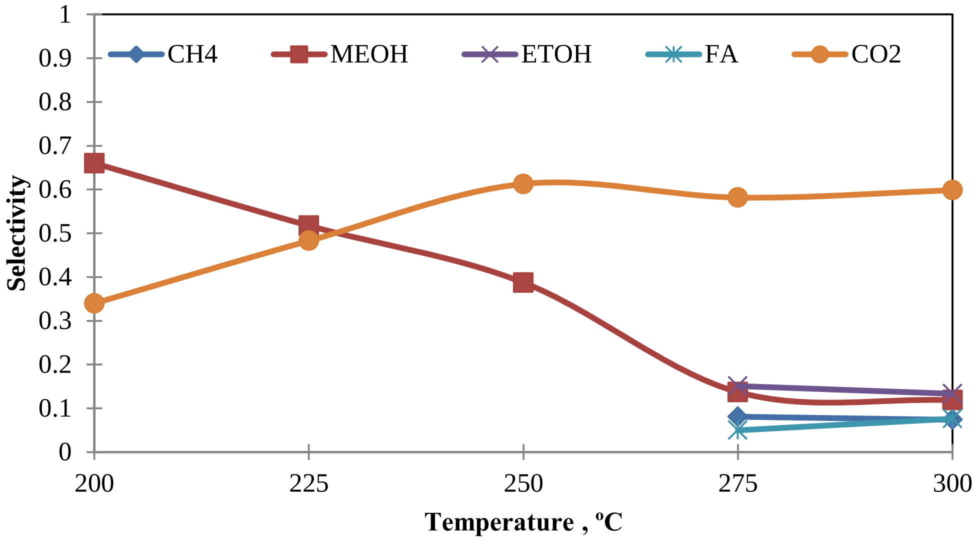

Figure 79. Product distribution obtained with copper zinc containing co-precipitated catalyst, CZ, (Space time of 0.48 s.gr/cc, catalyst amount: 0.2 gr, Mixture-1 feed stream: 50% CO + 50% H_2)

Formation of CO_2 at low temperatures could be due to Boudouard reaction, reaction 13. Boudouard reaction is thermodynamically favorable at reaction conditions. Equilibrium conversion at reaction conditions is given with respect to temperature in Figure 80.

$2CO \rightarrow CO_2 + C_{(s)}$ [13]

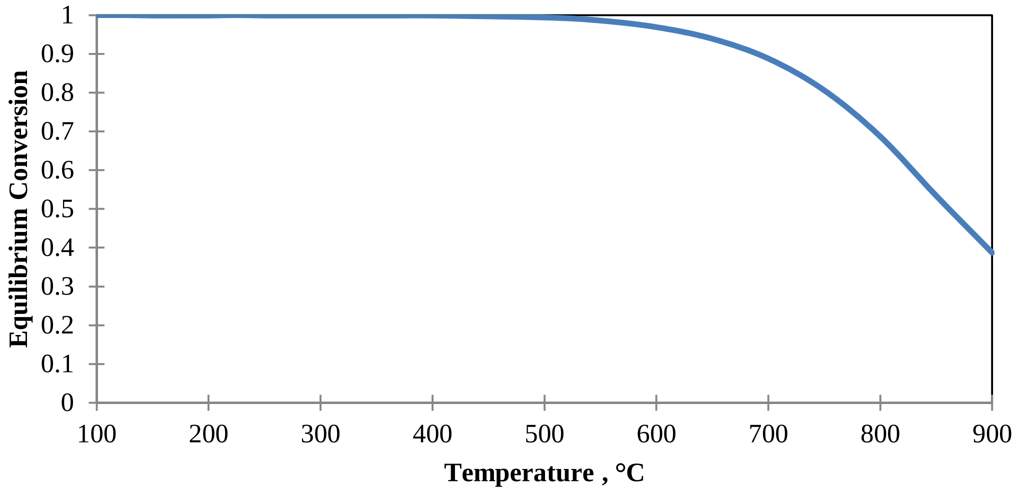

Figure 80. The equilibrium conversion curve for reaction-13 (2CO → $CO_2 + C_{(s)}$) with respect to temperature at 50 bar

On the other hand, CO_2 could also be produced by trace of surface oxygen, from reactions 14, 15, and 16. This point is further explained in the activity test of copper, zinc and zirconia containing co-precipitated catalyst.

$$CO + CuO \rightarrow Cu + CO_2 \qquad [14]$$
$$CO + 2CuO \rightarrow Cu_2O + CO_2 \qquad [15]$$
$$CO + Cu_2O \rightarrow 2Cu + CO_2 \qquad [16]$$

Without promoters, copper and zinc based, co-precipitated methanol synthesis catalyst showed low activity in methanol synthesis from synthesis gas. Addition of promoter was proposed to enhance the activity [25-27, 33-35] and for this reason, aluminum, zirconium and ceria metals were incorporated to the co-precipitated catalysts as promoters. Comparison of carbon monoxide conversions from carbon monoxide hydrogenations of these catalysts were given in Figure 81.

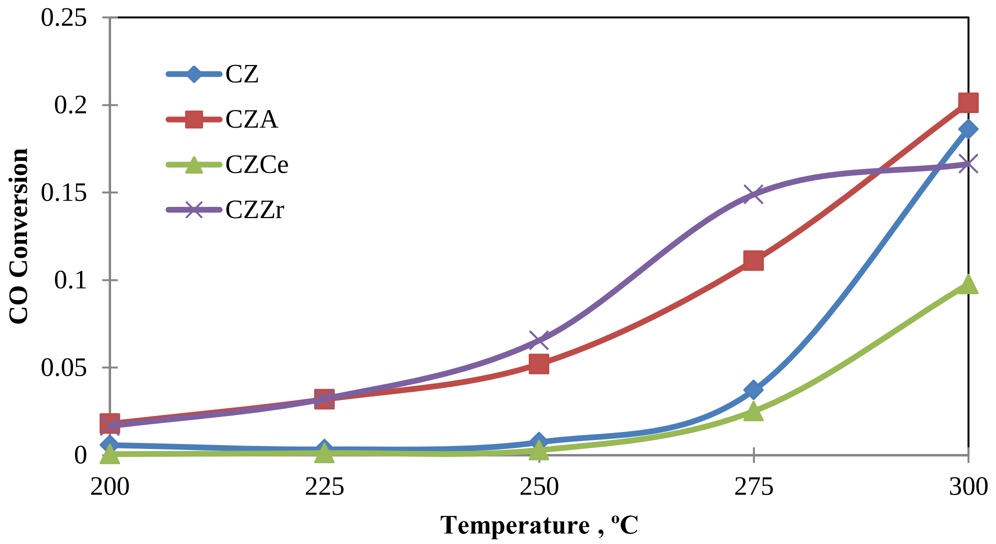

Figure 81. Comparison of carbon monoxide conversion values obtained with copper, zinc and promoter containing co-precipitated catalyst; CZ, without promoter; CZA, Aluminum promoter; CZCe, Ceria promoter; CZZr, Zirconia promoter. (Space time of 0.48 s.gr/cc, catalyst amount: 0.2 gr, Mixture-1 feed stream: 50% CO + 50% H_2)

Addition of zirconia and aluminum enhanced the carbon monoxide conversion to a large extent. Zirconia promoted catalyst CZZr exhibited 14.9% carbon monoxide conversion at 275 °C and aluminum promoted catalyst gave 11.1% carbon monoxide conversion at 275 °C. Carbon monoxide conversion of the catalyst without promoter was only 3.7% at this temperature. Addition of ceria to the precipitated catalyst gave lower conversion than the catalyst without promoter. As temperature increased to 300 °C, catalytic activity of zirconia promoted catalyst was lower than the carbon monoxide conversion of no-promoter catalyst.

Product distribution of the CZZr catalyst is given in Figure 82. In all the temperatures in which activity test was conducted, methanol selectivities were very high. Highest methanol selectivity was obtained at 250 °C as 94%. A sharp decrease in the methanol selectivity was observed at temperatures 275 °C and 300 °C whereas carbon dioxide selectivity increased at these temperatures. At 300 °C, carbon dioxide selectivity was higher than the methanol selectivity. Formation of other minor products was observed at 275 °C and 300 °C.

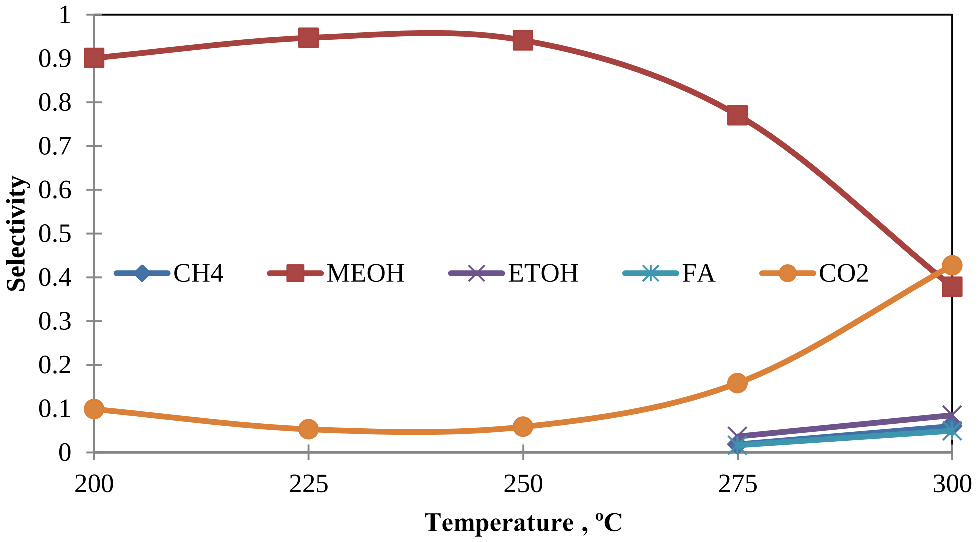

Figure 82. Product distribution obtained with copper, zinc, and zirconium containing co-precipitated catalyst, CZZr, (Space time of 0.48 s.gr/cc, catalyst amount: 0.2 gr, Mixture-1 feed stream: 50% CO + 50% H_2)

At temperatures below 275 °C, products were methanol and carbon dioxide. Formation of CO_2 at low temperatures could be due to thermodynamically favored (Figure 80) Boudouard reaction, reaction 13.

$$2CO \rightarrow CO_2 + C_{(s)} \qquad [13]$$

CO_2 could also be produced by trace of surface oxygen, reaction 14-16. It is known that copper is the active metal in methanol synthesis and CO could be oxidized to CO_2 on the copper surface. The presence of CO_2 with methanol at temperatures below 275 °C in the activity test of copper and zinc containing co-precipitated catalyst could be attributed to oxidizing adsorption of CO [73].

$$CO + CuO \rightarrow Cu + CO_2 \qquad [14]$$

$CO + 2CuO \rightarrow Cu_2O + CO_2$ [15]

$CO + Cu_2O \rightarrow 2Cu + CO_2$ [16]

Considering Boudouard reaction and surface oxidation of CO reactions, high amount of CO_2 may be expected at first. Since copper in the copper, zinc, and zirconia containing catalyst (CZZr) is at +2 oxidation level as shown by XRD pattern in Figure 14, firstly reduction of copper with formation of CO_2 could occur. Then, produced CO_2 could be converted to methanol and as a result, CO_2 selectivity would decrease upon time and reach a steady state value. This proposal was also supported by the activity test results of CZZr catalyst at 200 °C and 50 bar from a feed mixture of CO and H_2. Selectivity changes of CO_2 and methanol with respect to time at 200 °C is given in Figure 83. As it can be seen from Figure 83, CO_2 selectivity at first half hour was very high and as time passed, selectivity of carbon dioxide decreased whereas methanol selectivity increased. Since copper in the CZZr catalyst was non-reduced, firstly reduction of copper particles occurred with formation of CO_2 through reactions 14-16.

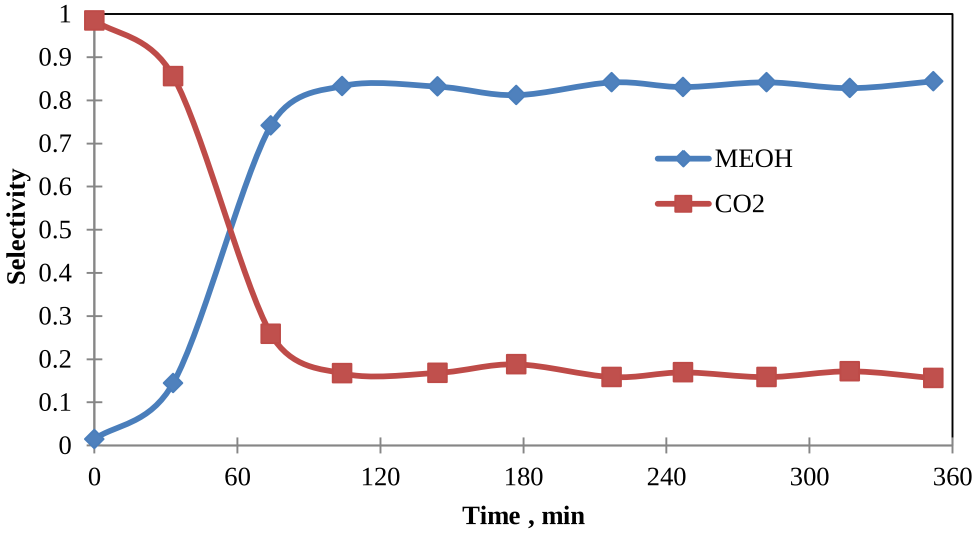

Figure 83. Methanol and CO_2 selectivity changes of copper, zinc, and zirconium containing co-precipitated catalyst, CZZr with respect to time at 200 °C (Space time of 0.48 s.gr/cc, catalyst amount: 0.2 gr, Mixture-1 feed stream: 50% CO + 50% H_2)

Co-precipitated catalyst with promoter alumina has given a similar product distribution with respect to catalyst with promoter zirconia. Product distribution of the CZA catalyst is given in Figure 84. In all the temperatures in which activity test was conducted, methanol selectivities were very high. Highest methanol selectivity was observed at 225 °C as 95.5%. Major side product was carbon dioxide for all the temperatures and formation of methane, dimethyl ether and ethanol were observed at 275 °C and 300 °C.

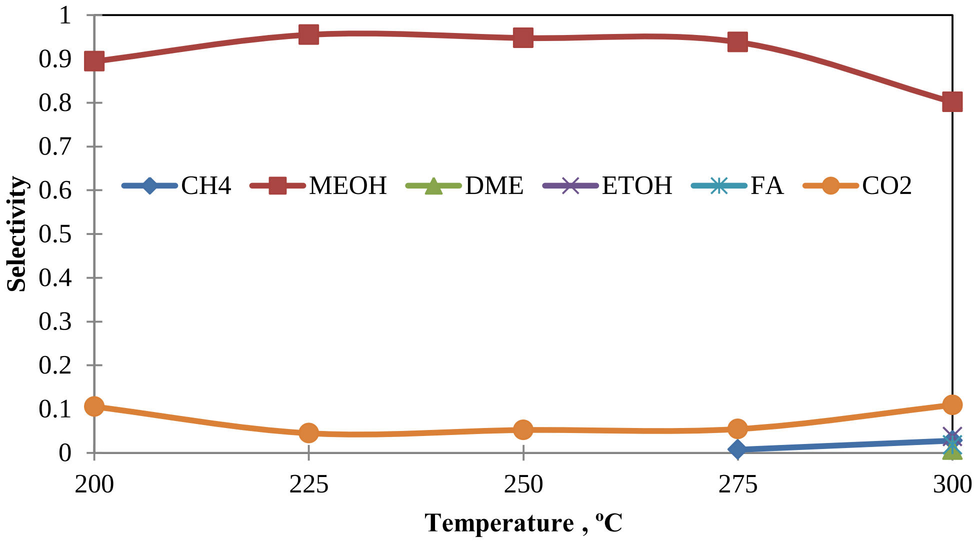

Figure 84. Product distribution obtained with copper, zinc, and aluminum containing co-precipitated catalyst, CZA, (Space time of 0.48 s.gr/cc, catalyst amount: 0.2 gr, Mixture-1 feed stream: 50% CO + 50% H_2)

For the ceria promoted catalyst, there was no transformation of syngas to methanol until 275 °C. Product distribution of this catalyst is given in Figure 85. Carbon monoxide - hydrogen gas mixture was only converted to the carbon dioxide at temperatures 200 °C - 250 °C. Formation of side products was seen at temperatures higher than the 275 °C. It can be concluded that ceria promoted catalysts was not active in methanol synthesis from the synthesis gas. For the ceria promoted catalyst, ethanol formation was observed with a selectivity value of 19% at 275 °C. Ethanol formation was possibly through reactions 9 and 10.

$2CO + 4H_2 \rightarrow C_2H_5OH + H_2O$ [9]

$3CO + 3H_2 \rightarrow C_2H_5OH + CO_2$ [10]

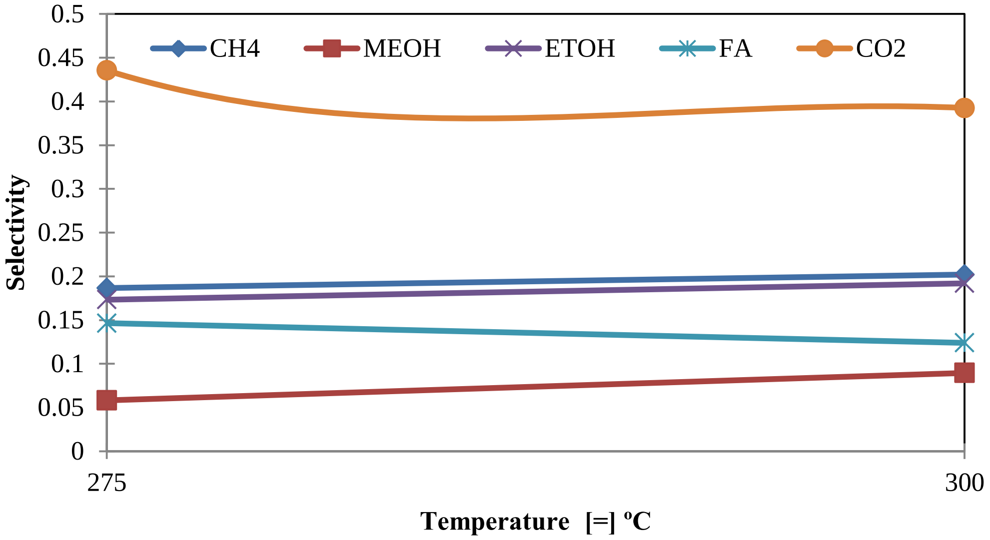

Figure 85. Product distribution obtained with copper, zinc, and ceria containing co-precipitated catalyst, CZCe, (Space time of 0.48 s.gr/cc, catalyst amount:0.2 gr, Mixture-1 feed stream: 50% CO + 50% H_2)

When the promoter type was changed, activity of the copper zinc based co-precipitated methanol synthesis catalysts was enhanced for the zirconia and aluminum promoted catalysts to a large extent. Comparison of promoter effects is tabulated in Table 25 for 250 °C and 275 °C. As it can be seen from the table, carbon monoxide conversion of the aluminum promoted catalyst was three times and zirconia promoted catalyst was four times of the catalyst without promoter at this temperature. For the product distribution, almost all the product was methanol with a selectivity value of 93.8% for the aluminum promoted catalyst. For the zirconia promoted catalyst, methanol selectivity was 77.1% and major side product was carbon dioxide with a selectivity of 15.8%. Highest methanol yield was 11.5% obtained with copper, zinc, and zirconia containing catalyst at 275 °C. In the copper, zinc and alumina or zirconia promoted catalysts, particle sizes of CuO were 8.1 nm for alumina promoted catalyst and 5.0 nm for zirconia promoted catalyst as shown in

Table 8. Higher activity of zirconia promoted catalyst to alumina promoted catalyst could be attributed to CuO particle size.

Table 25. Comparison of carbon monoxide conversion, methanol selectivity and methanol yield for co-precipitated catalysts at 250 °C and 275 °C (Space time of 0.48 s.gr/cc, catalyst amount: 0.2 gr, Mixture-1 feed stream: 50% CO + 50% H_2)

	CO Conversion , %	**CO Conversion , %**	**CH_3OH Selectivity , %**	**CH_3OH Selectivity , %**	**CH_3OH Yield , %**	**CH_3OH Yield , %**
T , °C	250	275	250	275	250	275
CZ	0.7	3.7	38.7	13.7	0.3	0.5
CZA	5.2	11.1	94.8	93.8	4.9	10.4
CZZr	6.6	14.9	94.1	77.1	6.2	11.5
CZCe	0.3	2.5	0	5.8	0	0.1

Aluminum promoted, copper zinc based, co-precipitated catalyst has shown very good activity toward methanol with high conversion and selectivity values. In the preparation of CZA catalyst, aging time was kept constant at 3 hours. It was proposed that changing the aging time could affect the activity of the catalyst in methanol synthesis reaction [31]. Two additional catalysts were prepared at different aging times of 1 hour and 6 hours. Comparison of CZA catalysts aged for 1, 3, and 6 hours is given in Figure 86.

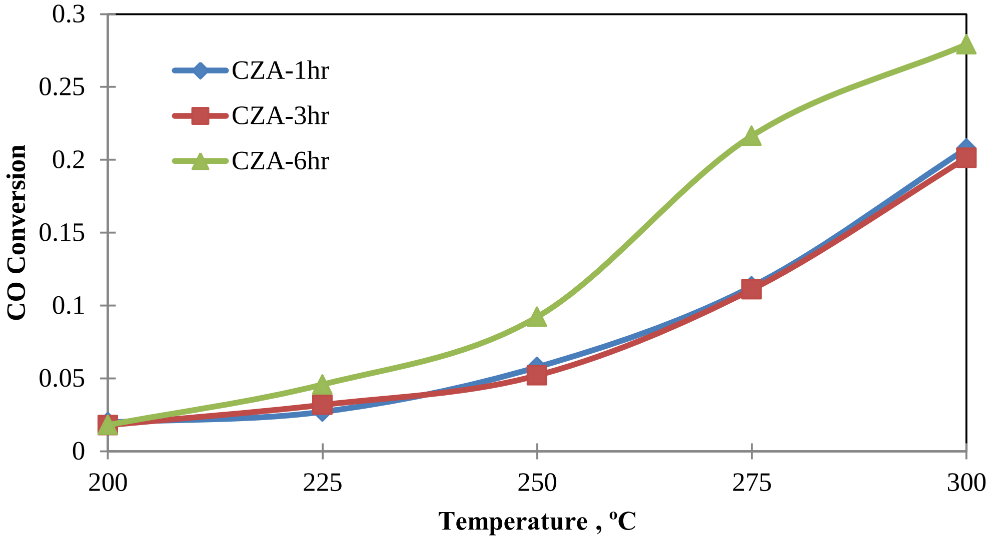

Figure 86. Comparison of carbon monoxide conversions obtained with CZA aged for 1 hour, 3 hours and 6 hours, (Space time of 0.48 s.gr/cc, catalyst amount:0.2 gr, Mixture-1 feed stream: 50% CO + 50% H_2)

As it can be seen from Figure 86, aluminum promoted catalyst aged for 1 hour and 3 hours exhibited almost same carbon monoxide conversions whereas catalyst aged for 6 hours exhibited much more activity. Catalyst aged for 6 hours showed 21.6% carbon monoxide conversion at 275 °C whereas catalyst aged for 3 hours showed 11.1% carbon monoxide conversion at the same temperature. Carbon monoxide conversion was increased by increasing temperature.

When the product selectivities of the one hour aged aluminum promoted catalyst was examined, the main product was methanol as expected. Product distrubition of this catalyst is given in Figure 87. Highest methanol selectivity was obtained at 225 °C as 94.8%. Methanol selectivity decreased upon the increase in temperature due to the exothermic nature of the methanol synthesis reaction. There was a sharp decrease of the methanol selectivity at 300 °C and carbon dioxide selectivity reached to 46.8% at 300 °C which is greater than methanol selectivity at the same temperature. Formation of side products methane, ethanol and formic acid were also seen at high temperatures. At low temperatures, co-existence of methanol and carbon dioxide could be attributed to Boudouard reaction and surface oxidization of CO on copper particles.

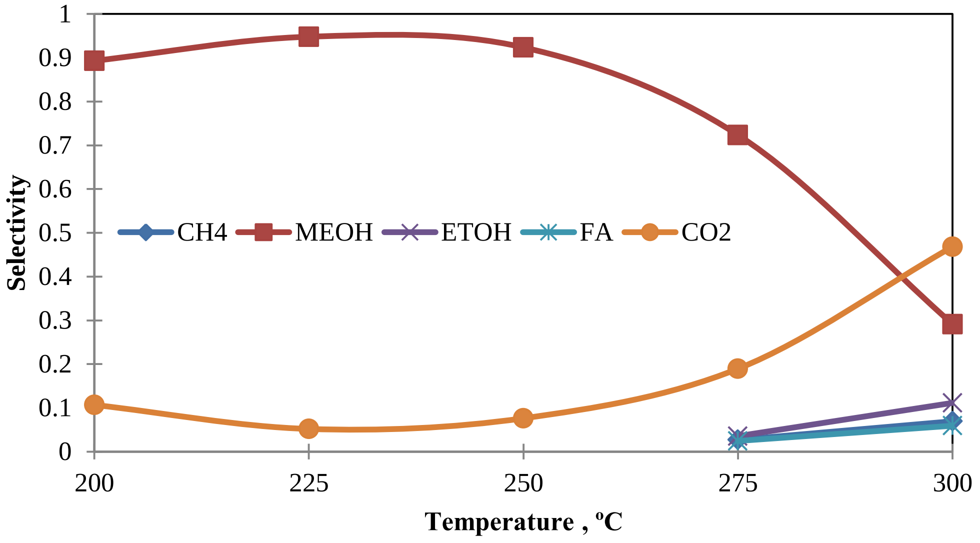

Figure 87. Product distribution obtained with CZA aged for 1 hour (Space time of 0.48 s.gr/cc, catalyst amount: 0.2 gr, Mixture-1 feed stream: 50% CO + 50% H_2)

Six hours aged aluminum promoted catalyst, product distribution of which is given in Figure 88, gave the highest selectivity at 225 °C and 250 °C as 95.4%. Similar to the one hour aged catalyst, methanol selectivity decreased sharply for temperatures 275 °C and 300 °C. Major side product was carbon dioxide at all temperatures and its selectivity increased steadily after 250 °C. However, carbon dioxide selectivity at 300 °C was still lower than the methanol selectivity at 300 °C. Formation of carbon dioxide with methanol at temperatures between 200 °C – 275 °C could be attributed to Boudouard reaction and surface oxidization of CO on copper particles. These reactions were discussed for CZZr catalyst in detail.

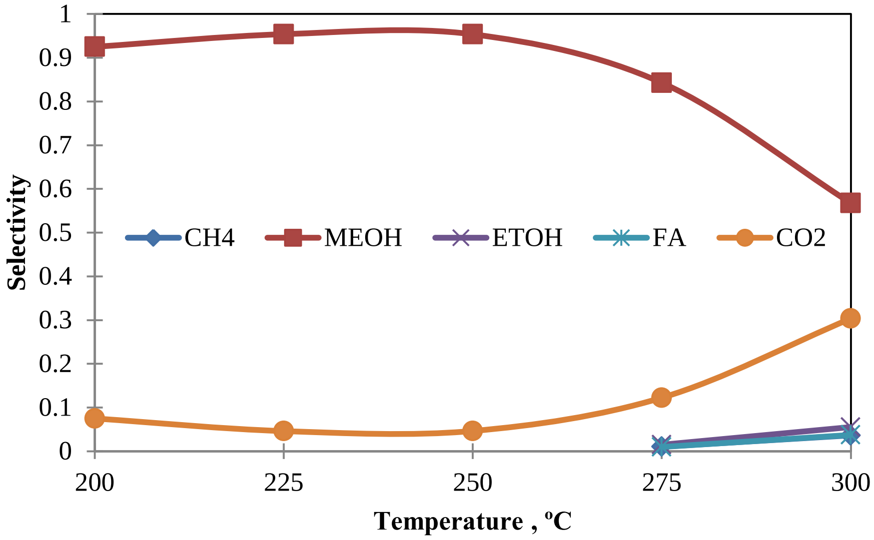

Figure 88. Product distribution obtained with CZA aged for 6 hours (Space time of 0.48 s.gr/cc, catalyst amount: 0.2 gr, Mixture-1 feed stream: 50% CO + 50% H_2)

When the methanol selectivities of different time aged catalysts were compared, it could be seen from Figure 89 that they showed nearly same methanol selectivities up to 250 °C. However, there was a similar trend in the decrease of methanol selectivities upon the increase of temperature from 250 °C. One hour aged catalysts underwent very sharp selectivity decrease among the studied catalysts.

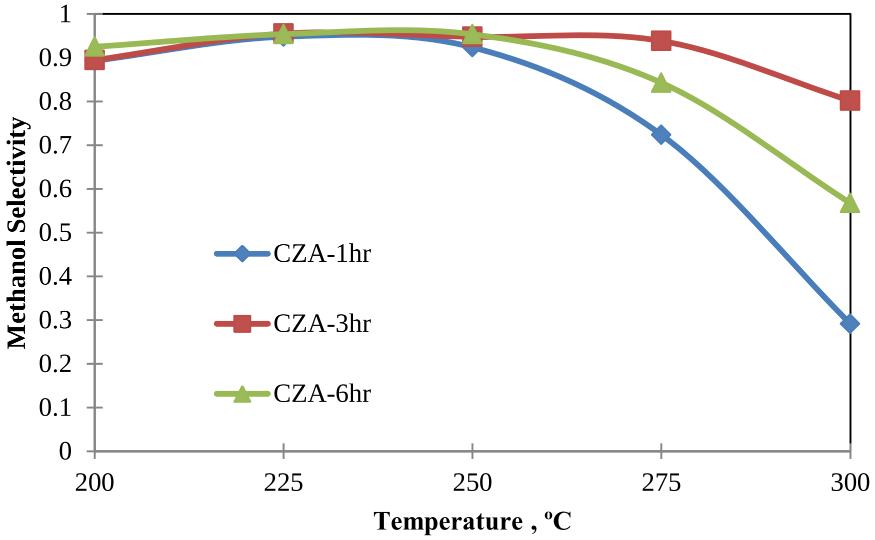

Figure 89. Comparison of methanol selectivities obtained with CZA aged for 1 hour, 3 hours and 6 hours, (Space time of 0.48 s.gr/cc, catalyst amount:0.2 gr, Mixture-1 feed stream: 50% CO + 50% H_2)

Summary of the activity results at 250 °C and 275 °C for different timely aged catalyst is tabulated in Table 26. As it can be seen from the table, highest carbon monoxide conversion was 21.6% for the six hours aged catalyst whereas highest methanol selectivity was obtained at three hours aged catalyst. Highest methanol yield was 18.2% obtained with 6 hours aged catalyst. Dependence of CuO particle size on the activity of co-precipitated catalysts can be better seen with different time aged catalysts. Catalytic activity of different time aged catalysts can be ordered as CZA-6hr > CZA-3hr > CZA-1hr and smallest CuO particle size was obtained with CZA-6hr catalyst as 7.6 nm whereas largest CuO particles were obtained with CZA-1hr catalyst as 9.4 nm.

Table 26. Comparison of carbon monoxide conversion, methanol selectivity and methanol yield for different time aged co-precipitated catalysts at 250 °C and 275°C (Space time of 0.48 s.gr/cc, catalyst amount:0.2 gr, Mixture-1 feed stream: 50% CO + 50% H_2)

Catalyst	**CO Conversion , %**	**CO Conversion , %**	**CH_3OH Selectivity , %**	**CH_3OH Selectivity , %**	**CH_3OH Yield , %**	**CH_3OH Yield , %**
T , °C	250	275	250	275	250	275
CZA-1hr	5.8	11.3	92.4	72.4	5.4	8.2
CZA-3hr	5.2	11.1	94.8	93.8	4.9	10.4
CZA-6hr	9.2	21.6	95.4	84.3	8.8	18.2

In the catalyst preparation, washing was made to remove the undesired and useless ions from the suspension of product containing solution. It also has been reported that ion exchange efficiency could increase upon washing with hot water at ~90 °C [52]. Starting from this point; copper, zinc, and aluminum containing co-precipitated catalyst were prepared and washed with hot water as described in section 6.1 and denoted as "CZA-Hot". Activity test was conducted at 50 bar, space time of 0.48 s.gr/cc, catalyst amount of 0.2 gr for the equimolar feed mixture of carbon monoxide and carbon dioxide. CO conversions are given in Figure 90 in comparison to cold water washed catalyst. Results showed that washing with hot deionized water did not result in any significant change on the carbon monoxide conversion. Conversions were nearly same at all temperatures except 300 °C. CO conversion was 20.1% at 300 °C for the catalyst washed with cold water whereas it was 12.0% for the catalyst washed with hot water at the same temperature.

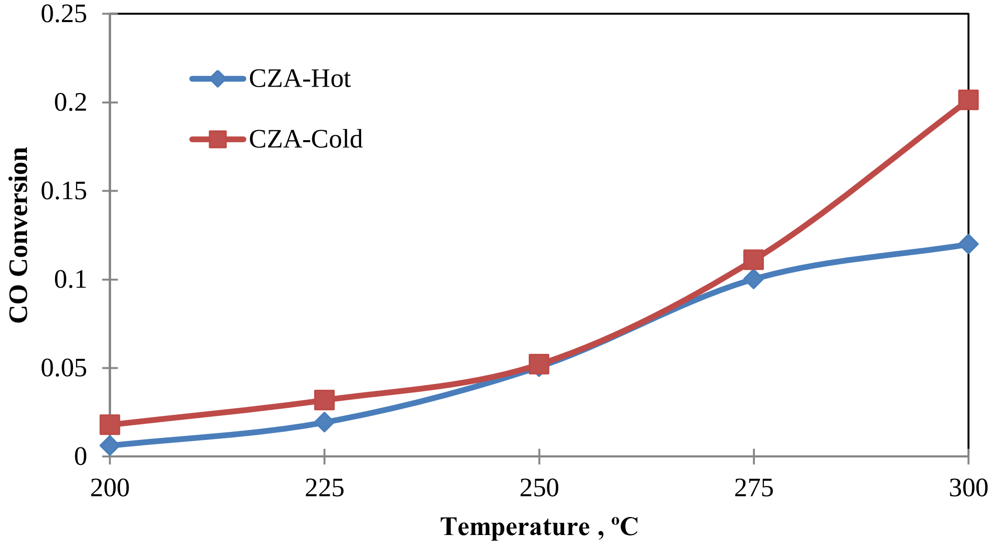

Figure 90. Comparison of carbon monoxide conversions obtained with CZA catalyst washed with hot deionized water (CZA-Hot) and washed with cold deionized water (CZA-Cold) (Space time of 0.48 s.gr/cc, catalyst amount:0.2 gr, Mixture-1 feed stream: 50% CO + 50% H_2)

Product distribution of catalyst washed with hot deionized water is given in Figure 91. As it can be seen from the figure, major product was methanol as expected. Methanol selectivity was the highest at 250 °C as 86.7%. As temperature increased, increase of methanol selectivity was observed until 250 °C and methanol selectivity was 86.7% at this temperature. Major side product was CO_2 at all temperatures and formation of CO_2 and methane showed a parallel trend, indicating reverse dry reforming of methane.

$$2CO + 2H_2 \rightarrow CH_4 + CO_2 \qquad [7]$$

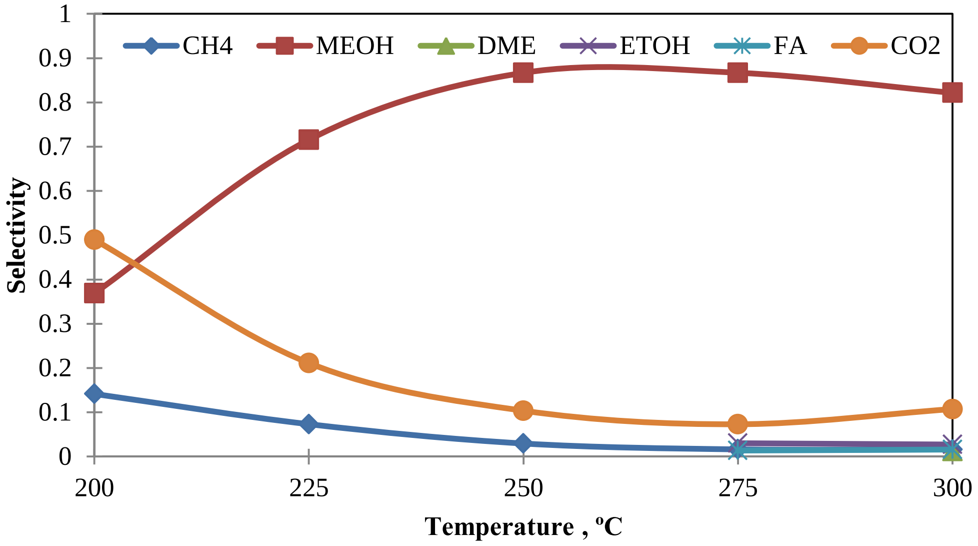

Figure 91. Product distribution obtained with CZA catalyst washed with hot deionized water (CZA-Hot) (Space time of 0.48 s.gr/cc, catalyst amount: 0.2 gr, Mixture-1 feed stream: 50% CO + 50% H_2)

Methanol selectivities of the catalyst washed with hot water were always lower than cold water washed catalyst as it can be seen from Figure 92. At 275 °C, methanol selectivity was 93.8% at 275 °C for CZA-Cold whereas it was 86.7% for CZA-Hot catalyst at the same temperature.

Lower activity of copper, zinc, and alumina containing catalyst washed with hot water can be attributed to the CuO particles size. CuO particle size of CZA-Hot was calculated as 8.4 nm whereas CuO particle size of CZA-Cold was 8.1 nm from XRD patterns. Smaller CuO particle size could be beneficial in catalytic activity in methanol synthesis from CO hydrogenation.

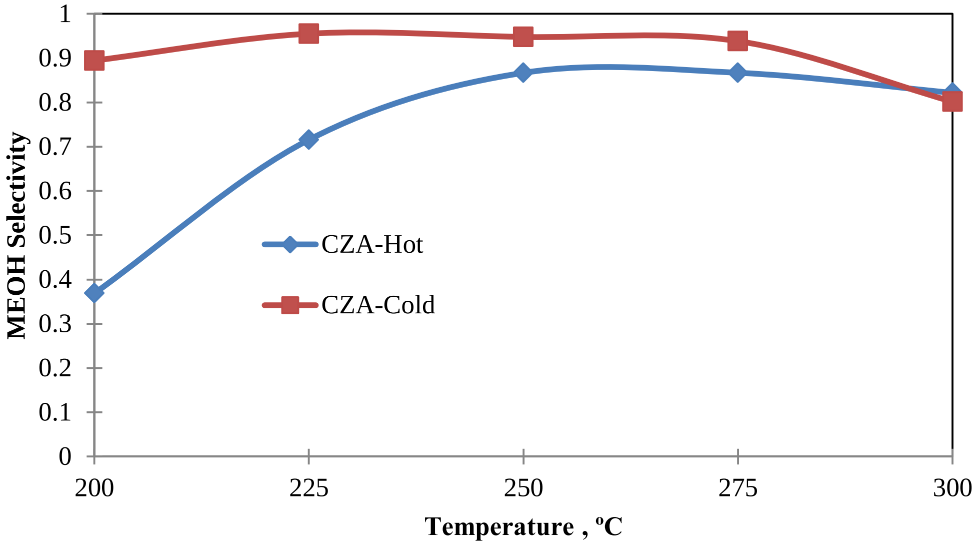

Figure 92. Comparison of methanol selectivities obtained with CZA catalyst washed with hot deionized water (CZA-Hot) and washed with cold deionized water (CZA-Cold) (Space time of 0.48 s.gr/cc, catalyst amount:0.2 gr, Mixture-1 feed stream: 50% CO + 50% H_2)

Effect of calcination temperature was also investigated by the activity tests on the copper, zinc, aluminum containing co-precipitated catalysts. Since the calcination temperature is very important to determine the catalyst properties [17], calcination was conducted in two temperatures. One of them is at high temperature of 550 °C and denoted as "CZA-C550" whereas other is at low temperature of 350 °C and denoted as "CZA-C350". Comparison of carbon monoxide conversions of CZA-C550 and CZA-C350 is given in Figure 93.

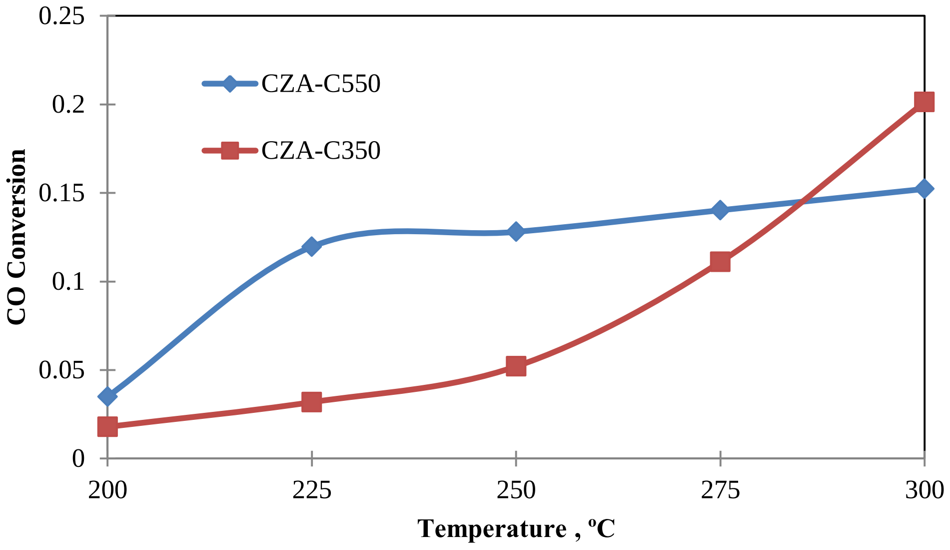

Figure 93. Comparison of carbon monoxide conversions obtained with CZA catalyst calcined at 550 °C (CZA-C550) and at 350 °C (CZA-C350). (Space time of 0.48 s.gr/cc, catalyst amount: 0.2 gr, Mixture-1 feed stream: 50% CO + 50% H_2)

When the copper and zinc containing and aluminum promoted co precipitated catalyst was calcined at high temperatures, carbon monoxide conversion differed than the catalyst calcined at low temperature. At low temperatures, CO conversion of high temperature calcined catalyst, CZA-C550, was higher than low temperature calcined catalyst, CZA-C350. CO conversion was 12.0% at 225 °C whereas CO conversion was 3.2% at the same temperature. With increase in temperature, low temperature calcined catalyst exhibited more CO conversion than high temperature calcined catalyst. Increase of the conversion in the range of 200 °C – 225 °C was not observed with further increase in temperature. Although this could be due to the exothermic nature of methanol synthesis, catalyst deactivation could be the main reason for such a conversion change. Methanol synthesis catalysts undergo deactivation due to copper sintering and coke formation [24, 39, 74]. However, copper sintering at 225 °C would not be the main reason of deactivation since copper particles begin sintering at the onset of 300 °C. High initial activity could result in coke formation in the temperature range of 200 °C – 225 °C and activity increase would not continue after 225 °C.

Product distribution of the high temperature calcined catalyst is given in Figure 94. Methanol was the major product and carbon dioxide the major side product at different temperatures. At 225 °C, highest methanol selectivity was obtained as 88.3% whereas its selectivity decreased to the 66.9% at 300 °C. However, lowest methanol selectivity was 56.7% and obtained at 200 °C. Minor side products were methane, formic acid, and ethanol. Methane and carbon dioxide selectivities showed a similar trend at low temperatures which could be attributed to the reverse methane dry reforming reaction (reaction-7).

$$2CO + 2H_2 \rightarrow CH_4 + CO_2 \qquad [7]$$

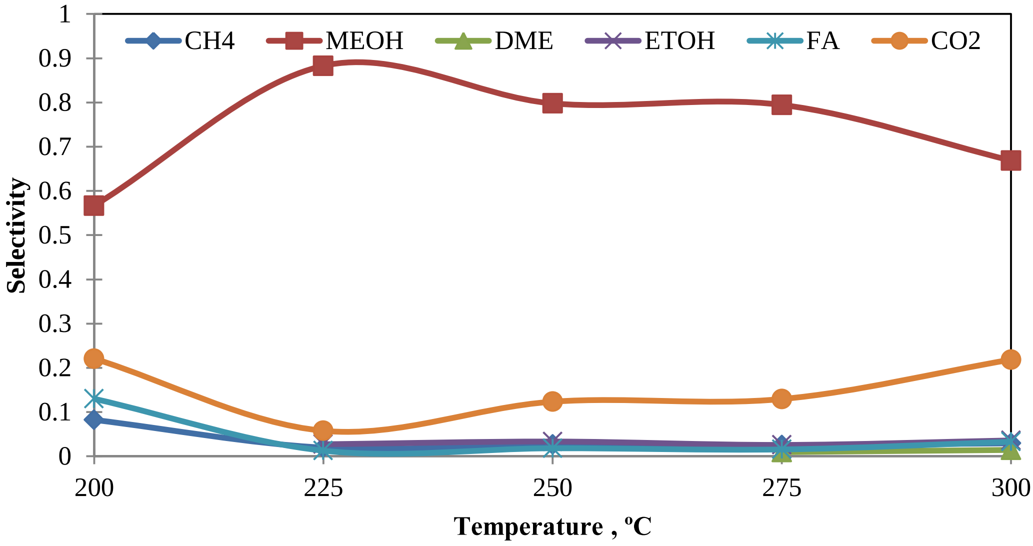

Figure 94. Product distribution obtained with CZA calcined at 550 °C (CZA-C550) (Space time of 0.48 s.gr/cc, catalyst amount: 0.2 gr, Mixture-1 feed stream: 50% CO + 50% H_2)

Methanol selectivities obtained from high temperature calcined co-precipitated catalyst (CZA-C550) and low temperature calcined co-precipitated catalyst (CZA-C350) are compared in Figure 95. Methanol selectivity of the low temperature calcined catalyst was always greater than the high temperature calcined catalyst. Methanol selectivity difference could be attributed to the aggregation of copper crystals due to calcining at 550 °C. Copper particles sinter at temperatures higher than 300 °C [24].

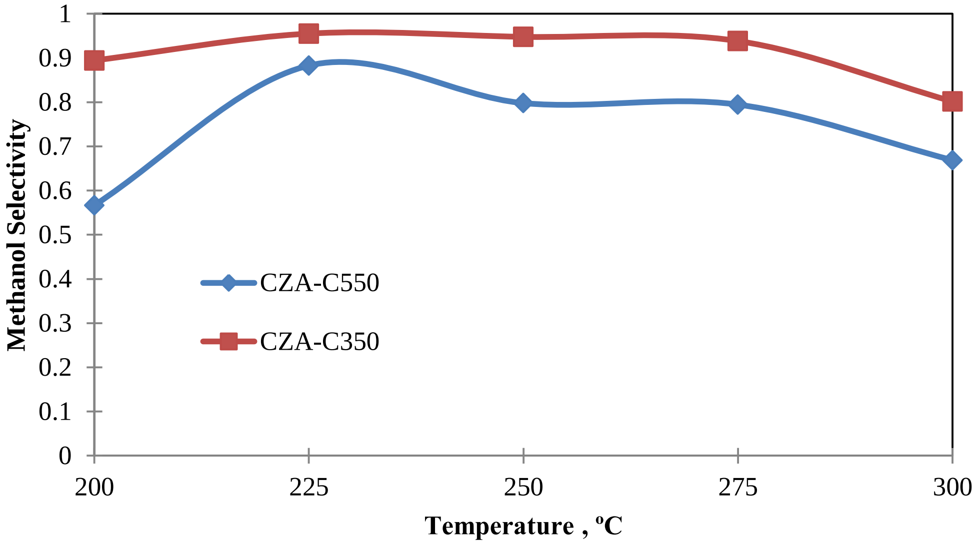

Figure 95. Comparison of methanol selectivities obtained with CZA catalyst calcined at 550 °C (CZA-C550) and at 350 °C (CZA-C350). (Space time of 0.48 s.gr/cc, catalyst amount: 0.2 gr, Mixture-1 feed stream: 50% CO + 50% H_2)

Methanol yields were calculated so as to determine the effect of calcination temperature. Selectivity of methanol obtained with high temperature calcined catalyst was always lower than the selectivity of methanol obtained with low temperature calcined catalyst. On the other hand, high temperature calcined catalyst exhibited more CO conversion than low temperature calcined catalyst. For this reason, yield calculations were made and given in Table 27. Highest methanol yield was 16.1% obtained with low temperature calcined catalyst at 300 °C. On the other hand, very high yield was obtained with high temperature calcined catalyst at 225 °C. In addition, methanol yield of high temperature calcined catalyst was higher than low temperature calcined catalyst at 250 °C and 275 °C. Based on yield calculations, high calcination temperature, 550 °C, exhibited more activity than low temperature calcined catalyst. On the other hand, methanol selectivity of low temperature calcined catalyst was almost close to 1.

Table 27. Comparison of methanol yields obtained with copper, zinc and alumina based co-precipitated catalyst calcined at 550 °C (CZA-C550) and at 350 °C (CZA-C350). (Space time of 0.48 s.gr/cc, catalyst amount: 0.2 gr, Mixture-1 feed stream: 50% CO + 50% H_2)

Temperature , °C	**Methanol Yields , %**	
	CZA-C350	**CZA-C550**
200	1.6	2.0
225	3.1	10.6
250	4.9	10.2
275	10.4	11.1
300	16.1	10.1

Hydrogen reduction was applied to copper, zinc and alumina containing co-precipitated catalyst as described in section 6.1.1. Among the reduction, it was seen from Figure 18 that all CuO particles were reduced to metallic copper, completely. Activity test of reduced catalyst was made and CO conversion is given in Figure 96. CO conversion of reduced catalyst was always greater than non-reduced catalyst except at 300 °C. Conversion difference of reduced catalyst to non-reduced catalyst decreased above 250 °C. CO conversion of reduced catalyst was 12.8% at 250 °C whereas it was 5.2% for no-reduced catalyst.

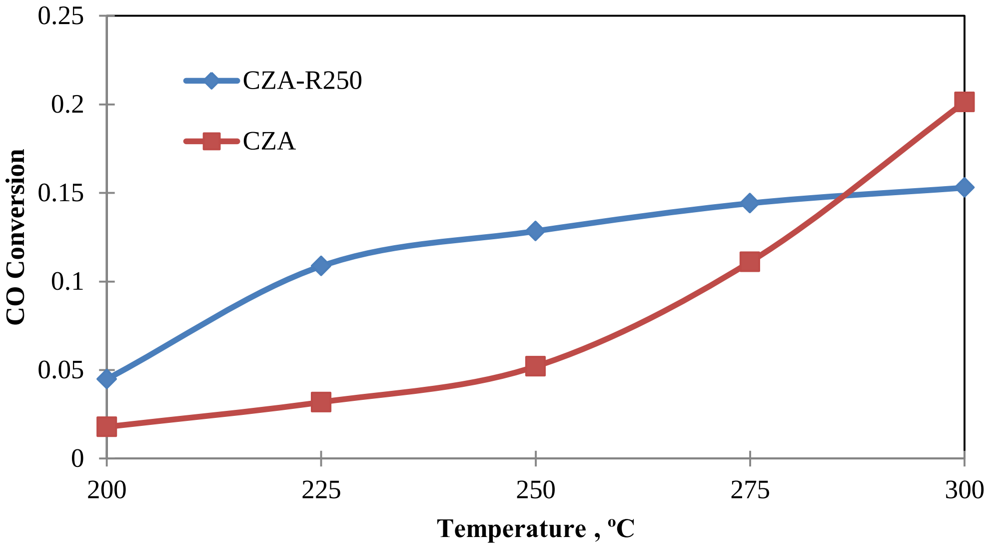

Figure 96. Comparison of carbon monoxide conversions obtained with CZA catalyst reduced at 250 °C (CZA-R550) and no-reduced catalyst (Space time of 0.48 s.gr/cc, catalyst amount:0.2 gr, Mixture-1 feed stream: 50% CO + 50% H_2)

Product distribution of catalyst reduced at 250 °C is given in Figure 97. As it can be seen from figure, major product was methanol as expected. Methanol selectivity was the highest at 225 °C as 83.2%. As temperature increased, decrease of methanol selectivity was observed and methanol selectivity was 70.0% at 300 °C. Major side product was CO_2 at all temperatures and formation of CO_2 and methane showed a parallel trend, indicating reverse dry reforming of methane.

$$2CO + 2H_2 \rightarrow CH_4 + CO_2 \qquad [7]$$

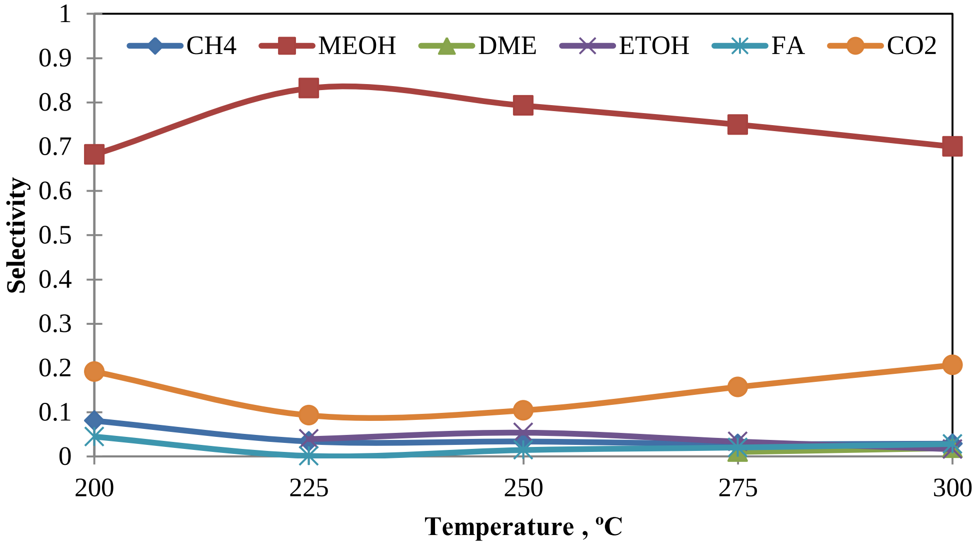

Figure 97. Product distribution obtained with CZA catalyst reduced at 250 °C (CZA-R550) (Space time of 0.48 s.gr/cc, catalyst amount: 0.2 gr, Mixture-1 feed stream: 50% CO + 50% H_2)

Methanol selectivities of reduced catalyst were always lower than no-reduced catalyst as it can be seen from Figure 98. At 275 °C, methanol selectivity was 75.0% for reduced catalyst at 250 °C whereas it was 93.8% for no-reduced catalyst at the same temperature.

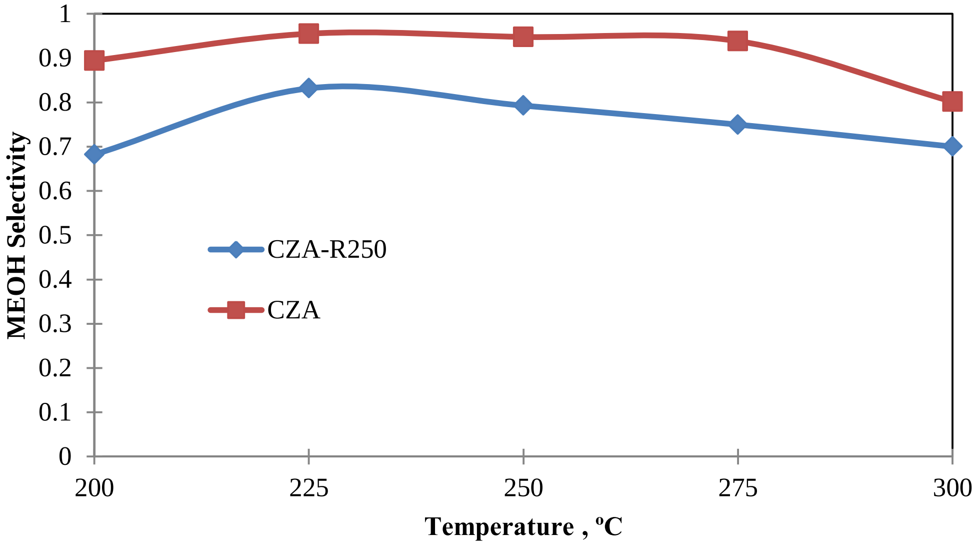

Figure 98. Comparison of methanol selectivities obtained with CZA catalyst reduced at 250 °C (CZA-R550) and no-reduced catalyst (Space time of 0.48 s.gr/cc, catalyst amount:0.2 gr, Mixture-1 feed stream: 50% CO + 50% H_2)

To investigate the effect of reduction on the catalytic activity, yields, obtained by multiplying the conversion with selectivity of desired product, are given in Table 28. According to table, reduced catalyst has higher yield than no-reduced catalyst until 275 °C, in which methanol yields were nearly the same. However, at 300 °C, methanol yield of no-reduced catalyst was greater than reduced catalyst.

Table 28. Comparison of methanol yields obtained with CZA catalyst reduced at 250 °C (CZA-R550) and no-reduced catalyst (Space time of 0.48 s.gr/cc, catalyst amount:0.2 gr, Mixture-1 feed stream: 50% CO + 50% H_2)

Temperature , °C	**Methanol Yields , %**	
	CZA-R250	**CZA**
200	3.1	1.6
225	9.0	3.0
250	10.2	4.9
275	10.8	10.4
300	10.7	16.1

Co-precipitated catalysts could be considered to be very active in methanol synthesis from carbon monoxide hydrogenation. Among the activity test conducted catalysts, it has been concluded that aluminum promoted catalyst which was aged six hours and calcined at 350 °C exhibited the highest activity. Other catalysts also give promising results. This can be seen in Figure 99, 100, and 101. Among co-precipitated catalysts, highest CO conversion was obtained at 300 °C with 6 hour aged catalyst, CZA-6hr. Moreover, at low temperatures, high temperature calcined catalyst, CZA-C550, and reduced gas with hydrogen at 250 °C catalyst, CZA-R250, showed promising CO conversions.

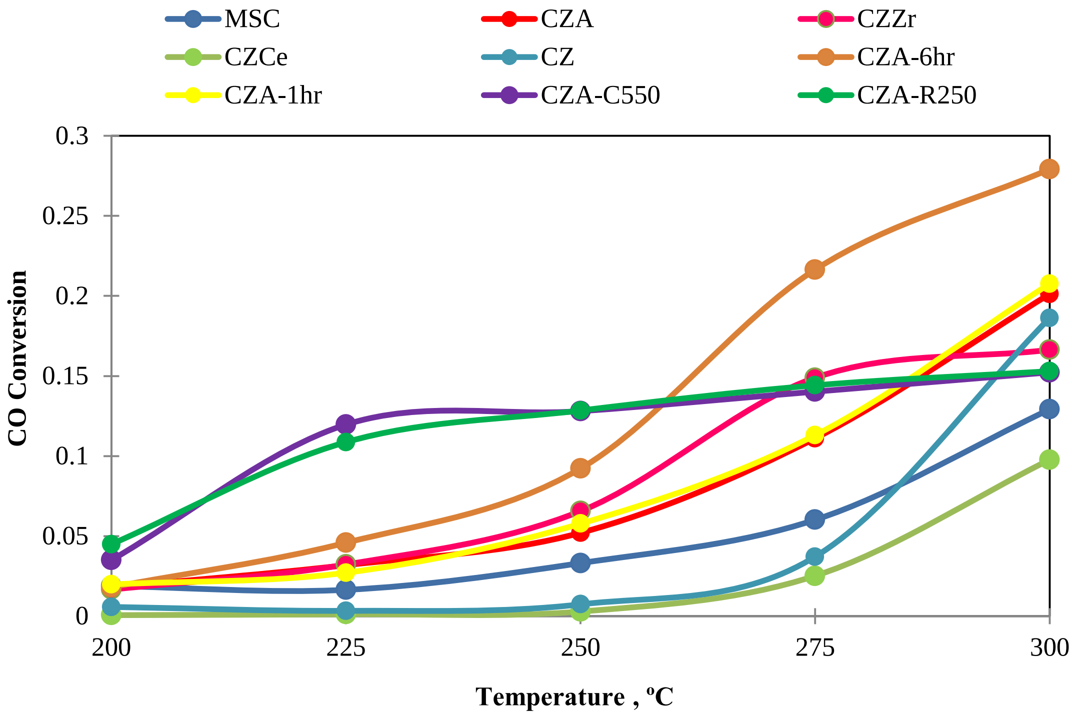

Figure 99. Comparison of carbon monoxide conversions obtained with co-precipitated catalyst and commercial methanol synthesis catalyst (MSC) (Space time of 0.48 s.gr/cc, catalyst amount: 0.2 gr, Mixture-1 feed stream: 50% CO + 50% H_2)

When it comes to methanol selectivity, higher methanol selectivities were obtained than commercial methanol synthesis catalyst (MSC) at all temperatures except 300

°C. Variation of methanol selectivities of co-precipitated catalysts and methanol synthesis catalyst can be seen in Figure 100.

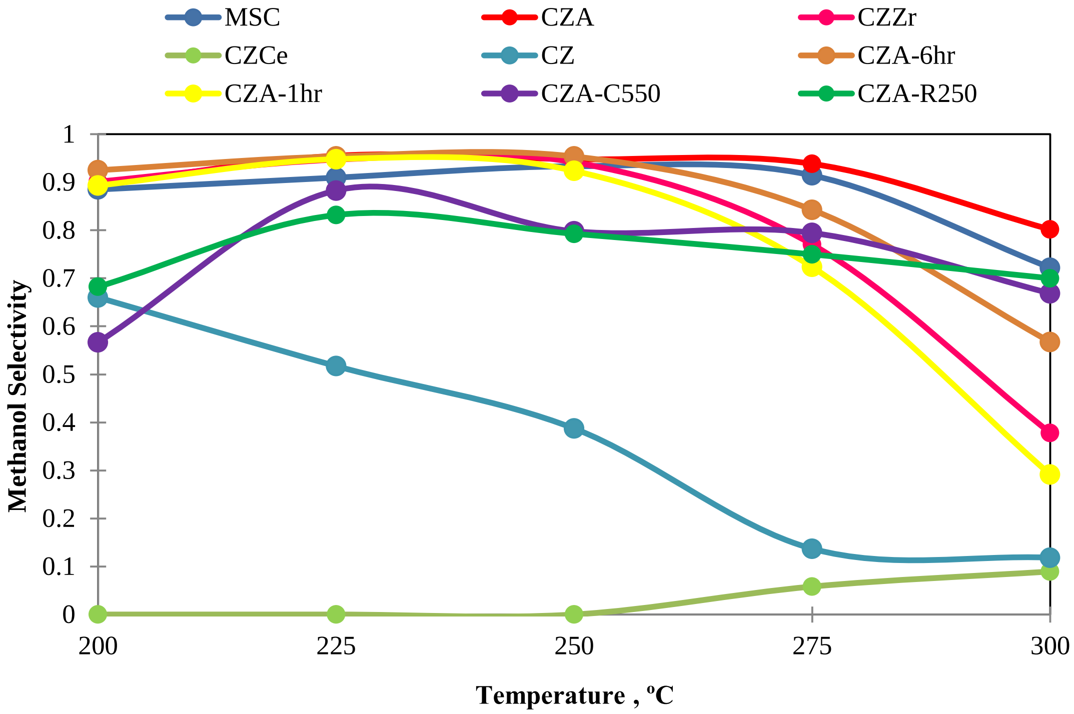

Figure 100. Variation of methanol selectivities over co-precipitated catalysts and commercial methanol synthesis catalyst (MSC) (Space time of 0.48 s.gr/cc, catalyst amount: 0.2 gr, Mixture-1 feed stream: 50% CO + 50% H_2)

Methanol yields of co-precipitated catalysts and methanol synthesis catalyst were compared in Figure 101. Among the activity tests made catalysts, highest methanol yield was 18.2% obtained with 6 hour aged copper, zinc, and alumina containing catalyst, CZA-6hr at 275 °C. Methanol yields of high temperature calcined catalyst and reduced catalyst were very promising.

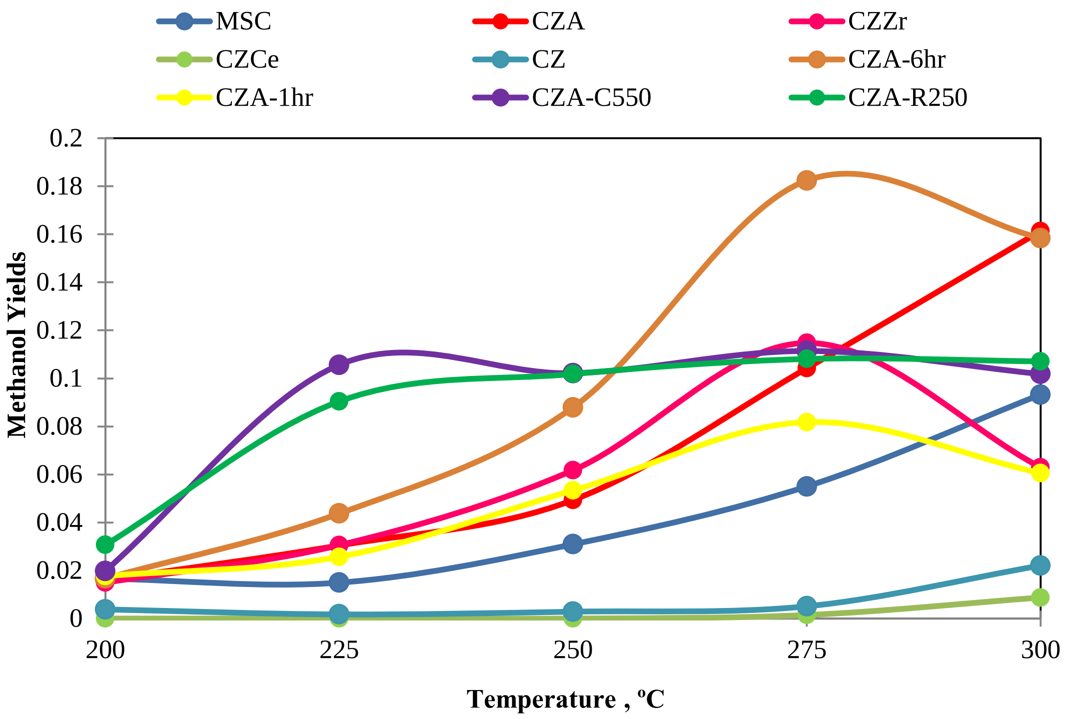

Figure 101. Variation of methanol yields over co-precipitated catalysts and commercial methanol synthesis catalyst (MSC) (Space time of 0.48 s.gr/cc, catalyst amount: 0.2 gr, Mixture-1 feed stream: 50% CO + 50% H_2)

When activity results of co-precipitated catalysts were compared, effects of investigated parameters on the activity were observed. It was seen that promoter addition enhanced the activity. Choice of promoter also affected the activity and zirconia was the best promoter in comparison with alumina and ceria. Aging time was found to be beneficial and washing the catalyst with hot water resulted the decrease in catalytic activity. Calcination at 550 °C and reduction at 250 °C not only enhanced catalytic activity but also very promising yields were obtained at 225 °C.

Activity results of the co-precipitated catalysts exhibited the superiority of the synthesized catalysts in methanol synthesis from carbon monoxide hydrogenation. No significant formation of DME was observed in activity tests since co-precipitated catalysts were weak in acidic functions. These results are encouraging to be used as catalysts for the methanol synthesis step in the direct synthesis of dimethyl ether. By choosing a proper acid catalyst, the obtained methanol could be dehydrated to dimethyl ether. Continuous dehydration of methanol to DME will favor shifting the equilibrium toward DME formation. As a result, carbon monoxide conversion increases. Use of these catalysts in direct DME synthesis is very promising and very high conversions and yield values could be obtained in the direct synthesis of dimethyl ether from the syngas.

8.4.2. Activity results of bi-functional co-precipitated catalyst, H-CZA-TOYO, from Mixture-1 ($CO:H_2=50:50$)

Bi-functional co-precipitated catalyst was prepared and its preparation was explained in detail in the experimental procedure. Bi-functional catalyst was denoted as “H-CZA-TOYO” and its catalytic activity was made for a reactant flow rate of 25 cc/min from mixture-1 stream. Carbon monoxide conversion of bi-functional catalyst is given in Figure 102 in comparison with copper, zinc, and aluminum containing co-precipitated catalyst CZA.

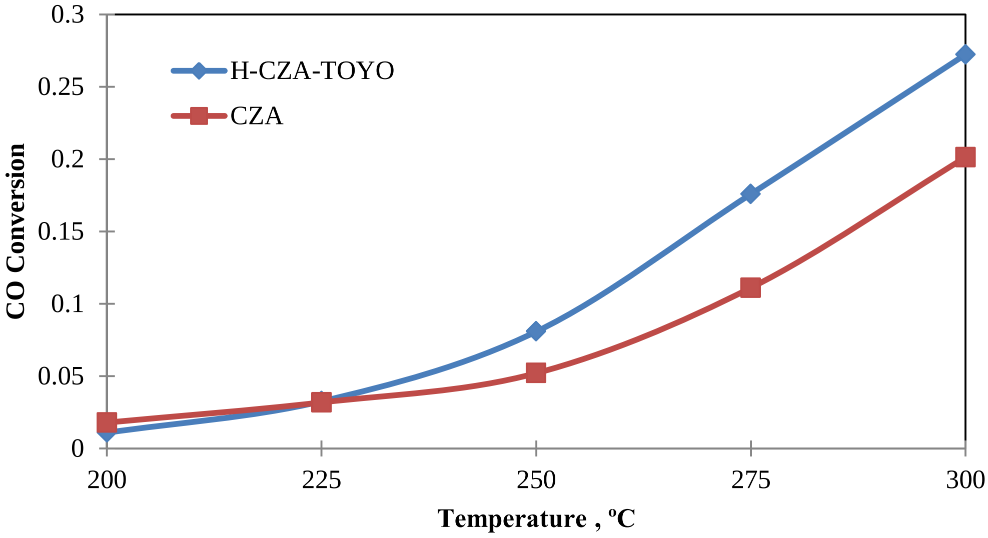

Figure 102. Comparison of carbon monoxide conversions obtained with bi-functional co-precipitated catalyst H-CZA-TOYO copper, zinc, and aluminum containing co-precipitated catalyst CZA (Space time of 0.48 s.gr/cc, catalyst amount: 0.2 gr, Mixture-1 feed stream: 50% CO + 50% H_2)

Carbon monoxide conversion of bi-functional catalyst was higher than the methanol synthesis catalyst above 225 °C and it smoothly increases with increasing temperature. Carbon monoxide conversion of bi-functional catalyst H-CZA-TOYO was 27.2% at 300 °C whereas conversion of copper, zinc and alumina containing co-precipitated catalyst was 20.1% at the same temperature. Product distribution obtained with bi-functional catalyst is given in Figure 103.

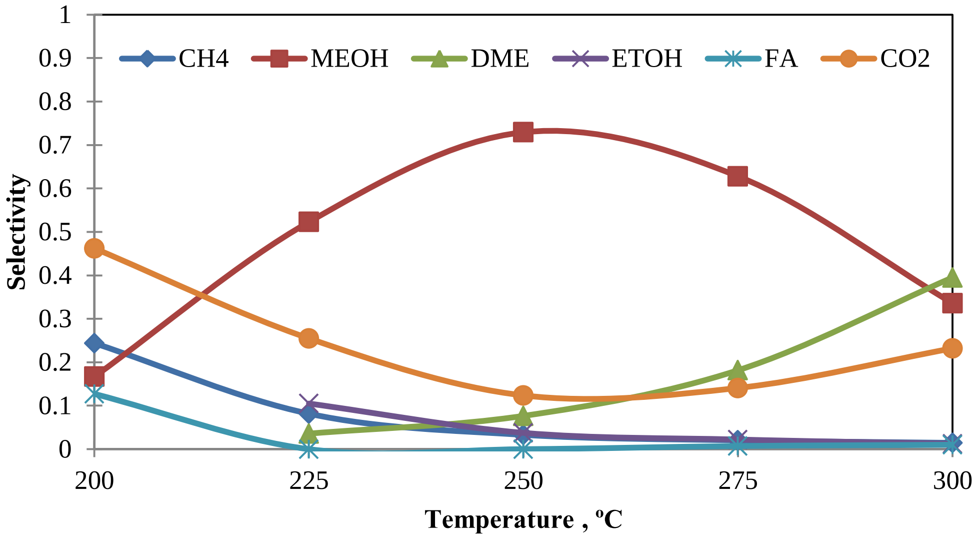

Figure 103. Product distribution obtained with H-CZA-TOYO catalyst (Space time of 0.48 s.gr/cc, catalyst amount: 0.2 gr, Mixture-1 feed stream: 50% CO + 50% H_2)

Product distribution shows that main product was methanol with a selectivity of 72.9% at 250 °C. Methanol selectivity exhibited a volcano type relation with temperature giving a maximum at 250 °C. At 200 °C, main product was carbon dioxide and significant amount of methane was present. Moreover, similar decay in selectivities of methane and carbon dioxide until 250 °C can be attributed to the reverse dry reforming of methane.

$$2CO + 2H_2 \rightarrow CH_4 + CO_2 \qquad [7]$$

After 250 °C, methanol selectivity decreased and dimethyl ether and carbon dioxide selectivity increased. Since there was no methane at high temperatures and carbon dioxide formation was showing an increasing trend with dimethyl ether, it was likely that dimethyl ether was produced from the reaction-1.

$$3CO + 3H_2 \rightarrow C_2H_5OH + CO_2 \qquad [1]$$

The selectivity ratio of dimethyl ether to carbon dioxide is 2 if reaction-6 occurs only. At 300 °C, ratio of selectivities was equal to 1.7. Since selectivity ratio is closer to the ratio obtained with reaction-6, it could be concluded that DME was produced mostly from reaction-6. However, formation of DME through other reactions was also possible.

$$2CO + 4H_2 \rightarrow C_2H_5OH + H_2O \qquad [2]$$

Although bi-functional catalyst had acidic sites to convert produced methanol into dimethyl ether, conversion to dimethyl ether was not successful. Methanol was the main product at almost all temperatures. Dimethyl ether formation was first observed at 225 °C and selectivity of it reached 39.5% at 300 °C which was greater than the selectivity of methanol. It is clear that acidity of the bi-functional catalyst was not strong enough to convert methanol into DME, completely. Drift spectra of pyridine adsorption also confirmed the low acidity of bi-functional catalyst as shown in Figure 34

To enhance the catalytic activity of bi-functional H-CZA-TOYO catalyst in direct synthesis of DME, experimental procedure should be modified so as to increase the acidity. This could be done by changing the weight percentages of methanol dehydration component to methanol synthesis one. Moreover, presence of carbon dioxide in the feed gas inhibits the reverse methane dry reforming and less amount of carbon dioxide forms.

8.5. ACTIVITY RESULTS OF STA IMPREGNATED SBA-15

In this part, methanol reforming catalyst, MRC, and methanol dehydration catalyst, silica tungstic acid (STA) impregnated SBA-15 were physically mixed in equal weights. That is, a mixed catalyst mixture was prepared by mixing the 0.1 gr of catalysts which is responsible for methanol synthesis and 0.1 gr catalysts which is responsible for methanol dehydration and denoted as "HF-STBA-C". Activity test was co-worked with Arslan. A. and results were reported in elsewhere [69]. Activity tested was conducted with feed mixture-1 (50% CO, 50% H_2) at 50 bar and at a flow rate of 50 cc/min in the temperature range of 200 °C – 300 °C. Carbon monoxide conversion values are given in Figure 104 in comparison to methanol reforming catalyst (MRC) HIFUEL R120.

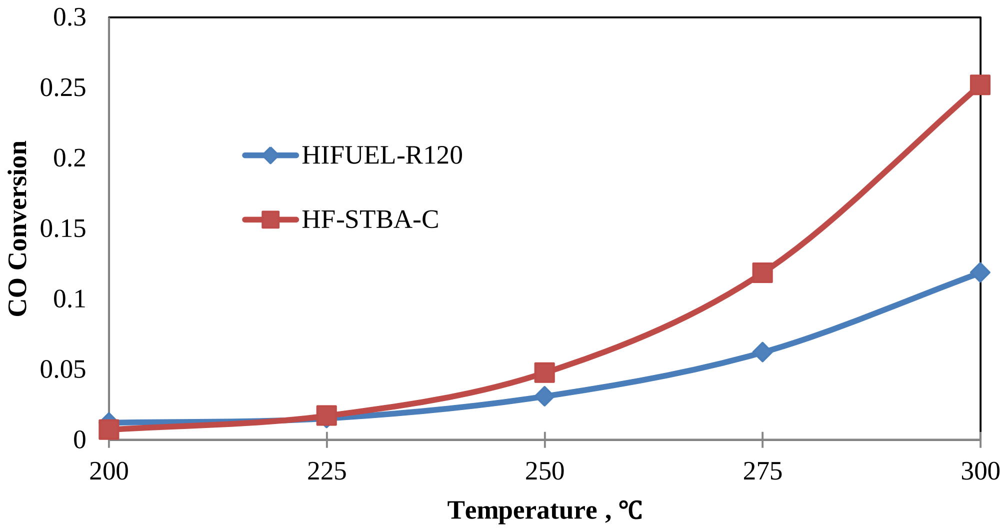

Figure 104. Comparison of carbon monoxide conversions obtained with methanol reforming catalyst and STA impregnated SBA-15 catalyst, HF-STBA-C (space time of 0.48 s.gr/cc, catalyst amount: 0.2 gr, Mixture-1 feed stream: 50%CO +50%H_2)

As it can be seen from Figure 104, mixing of the silica tungstic acid containing dehydration catalyst to the commercial methanol reforming catalyst increased the CO conversion from 11.9% to 25.1% as expected. In situ removal of methanol in the reactor system using the acid impregnated catalyst leads to the part of that increase by overcoming the equilibrium limitations of methanol synthesis reaction by obeying the Le Chatelier's principle above 225 °C. The other reason of the increase of CO conversion is the formation of side products such as formic acid and ethanol. Continuous increase of conversion was seen with temperature increase.

Product distribution of HF-STBA-C is given in Figure 105. Product distribution shows that main product was methanol and dimethyl ether with side products of formic acid, and ethanol. Dimethyl ether selectivity exhibited a volcano type relation with temperature giving a maximum at 250 °C as 47.8%. At 200 °C, main product was carbon dioxide and significant amount of formic acid was present with selectivity 29.7%.

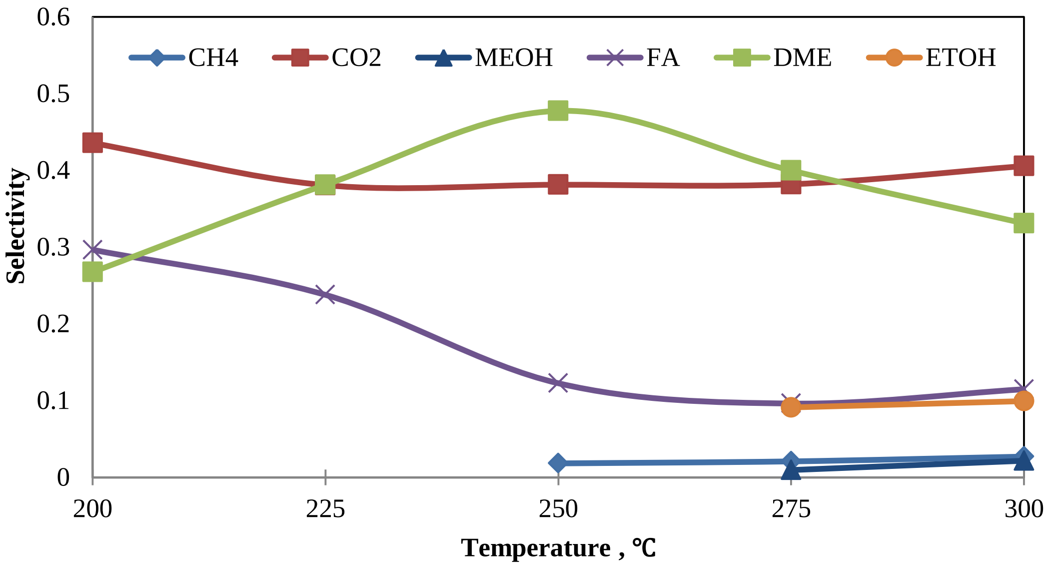

Figure 105. Product distributions obtained with HF-STBA-C catalyst (space time of 0.48 s.gr/cc, catalyst amount: 0.2 gr, Mixture-1=50%CO +50%H_2)

Acidity of the STA impregnated catalyst is adequate to convert all methanol into the dimethyl ether. Strong Brönsted acid sites were present in the methanol dehydration component of direct synthesis catalyst as shown in Figure 39. Methanol was not produced until 275 °C. At this temperature, presence of methanol could be attributed to the activity loss of the methanol dehydration component. Coking of the acidic catalyst could be one of the main reasons for the deactivation [24].

For all the temperatures, significant amount of carbon dioxide was present. Formation of carbon dioxide could follow water gas shift reaction (reaction 5) and direct synthesis of DME reaction (reaction-1).

$CO + H_2O \rightarrow CO_2 + H_2$ [5]

$3\ CO + 3\ H_2 \rightarrow DME + CO_2$ [1]

To prevent the enormous amount of carbon dioxide in the product stream, carbon dioxide could be added to the feed in small amount. By this way, it would prevent the formation of carbon dioxide simply by Le chatelier principle.

CHAPTER 9

CONCLUSIONS

In this study, dimethyl ether, which is an excellent green diesel fuel alternate, was synthesized successfully by direct synthesis route from the synthesis gas. For this purpose, novel catalytic materials for methanol synthesis, methanol dehydration, and direct synthesis of DME from syngas were synthesized and commercial catalysts were also used. In catalyst synthesis; co-precipitation, one-pot hydrothermal synthesis and impregnation methods were applied. Catalyst beds were prepared either by physical mixing of methanol synthesis component with methanol dehydration component or by loading them in series to the fixed bed flow reactor operating at 50 bar. In the case of bi-functional catalysts, catalyst bed was composed of only one catalyst since active sites necessary for the direct synthesis of DME was already present. Catalysts were characterized by XRD, N_2 physisorption, EDS, SEM and DRIFTS of pyridine adsorption. Activity tests were carried out at 50 bar and in a temperature range of 200 °C – 400 °C from two different compositions of feed gas, namely mixture-1 and mixture-2. Mixture-1 was an equimolar composition of CO and H_2 and Mixture-2 was composed of CO, CO_2 and H_2 with a composition $CO:CO_2:H_2=40:10:50$.

Characterization results indicated that catalysts were synthesized successfully. Catalysts with very narrow CuO particles as small as 3 nm were obtained and CuO was reduced completely to Cu by H_2 reduction at 250 °C. High temperature treatments resulted in more crystalline structure with increase in particle sizes due to agglomeration and decrease in surface area due to thermal sintering was also observed. Rod-like morphologies were obtained as shown by SEM images. For the one-pot hydrothermally synthesized materials, very high surface areas such as 800 m^2/g were obtained by the SBA-15 and impregnation of STA was successful. Upon impregnation, decrease on the surface areas was observed due to pore blockage. However, mesoporous structure was still retained as reflected by adsorption-desorption isotherms. In addition to synthesized catalysts, characterization studies of the commercial catalysts were also conducted and results showed that similar morphologies and textural properties were obtained with the synthesized catalysts.

Activity results of the co-precipitated catalysts exhibited the superiority of the synthesized catalysts in methanol synthesis from carbon monoxide hydrogenation. Methanol was synthesized from synthesis gas with very high yield and selectivity values. Aging time, promoter additions, high calcination temperature and reduction with hydrogen enhanced the catalytic activity whereas washing with hot water decreased the catalytic activity. Based on the co-precipitation activity results, best catalyst would be the combination of catalyst preparation parameters of zirconia promoted, 6 hours aged, cold water washed, 550 °C calcined and 250 °C reduced.

Co-precipitated methanol synthesis catalysts were more active than commercial methanol synthesis and methanol reforming catalysts in terms of both selectivity and conversions in carbon monoxide hydrogenation. These results are encouraging to be used as catalysts for the methanol synthesis step in the direct synthesis of dimethyl ether. When used with a proper acid catalyst, continuous dehydration of methanol to DME will favor shifting the equilibrium toward DME formation and as a result, carbon monoxide conversion will increase. Furthermore, bi-functional co-precipitated catalyst, H-CZA-TOYO, did not function very well in the catalytic conversion of methanol to DME due to low acidity. However, CO conversion increase was observed by in-situ conversion of produced methanol to DME.

Results proved that, with the bi-functional catalyst TRC-75(L)-C, HF-AL-C, and STA impregnated SBA-15, very high DME yield values were obtained in direct synthesis of DME from syngas. The performance of the tungsto silisic acid incorporated mesoporous catalyst TRC-75(L) developed in our laboratory was better than the conventional γ-alumina catalyst for the dehydration function of bi-functional catalyst. Higher DME selectivity values were obtained with the TRC-75(L)-C and STA@SBA-15 than the bi-functional catalyst composed of commercial Cu-Zn-alumina and γ-alumina.

Results indicated that presence of CO_2 in the feed stream was shown to have a positive effect on DME selectivity. DME selectivity reached very high values in a temperature range of 250 °C - 275 °C, in the presence of CO_2 (Mixture-2). However, in the absence of CO_2 in the feed stream (Mixture-1), DME selectivity was decreased in the same temperature range. Results indicated that some CO_2 was also converted to DME at temperatures lower than 250°C. Apparently, in the absence of CO_2 in the feed stream, DME was essentially produced through Reaction 1, in which DME and CO_2 are the products. However, presence of CO_2 in the feed stream (Mixture-2), shifted DME formation through Reaction 2, in which water was formed, together with DME. Presence of CO_2 in the feed stream not only enhanced the catalytic activity but also utilization of the most important greenhouse gas was also accomplished.

$$3CO + 3H_2 \rightarrow CH_3OCH_3 + CO_2 \quad [1]$$
$$2CO + 4H_2 \rightarrow CH_3OCH_3 + H_2O \quad [2]$$

Comparison of activity results of DME synthesis obtained by using the bi-functional system, which was composed of methanol reforming catalyst and TRC-75(L) methanol dehydration catalyst, with the results obtained in a system in which these catalysts were charged to the reactor in series, clearly showed the advantages of in-situ conversion of produced methanol to DME. The bi-functional catalytic system prepared in this work functioned very well in DME synthesis directly from synthesis gas. It was concluded that direct synthesis of DME from synthesis gas had significant superiorities in terms of CO conversion and DME yield, over the two step process, involving methanol synthesis and dehydration reactions taking place in consecutive reactors.

Use of these catalysts in direct DME synthesis is very promising and very high conversions and yield values could be obtained in the direct synthesis of dimethyl ether from the syngas.

REFERENCES

[1] Olah G.A., Goeppert A., Prakash G.K.S., Chemical Recycling of Carbon Dioxide to Methanol and Dimethyl Ether: From Greenhouse Gas to Renewable, Environmentally Carbon Neutral Fuels and Synthetic Hydrocarbons, Journal of Organic Chemistry, 74:487-498, 2009.

[2] Dogu T., Varisli D., Alcohols as Alternatives to Petroleum for Environmentally Clean Fuels and Petrochemicals, Turkish Journal of Chemistry, 31:551-567, 2007.

[3] Yoon E.S., Han C., A Review of Sustainable Energy-Recent Development and Future Prospects of Dimethyl Ether (DME), 10th International Symposium on Process System Engineering, PSE2009, 169-175, 2009.

[4] Semelsberger T.A., Borup R.L., Greene H.L., Dimethyl ether (DME) as an Alternative Fuel, Journal of Power Sources, 156:497-511, 2006.

[5] Fleisch T.H., Basu A., Gradassi M.J., Masin J.G., Dimethyl ether: a Fuel for the 21st Century, Natural Gas Conversion IV, Studies in Surface Science and Catalysis, 107:117-125, 1997.

[6] Taupy J.A., DME , a New Energy Carrier, Global Forum: Flaring Reduction and Gas Utilisation, 2006.

[7] Olah, G.A., Goeppert, A., Prakash, G.K.S., Beyond Oil and Gas: The Methanol Economy, Wiley-VCH, Weinheim, 2006.

[8] Arınan, A., Direct Synthesis of Dimethyl Ether (DME) from Synthesis Gas Using Novel Catalysts, M. Sc. Thesis, Middle East Technical University, Ankara, January 2010.

[9] Dme applications. Retrieved from http://www.aboutdme.org/index.asp?bid=219

[10] Dimethyl Ether Technology and Markets, Nexant, PERP07/08-S3, December 2008.

[11] Serov A., Kwak C, Progress in Development of Direct Dimethyl Ether Fuel Cells, Applied Catalysis B: Environmental, 91:1-10, 2010.

[12] Yoon E.S., Han C., A Review of Sustainable Energy - Recent Development and Future Prospects of Dimethyl Ether (DME), 10th International Symposium on Process System Engineering – PSE2009:169-175, 2010.

[13] Ogawa T., Inoue N., Shikada T., Inokoshi O., Ohno Y., Direct Dimethyl Ether (DME) Synthesis from Natural Gas, Studies in Surface Science and Catalysis, 147:379-384, 2004.

[14] Zhang Y., Fei J., Yu Y., Zheng X., Methanol Synthesis from CO_2 Hydrogenation over Cu Based Catalyst Supported on Zirconia Modified ɣ-Al_2O_3, Energy Conversion and Management, 47:3360-3367, 2006.

[15] Sun, K., Lu W., Wang M., Xu X., ‘Low-temperature synthesis of DME from CO_2/H_2 over Pd-modified $CuO–ZnO–Al_2O_3–ZrO_2$/HZSM-5 catalysts, Catalyst Communications, 5:367-370, 2004.

[16] Yoo K.S., Kim J.H., Park M.J., Kim S.J., Joo O.S., Jung K.D., Influence of Solid Acid Catalyst on DME Production Directly from Synthesis Gas Over the Admixed Catalyst of $Cu/ZnO/Al_2O_3$ and Various SAPO Catalysts Applied Catalysis A: General, 330:57-62, 2007.

[17] Mao D., Yang W., Xia J., Zhang B., Lu G., The Direct Synthesis of Dimethyl Eher from Syngas Over Hybrid Catalysts With Sulfate-modified γ-alumina as Methanol Dehydration Components, Journal of Molecular Catalysis A: Chemical, 250:138-144, 2006.

[18] Sofianos A.C., Scurrell M.S., Conversion of Synthesis Gas to Dimethyl Ether Over Bifunctional Catalytic Systems, Ind. Eng. Chem. Res., 30:2372-2378, 1991.

[19] Sun K., Lu W., Qiu F., Liu S., Xu X., Direct Synthesis of DME Over Bifunctional Catalyst: Surface Properties and Catalytic Performance, Applied Catalysis A: General, 252:243-249, 2003.

[20] Sierra I., Erena J., Aguayo A.T., Arandes J.M., Bilbao J., Regeneration of CuO-ZnO-Al_2O_3/ɣ-Al_2O_3 Catalyst in the Direct Synthesis of Dimethyl Ether, Applied Catalysis B: Environmental 94:108-116, 2010.

[21] Tijm P.J.A., Waller F.J., Brown D.M., Methanol Technology Developments for the New Millenium, Applied Catalysis A: General, 221:275-282, 2001.

[22] Klier K., Beretta A., Sun Q., Feeley O. C., Herman R. G., Catalytic Synthesis of Methanol, Higher Alcohols and Ethers, Catalysis Today, 36:3-14, 1997.

[23] Hansen, J.B., Højlund Nielsen P.E, Methanol Synthesis, Handbook of Heterogeneous Catalysis, 2920–2949, 2008.

[24] Twigg, M. V., Spencer, M. S., Deactivation of Supported Copper Metal Catalysts for Hydrogenation Reactions, Appl. Catal. A: Gen., 212:161, 2001.

[25] Arena F., Italiano G., Barbera K., Bonura G., Spadaro L., Frusteri F., Basic Evidences for Methanol-Synthesis Catalyst Design, Catalysis Today, 143:80-85, 2009.

[26] Saito M., Fujitani T., Takeuchi M., Watanabe T., Development of Copper/zinc Oxide-based Multicomponent Catalysts for Methanol Synthesis from Carbon Dioxide and Hydrogen, Applied Catalysis A: General, 138:311-318, 1996.

[27] Meshkini F., Taghizadeh M., Bahmani M., Investigating the Effect of Metal Oxide Additives on the Properties of Cu/ZnO/Al_2O_3 Catalysts in Methanol Synthesis from Syngas Using Factorial Experimental Design, Fuel, 89:170-175, 2010.

[28] Dai W.L., Sun Q., Deng J.F., Wu D., Sun Y.H., XPS studies of Cu/ZnO/Al_2O_3 Ultra-fine Catalysts Derived by a Novel Gel Oxalate Co-precipitation for Methanol Synthesis by CO_2+H_2, Applied Surface Science, 177:172-17, 2001.

[29] Spencer M.S., The role of zinc oxide in Cu/ZnO Catalysts for Methanol Synthesis and the Water-gas Shift Reaction, Topics in Catalysis, 8:259-266, 1999.

[30] Ma Y., Sun Q., Wu D., Fan W.H., Zhang Y.L., Deng J.F., A Practical Approach for the Preparation of High Activity Cu/ZnO/ZrO_2 Catalyst for Methanol Synthesis from CO_2 Hydrogenation, Applied Catalysis A: General, 171:45-55, 1998.

[31] Raudaskoski R., Niemela M.V., Keiski R.L., The Effect of Ageing Time on Co-precipitated Cu/ZnO/ZrO_2 Catalysts Used in Methanol Synthesis from CO_2 and H_2, Topics in Catalysis, 45:57-60, 2007.

[32] Sun K., Lu W., Qiu F., Liu S., Xu X., Direct synthesis of DME Over Bifunctional Catalyst: Surface Properties and Catalytic Performance, Applied Catalysis A: General, 252:243-249, 2003.

[33] Flores J.H., Peixoto D.P.B., Appel L.G., Avillez R.R., Pais da Silva M.I., The Influence of Different Methanol Synthesis Catalysts on Direct Synthesis of DME from Syngas, Catalysis Today, 172:218-225, 2011.

[34] Słoczynski J., Grabowski R., Olszewski P., Kozłowska A., Stoch J., Lachowska M., Skrzypek J., Effect of Metal Oxide Additives on the Activity and Stability of Cu/ZnO/ZrO_2 Catalysts in the Synthesis of Methanol from CO_2 and H_2, Applied Catalysis: A General, 310:127-137, 2006.

[35] Shen W.J., Ichihashi Y., Matsumura Y., Low Temperature Methanol Synthesis from Carbon Monoxide and Hydrogen Over Ceria Supported Copper Catalyst, Applied Catalysis A: General, 282:221-226, 2005.

[36] Pokrovski Konstantin A., Rhodes M.D., Bell A.T., Effects of Cerium Incorporation into Zirconia on the Activity of Cu/ZrO_2 for Methanol Synthesis via CO Hydrogenation, Journal of Catalysis, 235:368-377, 2005.

[37] Kaluza, S., Behrens, M., Schiefenhövel N., Kniep B., Fischer R., Schlögl R. and Muhler M., A Novel Synthesis Route for Cu/ZnO/Al_2O_3 Catalysts Used in Methanol Synthesis: Combining Continuous Consecutive Precipitation with Continuous Aging of the Precipitate, Chem. Cat. Chem., 3: 189–199,2011.

[38] Guo X., Mao D., Lu G., Wang S., Wu G., Glycine-nitrate Combustion Synthesis of CuO-ZnO-ZrO_2 Catalysts for Methanol Synthesis from CO_2 Hydrogenation, Journal of Catalysis, 271:178-185, 2010.

[39] Kim J.-H., Park M.J., Kim S.J., Joo O.-S., Jung K.-D., DME Synthesis from Synthesis Gas on the Admixed Catalysts of Cu/ZnO/Al_2O_3 and ZSM-5, Applied Catalysis A: General 264:37-41, 2004.

[40] Yaripour F., Mollavali M., Mohammadi Jam Sh., Atashi H., Catalytic Dehydration of Methanol to Dimethyl Ether Catalyzed by Aluminum Phosphate Catalysts, Energy&Fuels, 23:1896-1900, 2009.

[41] Yaripour F., Baghaei F., Schmidt I., Perregaard J., Synthesis of Dimethyl Ether from Methanol Over Aluminum Phosphate and Silica–Titania Catalysts, Catalysis Communications, 6:542-549, 2005.

[42] Khaleel A., Methanol Dehydration to Dimethyl Ether over Highly Porous Xerogel Alumina Catalyst: Flow Rate Effect, Fuel Processing Technology, 91:1505-1509, 2010.

[43] Fu Y., Hong T., Chen J., Auroux A., Shen J., Surface Acidity and the Dehydration of Methanol to Dimethyl Ether, Thermochimica Acta, 434:22-26, 2005.

[44] Vishwanathan V., Jun K.W., Kim J.W., Roh H.S., Vapour Phase Dehydration of Crude Methanol to Dimethyl Ether Over Na-modified H-ZSM-5 Catalysts, Applied Catalysis A: General, 276:251-255, 2004.

[45] Tokay K.C., Dogu T., Dogu G., Dimethyl Ether Synthesis Over Alumina Based Catalyst, Chemical Engineering Journal, 184:278-285, 2012.

[46] Xu, M., Lunsford, J.H., Goodman, D.W., Synthesis of Dimethyl Ether (DME) from Methanol over Solid-acid Catalysts, Applied Catalysis A: General, 149: 289-301, 1997.

[47] Çiftçi A., Sezgi N.A., Dogu T., Nafion incorporated silicate structured Nanocomposites Catalysts for DME Synthesis, Ind. Eng. Chem. Res., 49:6756-6752, 2010.

[48] Ciftci A., Varisli D., Dogu T, Dimethyl Ether Synthesis over Novel Silicotungstic Acid Incorporated Nanostructured Catalysts, Int. J. Chemical Reactor Eng, 8, A45, 2010.

[49] Sandler S.I., Chemical and Engineering Thermodynamics, 3th Ed., Wiley, New York, 1999.

[50] Wijngaarden R.J., Kronberg A., Westerterp K.R., Industrial Catalysis Optimizing Catalysts and Processes, Wiley-vch, 1998.

[51] Haber J., Block J.H., Delmon, B.,Methods and Procedures for Catalysts Characterization, Handbook of Heterogeneous Catalysis, Wiley-VCH Verlag GmbH, Weinheim, Germany., 1230-1232, 2008.

[52] Perego C., Villa P., Catalyst Preparation Methods, Catalysis Today, 34:281-305, 1994.

[53] Schüth, F., Hesse, M. and Unger K. K., Precipitation and Co-precipitation: Handbook of Heterogeneous Catalysis, 100–119, 2008.

[54] Baerns M., Basic Principles in Applied Catalysis, New York, Springer - Verlag, 2004.

[55] Sener C., Synthesis and Characterization of Pd-MCM Type Mesoporous Nanocomposite Materials, M. Sc. Thesis, Middle East Technical University, January 2006.

[56] Kleitz F., Ordered Mesoporous Materials, Handbook of Heterogeneous Catalysis, 178–219, 2008.

[57] Kresge, C.T., Leonowicz, M.E., Roth W.J., Varuli J.C., Beck, J.S. Ordered Mesporous Molecular Sieves Synthesized by a Liquid Crystal Template Mechanism, Nature, 359:710, 1992.

[58] Gucbilmez Y., Dogu T., Balci S., Ethylene and Acetaldehyde Production by Selective Oxidation of Ethanol Using Mesoporous V-MCM-41 Catalysts. Ind. Eng. Chem. Res., 45:3496, 2006.

[59] Varisli D., Dogu T., Dogu G., Novel Mesoporous Nanocomposite WO_x-Silicate Acidic Catalysts: Ethylene and DEE from Ethanol, Ind. Eng. Chem. Res., 48:9394, 2009.

[60] Varisli D., Dogu T., Dogu G, Petrochemicals from Ethanol over a W-Si-based Nanocomposite Bidisperse Solid Acid Catalyst, Chem. Eng. Sci., 65, 153, 2010.

[61] Varisli D., Dogu T., Dogu G. Silicotungstic Acid Impregnated MCM-41-Like Mesoporous Solid Acid Catalysts for Dehydration of Ethanol, Ind. Eng. Chem. Res., 47:4071, 2008.

[62] Zhao D., Jianglin F., Qisheng H., Melosh N., Fredrickson G. H., Chmelka B. F., Stucky G. D., Triblock Copolymer Syntheses of Mesoporous Silica with Periodic 50 to 300 Angstrom Pores, Science, 279:548-552, 1998.

[63] Aktas O., Yasyerli S., Dogu T., Dogu G., Structural Variations of MCF and SBA-15-like Mesoporous Materials as a Result of Differences in Synthesis Solution pH, Materials Chemistry and Physics, 131:151-159, 2011.

[64] Chorkendorff I., Niemantsverdriet J.W., Concept of Modern Catalysis and Kinetics, 2nd ed., Wiley-VCH, 2007.

[65] Yao N., Synthesis and Characterization of Pt/Sn-MCM-41 Petroleum Reforming Catalysts, PhD Thesis, Yale University, January 2002.

[66] Singh K.S.W., Neimark A.V., Thommes M., Characterization of Solid Catalysts: Handbook of Heterogeneous Catalysis, Wiley-VCH Verlag GmbH, Weinheim, 721-725, 2008.

[67] Walker , C. Surface science techniques. Retrieved from http://www.uksaf.org/tech/ftir.html

[68] Arslan A., Direct synthesis of DME from Syngas, ChE499-Topics in Chemical Engineering, Middle East Technical University, January 2012.

[69] Mbaraka I.K., Shanks B.H., Design of multifunctionalized mesoporous silicas for esterification of fatty acid**,** Journal of Catalysis, 229:365-373, 2005.

[70] Varışlı D., Kinetic Studies for Dimethyl Ether and Diethyl Ether Production, PhD. Thesis, Middle East Technical University, Ankara, September 2007.

[71] Tennyson W., X-Ray Diffraction: The Basics Followed by a few Examples of Data Analysis, Nanolab/NSF NUE/Bumm, 2005.

[72] Damyanova S., Fierro J.L., Sobrados I., Sanz J., Surface Behavior of Supported 12-Heteropoly Acid As Revealed by Nuclear Magnetic Resonance, X-ray Photoelectron Spectroscopy and Fourier Transform Infrared Techniques, Langmuir, 15(2):469-476, 1999.

[73] Vanden Bussche K.M., Froment G.F., A Steady State Kinetic Model for Methanol Synthesis and the Water Gas Shift Reaction on a Commercial $Cu/ZnO/Al_2O_3$ Catalyst, J. Catal., 161:1-10, 1996.

[74] Erena J., Sierra I., Olazar M., Gayubo A.G., Aguayo A.T., Deactivation of a $CuO\text{-}ZnO\text{-}Al_2O_3/\gamma\text{-}Al_2O_3$ Catalyst in the Synthesis of Dimethyl Ether, Ind. Eng. Chem. Res., 47:2238-2247, 2008.

APPENDICES

APPENDIX A

FUGACITY COEFFICIENTS OF SPECIES INVOLVED IN DME SYNTHESIS

Fugacity coefficients of the species involved in DME synthesis was calculated by Peng Robinson equation of state and coefficients are tabulated with respect to temperature in the range of 100 °C – 400 °C and pressure in the range of 1 bar – 70 bar in Tables 29-33. K_{ϕ} values for DME reactions (reaction1&2) and methanol synthesis reaction (reaction-3) are also given in these tables. K_{ϕ} values were given in equations A1-A3.

$3CO + 3H_2 \rightarrow CH_3OCH_3 + CO_2$ [1]

$$K_{\phi 1} = \frac{\phi_{CH3OH} * \phi_{CO2}}{(\phi_{CO})^3 * (\phi_{H2})^3} \qquad [A1.]$$

$2CO + 4H_2 \rightarrow CH_3OCH_3 + H_2O$ [2]

$$K_{\phi 2} = \frac{\phi_{CH3OH} * \phi_{H2O}}{(\phi_{CO})^2 * (\phi_{H2})^4} \qquad [A2.]$$

$CO + 2H_2 \rightarrow CH_3OH$ [3]

$$K_{\phi 3} = \frac{\phi_{CH3OH}}{\phi_{CO} * (\phi_{H2})^2} \qquad [A3.]$$

Table 29. Fugacity coefficients of the species involved in DME synthesis calculated by Peng Robinson equation of state at 1 bar

T , ºC	ϕ_{CO}	ϕ_{CO2}	ϕ_{H2}	ϕ_{DME}	ϕ_{H2O}	ϕ_{CH3OH}	$K_{\phi 1}$	$K_{\phi 2}$	$K_{\phi 3}$
100	1.000	0.997	1.000	0.991	0.992	0.987	0.988	0.982	0.986
125	1.000	0.998	1.000	0.993	0.993	0.989	0.989	0.984	0.988
150	1.000	0.998	1.000	0.994	0.994	0.991	0.991	0.986	0.990
175	1.000	0.999	1.000	0.995	0.995	0.993	0.992	0.988	0.992
200	1.000	0.999	1.000	0.996	0.996	0.994	0.993	0.990	0.993
225	1.000	0.999	1.000	0.996	0.996	0.995	0.994	0.991	0.994
250	1.000	0.999	1.000	0.997	0.997	0.996	0.995	0.992	0.995
275	1.000	1.000	1.000	0.997	0.997	0.996	0.995	0.993	0.995
300	1.000	1.000	1.000	0.998	0.998	0.997	0.996	0.994	0.996
325	1.000	1.000	1.000	0.998	0.998	0.997	0.996	0.995	0.997
350	1.000	1.000	1.000	0.998	0.998	0.998	0.996	0.995	0.997
375	1.000	1.000	1.000	0.999	0.998	0.998	0.997	0.995	0.997
400	1.000	1.000	1.000	0.999	0.998	0.998	0.997	0.996	0.998

Table 30. Fugacity coefficients of the species involved in DME synthesis calculated by Peng Robinson equation of state at 10 bar

T , ºC	ϕ_{CO}	ϕ_{CO2}	ϕ_{H2}	ϕ_{DME}	ϕ_{H2O}	ϕ_{CH3OH}	$K_{\phi 1}$	$K_{\phi 2}$	$K_{\phi 3}$
100	1.000	0.974	1.003	0.913	0.915	0.869	0.880	0.825	0.863
125	1.001	0.979	1.003	0.928	0.929	0.893	0.897	0.850	0.886
150	1.002	0.984	1.003	0.940	0.940	0.911	0.911	0.870	0.904
175	1.003	0.987	1.003	0.950	0.949	0.926	0.923	0.887	0.919
200	1.003	0.990	1.003	0.958	0.956	0.939	0.932	0.901	0.931
225	1.003	0.992	1.003	0.965	0.962	0.949	0.940	0.912	0.941
250	1.003	0.994	1.003	0.970	0.967	0.957	0.947	0.922	0.949
275	1.003	0.995	1.003	0.975	0.971	0.964	0.953	0.931	0.956
300	1.004	0.996	1.003	0.979	0.975	0.970	0.958	0.938	0.961
325	1.004	0.997	1.003	0.982	0.978	0.974	0.962	0.944	0.966
350	1.004	0.998	1.002	0.985	0.981	0.978	0.966	0.950	0.970
375	1.004	0.999	1.002	0.987	0.983	0.982	0.969	0.955	0.974
400	1.004	1.000	1.002	0.989	0.985	0.985	0.972	0.959	0.977

Table 31. Fugacity coefficients of the species involved in DME synthesis calculated by Peng Robinson equation of state at 30 bar

T , ºC	ϕ_{CO}	ϕ_{CO2}	ϕ_{H2}	ϕ_{DME}	ϕ_{H2O}	ϕ_{CH3OH}	$K_{\phi 1}$	$K_{\phi 2}$	$K_{\phi 3}$
100	1.002	0.924	1.009	0.744	0.740	0.121	0.666	0.529	0.119
125	1.004	0.940	1.009	0.790	0.785	0.242	0.714	0.594	0.237
150	1.006	0.952	1.009	0.826	0.819	0.734	0.752	0.646	0.717
175	1.008	0.962	1.009	0.855	0.846	0.782	0.784	0.689	0.763
200	1.009	0.970	1.008	0.879	0.869	0.819	0.810	0.725	0.799
225	1.010	0.976	1.008	0.898	0.887	0.849	0.832	0.756	0.828
250	1.010	0.982	1.008	0.914	0.902	0.874	0.850	0.783	0.851
275	1.010	0.986	1.008	0.927	0.915	0.894	0.866	0.805	0.871
300	1.011	0.990	1.008	0.939	0.925	0.911	0.880	0.825	0.888
325	1.011	0.993	1.007	0.948	0.935	0.925	0.891	0.842	0.902
350	1.011	0.950	1.007	0.956	0.943	0.937	0.861	0.857	0.914
375	1.011	0.997	1.007	0.963	0.949	0.947	0.911	0.870	0.924
400	1.011	0.999	1.007	0.969	0.955	0.956	0.918	0.882	0.932

Table 32. Fugacity coefficients of the species involved in DME synthesis calculated by Peng Robinson equation of state at 50 bar

T , ºC	ϕ_{CO}	ϕ_{CO2}	ϕ_{H2}	ϕ_{DME}	ϕ_{H2O}	ϕ_{CH3OH}	$K_{\phi 1}$	$K_{\phi 2}$	$K_{\phi 3}$
100	1.004	0.876	1.015	0.497	0.020	0.075	0.412	0.009	0.073
125	1.008	0.902	1.015	0.654	0.046	0.150	0.551	0.028	0.145
150	1.011	0.922	1.015	0.719	0.094	0.266	0.614	0.062	0.256
175	1.013	0.938	1.015	0.767	0.741	0.427	0.662	0.522	0.410
200	1.015	0.951	1.014	0.805	0.780	0.699	0.702	0.577	0.670
225	1.016	0.962	1.014	0.836	0.812	0.753	0.735	0.622	0.721
250	1.017	0.970	1.013	0.862	0.837	0.794	0.764	0.661	0.760
275	1.018	0.977	1.013	0.883	0.859	0.827	0.788	0.695	0.792
300	1.018	0.983	1.013	0.901	0.877	0.855	0.809	0.725	0.819
325	1.018	0.988	1.012	0.917	0.892	0.878	0.827	0.751	0.841
350	1.018	0.992	1.012	0.930	0.905	0.897	0.843	0.774	0.860
375	1.018	0.996	1.012	0.941	0.916	0.914	0.857	0.794	0.877
400	1.018	0.998	1.012	0.951	0.926	0.928	0.869	0.812	0.891

Table 33. Fugacity coefficients of the species involved in DME synthesis calculated by Peng Robinson equation of state at 70 bar

T , ºC	ϕ_{CO}	ϕ_{CO2}	ϕ_{H2}	ϕ_{DME}	ϕ_{H2O}	ϕ_{CH3OH}	$K_{\phi 1}$	$K_{\phi 2}$	$K_{\phi 3}$
100	1.006	0.832	1.022	0.377	0.014	0.056	0.288	0.005	0.053
125	1.012	0.866	1.021	0.505	0.033	0.111	0.396	0.015	0.105
150	1.016	0.894	1.021	0.615	0.068	0.197	0.493	0.037	0.186
175	1.019	0.916	1.021	0.685	0.126	0.316	0.558	0.076	0.298
200	1.022	0.934	1.020	0.738	0.214	0.466	0.609	0.140	0.438
225	1.023	0.948	1.020	0.779	0.734	0.632	0.651	0.506	0.595
250	1.024	0.960	1.019	0.814	0.772	0.716	0.687	0.556	0.673
275	1.025	0.970	1.019	0.843	0.803	0.763	0.719	0.599	0.718
300	1.025	0.978	1.018	0.867	0.828	0.802	0.745	0.636	0.754
325	1.026	0.984	1.018	0.888	0.850	0.833	0.769	0.669	0.785
350	1.026	0.990	1.017	0.906	0.868	0.860	0.789	0.698	0.810
375	1.026	0.994	1.017	0.921	0.884	0.882	0.808	0.724	0.832
400	1.026	0.998	1.016	0.934	0.898	0.902	0.824	0.747	0.851

APPENDIX B

CONVERSION AND SELECTIVITY CALCULATIONS

In the activity tests, products and unconverted gases were analyzed with an online GC connected to experimental set-up. Details of experimental system are explained in Section 6.3. From GC analyses, peaks regarding to component(s) were obtained. Retention time of each peak was found by calibration and calibration factors are given in Table 7. In this appendix, sample calculations for conversion and selectivity calculations are illustrated for two different feed gas compositions.

B1. ACTIVITY RESULTS OF TRC-75(L)-C from mixture-1 (50% H_2, 50% CO)

Activity test of TRC-75(L)-C was made at a pressure of 50 bar and in a temperature range of 200 °C – 400 °C. Reactant gas flow rate was 50 cc/min and 0.2 gr catalyst was loaded to reactor. Activity results were given in Section 8.2.1.

In experiments, steady state was reached at around 30 minutes that corresponds to duration of one complete GC analysis. After steady state reached, four successive runs were carried out and peak areas corresponding to any component was recorded. For conversion and selectivity calculations, average of them was taken and average values are given in Table 34.

Table 34. Average area values of chemicals obtained from GC analyses

T , °C	**A_{CO}**	**A_{CH_4}**	**A_{CO_2}**	**A_{MEOH}**	**A_{FA}**	**A_{DME}**	**A_{ETOH}**
200	416.72	0	2.44	0	0	0	0
250	403.69	0.36	20.66	1.64	0.56	27.37	0.00
275	403.83	0.34	24.42	5.58	0.71	36.97	0.82
300	371.54	5.96	65.55	6.16	4.19	25.20	5.92
350	357.38	9.25	72.49	7.56	6.74	12.65	7.12
400	359.14	13.99	75.74	4.90	7.30	3.13	8.01

Peak areas obtained from GC were converted to mole numbers with respect to reference calibration chemical CO by multiplying peak areas with calibration factors from equation B1.

$$n_i = A_i * \beta_i \quad [B1]$$

Average area values were converted to respective mole numbers and given in Table 35. Hand calculations for 275 °C are given below.

$n_{CO} = A_{CO} \times \beta_{CO} = 403.83 \times 1.00 = 403.83$

$n_{CH_4} = A_{CH_4} \times \beta_{CH_4} = 0.34 \times 1.36 = 0.46$

$n_{CO_2} = A_{CO_2} \times \beta_{CO_2} = 24.42 \times 0.83 = 20.27$

$n_{MEOH} = A_{MEOH} \times \beta_{MEOH} = 5.58 \times 1.40 = 7.82$

$n_{FA} = A_{FA} \times \beta_{FA} = 0.71 \times 1.80 = 1.27$

$n_{DME} = A_{DME} \times \beta_{DME} = 36.97 \times 0.49 = 18.11$

$n_{ETOH} = A_{ETOH} \times \beta_{ETOH} = 0.82 \times 1.44 = 1.19$

Table 35. Respective mole numbers of chemicals obtained from GC analyses

T , °C	**n_{CO}**	**n_{CH_4}**	**n_{CO_2}**	**n_{MEOH}**	**n_{FA}**	**n_{DME}**	**n_{ETOH}**
200	416.72	0	2.02	0	0	0	0
250	403.69	0.49	17.15	2.29	1.00	13.41	0.00
275	403.83	0.46	20.27	7.82	1.27	18.11	1.19
300	371.54	8.11	54.41	8.62	7.54	12.35	8.52
350	357.38	12.59	60.17	10.58	12.13	6.20	10.26
400	359.14	19.02	62.87	6.86	13.15	1.53	11.53

To determine the CO amount that was fed to reactor ($n_{CO,0}$), total carbon balance was made and number of total carbon monoxide entering to system is found from Equation B2. As it can be noticed from chemical structure of chemicals, CO, CH_4, CO_2, FA and methanol contains only one carbon atom whereas DME and ethanol contains two carbon atoms. For this reason, respective mole numbers of DME and ethanol was multiplied by 2.

$$n_{CO,0} = n_{CO} + n_{CH_4} + n_{CO_2} + n_{FA} + n_{MEOH} + 2 * n_{DME} + 2 * n_{ETOH} \qquad [B2]$$

CO conversion was defined as the ratio of amount of CO reacted to amount of CO fed to reactor and expressed as in 6.1 and mathematical expression of it is given with B.3.

X = (Moles of CO fed to system – Moles of CO emerged from system)/ Moles of CO fed to system [6.1]

$$X = \frac{n_{CO,0} - n_{CO}}{n_{CO,0}} \qquad [B3]$$

Total numbers of CO fed to system and CO conversions are given in Table 36 and hand calculations are given below for 275 °C.

$$\begin{aligned} n_{CO,0} &= n_{CO} + n_{CH_4} + n_{CO_2} + n_{FA} + n_{MEOH} + 2 * n_{DME} + 2 * n_{ETOH} \\ &= 403.83 + 0.46 + 20.27 + 1.27 + 7.82 + 2 * 18.11 + 2 * 1.19 \\ &= 472.25 \end{aligned}$$

Table 36. Total numbers of CO fed to system and CO conversions

T , °C	**$n_{CO,0}$**	**X**
200	418.74	0.00
250	451.45	0.11
275	472.25	0.14
300	491.96	0.24
350	485.76	0.26
400	487.16	0.26

Product selectivities were defined as the ratio of moles of CO converted to a specific component to total moles of CO converted to the products. According to this definition, DME methanol and CO_2 selectivities were expressed as;

S_{DME} = 2(Moles of DME formed)/ (Moles of CO converted to products) 6.2.

S_{MEOH}= (Moles of MEOH formed)/ (Moles of CO converted to products) 6.3.

S_{CO_2} = (Moles of CO_2 formed)/ (Moles of CO converted to products) 6.4.

Mathematical expressions for equations 6.2, 6.3, and 6.4 are given with following equations.

$$S_{DME} = 2\frac{n_{DME}}{n_{CO,0} - n_{CO}} \quad [B4]$$

$$S_{MEOH} = \frac{n_{MEOH}}{n_{CO,0} - n_{CO}} \quad [B5]$$

$$S_{CO2} = \frac{n_{CO2}}{n_{CO,0} - n_{CO}} \quad [B6]$$

Product selectivities of each chemical are given in Table 37 and hand calculations are shown below for 275 °C.

$$S_{DME} = 2\frac{n_{DME}}{n_{CO,0} - n_{CO}} = 2 \times \frac{18.11}{472.25 - 403.83} = 0.53$$

$$S_{MEOH} = \frac{n_{MEOH}}{n_{CO,0} - n_{CO}} = \frac{7.82}{472.25 - 403.83} = 0.11$$

$$S_{CO2} = \frac{n_{CO2}}{n_{CO,0} - n_{CO}} = \frac{20.27}{472.25 - 403.83} = 0.30$$

Table 37. Product selectivities defined with respect to moles of CO converted to products

T , °C	S_{CH_4}	S_{CO_2}	S_{MEOH}	S_{FA}	S_{DME}	S_{ETOH}
200	0	1.00	0	0	0	0
250	0.01	0.36	0.05	0.02	0.56	0.00
275	0.01	0.30	0.11	0.02	0.53	0.03
300	0.07	0.45	0.07	0.06	0.21	0.14
350	0.10	0.47	0.08	0.09	0.10	0.16
400	0.15	0.49	0.05	0.10	0.02	0.18

In some experiments, yields were calculated. Yields were obtained by multiplying selectivity of any component with conversion and can be expressed as the ratio of moles of desired product formed to moles of reactant fed to the system. Yields, conversion and DME selectivities are given in Table 38.

$$Y = S \times X \qquad [B7]$$

Table 38. DME selectivity, conversion, and product yields

T , °C	S_{DME}	X	Y
200	0.00	0.00	0.00
250	0.56	0.11	0.06
275	0.53	0.14	0.08
300	0.21	0.24	0.05
350	0.10	0.26	0.03
400	0.02	0.26	0.01

B2. ACTIVITY RESULTS OF TRC-75(L)-C FROM MIXTURE-1 (50% H_2, 40% CO, 10% CO_2)

Activity test of TRC-75(L)-C was made at a pressure of 50 bar and in a temperature range of 200 °C – 400 °C. Reactant gas flow rate was 50 cc/min and 0.2 gr catalyst was loaded to reactor. Feed gas was composed of carbon monoxide, carbon dioxide and hydrogen with a composition H_2:CO:CO_2=50:40:10. Activity results were given in Section 8.2.2.

In experiments, steady state was reached at around 30 minutes that corresponds to duration of one complete GC analysis. After steady state reached, four successive runs were carried out and peak areas corresponding to any component was recorded. For conversion and selectivity calculations, average of them was taken and average values are given in Table 39.

Table 39. Average area values of chemicals obtained from GC analyses

T , °C	A_{CO}	A_{CH_4}	A_{CO_2}	A_{FA}	A_{DME}	A_{ETOH}
200	307.03	0.00	86.61	0.00	2.64	0.00
250	295.87	0.24	99.32	0.26	19.72	0.00
275	274.67	0.53	120.91	0.69	43.91	0.00
300	275.26	0.92	118.90	0.96	36.47	1.44
350	290.01	3.71	108.85	2.20	12.45	2.09
400	289.12	8.87	109.11	3.64	2.33	2.70

Peak areas obtained from GC were converted to mole numbers with respect to reference calibration chemical CO by multiplying peak areas with calibration factors from equation B1.

$$n_i = A_i * \beta_i \qquad [B1]$$

Average area values were converted to respective mole numbers and given in Table 40. Hand calculations for 250 °C are given below.

$n_{CO} = A_{CO} \times \beta_{CO} = 295.87 \times 1.00 = 295.87$

$n_{CH_4} = A_{CH_4} \times \beta_{CH_4} = 0.24 \times 1.36 = 0.33$

$n_{CO_2} = A_{CO_2} \times \beta_{CO_2} = 99.32 \times 0.83 = 82.43$

$n_{FA} = A_{FA} \times \beta_{FA} = 0.26 \times 1.80 = 0.47$

$n_{DME} = A_{DME} \times \beta_{DME} = 19.72 \times 0.49 = 9.66$

Table 40. Respective mole numbers of chemicals obtained from GC analyses

T , °C	n_{CO}	n_{CH_4}	n_{CO_2}	n_{FA}	n_{DME}	n_{ETOH}
200	307.03	0	71.89	0	1.30	0
250	295.87	0.33	82.43	0.47	9.66	0
275	274.67	0.72	100.36	1.24	21.51	0
300	275.26	1.25	98.69	1.72	17.87	2.07
350	290.01	5.05	90.34	3.95	6.10	3.00
400	289.12	12.06	90.56	6.56	1.14	3.89

To determine inlet carbon amount that was fed to reactor ($n_{C,0}$), total carbon balance was made and number of total carbons entering to system is found from Equation B2. As it can be noticed from chemical structure of chemicals, CO, CH_4, CO_2, and FA contains only one carbon atom whereas DME and ethanol contains two carbon atoms. For this reason, respective mole numbers of DME and ethanol was multiplied by 2.

$$n_{C,0} = n_{CO} + n_{CH_4} + n_{CO_2} + n_{FA} 2 * n_{DME} + 2 * n_{ETOH} \qquad [B2]$$

Since the composition of feed gas was known, initial amounts of CO and CO_2 can be calculated as follows.

$$n_{CO,0} = 0.80 * n_{C,0} \qquad [B8]$$

$$n_{CO_2,0} = 0.20 * n_{C,0} \qquad [B9]$$

CO conversion was defined as the ratio of amount of CO reacted to amount of CO fed to reactor and expressed as in 6.1 and mathematical expression of it is given with B.3.

X_{CO} = (Moles of CO fed to system – Moles of CO emerged from system)/ Moles of CO fed to system

$$x_{CO} = \frac{n_{CO,0} - n_{CO}}{n_{CO,0}} \qquad [B3]$$

Total numbers of carbon ($n_{C,0}$) and carbon monoxide ($n_{CO,0}$) fed to system and CO and CO_2 conversions are given in Table 41 and hand calculations are illustrated for 250 °C.

$$n_{C,0} = n_{CO} + n_{CH_4} + n_{CO_2} + n_{FA} + 2 * n_{DME} + 2 * n_{ETOH}$$

$$= 295.87 + 0.33 + 82.43 + 0.47 + 2 * 9.66 = 398.42$$

$$n_{CO,0} = 0.80 * n_{C,0} = 0.80 * 398.42 = 318.74$$

$$n_{CO_2,0} = 0.20 * n_{C,0} = 0.20 * 398.42 = 79.68$$

$$x_{CO} = \frac{n_{CO,0} - n_{CO}}{n_{CO,0}} = \frac{318.74 - 295.87}{318.74} = 0.07$$

Table 41. Total numbers of carbon, CO, and CO_2 fed to system and CO conversions

T , °C	$n_{C,0}$	$n_{CO,0}$	$n_{CO_2,0}$	x_{CO}
200	381.51	305.21	76.3	-0.01
250	398.42	318.74	79.7	0.07
275	420.02	336.02	84.0	0.18
300	416.80	333.44	83.4	0.17
350	407.56	326.05	81.5	0.11
400	408.36	326.69	81.7	0.12

Product selectivities were defined as the ratio of moles of CO converted to a specific component to total moles of CO converted to the products. According to this definition, DME and CO_2 selectivities were expressed as;

S_{DME} = 2(Moles of DME formed)/ (Moles of CO converted to products) 6.2.

S_{CO_2} = (Moles of CO_2 formed)/ (Moles of CO converted to products) 6.4.

Mathematical expressions for equations 6.2 and 6.4 are given with following equations.

$$S_{DME} = 2\frac{n_{DME}}{n_{CO,0}-n_{CO}} \qquad [B4]$$

$$S_{CO2} = \frac{n_{CO2,0}-n_{CO2}}{n_{CO,0}-n_{CO}} \qquad [B6]$$

Product selectivities of each chemical are given in Table 42 and hand calculations are shown below for 250 °C.

$$S_{DME} = 2\frac{n_{DME}}{n_{CO,0}-n_{CO}} = 2\frac{9.66}{318.74-295.87} = 0.85$$

$$S_{CO_2} = \frac{n_{CO2,0} - n_{CO2}}{n_{CO,0} - n_{CO}} = \frac{82.43 - 79.7}{318.74 - 295.87} = 0.12$$

Table 42. Product selectivities defined with respect to moles of CO converted to products

T , °C	S_{CH_4}	S_{CO_2}	S_{FA}	S_{DME}	S_{ETOH}
200	0	2.42	0	-1.42	0
250	0.01	0.12	0.02	0.85	0
275	0.01	0.27	0.02	0.70	0
300	0.02	0.26	0.03	0.61	0.07
350	0.14	0.25	0.11	0.34	0.17
400	0.32	0.24	0.17	0.06	0.21

Similarly, CO_2 conversion was defined as the ratio of amount of CO_2 reacted to amount of CO_2 fed to reactor and expressed as in 6.6 and mathematical expression of it is given with B10.

X_{CO_2} = (Moles of CO_2 fed to system – Moles of CO_2 emerged from system)/ Moles of CO_2 fed to system 6.6

$$x_{CO_2} = \frac{n_{CO_2,0} - n_{CO_2}}{n_{CO_2,0}} \qquad [B10]$$

CO_2 conversions were calculated at different temperatures and given in Table 43. Hand calculations are also given for 250 °C.

$$x_{CO_2} = \frac{n_{CO_2,0} - n_{CO_2}}{n_{CO_2,0}} = \frac{79.7 - 82.43}{79.7} = -0.03$$

Table 43. CO_2 conversion with respect to temperature

T , °C	200	250	275	300	350	400
X_{CO_2}	0.06	-0.03	-0.19	-0.18	-0.11	-0.11

As it could be seen from Table 41, CO conversion was negative at 200 °C. Moreover, DME selectivity was negative and CO_2 selectivity was positive and greater than one at 200 °C. Negative CO conversion indicated that CO was a product rather than a reactant at 200 °C. Based on CO_2 conversion results, which is shown in Table 43, CO_2 conversion was positive at 200 °C, meaning that CO_2 acted as reactant instead of being a product. Therefore, selectivity definition which was made with respect to converted CO to products was meaningless for positive CO_2 definition. Selectivity must be defined with respect to total amount of converted CO & CO_2. According to this definition, DME and methanol selectivities were expressed as;

S_{DME} = 2(Moles of DME formed)/ (Moles of CO&CO_2 converted to products) 6.7.
S_{MEOH}= (Moles of MEOH formed)/ (Moles of CO&CO_2 converted to products) 6.8.

Mathematical expressions for 6.7 and 6.8 are given with B11 and B12.

$$S_{DME} = \frac{2 * n_{DME}}{n_{C,0} - (n_{CO} + n_{CO_2})} \quad [B11]$$

$$S_{MEOH} = \frac{n_{MEOH}}{n_{C,0} - (n_{CO} + n_{CO_2})} \quad [B12]$$

Product selectivities which were defined with respect to converted CO&CO_2 were calculated at different temperatures and given in Table 44. Hand calculations are also given for 200 °C.

$$S_{DME} = \frac{2 * n_{DME}}{n_{C,0} - \left(n_{CO} + n_{CO_2}\right)} = \frac{2 * 1.30}{381.51 - (307.03 + 71.89)} = 1.00$$

Table 44. Product selectivities defined with respect to moles of CO&CO_2 converted to products

T , °C	S_{CH_4}	S_{FA}	S_{DME}	S_{ETOH}
200	0	0	1	0
250	0.02	0.02	0.96	0
275	0.02	0.03	0.96	0
300	0.03	0.04	0.83	0.10
350	0.19	0.15	0.45	0.22
400	0.42	0.23	0.08	0.27

APPENDIX C

PARTICLE SIZE CALCULATIONS

Particle sizes of the metals and metal oxides were calculated by Scherrer's equation [74].

$$\mathrm{d_i} = \frac{\mathrm{K} \times \lambda}{\beta \times \cos(\theta)} \qquad 7.1.$$

where, d_i = particle size of i,
K = shape factor
λ = X-Ray wavelength
β = Full width at half max (FWHM)
θ = Bragg's angle

Particle size of CuO, Cu_2O, Cu, ZnO, γ-Al_2O_3, and SiO_2 were calculated from the Scherrer's equation for the peaks of 2θ at around 35° for CuO, 65° for Cu_2O, 43° for Cu, 31° for ZnO, and 66° for γ-Al_2O_3. X-Ray diffractions were taken at the wavelength of 0.154 nm and shape factor was taken as 0.89.

CuO particle size was calculated for 2θ angle of 35.6°. XRD results revealed that FWHM was 1.93°. FWHM and 2θ were converted to radians.

$$\text{FWHM (radians)} = \frac{\text{FWHM}(°) \times \pi}{180} = \frac{1.93 \ \times \pi}{180} = 0.034$$

$$2\theta(\text{radians}) = \frac{2\theta(°) \times \pi}{180} = \frac{35.6 \ \times \pi}{180} = 0.621$$

$$\mathrm{d_i} = \frac{0.89 \times 0.154}{0.034 \times \cos(0.621/2)} = 4.3 \text{ nm}$$

Corresponding particle sizes for metals and metal oxides were calculated from equation 7.1 in a similar way and given in Table 45.

Table 45: Particle sizes for metals and metal oxides calculated from Scherrer's equation

Catalyst	Peak	2θ , °	FWHM , °	cos(θ)	Particle Size , nm
CZ	CuO	35.6	0.034	0.95	4.3
	ZnO	31.7	0.030	0.96	4.9
CZA	ZnO	31.7	0.035	0.96	4.1
	CuO	35.2	0.018	0.95	8.1
CZZr	ZnO	31.8	0.057	0.96	2.5
	CuO	35.3	0.029	0.95	5.0
CZCe	CuO	35.6	0.053	0.95	2.8
CZA-1hr	ZnO	38.3	0.006	0.94	25.6
	CuO	43.3	0.006	0.93	26.0
CZA-6hr	ZnO	31.8	0.031	0.96	4.7
	CuO	35.3	0.015	0.95	9.4
CZA-Hot	CuO	35.4	0.017	0.95	8.4
CZA-C5550	ZnO	31.6	0.018	0.96	8.1
	CuO	35.3	0.011	0.95	13.0
CZA-R225	ZnO	31.5	0.008	0.96	18.5
	Cu_2O	64.9	0.016	0.84	10.3
CZA-R250	ZnO	31.7	0.014	0.96	10.6
	Cu	43.1	0.006	0.93	26.8
TOYO	γ-Al_2O_3	66.7	0.034	0.84	4.8
H-CZA-TOYO	ZnO	31.8	0.129	0.96	1.1
	Cu	35.4	0.021	0.95	6.9
	γ-Al_2O_3	66.6	0.043	0.84	3.9
MSC	ZnO	31.8	0.042	0.96	3.4
	CuO	35.5	0.032	0.95	4.6
	SiO_2	26.4	0.005	0.97	29.8
MRC	ZnO	32.0	0.022	0.96	6.4
	CuO	35.4	0.023	0.95	6.5
	SiO_2	26.4	0.005	0.97	29.3

APPENDIX-D

ADSORPTION-DESORPTION ISOTHERMS

Adsorption-Desorption isotherms of the co-precipitated catalysts are given in Figures 106-116.

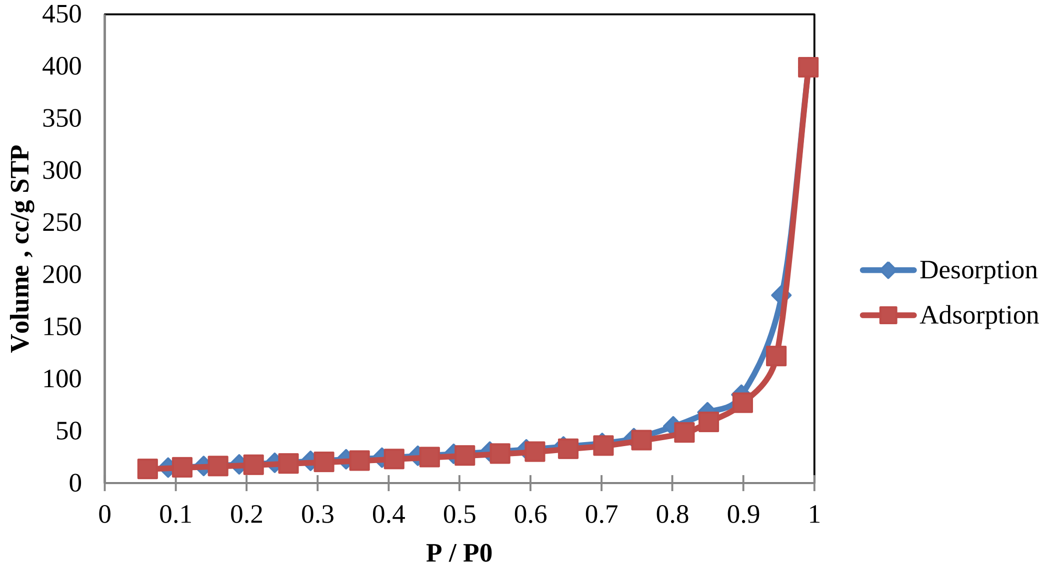

Figure 106. Adsorption desorption isotherm of copper and zinc containing co-precipitated catalyst, CZ

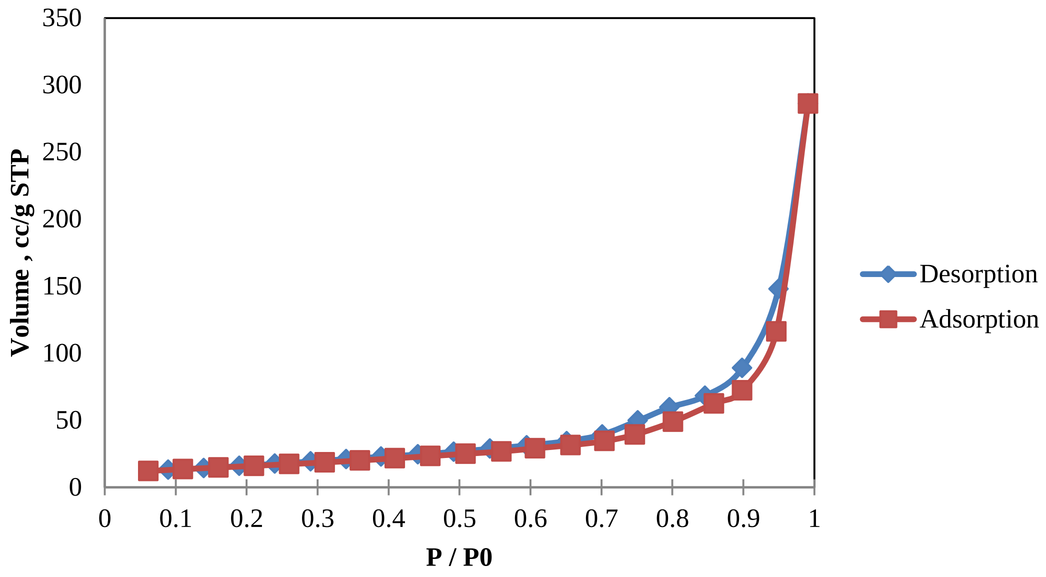

Figure 107. Adsorption desorption isotherm of copper, zinc, and alumina containing co-precipitated catalyst, CZA

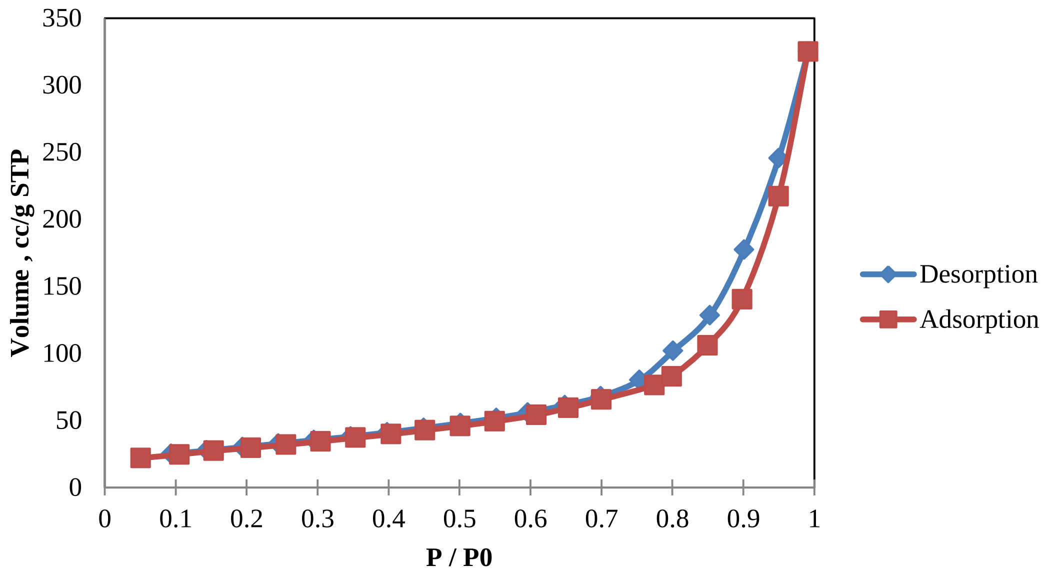

Figure 108. Adsorption desorption isotherm of copper, zinc, and zirconia containing co-precipitated catalyst, CZZr

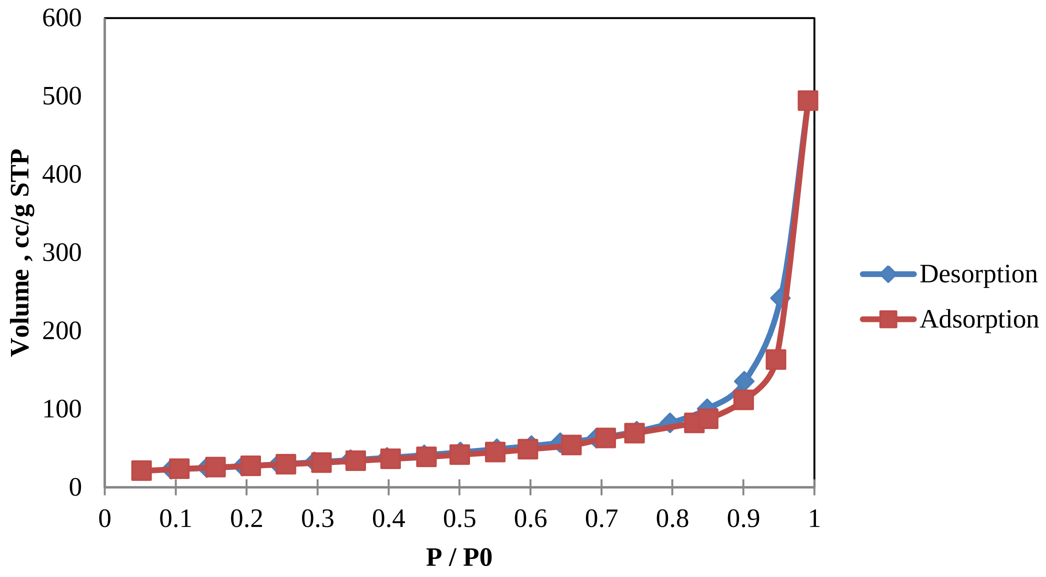

Figure 109. Adsorption desorption isotherm of copper, zinc, and ceria containing co-precipitated catalyst, CZCe

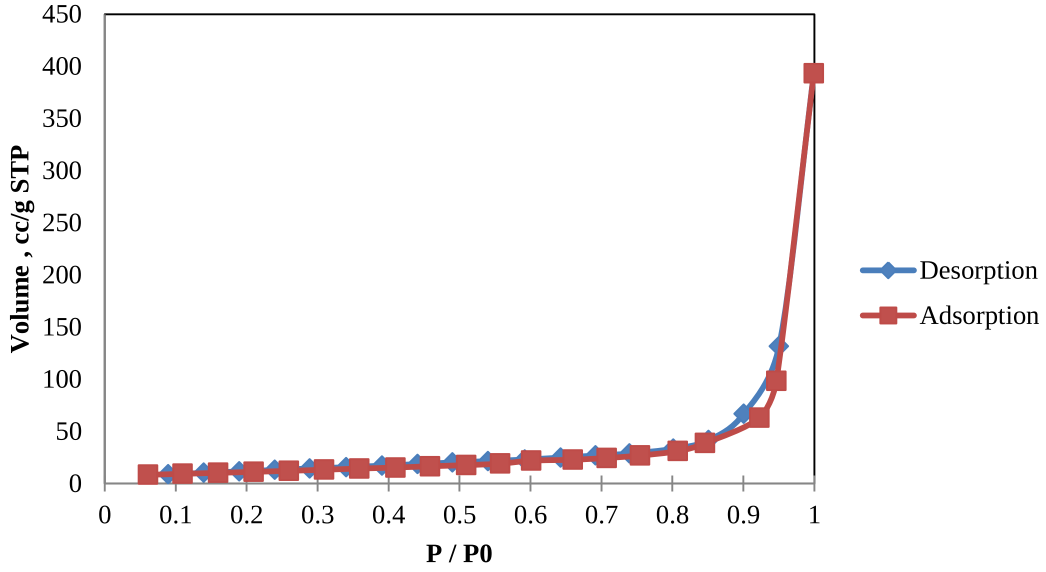

Figure 110. SEM images of copper, zinc, and alumina containing co-precipitated catalyst calcined at 550 °C, CZA-C550

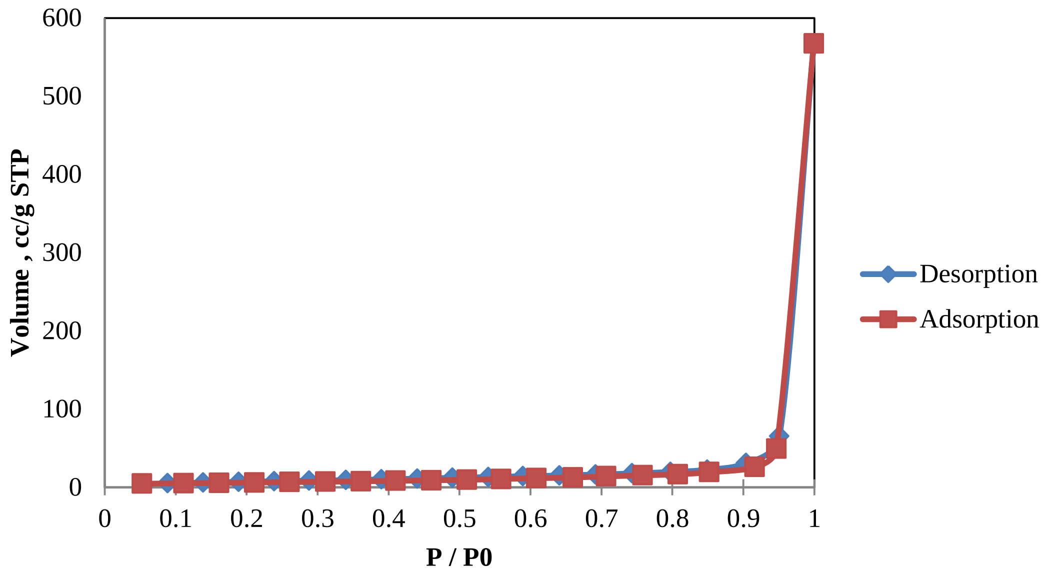

Figure 111. Adsorption desorption isotherm of copper, zinc, and alumina containing co-precipitated catalyst reduced at 225 °C, CZA-R225

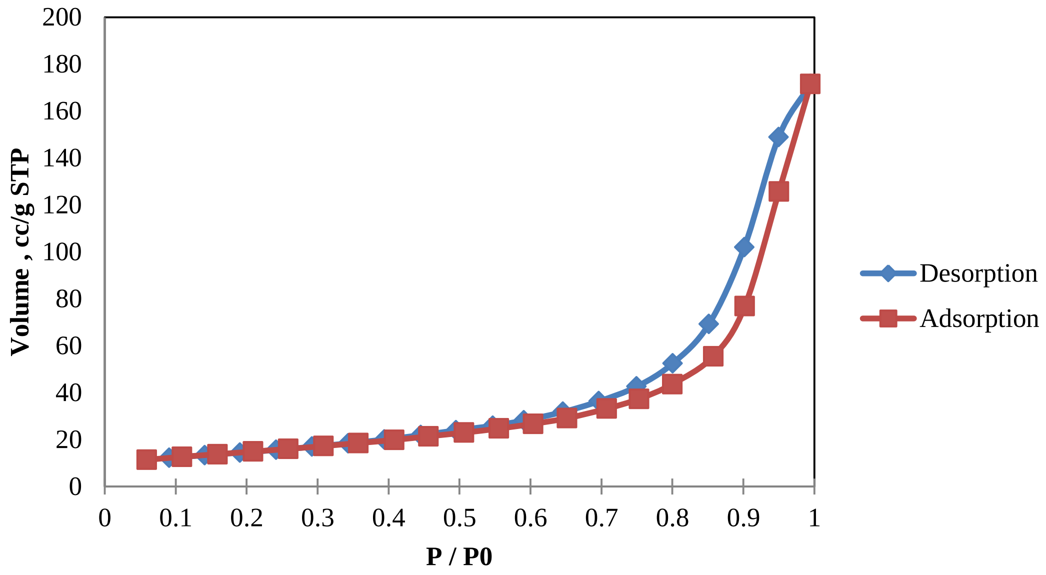

Figure 112. Adsorption desorption isotherm of copper, zinc, and alumina containing co-precipitated catalyst reduced at 250 °C, CZA-R250

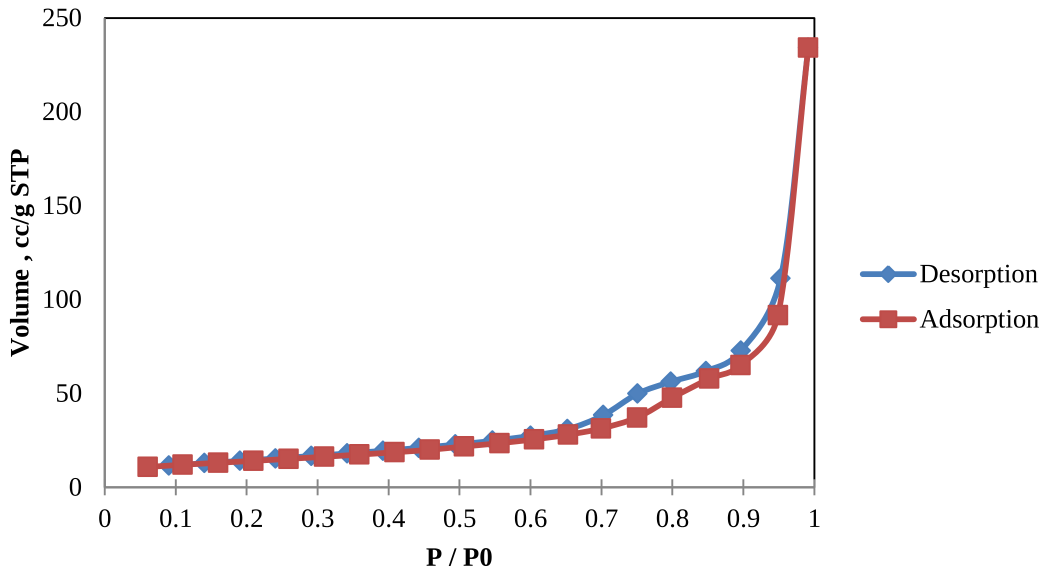

Figure 113. Adsorption desorption isotherm of copper, zinc, and alumina containing co-precipitated catalyst aged for 6 hours, CZA-6 hr

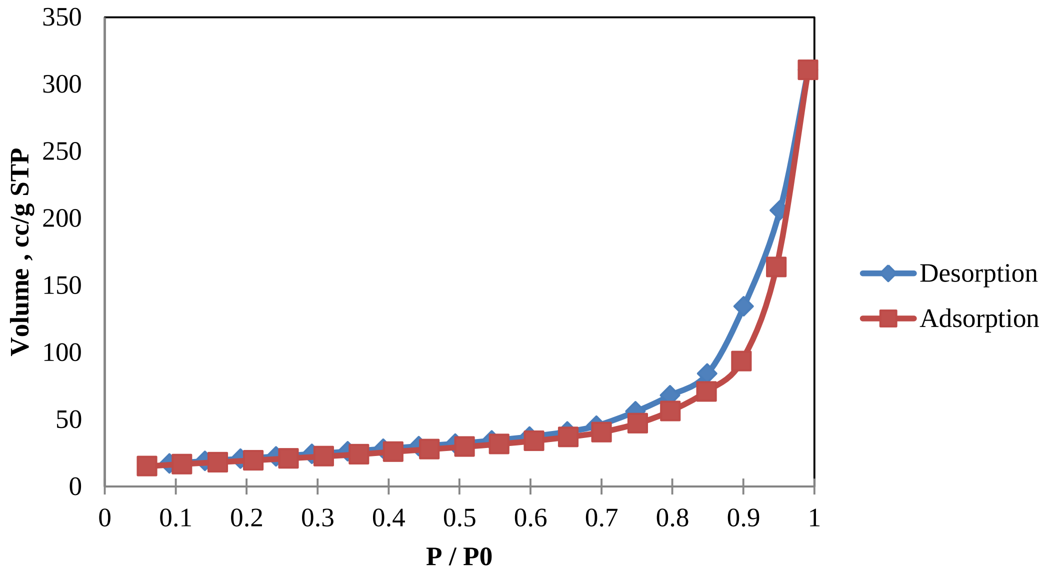

Figure 114. Adsorption desorption isotherm of copper, zinc, and alumina containing co-precipitated catalyst aged for 1 hour, CZA-1 hr

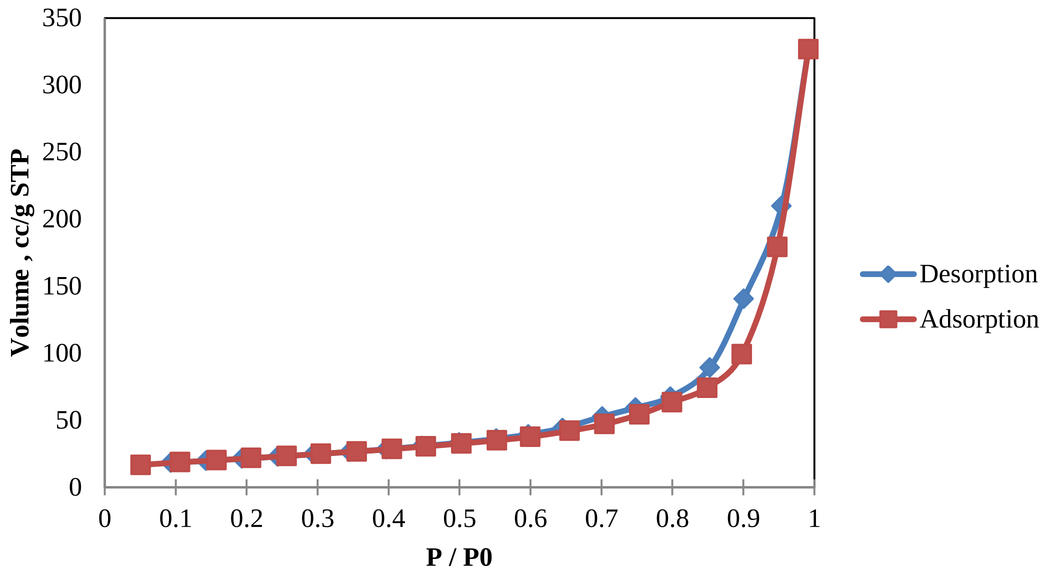

Figure 115. Adsorption desorption isotherm of copper, zinc, and alumina containing co-precipitated catalyst washed with hot water, CZA-Hot

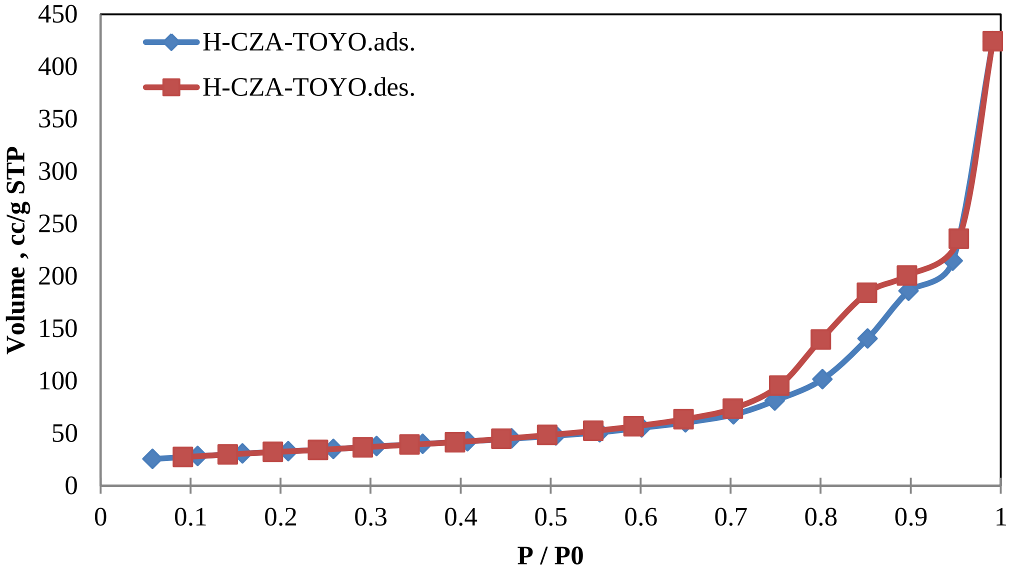

Figure 116. Adsorption desorption isotherm of bi-functional, copper, zinc, and alumina containing co-precipitated catalyst, H-CZA-TOYO